# THE INFLUENCE OF MINERALS CONTENT AND PETROGRAPHIC COMPOSITION ON THE GASIFICATION OF INERTINITE RICH HIGH ASH COAL

AF Koekemoer, B. Eng (Chemical Engineering)

Dissertation submitted in fulfilment of the requirements for the degree Magister in Engineering at the School of Chemical and Minerals Engineering at the North-West University, Potchefstroom Campus

Supervisor: Prof. H.W.J.P. Neomagus.
Co-supervisor: Prof. J.R. Bunt.
Co-supervisor: Prof. R.C. Everson.

Potchefstroom.

# Declaration

"I, Andrei Frederik Koekemoer, hereby declare that the thesis entitled:

**The influence of minerals content and petrographic composition on the gasification of inertinite rich high ash coal.**

Which I herewith submit to the North-West University in completion of the requirements set for the degree Magister in Engineering is my own original work and has not previously been submitted to any institution. If there was the need to quote, it was indicated and shown in a reference list."

Signed at Potchefstroom on this 20th November 2009.

.....
A.F. Koekemoer.

# Synopsis

Coal particles with different densities have different mineral and maceral compositions and this affects the gasification reaction rates, especially in coals with high ash contents. This study involved the characterization of six Highveld coals (coals A – F) as well as a coal blend (coal G) consisting of several of these single-source coals in terms of chemical, maceral, mineral and structural properties. This initial characterization was supported by the evaluation of the pyrolysis gas compositions (at 600 ºC) that can be obtained from the seven parent coals. The second part of this study included the density separation of two coals (coals B and G) into five density fractions by means of dense medium separation. This allowed the evaluation of chemical, maceral, mineral and structural properties of the coal fractions as a function of particle density. Finally these coal fractions (1 mm) were gasified under a pure $CO_2$ atmosphere at atmospheric pressure (87.5 kPa) and temperatures ranging from 1000 ºC to 1070 ºC to study the effect of particle density on gasification behaviour of coals. These gasification experiments were modelled with the random pore model and the activation energy of each fraction was calculated.

From the initial characterization it was found that the parent coals have ash contents in excess of 18.6 % and are inertinite rich (> 68 %); properties which are typical of coals derived from the Highveld coal field. It was observed that coal B has a very low calorific value (17.5 $MJ.kg^{-1}$) considering the amount of fixed carbon contained in this coal (48.1 %). This motivated further research into the properties and gasification kinetics of density separated fractions prepared from coals B and G. Density separation showed that five coal fractions with uniquely varying properties can be prepared by this procedure. Several trends were observed relating coal properties to particle density, the most prominent of which are:

- Ash increases from 8.9 % to 73 % with increasing particle density.
- Fixed carbon decreases from 60 % to 10 % with increasing density.
- Qualitative maceral segregation occurs, as inertinite tends to concentrate in the dense fractions (1.6 $g.cm^{-3}$ – 2.0 $g.cm^{-3}$), while vitrinite and liptinite remain in the lighter fractions (-1.4 $g.cm^{-3}$ – 1.6 $g.cm^{-3}$).
- The calorific value increases from 3.3 $MJ.kg^{-1}$ to 28.3 $MJ.kg^{-1}$ with decreasing particle density.

- The coal surface area increases from 38.0 $m^2.g^{-1}$ to 142.6 $m^2.g^{-1}$ with decreasing particle density.

It was found at low densities (< 1.8 $g.cm^{-3}$) that particle density does not have a significant influence on the $CO_2$ gasification reactivity. Further increase in particle density in excess of 1.8 $g.cm^{-3}$ results in increasing the gasification reactivity. The random pore model was found to give an adequate fit to the experimental gasification data in the temperature range of 1000 ºC to 1070 ºC. The activation energy for the $CO_2$ gasification reaction varies from 163 $kJ.mole^{-1}$ to 225 $kJ.mole^{-1}$ for the various coal fractions. It was observed that Ca, Mg and K act as catalysts in the $CO_2$ gasification reaction.

# Opsomming

Die digtheid van steenkool beinvloed die samestelling, veral van die minerale en maserale in die steenkool; wat dan indirek `n impak het op die tempo van vergassing veral in steenkool met `n hoë as inhoud. Die studie is gebaseer op ses enkelbron steenkole (steenkool A – F) sowel as `n mengsel wat saamgestel is uit `n aantal van die enkelbron steenkole. Die verskillende steenkole is word dan gekarakteriseer in terme van die chemiese, minerale, maserale en strukturele eienskappe. Hierdie karakterisering word aangevul deur `n meting van die pirolise gas samestelling wat van die steenkole verkry kan word by `n temperatuur van 600 ºC. Die tweede deel van die studie is om twee van die bogenoemde steenkole (steenkole B en G) te skei in vyf verskillende digthede deur middel van digte medium skeiding. Hierdie skeiding van verskillende digthede steenkool maak dit dan moontlik om die chemiese, minerale, maserale en strukturele eienskappe van die steenkool as `n funksie van partikel digtheid te bestudeer. Die geskeide steenkool fraksies (1 mm) word ook vergas in die teenwoordigheid van suiwer $CO_2$ gas by atmosferiese druk (87.5 kPa) en temperature wat reik van 1000 ºC tot 1070 ºC om die effek van partikel digtheid op die vergassings-eienskappe van steenkool waar te neem. Hierdie vergassings eksperimente is gemodelleer deur gebruik te maak van die “random pore” model en die aktiverings energie van die $CO_2$ vergassings reaksie was bereken vir elke steenkool fraksie.

Vanuit die aanvanklike karakterisiering is gevind dat die enkelbron steenkole `n as inhoud het van hoër as 18.6 % en `n hoë inetriniet inhoud het (>68 %). Hierdie eienskappe is kenmerkend aan steenkool afkomstig vanaf die Hoëveld steenkool veld. Dit is opmerklik dat steenkool B `n relatiewe lae kalorie-waarde het (17.5 $MJ.kg^{-1}$) met inagneming dat die steenkool `n vaste koolstof inhoud van 48.1 % het. Hierdie waarneming is `n goeie motivering vir die verdere navorsing wat gedoen is aangaande die eienskappe en $CO_2$ vergassings kinetika van digtheid geskeide steenkool fraksies verkry vanaf steenkole B en G. Die opbrengs verkry vanaf digtheidskeiding dui daarop dat vyf uniek verskillende fraksies voorberei kan word met die prosedure. `n Aantal tendense is waargeneem wat die eienskappe van die steenkole korreleer met die partikel digtheid, waarvan die mees opmerklikste is:

- Die as inhoud neem toe vanaf 8.9 % na 73 % met toenemende partikel digtheid.
- Die vaste koolstof inhoud neem af van 60 % na 10 % met toenemende partikel digtheid.
- Die skeiding van maserale op grond van digtheid is kwalitatief waargeneem, aangesien inertiniet hoofsaaklik in die digte fraksies (1.6 $g.cm^{-3}$ – 2.0 $g.cm^{-3}$) gevind word, terwyl vitriniet en liptiniet in die ligter fraksies (-1.4 $g.cm^{-3}$ – 1.6 $g.cm^{-3}$) voorkom.
- Die kalorie-waarde van die steenkool verhoog vanaf 3.3 $MJ.kg^{-1}$ na 28.3 $MJ.kg^{-1}$ soos wat die partikel digtheid afneem.
- Die oppervlak area van die steenkool neem toe vanaf 38.0 $m^2.g^{-1}$ na 142.6 $m^2.g^{-1}$ soos wat die partikel digtheid afneem.

Daar is gevind dat by laer partikel digthede (< 1.8 $g.cm^{-3}$) dat die digtheid nie `n beduidende impak het op die tempo van vergassing nie. Die “random pore” model gee `n bevredigende voorstelling van die eksperimentele $CO_2$ vergassings data verkry by temperature wat reik van 1000 ºC tot 1070 ºC. Die aktiverings energie waardes vir die $CO_2$ vergassings reaksie is waargeneem en reik vanaf 163 $kJ.mol^{-1}$ tot 225 $kJ.mol^{-1}$ vir die verskeie steenkool fraksies. Daar was waargeneem dat Ca, Mg en K as kataliste optree in die $CO_2$ vergassings reaksie.

# Acknowledgements

I hereby wish to thank all of the persons and institutions who contributed to the completion of this research project. Your assistance and inputs are truly appreciated. The following persons deserve special thanks:

- Soli Deo Gloria.
- Sasol for the financial support of this project.
- My father and grand parents for always believing in me.
- The Coal Research Group at the North-West University for many valuable discussions. Here I make special mention of Prof. Hein Neomagus and Prof. John Bunt for their mentorship and guidance as study leaders.
- Rudi Coetzer and Sarel Du Plessis at Sasol Technology for their assistance in sample preparation as well as the pyrolysis test-rig.
- Chris van Alphen for his assistance with QEMSCAN analysis.
- Dr Nicola Wagner from the University of the Witwatersrand for her assistance with the petrographic analysis of coal.
- Rufaro Kaitano for his assistance and training on the gas adsorption equipment.
- Ome Jan Kroeze and Adrian Brock for assistance on the technical aspects.

# Contents

# List of Figures

# List of Tables

# List of Symbols

| Symbol | Description | Units |
|---|---|---|
| A | Pre-exponential factor | $s^{-1}.Pa^{-1}$ |
| $C_A$ | Concentration of species A | $mol.dm^{-3}$ |
| $D_{AVG}$ | Average pore diameter | Å |
| $D_{eff}$ | Effective diffusivity | $m^3.m^{-1}.s^{-1}$ |
| $D_K$ | Knudsen diffusivity | $m^3.m^{-1}.s^{-1}$ |
| $d_p$ | Particle diameter | m |
| $E_{act}$ | Activation energy | $Kj.mole^{-1}$ |
| $\Delta H_0$ | Heat of reaction | $Kj.mole^{-1}$ |
| k | Apparent rate constant | $s^{-1}$ |
| k'' | Reaction rate constant | $m^3.mole^{-1}.s^{-1}$ |
| $k_{s0}$ | Initial reaction rate constant | $m.s^{-1}.Pa^{-1}$ |
| $k_{s0}$' | Lumped pre-exponential factor | $s^{-1}.Pa^{-1}$ |
| L | Characteristic length | m |
| $L_0$ | Initial pore length per unit volume | $m.g^{-1}.m^{-3}$ |
| $M_0$ | Mass of sample at the beginning of gasification | mg |
| $M_{ASH}$ | Mass of ash | mg |
| $M_{CO2}$ | Molecular weight of $CO_2$ | $g.mol^{-1}$ |
| $M_t$ | Mass of sample at time (t) | mg |
| $M_W$ | Wagner-Weisz-Wheeler modulus | - |
| n | Reaction order with respect to $CO_2$ partial pressure | - |
| P | Pressure | Bar / kPa / mm Hg |
| $P_{CO2}$ | Carbon dioxide partial pressure | Bar / kPa |
| $P_{final}$ | Final degassing pressure | Bar / kPa / mm Hg |
| R | Universal gas constant | $J.K^{-1}.mole^{-1}$ |
| $R_A$ | Apparent reactivity | $min^{-1}$ |
| $R_I$ | Intrinsic reactivity | $g.m^{-2}.min^{-1}$ |
| RoV | Random vitrinite reflectance | % |
| $r_A'''$ | Reaction rate based on volume solids | $mol.m^{-3}.s^{-1}$ |
| $r_0/r_{s0}$ | Initial reaction rate | $m.s^{-1}$ |
| $r_s$ | Reaction rate | $m.s^{-1}$ |
| $S_0$ | Initial surface area | $m^2.m^{-3}$ |
| $S_{COAL}$ | Coal surface area | $m^2.g^{-1}$ |
| $S_{CHAR}$ | Char surface area | $m^2.g^{-1}$ |
| $S_{CO2}$ | Carbon dioxide adsorption surface area | $m^2.g^{-1}$ |
| $S_{N2}$ | Nitrogen adsorption surface area | $m^2.g^{-1}$ |

| Symbol | Description | Units |
|---|---|---|
| $T$ | Temperature | ºC / K |
| $T_{analysis}$ | Analysis temperature | ºC / K |
| $T_{degas}$ | Degassing temperature | ºC / K |
| $T_{HP}$ | High pressure analysis temperature | ºC / K |
| $T_{LP}$ | Low pressure analysis temperature | ºC / K |
| $t$ | Time | min |
| $t_x$ | Time to reach conversion x | min |
| $t_{50}$ | Time to reach 50 % conversion | min |
| $t_f$ | Time factor | $min^{-1}$ |
| $V_m$ | Volume of high density liquid | $cm^3$ |
| $V_t$ | Total volume of dense media mixture | $cm^3$ |
| $V_{MP}$ | Micro-pore volume | $cm^3.g^{-1}$ |
| $V_{N2}$ | Pore volume determined by nitrogen adsorption | $cm^3.g^{-1}$ |
| $w_0$ | Initial sample mass | mg |
| $X$ | Conversion | - |

## Greek Symbols

| Symbol | Description | Units |
|---|---|---|
| $\varepsilon_0$ | Initial porosity | % |
| $\mu$ | Mean value of continuous variable | - |
| $\rho$ | Density | $g.cm^{-3}$ |
| $\rho_m$ | Density of high density liquid | $g.cm^{-3}$ |
| $\rho_p$ | Density of low density liquid | $g.cm^{-3}$ |
| $\rho_t$ | Density of dense media mixture | $g.cm^{-3}$ |
| $\sigma$ | Standard deviation | - |
| $\tau$ | Dimensionless time | - |
| $\tau_t$ | Tortuosity | - |
| $\psi$ | Structural parameter | - |

# Nomenclature

| Abbreviation | Description |
|---|---|
| Afrox | African Oxygen Limited |
| BET | Brunauer-Emmett-Teller |
| BSI | Backscatter Electron Image |
| C-Arg | Carb-Argillite |
| C-Sil | Carbo-Silicate |
| CI | Confidence Interval |
| CTL | Coal To Liquids |
| daf | Dry ash free base |
| DR | Dubinin Raduschkevich |
| EE | Experimental Error |
| EDS | Energy Dispersive Spectrometry |
| GC | Gas Chromatograph |
| Inerto | Inertodetrinite |
| Inter | Intermediates |
| ISO | International Standards Organization |
| MIP | Mercury Intrusion Porosimetry |
| mmb | Mineral matter base |
| mmf | Mineral matter free base |
| N | Number of data points |
| s | Standard deviation |
| SABS | South African Bureau of Standards |
| SE | Standard Error of mean |
| SEM | Scanning Electron Microscope |
| SF | Semi-Fusinite |
| SG | Specific Gravity |
| TBE | Tetrabromoethane |
| TGA | Thermo-Gravimetric Analyzer |
| WITS | University of the Witwatersrand |
| XRD | X-ray Diffraction |
| XRF | X-ray Fluorescence |
| $\bar{x}$ | Mean value of data points |
| $x_i$ | Individual data point |
| z | 95 % Confidence interval critical value |

# Chapter 1: Introduction and Motivation

Coal has always been a very important natural resource, and one of the most important fossil fuels to be utilized by man. It has been reported that coal was used even as far back as 1000 BC in China, in Britain during pre-historic times as well as during the ancient Roman Empire (Tonge, 1907; Eddinger, 1974; WCI, 2007). More recently coal has played a great role in developing the technology of today by fuelling the Industrial Revolution of the 19$^{th}$ century as well as leading in the Electric Era of the 20$^{th}$ century (WCI, 2007). Both of these landmarks proved to make important contributions towards developing global technologies to the current level.

Coal was the most important source of the world's primary energy until the 1960's, when it was overtaken by oil as the primary energy source. Due to the current level of technological development as well as the rapid rate at which oil reserves are being depleted, it is forecast that coal will again become the main source of the world's primary energy during the first half of the century (WCI, 2007). Currently oil is responsible for providing 35 % of the global primary energy with natural gas and coal providing 21 % and 25 % respectively (WCI, 2007). The contributions of various energy sources to the global primary energy sector can be seen in Table 1.1.

Table 1. 1: Contributions to global primary energy (WCI, 2007).

| **Energy source** | **Contribution (%)** |
|---|---|
| Oil | 35 |
| Coal | 25 |
| Natural Gas | 21 |
| Nuclear | 6 |
| Hydro | 2 |
| Combustible and renewable waste | 10 |
| Other (including geothermal, solar and wind) | 1 |

Coal is also a very important resource in the global electricity sector, as most of the traditional electricity generation is done in pulverized coal combustion processes. Currently coal is the most important source of electricity in the world, as it is responsible for providing 40 % of the global electricity supply, with natural gas

generating 20 % of the global electricity supply, representing the second largest contribution to the global electricity sector. The generation of electricity by means of nuclear power plants is still a developing technology and represents 15 % of the global electricity supply, while the most important renewable source of electricity is hydro-generated power which represents 16 % of the global electricity supply. The contributions of the various sources of electricity are shown in Table 1.2.

Table 1. 2: Contributions to global electricity (WCI, 2007).

| Electricity source | Contribution (%) |
|---|---|
| Oil | 7 |
| Coal | 40 |
| Natural Gas | 20 |
| Nuclear | 15 |
| Hydro | 16 |
| Other (including geothermal, solar and wind) | 2 |

It is expected that the world energy demand will increase by 1.6 % annually from 2004 to 2030. The bulk of this growth will happen in developing countries such as South Africa; with these countries responsible for 70 % of the forecast growth, while China is expected to contribute to 30 % of the forecast increase in energy demand. It is anticipated that fossil fuels will be responsible for supplying 80 % of this forecast growth in electricity demand, emphasizing the importance of these fuels in the global energy sector (WCI, 2007).

Coal can be seen as the most important fossil fuel when looking into the future, as it is estimated that at current production levels, coal reserves will last another 141 years, while the other fossil fuels, oil and natural gas have 41 years and 65 years reserves left respectively (WCI, 2007). Coal is an abundant fossil fuel with reserves distributed across the globe, with recoverable coal reserves in approximately 70 countries, whereas the oil and natural gas reserves are concentrated in the Middle East and Russia; as 68 % of the current oil reserves and 67 % of the current natural gas reserves are located in these countries (WCI, 2007). Table 1.3 illustrates the top five hard coal producing countries. The Peoples Republic of China is the leading producer

of hard coal with an annual production of 2482 Mt, while South Africa is currently ranked fifth with an annual hard coal production of 244 Mt.

Table 1. 3: Leading global hard coal producers (WCI, 2007).

| Country | Production (Mt/year) |
|---|---|
| PR China | 2482 |
| USA | 990 |
| India | 427 |
| Australia | 309 |
| South Africa | 244 |

Another important use of coal is in the global steel industry, as 68 % of global steel production is based on coal-fired technologies. It is estimated that 592 Mt of coal was used in the steel industry during 2006 alone (WCI, 2007).

Coal is also used in the production of synthetic fuels. Sasol is a South African company which is the world leader in the conversion of coal to liquid fuels technology. This company was established in 1950 with the specific goal of converting low grade coal into petroleum products to make the country less dependant on foreign oil reserves. Sasol gasifies approximately 30 Mt of coal per annum at the Sasol II and III facilities in Secunda to produce 150 000 barrels per day of liquid fuels and petrochemicals. This liquid fuel production contributes to 40 % of the South African domestic liquid fuel requirements. With several global initiatives, there is a great need to further develop coal gasification technology (Sasol, 2007; Barker, 1999).

Coal is an important resource, specifically for South Africa as it is estimated that the South African coal reserves amount to 34 000 Mt (Campbell, 2002). The current production rate is approximately 244 Mt per annum and more than half of this coal is used to generate electricity. According to the Department of Minerals and Energy (DME, 2007), 21 % of South African coal is sold to the export market, 21 % is used locally (excluding the power-station coal) and the remaining 58 % is used according to Table 1.4.

Table 1. 4: Coal uses in South Africa (DME, 2007).

| Coal use | Contribution (%) |
|---|---|
| Electricity generation | 62 |
| Synthetic fuel production | 23 |
| General industry | 8 |
| Metallurgical industry | 4 |
| Sold locally or exported | 3 |

It is estimated that 93 % of the South African electricity supply depends on coal-fired technologies (WCI, 2007). This is significant, as South Africa is currently experiencing an energy crisis due to the electricity demand exceeding the supply. By developing new coal technologies or by improving on the current coal conversion efficiencies this problem may be resolved.

As the global population increases and the industries expand, it is important to note that the energy demand will also increase. Due to this, there is a great need to develop new coal technologies with greater efficiencies and which have a lower impact on the environment. Another motivation to optimize coal technologies is because coal, such as any other fossil fuel has finite reserves. The need exists to develop coal technology as to extract the maximum amount of energy per ton of coal, while minimizing the impact of coal utilization on the environment. Until nuclear energy and renewable energy sources such as hydro, wind and solar energy have been fully developed, coal must be used as efficiently as possible to ensure a smooth transition from fossil fuels to renewable energy sources. Another possibility is to co-fire biomass with coal in combustion and gasification processes as to further extend the current coal reserves into the future (Ericsson, 2006).

The greenhouse effect is a natural phenomenon, which is receiving increasingly more attention. This phenomenon is in effect the warming of the earth's surface due to greenhouse gases such as water vapour and carbon dioxide in the atmosphere. Exhaust gases from industries including, but not limited to the coal industry contribute to this effect which is then referred to as the enhanced greenhouse effect. Water vapour is known to be responsible for 67 % of the natural greenhouse effect, being the main cause of this phenomenon. The coal industries are responsible for

contributing 18.9 % to the enhanced greenhouse effect with the contribution of the various gases emitted from this industry shown in Table 1.5.

Table 1. 5: Coal industries contributions to enhanced Greenhouse effect (WCI, 2007).

| Gas | Contribution (%) |
|---|---|
| Carbon dioxide | 92 |
| Methane | 6 |
| Nitrous oxide | 2 |

Even though the coal industries are only responsible for a fraction of the greenhouse effect, it is still required to drastically reduce environmentally harmful emissions from coal-fired industries. By improving coal technology as to limit the environmental impact and improve the efficiency with which it is used, the term Clean Coal Technology comes to mind. Clean Coal Technologies have the following advantages (WCI, 2007):

- Reduction of environmentally harmful emissions.
- Reduction of waste material.
- Increasing the energy produced per ton of coal used.

In South Africa it is increasingly important for the coal to liquid fuels company, Sasol to improve on the efficiency with which gasifiers are used to produce synthesis gas from coal. This is needed as there is increased demand for gas and liquid fuels as well as increasing pressure from the global community to reduce potentially harmful emissions.

The heterogeneous nature of coal complicates the prediction of coal behaviour during gasification processes, and due to this nature of coal it follows that coal properties vary, even within a specific coal seam. Certain coal properties which influence coal fixed-bed gasification are (Bunt, 2006):

- Coal porosity and pore structure.
- Coal fixed carbon content.
- Volatile matter contained in the coal.
- Mineral matter contained in parent coal sample.
- Coal maceral composition and rank.

- Caking behaviour of the coal.

Apart from this, the gasification behaviour of coal is also affected by factors such as the temperature, heating rate and gases present within the gasifier itself. Due to this it is not possible to set up a universal model able to describe the kinetic behaviour of coal during the gasification process. In order to optimize the design and operation of coal processes, a deeper understanding into the coal gasification processes is needed and this motivates this study which will contribute to the understanding and prediction of coal gasification behaviour; especially as a function of particle density.

It is known that the petrographically characterized dense and intermediate char forms gasify at a lower rate when compared to the porous and carbominerite char types, leading to lower carbon efficiencies and gas yields. This behaviour has been observed by the Gas Production Operations of Sasol in Secunda, especially for coals which differ in molecular structure and have higher densities (Bunt, 2008). Due to this, it is possible that these high density coals will require more time to react and convert into gas. By better understanding the influence of density on coal gasification kinetics, the blends of coal used in gasification processes may be altered as to optimize the gas yield from the gasification processes.

**Scope**

Coal particles with different densities have different mineral and maceral compositions and this affects the gasification reaction rates, especially in coals with high ash contents. This paper presents results from a detailed study of characteristic properties of seven different coal feedstocks; which will include the chemical, petrographic, mineral and structural properties. Six of these coals are single-source, low grade, medium-rank C bituminous coals (coals A – F) which are rich in minerals and inertinite and currently used for energy and fuel production; and the seventh coal (coal G) is a blend consisting of several of these single-source coals.

From personal communication with Prof. J.R. Bunt (2008), it is known that coal blends containing more of coal B do not show good gasification behaviour, as it is associated with more carbon-in-ash as well as lower gas yields. This motivates a more specific study into the influence of coal particle density on the gasification reaction

rate of coal B and coal G. Coal G is chosen as it represents the benchmark for efficient gasification operations. The characteristic properties and $CO_2$ reactivity of different density fractions derived from these two coals (coals B and G) will also be evaluated. The focus of this work is to develop some insight into the intrinsic reactivity of the carbon/char; catalytic effect of mineral impurities; and pore structure effects of this coal type when gasified using $CO_2$ in a thermogravimetric analyser (TGA) at temperatures ranging from 1000 ºC to 1070 ºC. Although much gasification reactivity test work has been conducted on South African coals in the past, char reactivity as function of coal particle density is a new approach to understanding the factors that control the process when gasifying coals having a high ash content for coals of this region.

**Objectives**

The objectives of this research project are the following:

- Determine the chemical, petrographic, mineralogical and structural properties of the seven parent coal samples. This will be supported by an evaluation of the pyrolysis gases evolved from these seven coal samples to correlate this data with the parent coal properties.
- Perform density separation on coals B and G to produce 5 specific density fractions from each coal. For each of the density separated fractions, the chemical, petrographic, mineralogical and structural properties will be determined.
- Evaluate the carbon dioxide gasification reaction rate as a function of coal particle density for coals B and G; with the focus on relating the coal properties to the $CO_2$ reactivity as well as the gasification activation energy.
- The results from the $CO_2$ gasification experiments will be modelled and the relevant model parameters related to the coal properties.

# Chapter 2. Literature Survey

Coal is a very heterogeneous fossil fuel, which behaves differently under different conditions. In order to study the gasification behaviour of coal it is necessary to understand the formation and the building blocks which constitute this fossil fuel, as this will influence the properties of the coal to various degrees. When specifically looking at coal in the gasification process, it is important to note that the coal behaviour is influenced by the heating and reaction conditions in the gasification process. In order to fully understand and quantify the gasification behaviour of coal, several kinetic and particle models are available which can be evaluated against the reaction conditions.

This chapter will discuss coal under the following topics:

- Section 2.1 will discuss the formation of coal as well as the petrographic constituents of coal. This section will also look at Southern Hemisphere coals in terms of coal formation and origin.
- Section 2.2 will look at coal properties and will include discussions of the surface properties, petrographic properties, chemical properties, plastic properties as well as the density of coal.
- Section 2.3 will include a review of the mechanism of pyrolysis as well as the gas, liquid and char products formed during pyrolysis.
- Section 2.4 focuses on the behaviour of coal in the gasification reaction and the influence of various reaction conditions such as: temperature, reactant gas partial pressure, total pressure and the influence of diffusion effects on coal gasification.
- Section 2.5 looks at the specific gasification reactions taking place as well as the kinetic and particle models available to predict the gasification behaviour of coal.
- Section 2.6 will give a brief overview of previous research done on density separated coals.

## 2.1. Coal formation and constituents

Coal is the term used to describe the family of solid fossil fuels. These fossilized plant remains have a wide range of chemical and physical properties. Coal can also be described as a heterogeneous type of rock, which consists of different kinds of organic material as well as mineral matter in varying proportions (Sanders, 1996). Due to this heterogeneous nature of coal, it follows that no two coals are the same, as even coal samples from the same seam may vary in composition and exhibit varied properties.

### 2.1.1 Coal formation

Coal is formed in a marshy environment which allows for rapid plant growth. Another requirement for coal formation is enough water to restrict the oxygen supply to dead plant material as to prevent the breakdown of this organic material. This dead plant material undergoes a metamorphism by means of microbiological and geothermal factors which function as to alter it from the initial plant material to form coal.

The microbiological change is brought about by micro-organisms which function as to chemically change this dead plant material to form peat. This first step is known as the peatification process and the proportions and chemical composition of the organic constituents formed during this peatification process are the predecessors of macerals, which are the building blocks of coal and play an important role in determining the coal type (Grainger and Gibson, 1981). Here it follows that the grade of the resulting coal is determined by the amount of inorganic material washed into the peat swamp system (Falcon and Snyman, 1986).

The geothermal change in the organic matter is brought about by pressure and heat, as these peat swamps undergo physical and chemical changes (Neavel, 1982). These changes are due to peat swamps being buried deep under ground and then exposed to geothermal heat and pressure. This change in the organic material due to geological time is known as the coalification process. This coalification process is responsible for determining the rank of the resulting coal and it can therefore be said that the coal rank is independent of the coal type (Grainger & Gibson, 1981). The steps according

to which the coalification process takes place to form the different ranks of coal can be described as follows.

- Firstly there is the conversion of peat to form brown coal. This brown coal has a very high moisture content of approximately 20 % - 45 %. When dried, brown coal has a low heating value (Parks, 1963).
- Brown coal is then further coalified to form lignite, which is slightly more mature (Parks, 1963).
- The lignite maturity is further increased to form the sub-bituminous coals. These sub-bituminous coals have a glossy black colour and a moderately high moisture content of approximately 12 % - 30 %. The volatile matter contained in sub-bituminous coals is approximately 40 % (Neavel, 1982; Parks, 1963).
- The sub-bituminous coals undergo physical and chemical changes as well as becoming harder and more mature to form bituminous coals. These bituminous coals can also be sub-divided into 5 groups ranging from highly volatile to low volatile coals. The average volatile content of bituminous coals is 16.5 % (Neavel, 1982).
- Finally the bituminous coals are coalified to form semi-anthracite and anthracite coals. These anthracite coals have a low volatile content of less than 8 %, and have a high heating value. Due to this, anthracite coals are mainly used domestically for heating purposes (Parks, 1963).

### 2.1.2 Petrographic constituents

When looking at the building blocks which constitute coal, it follows that coal consists of maceral (organic) and mineral (inorganic) constituents on microscopic level. The maceral groups refer to the various plant material from which the coal was derived (Falcon, 1981). These maceral groups are:

- Vitrinite. The vitrinite maceral group is derived from cell walls, cell contents as well as precipitated gels. This maceral group is usually rich in oxygen (Falcon and Falcon, 1987).
- Liptinite. The liptinite maceral group is derived from algae, spores as well as waxy leaves. This maceral group is known to be rich in hydrogen (Falcon and Falcon, 1987).

- Inertinite. The inertinite maceral group is derived from plant material that had been oxidized, degraded or burned during the peat stage of the coalification process. This maceral group has a high carbon content (Falcon and Falcon, 1987).

Microscopic bands of macerals or maceral groups are called microlithotypes, and successions of these bands which form macroscopic bands are called lithotypes (Falcon, 1981). It follows that both the physical as well as the chemical properties of the coal depends on the original plant material, the environment under which the coal was formed as well as the degree of alteration that took place during the coalification process. It is possible to distinguish between coal macerals on a microscopic level, as these macerals differ in reflectivity, colour, shape and hardness. Here it follows that the term petrography refers to the microscopic study of the organic and inorganic constituents of the coals (Falcon and Snyman, 1986). The main properties of the coal macerals are described in the following paragraphs.

Vitrinite is the oxygen rich coal maceral group (Falcon and Falcon, 1987). Here it follows that the oxygen content decreases as the rank of the coal increases. It is also known that the porosities of vitrinite coals increase as the rank decreases (Jones et al., 1985). This behaviour is due to the increased amount of volatile matter contained in low rank coals. This maceral group is harder than the liptinite maceral group, but not as hard as the inertinite maceral group (Neavel, 1982). It follows that vitrinite-rich coals derived from bituminous coals soften during heating, forming porous char structures which expand the surface area required for the gasification reaction to take place. The density of this maceral group varies from 1.27 $g.cm^{-3}$ to 1.8 $g.cm^{-3}$ (Borrego et al., 1997).

Liptinite is the hydrogen-rich maceral group containing the greatest amount of volatile matter compared to the other maceral groups (Neavel, 1982). Due to the large volatile matter content, liptinite-rich coals produce high tar and gas yields during pyrolysis. This is the maceral group with the lowest hardness as well as the lowest density compared to the other maceral groups. The density of the liptinite maceral group varies from 1.18 $g.cm^{-3}$ to 1.25 $g.cm^{-3}$ (Grainger and Gibson, 1981; Borrego et al., 1997).

The inertinite maceral group is known to be rich in carbon, also containing the smallest amount of volatile matter compared to the other maceral groups (Neavel, 1982). This maceral group has the highest density varying from 1.35 $g.cm^{-3}$ to 1.7 $g.cm^{-3}$ (Borrego et al., 1997). The inertinite maceral group is highly aromatic and does not soften or develop porous char structures during heating, but rather forms a dense char which is difficult to ignite (Falcon and Snyman, 1986).

As previously mentioned, the macerals band together to form microscopic bands known as microlithotypes. These bands usually have a thickness of less than 50µm (Falcon and Snyman, 1986). The main microlithotypes are:

- Vitrite.
- Inertite.
- Liptite.
- Durite.
- Clarite.
- Vitrinertite.

The vitrite microlithotype is composed mainly of vitrinite, as it contains more than 95 % (vol) vitrinite, hence the name vitrite. The inertite microlithotype is composed mainly of the inertinite maceral group, as it contains more than 95 % (vol) inertinite and similarly liptite contains more than 95 % (vol) liptinite. It follows that vitrite, inertite and liptite are known as mono maceral microlithotypes, as they consist of mainly one maceral group; and the other constituting macerals contributing less than 5 % (vol) each.

Bi-macerals microlithotypes refer to those microscopic bands consisting of a combined maceral content of two macerals in excess of 95 % (vol), with a minimum contribution of 5 % (vol) from each maceral group. Durite is a bi-maceral microlithotype consisting of inertinite and liptinite, clarite is the bi-maceral microlithotype which consists of vitrinite and liptinite; and vitrinertite is the bi-maceral microlithotype which consists of vitrinite and inertinite. Then there is a microlithotype which consists of three main maceral groups known as trimacerite,

with a combined vitrinite, inertinite and liptinite content in excess of 5 % (vol) each (Falcon and Snyman, 1986).

As previously mentioned, these microlithotypes band together to form macroscopic bands known as lithotypes. The main lithotypes are (Falcon and Falcon, 1987):

- Vitrain.
- Clarain.
- Durain.
- Fusain.

Minerite refers to the more inorganic microlithotypes, containing more than 60 % (vol) mineral matter. The term carbominerite refers to the interaction and association between the organic and inorganic microlithotypes (Wagner, 1998). The main groups that are identified as carbominerite groups are shown in Table 2.1.

Table 2. 1: Main carbominerite groups (ISO 1213, 1992).

| **Carbominerite group.** | **Mineral association (Volume %)** |
|---|---|
| Carbargillite. | 20 – 60 Clay minerals. |
| Carbopyrite. | 5 – 20 Sulphide minerals. |
| Carbankerite. | 20 – 60 Carbonate minerals. |
| Carbosilicate. | 20 – 60 Quartz minerals. |

The mineral matter contained in coal is responsible for the formation of ash which is left behind at the end of combustion/gasification processes. These mineral constituents consist of two types (Grainger and Gibson, 1981):

- Intrinsic mineral matter.
- Extrinsic mineral matter.

The intrinsic mineral matter refers to the minerals which are contained in the original plant material. The extrinsic mineral matter can be sub-divided into two types: syngenetic and epigenetic. The syngenetic or primary extrinsic mineral matter can be defined as those minerals which were accumulated in the organic matter up to the peatification process (Falcon and Falcon, 1983). These minerals are usually inter-grown into the coal structure. The epigenetic or secondary extrinsic mineral matter

refers to those minerals which were deposited into fractures, cavities and cleats of the coal beds after solidification took place. These minerals are not as interwoven into the coal structure and are thus easier to remove from the parent coals (Falcon and Falcon, 1983). The most common minerals to occur in coals are (Alpern et al., 1984; Matjie et al., 2008; Mèndez et al., 2003):

- Kaolinite.
- Quartz.
- Pyrite.
- Calcite.
- Dolomite.

### 2.1.3 Southern Hemisphere coals

The coals found in the Southern Hemisphere are referred to as Gondwanaland coals, while the Northern Hemisphere coals are referred to as Laurasian coals. The Gondwanaland coals differ from the Laurasian coals in the following ways (Plumstead, 1966; Barker, 1999):

- The climate during coal formation and organic matter deposition is different, with the Gondwanaland coals formed under cooler conditions during alternating wet and dry seasons.
- The vegetation from which the organic matter constituting the coals was derived differs for Gondwanaland and Laurasian coals.
- Due to the shallow deposition of Gondwanaland coals, these coals are chemically changed rather than physically changed. This is also as result of the lack of pressure effects on the coal, as well as the significant temperature effects of igneous intrusions into the coal seams.

Gondwanaland coals are known to contain larger amounts of the inertinite maceral group, while the Laurasian coals are rich in vitrinite. The mineral matter contained in Gondwanaland coals is mainly the syngenetic mineral type. This is because of the sedimentary, porous nature of the layers surrounding the coal in the Southern Hemisphere which in turn leads to the ground water seepage and mineral matter deposition. Up to 70 % of the mineral matter contained in these Southern Hemisphere coals consists of clay, while the other main contribution to the mineral matter is made

by quartz, which is responsible for up to 20 % of the mineral matter contained in Gondwanaland coals (Sanders, 1996; Barker, 1999).

## 2.2. Coal properties

Due to the heterogeneous nature of coal, it follows that the individual coal properties will influence the heating and gasification behaviour of coal. These coal properties are discussed in the following section and include:

- Coal surface properties.
- Coal petrography.
- Chemical composition of the coal.
- Plasticity or coking behaviour of the coal.
- Coal density.

### 2.2.1 Surface properties

The surface properties of coal chars play an important role in the gasification reaction, because the solid-gas reaction of the carbon with the reactant gas takes place at the surface of the char particle. More specifically, the reaction takes place on the active sites on the particle surface. Here the reactant gases form carbon-oxygen complexes. After the surface reaction has been completed, product gases such as carbon dioxide and carbon monoxide are released from these sites (Walker et al., 1959). Thus the surface properties of the char can be linked to the reaction rate limiting step, as the diffusion of reactant gases to the active sites and product gases away from the active sites may govern the reaction rate. The number of active sites, the nature of these sites, as well as the absorbed reactant gas molecules affect the intrinsic reaction kinetics in the following areas (Walker et al., 1959; Laine et al., 1963):

- Activation energy required for the gasification reaction.
- Pre-exponential factor.
- The dependence of the reaction on reactant gases.

The surface area and the porosity of chars are severely affected by the pyrolysis procedure, most importantly, the temperature at which the coal is exposed to as well

as the duration of the charring procedure (Zong et al., 2007; Feng and Bhatia, 2003). As the charring temperature is increased, the surface area of the resultant char is decreased. This decrease is due to the micro-pores becoming blocked during the heat treatment process. The same effect of pore blockage and the associated decrease in surface area is observed as the pyrolysis time is increased (Feng and Bhatia, 2003). This decrease in available surface area then leads to a lower gasification reactivity, as there are less active sites available for the reaction to take place. This can be seen as a type of thermal annealing process.

This effect can be linked to the maceral types contained in the coal, as vitrinite has the greatest degree of carbon re-structuring along with the associated deactivation of the formed char (Lu et al., 2000). It is known that the aromacity and the crystalline structure of the coal increases as the pyrolysis temperature increases due to the aliphatic hydrogen being evolved at lower temperatures (Gilfillan et al., 1999).

### 2.2.2 Petrography

The properties associated with the petrographic constituents in coal have a great influence on coal behaviour during heating and gasification. These petrographic properties include:

- Vitrinite reflectance.
- Maceral composition of the coal.
- Microlithotype composition of the coal.

The reflectance of a coal sample gives an indication of the degree to which the coal is matured, which varies from brown coal to anthracite. The reflectance value increases with an increase in rank, and thus, also with an increase in the carbon content of the coal (Berkowitz, 1985). The vitrinite maceral group was chosen as the reference for coal reflectance measurements, as the vitrinite reflectance increases with an increasing degree of coalification. The vitrinite reflectance parameter is used as an indication of the coal rank, as it does not depend on the carbon/hydrogen ratio, or on the carbon/oxygen ratio, or volatile matter content (Cloke and Lester, 1994). Table 2.2 illustrates how the vitrinite reflectance of the coal increases with an increase in coal rank.

Table 2. 2: Coal rank dependence on random vitrinite reflectance (Cloke and Lester, 1994).

| Rank of coal | Sub-rank | % RoV |
|---|---|---|
| Low | Peat | 0-0.3 |
| | Lignite | 0.3-0.4 |
| | Sub-bituminous | 0.4-0.5 |
| Medium | High volatile bituminous | 0.5-1.1 |
| | Medium volatile bituminous | 1.1-1.6 |
| | Low volatile bituminous | 1.6-2 |
| High | Semi-anthracite | 2-2.5 |
| | Anthracite | 2.5-3.5 |
| | Meta-anthracite | +3.5 |

The chemical make-up related to the various maceral constituents in the coal also influences the gasification behaviour of the coal. The inertinite maceral group has the highest carbon content, as well as the lowest volatile yield; therefore it has the highest carbon/hydrogen ratio compared to the other maceral groups (Cloke and Lester, 1994). Inertinite-rich coals also have the highest degree of aromatic bonding compared to the other maceral groups. Inertinite is associated with the formation of dense, hard to ignite chars during pyrolysis, and is capable of forming any type of char depending on the rank of the inertinite coal (Cloke and Lester, 1994; Borrego et al., 1997). It is known that low-rank inertinite-rich coals exhibit swelling behaviour during pyrolysis which results in a slightly more porous char with increased reactivity (Cloke and Lester, 1994).

Vitrinite-rich coals contain a higher amount of volatile matter compared to the inertinite maceral group, but less than the liptinite group. The vitrinite maceral group is rich in oxygen, with the amount of oxygen contained in the coal decreasing with increasing rank (Borrego et al., 1997). Vitrinite-rich bituminous coals soften during pyrolysis and expand to form cellular structures, which increase the internal surface area resulting in a porous char. The degree of expansion and plastic behaviour is affected by the heating rate of the particle (Du Cann, 2002). It can be said that vitrinites undergo both a physical (porous structure) and a chemical (devolatilisation) change during pyrolysis.

Liptinite-rich coals have the highest volatile content and thus also the highest hydrogen content (Cloke and Lester, 1994; Grainger and Gibson, 1981). This maceral group has been shown to have the lowest reflectance value as well as the lowest aromacity (Grainger and Gibson, 1981). Most of the hydrogen present is aliphatically bonded and easily evolved at low temperatures. These liptinite-rich coals have the highest tar and gas yields during pyrolysis, due to the large amount of volatiles contained in the coal (Grainger and Gibson, 1981; Borrego et al., 1997).

It follows that the coal properties associated with microlithotypes, which are the combination of maceral groups also influence the gasification behaviour of the coal (Cloke and Lester, 1994). When vitrinite occurs in combination with another maceral group, the resulting coal has a higher reflectance compared to the pure vitrinite maceral; these coals also have a higher density compared to pure vitrinite. These microlithotypes are influenced by the pyrolysis temperature and have a low porosity compared to the pure vitrinite, which also results in lower reactivity due to the limited surface area available for the reaction to take place (Rosenburg et al., 1996).

The petrographic make-up of a typical gasification feed blend derived from the Highveld coal field is presented in Table 2.3.

Table 2. 3: Petrographic contents of a typical gasification feed coal (Wagner et al., 2008).

| **Maceral** | **Range (wt %)** |
|---|---|
| Vitrinite | 17 – 33 |
| Liptinite | 3 – 5 |
| Inert inertinite | 48 – 52 |
| Reactive inertinite | 16 – 22 |
| RoV | 0.58 – 0.64 |

The individual macerals present in the coal may react alone or interact with other macerals during the reactions, which results in the coal displaying different properties to that as predicted by the whole-coal chemistry. Due to this, the reactions observed on a single particle scale may be different to the predicted, analytical behaviour of the coal (Matjie et al., 2008).

### 2.2.3 Chemical composition

The chemical composition of coal plays an important role in predicting the gasification behaviour of coals. The amount of oxygen present in the coal is a parameter which may be used to approximate the amount of free active sites available on the char surface, which facilitates the solid-gas gasification reaction (Hashimoto et al., 1986). The moisture content of the coal is also indicative of the porosity of the resulting char formed during pyrolysis (Takarada et al., 1985). The carbon content of the coal, which can be linked to the vitrinite reflectance parameter of the coal, can give an indication of the coal reactivity (Berkowitz, 1985). This is because the reactivity decreases with an increase in the carbon content of the coal (Cloke and Lester, 1994). This can then be linked to the rank of the coal, as the carbon content increases with increasing rank from brown coal to anthracite. It can therefore be said that the reactivity of the coal decreases with an increase in the rank of the coal.

The volatile matter contained in the coal depends on the maceral composition of the coal, and decreases from liptinite to vitrinite, and finally to inertinite, which contains the least amount of volatiles. This volatile content impact on the properties of the chars formed during pyrolysis, as the evolution of volatile matter from the coal particles affects the porosity of the formed char and thus also influences the overall char reactivity. This is valid, as gasification is a solid-gas reaction, and is dependant on the available char surface area. Coals containing a larger amount of volatile matter will be more reactive due to the increased porosity of the formed chars.

### 2.2.4 Mineral matter

The mineral matter contained in coal also has an impact on the char reactivity. This is because the minerals can have a catalytic effect on the gasification reaction. Minerals, especially calcium, iron, sodium and potassium bond to oxygen-containing carboxyl groups in the place of the hydrogen, which usually occurs in that position (Hashimoto et al., 1986; Nishiyama, Y, 1986; Kyotani et al., 1993; Huttinger and Natterman, 1994; Ye et al., 1998; Zong et al., 2007). The minerals change the surface chemistry of the char, resulting in more active sites which facilitate the gasification reaction. Some researchers propose that this catalytic effect is observed due to the disintegration of the porous structure which results in a higher surface area, which is

then related to a higher concentration of active carbon sites per weight (Marques-Montesinos et al., 2002; Standish and Tanjung, 1988). Wigmans et al. (1983) proposed a mechanism to explain alkali metal carbonate-catalysed gasification of activated carbon in steam. It was stated that increased rate of carbon conversion observed during the high conversion range might correlate with the activation of the intercalated metal phase which forms during the pre-treatment. The catalyst (alkali metal) is then trapped in the intercalate-like structure, and can be released by reaction with $CO_2$. The mechanism which is believed to be associated with this is described according to:

$$2MC_X + CO_2 \rightarrow 2MO + CO + 2C_X \quad \text{.....(1)}$$

High rank coals are not as greatly affected by the catalytic effect of the minerals compared to the low rank coals. Coals with a carbon content of less than 80 % are greatly affected by the catalytic effect of minerals, whilst higher rank coals having a carbon content of more than 80 % show little or no catalytic effect, as the reaction is rather controlled by the intrinsic reactivity of the char. The catalytic effect is also negligible at very high temperatures (Miura et al., 1989). It follows that the reactivity of the char varies as the char conversion proceeds. This is because of the initial selective gasification of the most reactive carbon sites, which is then followed by the gasification of the less reactive carbon sites at a reduced reaction rate (Goyal et al., 1989; Feng and Bhatia, 2003).

Oki et al. (2004) stated that there are four main types of mineral matter contained in coal:

- High ash – low density group consists of those minerals which occur in high quantities in the ash and have a relatively low density such as kaolinite, quartz and illite.
- High ash – high density group refers to those minerals which are found in large quantities in the ash and have a relatively high density. The only mineral classified in this group is anatase.

- Low ash – low density group includes the minerals which are found in small quantities in the ash and have relatively low densities. This group includes minerals such as calcite and dolomite.
- Low ash – high density group consists of the minerals which are found in small quantities in the ash and have a relatively high density. The minerals identified in this group are siderite and pyrite.

In a study by Matjie et al. (2008) on the mineral matter and elemental composition of Highveld coals, it was found that the minerals contained in these Highveld coals consist mainly of kaolinite, quartz, dolomite and mica. There are also minor contributions from other minerals such as illite, calcite, pyrite, siderite and alumina-phosphates belonging to the goyazite mineral group. The minerals contained in a typical gasification feed coal derived from the Highveld coal field is presented in Table 2.4.

Table 2. 4: Typical range for minerals contained in a gasification feed coal (Matjie et al., 2008).

| Mineral | Range (wt %) | Chemical composition | Density (g.cm$^{-3}$) |
|---|---|---|---|
| Kaolinite | 44.0 – 51.4 | $Al_2Si_2O_5(OH)_4$ | 2.60 |
| Quartz | 15.2 – 21.5 | $SiO_2$ | 2.62 |
| Illite | 2.2 – 5.7 | $K_{0.6}(H_3O)_{0.4}Al_{1.3}Mg_{0.3}Fe^{2+}Si_{3.5}O_{10}(OH)_2.2H_2O$ | 2.75 |
| Mica | 4.5 – 10.4 | $KAl_3Si_3O_{10}(OH)_{1.8}F_{0.2}$ | 2.82 |
| Calcite | 1.2 – 9.8 | $CaCO_3$ | 2.71 |
| Dolomite | 6.4 – 15.2 | $CaMg(CO_3)_2$ | 2.84 |
| Siderite | 0 – 1.4 | $Fe^{2+}(CO_3)$ | 3.96 |
| Pyrite | 1.4 – 2.6 | $FeS_2$ | 5.01 |
| Bassanite | 1.4 – 2.5 | $2CaSO_4.2H_2O$ | 2.70 |
| Goyazite | 0.9 – 3 | $SrAl(PO_4)_2(OH)_5.H_2O$ | 3.22 |
| Anatase | 0.8 – 2.7 | $TiO_2$ | 3.90 |

The chemical make-up of the ash formed from the minerals contained in coal consists mainly of silicon oxide, aluminium oxide and other oxides. The chemical composition of the ash obtained from a typical gasification feed coal derived from the Highveld coal field is presented in Table 2.5.

Table 2. 5: Chemical make-up of ash obtained from a gasification feed coal (Matjie et al., 2008).

| Chemical composition | Range (wt %) |
|---|---|
| $SiO_2$ | 51.3 - 59.3 |
| $Al_2O_3$ | 26.6 – 29.1 |
| $Fe_2O_3$ | 1.5 – 2.7 |
| $TiO_2$ | 1.0 – 3.2 |
| $P_2O_5$ | 0.4 – 1.3 |
| CaO | 3.9 – 12.2 |
| MgO | 1.6 – 4.1 |
| $Na_2O$ | 0 |
| $K_2O$ | 0.9 – 1.6 |

The trace elements contained in the coals is of significance, as the environmental impact of coal gasification is not only limited to the gaseous emissions, but also the trace elements which are enriched in the ash particles. Clarke and Sloss (1992) stated that the trace elements which are of greatest concern include: As, B, Cd, Hg, Mo, Pb and Se, and the other elements of lesser concern include: Cr, Cu, Ni, V and Zn.

The physical distribution of mineral matter in the coal impacts on the reactivity of the given coal. When the inorganic material is more widely dispersed in the coal, there is enhanced diffusion of reaction gas between the macerals, and between the macerals and minerals, which in turn results in a higher reactivity (Mèndez et al., 2003).

The mineral matter contained in the coal can also affect the gasification reaction by impacting on the size of the coal particles (Smoot and Smith, 1985; Stubington and Linjewile, 1989). This happens by means of the thermal expansion of the mineral matter contained in the coal; as the minerals do not expand at the same rate as the organic constituents of the coal. This in turn leads to internal stress in the coal particles, which results in the particles breaking up into smaller fragments and increase the reaction rate due to the increased surface area available for the gasification reaction to take place.

It is known that the mineral matter contained within the coal has a larger specific heat compared to the organic constituents of the coal. That is why coals containing large amounts of minerals will absorb more heat, and slow the reaction down compared to

high rank coals. These coals also have less carbon available to generate heat in the combustion reaction and will require more energy to drive the endothermic gasification reactions. A coal particle containing large amounts of mineral matter has a higher density compared to a carbon-rich coal particle, and thus also a lower porosity compared to a carbon-rich coal particle. This decreased porosity leads to a decreased reactivity, as the internal surface area available for the gasification reaction is decreased (Lu and Do, 1994).

The mineral matter component of coal has an influence on the amount of energy that can be obtained from each unit of coal. This happens as there is a reduction in the heating value of the coal caused by the endothermic decomposition of the minerals at temperatures exceeding 900 ºC as well as the high heat capacity of these minerals. The following reactions describe the thermal decomposition of several prominent minerals found in coal (Shirazi et al., 1995).

Kaolinite decomposes at 900 ºC according to an endothermic reaction to form meta-kaolinite and water vapour:

$$Al_2Si_2O_5(OH)_4 \xrightarrow{900°C} Al_2Si_2O_7 + 2H_2O_{(g)} \qquad (\Delta H_0 = +270.98 kJ.mole^{-1}) \;.....(2)$$

The initial decomposition of kaolinite is followed by the secondary exothermic decomposition of meta-kaolinite at 1200 ºC:

$$3Al_2SiO_7 \xrightarrow{1200°C} Al_6Si_2O_{13} + 4SiO_2 \qquad (\Delta H_0 = -430.66 kJ.mole^{-1}) \;.....(3)$$

Pyrite is converted according to the following oxidation reaction to form iron(III)oxide and sulphur dioxide gas is released:

$$2FeS_2 + \frac{11}{2}O_2 \xrightarrow{900°C} Fe_2O_3 + 4SO_{2(g)} \qquad (\Delta H_0 = -343.23 kJ.mole^{-1}) \;.....(4)$$

Siderite is also oxidized similar to pyrite to form iron(III)oxide which is associated with the release of carbon dioxide gas:

$$2FeCO_3 + \frac{1}{2}O_2 \xrightarrow{900°C} Fe_2O_3 + 2CO_{2(g)} \qquad (\Delta H_0 = -258.82kJ.mole^{-1}) \ldots\ldots\ldots (5)$$

Quartz has a minor effect on the heat obtained from coal, as it is thermally decomposed from the α-form to the β-form:

$$\alpha - SiO_2 \xrightarrow{900°C} \beta - SiO_2 \qquad (\Delta H_0 = +0.73kJ.mole^{-1}) \ldots\ldots\ldots\ldots\ldots\ldots\ldots\ldots (6)$$

The main carbonate containing minerals are known to be calcite and dolomite. These minerals act as heat sinks due to the endothermic decomposition of these groups as shown in Equations 7 and 8 respectively:

$$CaCO_3 \xrightarrow{900°C} CaO + CO_{2(g)} \qquad (\Delta H_0 = +179.75kJ.mole^{-1}) \ldots\ldots\ldots\ldots\ldots\ldots (7)$$

$$CaMg(CO_3)_2 \xrightarrow{900°C} CaO + MgO + 2CO_{2(g)} \qquad (\Delta H_0 = +307.78kJ.mole^{-1}) \ldots (8)$$

Therefore an increase in the minerals content of coal will be associated with a decrease in the heating value of the coal, especially at higher temperatures. This will in-turn result in the slowing the gasification reaction, as the heat obtained from the exothermic combustion reaction of coal drives the endothermic gasification reaction of carbon contained in the coal with carbon dioxide.

The ash fusion temperature is the temperature at which the mineral matter in the coal starts to melt. It is important for industrial dry-bottom gasifiers to operate below this temperature, because when the gasification temperature rises above this temperature, the ash will melt and agglomerate, which will in-turn cause unstable gasifier operation (Nowaki, 1981). When the minerals melt, it covers the external surface area of the particle. This in turn results in a decrease in char reactivity due to the decrease in the available surface area for the gasification reaction to take place, because the reactant gases cannot diffuse to the active carbon sites on the char particle. Waanders and Govender (2005) found that when looking at the mineral oxides contained in coal ash, that an increase in the $SiO_2/Al_2O_3$ ratio as well as the $Fe_2O_3$ concentration in the ash indicates a lower ash fusion temperature.

### 2.2.5 Plastic properties

When coal particles are heated, the coal undergoes physical as well as chemical alterations, which are accompanied with the splitting off of volatile matter and condensable vapours. The solid structure left behind consists of carbon and mineral constituents, and is known as the char (Tsai, 1982). During the heating process, some coals especially vitrinite and liptinite coals exhibit plastic behaviour. Properties which are associated with the softening behaviour of coal are (Hsu et al., 1977):

- Swelling of the coal sample.
- Pressing and gas permeability of the softened coal mass.

Both of these properties are dependant on the viscosity of the plastic coal mass formed during pyrolysis. The metaplast theory gives the best explanation for the caking behaviour of the coal. This theory describes three stages of plastic behaviour (Chermin and Van Krevelen, 1956):

- Depolymerisation.
- Cracking.
- Secondary degassing.

The depolymerisation stage includes the formation of an unstable, intermediate phase, also known as the metaplast phase. This is followed by the cracking stage, where tar evaporates and the non-aromatic groups are evolved; this is because the aliphatic compounds have a higher molecular mobility compared to the aromatic compounds (Lynch et al., 1988). Recondensation here leads to the formation of semi-coke, while the primary gas formed during this stage is responsible for the swelling behaviour of the coal. The gas formed during this cracking stage cannot escape fast enough from the plastic mass due to the low permeability of the said mass. Finally, the secondary degassing stage is responsible for the increase of the semi-coke density to form coke. During this stage hydrogen and methane are evolved at increased temperatures, leading to a decrease in the volume of the plastic mass (Chermin and Van Krevelen, 1956). It follows that the type of coal and the particle size determines the temperature at which the caking behaviour is observed, while the amount of volatiles determines the pore structure of the resulting char after pyrolysis.

The pore structure of the coal particle undergoes various changes during the heating of the coal sample. Existing pores may grow leading to an increase in the available surface area which facilitates the gasification reaction. New pores can also be formed, or previously inaccessible pores can be opened up. This behaviour also leads to an increase in the available surface area. There is also a possibility of pores coalescing, thus falling into each other, which will result in a decrease in the available surface area and in turn also retard the gasification reaction (Simon, 1983; Feng and Bhatia, 2003).

All of these changes in the porous char structure lead to the formation of a non-uniform pore structure which consists of (Liu et al., 2000a):

- Micro-pores (< 2 nm).
- Meso-pores (2 nm – 50 nm).
- Macro-pores (> 50 nm).

The macro-pores are responsible for the porosity of the char formed during pyrolysis, while the micro-pores account for the largest internal surface area, which in turn facilitates the gasification reaction (Laurendeau, 1978; Dutta et al., 1977). The porous structure of the char affects the char reactivity, as the available surface area and porosity determines the amount and rate at which the reactant gases can reach the active carbon sites. As the pyrolysis temperature increases, the surface area of the char increases up to a maximum, and then decreases with a further increase in temperature. This is because of pore expansion and development as the volatile gases are evolved (Liu, 1999). Also as the pyrolysis temperature increases past the optimum, and the duration of the charring process increases, the surface area and the porosity of the char decreases (Zong et al., 2007; Feng and Bhatia, 2003). This decrease is due to the micro-pores becoming blocked during the heat treatment process; and is associated with the recondensation of large molecules, consisting of unstructured functional groups, which tend to react at a higher rate compared to the structured carbon molecules when exposed to reactant gases. Diffusion of reactant gases occurs fast through the macro-pores and meso-pores, which means that the reactant gas concentration at the mouths of the micro-pores is the same as the reactant

gas concentration of the external gas atmosphere surrounding the char particle (Walker et al., 1977).

### 2.2.6 Density

Coal density can be used as an industrial indicator used as part of a coal assessment program prior to gasification, as density can be related to several coal properties including the maceral and minerals content. Gilfillan et al. (1999) found that higher density coals tend to form thick walled chars. It is also known that the inertinite maceral group has the highest density, followed by the vitrinite maceral group, and finally the liptinite maceral group with the lowest density. It can thus be said that inertinite-rich coals form dense, thick walled chars during pyrolysis. As the density of the chars increase, the reactivity decreases, as there is less available surface area for the gasification reaction to take place because of the thick walled chars. Liptinite-rich coals on the other hand are the least dense and form thin walled chars, which increases the available surface area where the gasification reaction takes place, and thus increases the reactivity of these chars (Gilfillan et al., 1999).

The aromatic nature of the coal also increases with increasing density (Dyrcacz et al., 1984). Inertinites have the highest density as well as the highest degree of aromacity. Vitrinites have less condensed aromatic CH rings, but more aliphatic $CH_2$ groups compared to the inertinite maceral group. Liptinites have the lowest density and also the largest concentration of aliphatic $CH_2$ groups (Gilfillan et al., 1999, Machnikowska et al., 2002). Thus it can be concluded that the reactivity as well as the aliphatic nature of coals decrease with increasing density. Oki et al. (2004) studied the mineral matter as a function of coal density and stated that in coal particles having a density in excess of 2.0 $g.cm^{-3}$ the mineral matter occur as liberated mineral particles; while in coal particles with a density of less than 2.0 $g.cm^{-3}$ the mineral matter is present as locked particles along with coal substance.

## 2.3. Pyrolysis behaviour of coal

The gasification of coal proceeds according to two steps, firstly the rapid pyrolysis step where the volatile matter is evolved, and then the slower gasification reaction

where the carbon is consumed. The pyrolysis behaviour of coal is mostly dependant on the organic properties of the coal. Pyrolysis plays an important role in the determination of the product distribution, as well as controlling the char reactivity and char structure resulting from this pre-gasification process (Solomon et al., 1990).

By maximizing the yield of volatile matter from pyrolysis, less char is produced, which in turn reduces the reliance on the relatively slow solid/gas reactions as less carbon needs to be converted into gas (Scaroni et al., 1981). The products from the devolatilisation step include (O'Brien et al., 1990):

- Hydrogen-rich volatile product.
- Carbon rich solid product.

The volatile product consists of a low molecular weight fraction which contains mostly carbon and methane oxides; as well as a high molecular weight fraction which contains compounds such as light oils and tars. The solid char product on the other hand consists of the fixed carbon as well as the incombustible mineral matter (O'Brien et al., 1990). The pyrolysis reaction is responsible for both a chemical as well as a physical change in the coal which will be described in this section as follows:

- Mechanism of pyrolysis.
- Gaseous pyrolysis products.
- Liquid pyrolysis products.
- Solid pyrolysis products.

### 2.3.1 Pyrolysis mechanism

The physical mechanism according to which the pyrolysis reaction takes place relates to the mechanism as described in Section 2.2.5. The rate of the devolatilisation is controlled primarily by bond breaking, cross-linking as well as mass transport of molecules within the coal particle. Firstly there is the depolymerisation step, which happens when the weaker bridges in the coal macromolecule are broken which results in a release of the smaller fragments which now make up the metaplast phase. After the depolymerisation step, there is a possibility that some of the metaplast molecules may repolymerise or cross-link. Those light molecules formed during the

depolymerisation step which did not cross-link, are then transported to the coal surface by convection or diffusion within the pores of non-softening coals and by liquid phase transport in softening coals. This metaplast formation, transport and cross-linking impacts on the tar yield, as the tar yield is increased with increasing temperature in the absence of cross-linking (Solomon et al., 1990). The factors which are influenced by the metaplast behaviour of coal are:

- Molecular weight distribution of products.
- Fluidity.
- Char structure.

As previously mentioned, vitrinite and liptinite rich coals tend to exhibit plastic behaviour during pyrolysis. The plastic behaviour depends on (Moulijn and Tromp, 1985):

- Experimental conditions.
- Heating rate.
- Particle size.

These thermoplastic properties become more significant as the heating rate increases up to a maximum, after which it is observed to a lesser degree. This is because the cross-linking temperature is reached too fast. Higher rank coals, with a carbon content of more than 80 % exhibit little plasticity, as they keep the original pore structure, and transport takes place via pore diffusion. Low rank coals experience cross-linking at lower temperatures due to carbon dioxide evolution at these temperatures, while in bituminous coals the cross-linking reaction takes place at higher temperatures, due to the evolution of methane at these temperatures (Solomon et al., 1990).

There are three processes which take place prior to the primary pyrolysis steps (Solomon et al., 1992):

- Hydrogen bond disruption.
- The transport of non-covalently bonded molecular phase.
- In coals containing less than 10 % oxygen, the low temperature cross-linking reaction coincides with the release of carbon dioxide and water vapour.

It is known that 80 % - 90 % of the volatile mass loss is due to the initial release of tars, aliphatics, carbon dioxide and water vapour; while the remaining mass loss is due to the later slow evolution of carbon monoxide and hydrogen (Solomon et al., 1992). The pyrolysis behaviour of coal is influenced by the structure of the coal as well as the experimental conditions such as:

- Temperature.
- Pressure.
- Gas residence time.
- Heating rate.

The rate at which the liquid pyrolysis product is evolved increases with an increased heating rate, as higher temperatures result in more volatiles being released (Arendt and Van Heek, 1981). The mass of volatile matter released has a linear relationship with the rank of the coal, and increases with decreasing rank. Thus more volatiles are released from coals containing less carbon (Xu and Tomita, 1987). The tar-forming propensity from coal decreases as the particle size increases, while the gas released from the same particle remains constant with an increase in particle size (Park et al., 1989). This is because of transport limitations within the coal particle, where the increased residence time of the metaplast molecules in the particle allows the secondary cross-linking reactions to take place. An increase in the pressure results in a decrease in the tar yield, because the tar-forming compounds cannot evaporate fast enough from the char surface (Suuberg et al., 1978).

### 2.3.2 Gaseous pyrolysis products

The gaseous product formed during pyrolysis consists of low molecular weight hydrocarbons such as $CO_2$, CO, $CH_4$, $C_2H_6$, $C_2H_4$, $C_2H_2$, $C_6H_6$ and water vapour (Solomon et al., 1992). As the rank of the coal increases, the oxygen content decreases, this result in a decrease in oxygen-containing gas yield such as CO2, CO and water vapour. On the other hand, the yield of $C_1$-$C_3$ gases increase with the increase in coal rank up to a maximum carbon concentration of 87 %. This behaviour is observed, because the gas evolved from low rank coals is determined by the oxygenated species, while the gas produced from high rank coals is determined by the hydrocarbons contained in the coal (Moulijn and Tromp, 1985). The decrease after 87

% carbon content is because these coals do not contain enough hydrogen for the evolution of $C_1$-$C_3$ hydrocarbons.

The different pyrolysis gases are released at different temperatures. Water vapour is evolved from 130 ºC; while no gas release is observed until approximately 242 ºC. The evolution of methane begins at 500 ºC, carbon monoxide is liberated at between 600 ºC and 800 ºC, and the release of hydrogen reaches a maximum rate at 750 ºC (Das, 2001). An increase in temperature results in an increase in the yield of carbon monoxide and hydrogen gases due to the decomposition of oxygen-containing functional groups such as the carboxyl and hydroxyl groups in the coal. Carbon dioxide is evolved at lower temperatures than carbon monoxide. This is because carbon dioxide is evolved from carboxyl groups, while the carbon monoxide is released from the decomposition of phenolic hydroxyl groups (Xu and Tomita, 1987).

### 2.3.3 Liquid pyrolysis product

The heavy tar product from pyrolysis consists of high molecular weight hydrocarbons. This is the main product from the pyrolysis of bituminous coals (Gönenç and Sunol, 1994). It is known that tars formed from highly aromatic coals are more stable when compared to those evolved from aliphatic coals (Freihaut et al., 1982). Tar is formed according to the following steps (Khan, 1989):

- Formation of tar fragments by means of the evaporation of the mobile phase as well as primary disruption reactions.
- The growth of tar fractions due to nucleation while being transported to the surface of the char.
- Transport of tar molecules to the char surface as well as the evaporation of these molecules from the char surface.
- Secondary reactions of the tar molecules with the gas or with the char while being transported to the char surface.

The yield of tars evolved during pyrolysis increases with an increase in temperature up to a maximum at approximately 727 ºC, after which a decreased tar yield is observed (Xu and Tomita, 1987). This is because the secondary cross-linking reaction takes place too fast at high temperatures. The tar yield is decreased as the pressure is

increased because high pressure conditions prevent the liquid tar products from evaporating from the char surface. This results in an increased residence time of the tar-forming compounds within the char particle, which allows the secondary reactions to take place (Arendt and Van Heek, 1981).

### 2.3.4 Solid pyrolysis product

The solid product from the pyrolysis process is referred to as the char. This char consists of the fixed carbon as well as incombustible mineral impurities. Pyrolysis impacts on the surface reactivity, pore structure, as well as the initial surface area of the resulting char (Yu et al., 2002).

As the pyrolysis temperature increases, the reactivity of the char decreases due to thermal annealing, this takes place because of the re-structuring of carbon molecules in the char matrix, as well as the blockage of micro-pores during the heat treatment process (Hurt and Gibbons, 1995; Feng and Bhatia, 2003). The reactivity of high rank bituminous coals increase with an increase in heating rate, while the reactivity of high rank lignite coals decrease with an increased heating rate. Low rank coals are not greatly influenced by the heating rate and exhibit little or no change in reactivity.

The char structure resulting from the pyrolysis procedure is greatly affected by the pyrolysis conditions, and also depends on several other factors such as:

- Parent coal rank.
- Initial structure of the coal.
- Caking properties of the coal.

The pyrolysis conditions which have the greatest impact on the char formation are (Yu et al., 2002):

- Temperature.
- Heating rate.
- Pressure and nature of pyrolysis gases.

As the pyrolysis temperature is increased, there is a decrease in the micro-porosity of the char (Baily et al., 1990; Cai et al., 1996; Feng and Bhatia, 2003). High

temperature favours the formation of large central pores, as well as a decrease in the formation of high density, thick walled chars. As the heating rate is increased, there is an increase in the amount of micro-pores and meso-pores in the char, which provides an extended initial surface area, which in turn facilitates the gasification reaction, thus increasing the reactivity (Griffin et al., 1994).

## 2.4. Reaction conditions

It is known that in industrial gasification reactors that the reactor operating conditions such as gas composition, temperature and pressure all influence the optimal operation of these reactors and the product quality from these reactors. By understanding the influence of these parameters on the gasification reaction, the behaviour of coal in such processes may be described in a more accurate way.

### 2.4.1 Diffusion effects

When considering any solid-gas reaction, it is important to keep in mind that the reaction will be influenced by diffusion in one of two ways:

- Boundary layer diffusion, also known as inter-particle diffusion.
- Internal pore diffusion, also known as intra-particle diffusion.

This gas-solid reaction can be simplified and presented as seven steps (Levenspiel, 1972):

- Transport of gaseous reactants from the bulk gas stream to the particle surface.
- Transport of the reactant gas molecules into the pores of the particle.
- Adsorption of these reactant molecules onto the reaction sites.
- Surface chemical reaction.
- Desorption of the product gases.
- Transport of product gas to the particle surface via pore diffusion.
- Transport of product gas from particle surface back to the bulk gas stream.

This model is applicable to gasification reactions, although the total process may be changed as to fit a specific reaction mechanism (Levenspiel, 1972). The diffusion steps which are responsible for the transport of reactant gases into the particle, or

product gases out of the particle, depends on the concentration gradient, as well as on the molecular velocity of the gas stream near the particle surface which facilitates the gasification reaction.

The chemical reaction step on the other hand depends on the external and pore interactions with the reactant gas (Hashimoto et al., 1986). The gas-solid interactions in turn depend on the number of impurities which are present on the particle surface, also referred to as active sites (Tsai, 1982; Essenhigh, 1981).

The properties of coals can be linked to the diffusion resistance of the reaction, as it is known that the diffusion resistance increases as the reaction rate increases. The diffusion resistance also increases with an increase in the particle size as well as with a decrease in pore size.

### 2.4.2 Temperature

It has been observed that higher temperatures result in increased reaction rates as well as lower activation energies. This shows that there must be a transition in the controlling mechanism of the gas-solid reactions, i.e. from a chemical reaction controlled mechanism at low temperatures, to a diffusion controlled mechanism at higher temperatures (Essenhigh, 1981; Johnson, 1979; Zong et al., 2007). Wicke (1955) proposed that the combustion reaction of a porous solid such as coal may be divided into three distinct temperature regions, known as the three-zone concept.

Reaction zone 1. This zone is represented by low temperatures (ambient – 500 ºC). Here the reaction rate is sufficiently low enough to allow the reactant gases to diffuse uniformly throughout the particle at a higher rate than they can be consumed by the reaction with the solid particle surface. This is also known as the chemical reaction limiting step (Walker et al., 1959; Zong et al., 2007).

Reaction zone 2. This zone is represented by moderately higher temperatures (500 ºC – 800 ºC) compared to the reaction zone 1 temperatures. Here the reactant gases which diffuse into the porous particle are consumed in a distinctive reaction zone, which does not extend to the core of the particle, thus leaving an unreacted core. The

reaction in this zone is limited by pore diffusion, but not controlled, as the controlling mechanism is rather reaction-diffusion controlled (Walker et al., 1959; Zong et al., 2007).

Reaction zone 3. This zone is represented by very high temperatures, exceeding 800 ºC. Here the reaction takes place at such a rapid rate that there is little or no penetration of the reactant gases into the char matrix. This means that the reaction is limited to the external particle surface and is therefore controlled by external diffusion. This is also known as the film diffusion limiting zone (Walker et al., 1959; Zong et al., 2007).

More recently Kajitani et al. (2002) demonstrated this transition of controlling mechanism for a char gasification system using both steam and $CO_2$. In this study it was observed that the reaction zone one (chemical reaction limited) conditions are applicable up to temperatures of 1300 ºC for $CO_2$ gasification reactions. At temperatures exceeding 1300 ºC, the rate of reaction will become more affected by pore diffusion of the reactant gas into the micro-pores (reaction zone 2). Hodge et al. (2010) made similar observations for a $CO_2$ gasification system, and found that the rate controlling mechanism changes from intrinsic kinetics controlled to pore diffusion with intrinsic kinetic control at temperatures exceeding 1200 ºC. It was also observed that the type of chars formed during pyrolysis impacts on the transition temperature where pore diffusion starts to play a significant role in the rate controlling mechanism.

### 2.4.3 Reactant gas partial pressure

The partial pressure of reactant gases in the gasification reaction influences the reaction differently at different temperatures. At sufficiently low temperatures, an increase in the partial pressure of carbon dioxide will result in an increased reaction rate. This is because the reactant gas is allowed to diffuse uniformly throughout the porous char particle before being consumed in the reaction. At higher temperatures, the carbon dioxide partial pressure has a lesser impact on the gasification rate. This is because the reactant gas is consumed in the reaction zone on the particle surface before it has time to diffuse into the char particle; thus a limited surface area is

available for the reaction to take place (Kajitani et al., 2006). Roberts and Harris (2000) observed that the reaction order with respect to $CO_2$ partial pressure does not stay constant over a pressure range (atmospheric pressure up to 15 bar). This change in reaction order is assumed to be related to the rate of the reaction. In addition to the reaction order changing, it was seen that the activation energy values stay approximately constant over the pressure range. Therefore it was concluded that this slight increase of the reaction rate with increasing pressure can be related to a physical, rather than a chemical transition in the gasification mechanism.

This increase can also be ascribed to the degree of surface utilization. This is because increasing the pressure of the gasification system will lead to a greater concentration of adsorbed surface complexes up to a pressure where the surface will be saturated with complexes and a further increase in pressure will not lead to the formation of new surface complexes (Roberts and Harris, 2000).

### 2.4.4 Pressure

The total pressure at which the gasification reaction takes place does not have a large impact on the gasification reaction rate. Kajitani and Matsuda (2002) found that by increasing the total pressure of the system from 0.2 MPa to 2.0 MPa resulted in a 20 % increase in the reaction rate. Megaritis et al. (1999) also observed that the gasification reaction rate increased slightly with an increase in the total pressure of the system. These results do not warrant the inclusion of a total pressure variable into the reaction rate equation.

## 2.5 Gasification

This section will discuss coal gasification under three main headings, including the gasification reactions taking place (Section 2.5.1), the gasification reaction kinetics (Section 2.5.2), as well as proposed gasification models (Section 2.5.3) which may be used as to predict the gasification behaviour of coal particles under various reaction conditions.

### 2.5.1 Reactions

The gasification of coal is a process applied globally in a number of different reactors under different reaction conditions (Simbeck et al., 1993). The main reactor types that are used in the industry are:

- Moving bed gasifier.
- Fluidized bed gasifier.
- Entrained flow gasifier.

When coal enters a gasification reactor, there are essentially two processes taking place:

- Pyrolysis.

  $$Coal + Heat \rightarrow Char + Liquid + Gas \quad \text{.....(9)}$$

- Gasification.

  $$Char + Gasifying\ agent + Heat \rightarrow Gas + Ash \quad \text{.....(10)}$$

Initially the coal is dried as it enters the gasifier. As the temperature in the reactor exceeds 400 ºC, it follows that the pyrolysis reactions start taking place. These pyrolysis reactions involve the evolution of volatile gas species from the coal, leaving behind the fixed carbon, as well as the incombustible minerals, commonly known as the char. When the temperature increases to above 700 ºC, the gasification reactions commence. These gasification reactions include the reaction of the carbon with steam, hydrogen and carbon dioxide.

The reaction of carbon with steam is known as the water-gas reaction. This gasification reaction is endothermic and is inhibited by the formation of product gases (Shilling et al., 1981). The reaction scheme for the water-gas reaction is shown below.

$$C + H_2O \rightarrow CO + H_2 \qquad (\Delta H_0 = +118.9\, kJ.mole^{-1}) \quad \text{.....(11)}$$

The reaction of carbon with hydrogen also takes place in industrial reactors. This reaction is commonly known as the hydro-gasification reaction. This reaction is very slow at high pressures. The reaction scheme for this gasification reaction is shown below (Shilling et al., 1981).

$$C + 2H_2 \rightarrow CH_4 \qquad (\Delta H_0 = -87.4\,kJ.mole^{-1}) \quad \text{.....(12)}$$

The two reactions mentioned above, as well as the gasification reaction with carbon dioxide (as described later), are the only three actual gasification reactions taking place, but the consumption of carbon in industrial reactors also includes the combustion reaction, as well as two gas-phase reactions as described in the following paragraphs.

The reaction of carbon with oxygen is known as the combustion reaction. Depending on the amount of oxygen present during the reaction, the char can be completely combusted in an excess oxygen environment, or partially combusted when the oxygen environment is limited (Shilling et al., 1981). The reaction schemes for the combustion reactions are shown below.

$$C + \frac{1}{2}O_2 \rightarrow CO \qquad (\Delta H_0 = -123\,kJ.mole^{-1}) \quad \text{..... .... (13)}$$

$$C + O_2 \rightarrow CO_2 \qquad (\Delta H_0 = -405.9\,kJ.mole^{-1}) \quad \text{.....(14)}$$

The first of the two gas-phase reactions is the reaction of carbon monoxide with water. This reaction is commonly known as the water-gas shift reaction and influences the CO:$H_2$ ratio in the product gas; which is very important in the production of synthesis gases (Shilling et al., 1981). This reaction proceeds according to the following reaction scheme.

$$CO + H_2O \rightarrow H_2 + CO_2 \qquad (\Delta H_0 = -40.9\,kJ.mole^{-1}) \quad \text{.....(15)}$$

The other gas-phase reaction is the reaction of carbon monoxide with hydrogen. This reaction is commonly known as the methanation reaction. This reaction has an impact on the calorific value of the product gas from the gasifier (Shilling et al., 1981). The methanation reaction proceeds according to the following reaction scheme.

$$CO + 3H_2 \rightarrow CH_4 + H_2O \qquad (\Delta H_0 = -206.3\,kJ.mole^{-1}) \quad \text{.....(16)}$$

The most relevant gasification reaction for this study is the reaction of carbon with carbon dioxide. This reaction is known as the Boudouard reaction. The reaction proceeds according to the following reaction scheme (Shilling et al., 1981).

$$C + CO_2 \rightarrow 2CO \qquad (\Delta H_0 = +159.7\, kJ.mole^{-1}) \quad \text{.....(17)}$$

This reaction is endothermic and is known to be inhibited by product gas formation. The gasification reaction is very slow in the absence of a catalyst at relatively low temperatures (< 1000 ºC). A more specific reaction scheme is proposed by Ergun (1962). This scheme takes into account the interaction of the reactant gas with the active carbon sites and is presented below.

$$C(\,) + CO_2 \leftrightarrow C(O) + CO \quad \text{.....(18)}$$

$$C(O) \rightarrow CO + C(\,) \quad \text{.....(19)}$$

$$C(\,) + CO \leftrightarrow C(CO) \quad \text{.....(20)}$$

Here the first step in the gasification with carbon dioxide is the dissociation of the carbon dioxide at the active carbon site. This dissociation releases a molecule of carbon monoxide, and also forms the oxidized surface complex at the active carbon site. The second reaction step is the actual gasification step in which the carbon-oxygen complex produces one molecule of carbon monoxide as well as another active carbon site. The rate limiting step in this scheme is step two, which is the desorption of the carbon-oxygen surface complex. It can also be seen that the formation of product gases, especially carbon monoxide will inhibit the gasification of carbon with carbon dioxide as shown in Equation 18 in the abovementioned reaction scheme.

When looking at the rate at which the gasification and combustion reactions take place, the reactions can be ranked from fastest to slowest as follows (Everson et al., 2006):

- Combustion with oxygen.
- Steam gasification.
- Carbon dioxide gasification.
- Hydrogen gasification.

### 2.5.2 Reaction kinetics

This section describes the kinetic rate equation, as it will be required to determine the intrinsic reaction kinetics of the char gasification reaction. Also discussed in this section, is the Arrhenius equation parameters, including the activation energy, as well as the pre-exponential factor which are related to the reaction rate constant.

**Kinetic rate equation**

In order to develop an expression which is able to relate the physical changes occurring during gasification reaction to the reaction conditions, it is necessary to take into account the two main process parameters: temperature and carbon dioxide partial pressure. The kinetic rate equation which describes the reaction of the char as a function of these two parameters, as well as the physical behaviour of the char can be presented as follows:

$$\frac{dX}{dt} = g(T).h(P_{CO2}).f(X) \quad \text{..... (21)}$$

Here g(T) represents the function which describes the influence of temperature on the reaction kinetics, $h(P_{CO2})$ refers to the function which describes the influence of carbon dioxide partial pressure on the reaction kinetics, and f(X) is a function describing the physical behaviour of the char during gasification. By now assuming a power-law dependence applicable to the first two functions in the rate equation, it follows that Equation 21 can be described as

$$\frac{dX}{dt} = k''.(P_{CO2})^n.f(X) \quad \text{..... (22)}$$

**Arrhenius equation parameters.**

From Equation 22 above, the reaction rate constant (k''); which depends mainly on the gasification temperature and the coal specific activation energy, may be described by the Arrhenius equation as follows:

$$k'' = A.\exp(\frac{-E_{act}}{RT}) \quad \text{..... (23)}$$

By then substituting this representation of the reaction rate constant into the kinetic rate equation (22) it follows that:

$$\frac{dX}{dt} = A.\exp(\frac{-E_{act}}{RT}).(P_{CO2})^{n}.f(X) \quad \text{..... (24)}$$

### 2.5.3 Gasification models

There exist a number of models which were developed to describe the kinetics, surface area, and the development of the pore structure of coal particles during gasification.

The physical behaviour of the char particle plays an important role in determining which model is applicable to the gasification of that specific char particle. The model will be a function of the physical behaviour of the char particle subject to the specific reaction conditions. This is mainly because the char particle undergoes changes as it reacts with the gas. These changes include the development of the char pore structure, thermal cracking of the particle, and the formation of an ash layer on the particle as the conversion of carbon proceeds. The ash formed during the reaction may be a flaking ash product, which does not inhibit the penetration of the reactant gas mixture to the active carbon sites, or a non-flaking ash product where the particle does not change in shape or size (Johnson, 1979; Bhatia and Perlmutter, 1980). Three of the most common models used in the prediction of the gasification and combustion behaviour of coal are:

- Shrinking core models.
- Percolation models.
- Capillary models.

**Shrinking core model**

The shrinking core models can be divided into two main sub-models known as the shrinking reacted core model and the shrinking unreacted core model (Levenspiel, 1972).

**Shrinking reacted core model**

Here it is assumed that the char particle consists of a heterogeneous mixture of carbon and incombustible minerals. It is also assumed that the char particle is porous, as to allow the reactant gases to diffuse uniformly throughout the char particle before being consumed by the gasification reactions. Due to this uniform diffusion of the reactant gases, it follows that the reaction takes place throughout the char particle, and that the carbon reacting on the inside of the char particle will result in further structural changes in the particle, thus influencing the diffusion coefficient applicable to the reaction conditions. As the conversion of carbon proceeds, the active carbon sites decrease and an ash layer is formed, mainly because the carbon on the surface reacts faster than that in the inner core of the particle. This ash layer is assumed to have a negligible resistance, thus not affecting the diffusion of reactant gases to the active carbon sites.

**Shrinking unreacted core model**

Here it is assumed that the char is non-porous, and that the reactant gas cannot penetrate into the core of the char particle, hence the name unreacted core model. Due to this assumption, the gasification reaction takes place at the outer surface of the char particle. As the reaction proceeds, the carbon is consumed in a reaction zone on the particle outer surface forming an ash layer. This ash layer is assumed to be porous and to allow the reactant gases to diffuse into the receding reaction zone. This model has three possible rate controlling mechanisms:

- Diffusion of the reactant gas through the boundary layer.
- Diffusion of the reactant gas through the ash layer.
- Reaction of the reactant gas at the ash-carbon interface.

**Percolation models**

The percolation models better compensate for the changes in connectivity of the pores and the development of the porous structure compared to the shrinking core models. The following changes in connectivity are considered:

- Opening of initially closed pores.
- Disintegration of the char particle (loss of connectivity).
- Pore closure, due to the blockage of connecting pores.

These models are similar to the reaction diffusion models (Bhatia and Gupta, 1992). The percolation models are known to predict the initial part of the gasification reactions more accurately compared to other models, due to the opening of initially closed pores during the reaction (Lu and Do, 1992).

**Capillary models**

Capillary models assume the char particle to consist of randomly intersecting cylindrical pores of uniform size (Peterson, 1957). This assumption is then used to calculate the surface area as well as the porosity of the char particle. The capillary models have limited applicability due to this assumption of uniform pore size. This is because char particles commonly contain wide pore size distributions, consisting of micro-pores, meso-pores and macro-pores. Due to this limitation, Bhatia and Perlmutter (1980) developed an adapted model known as the Random Pore Model, which is based on the random nucleation of crystals.

The main assumption of the Random Pore Model is that the volume of the char particle is enclosed by continuously developing pore structures which are randomly distributed throughout the char particle. This model compensates for the development of the pore structure, including the growth and collapse of pores in the particle during the solid-gas reaction. The initial structure of the char particle is described by a single parameter, known as the structural parameter ($\psi$), which is an important variable in the Random Pore Model (Bhatia and Perlmutter, 1981). The char properties incorporated into the structural parameter include:

- Pore volume.
- Pore surface area.
- Pore length.

The equation describing the surface area of the char particle as given by the Random Pore Model is given by:

$$f(X) = \frac{S_0.(1-X).\sqrt{1-\Psi \ln(1-X)}}{(1-\varepsilon_0)} \quad \text{..... (25)}$$

This equation reaches a maximum value for a structural parameter value above 2 and a char conversion of less than 40 %. It is also possible to further develop this model as to include the mineral content of the char (Lu and Do, 1992).

**Random Pore Model**

The basic rate equation for the Random Pore Model can be given as (Bhatia and Perlmutter, 1980):

$$\frac{dX}{dt} = r_0\sqrt{1-\Psi\ln(1-X)}.(1-X) \quad \text{..... (26)}$$

This equation describes the reaction rate as a function of conversion, assuming a uniform gas composition throughout the char particle, thus eliminating the effect of the diffusion of reactant gases into the particle. The dimensionless structural parameter (ψ) which is characteristic of the Random Pore Model, describes the initial char structure.

When considering a chemical reaction controlled, or pore diffusion controlled reaction mechanism, with a varying reactant gas concentration profile along the radius of the char particle, this equation is then applicable at a certain point along the radius of the particle, and the Thiele Modulus will then be required to compensate for the effect of diffusion on the reaction.

For the evaluation of the overall reaction rate model applicable to Regime 1 (Chemical Reaction Controlled) kinetics, considering the intrinsic kinetics, structural properties of the char, as well as the reaction conditions, the following equations are applicable:

$$\frac{dX}{dt} = \frac{r_s.(1-X).S_0.\sqrt{1-\Psi\ln(1-X)}}{(1-\varepsilon_0)} \quad \text{..... (27)}$$

Here ψ is a parameter obtained by data regression, which accounts for possible structural variations within the coal char particle and is given by:

$$\Psi = \frac{4\pi L_0 (1-\varepsilon_0)}{S_0{}^2} \quad \text{.....(28)}$$

And by defining the dimensionless time ($\tau$) as:

$$\tau = \frac{r_s S_0 t}{(1-\varepsilon_0)} \quad \text{.....(29)}$$

Then by writing Equation 27 in terms of the dimensionless time parameter:

$$\frac{dX}{d\tau} = (1-X).\sqrt{1-\Psi \ln(1-X)} \quad \text{.....(30)}$$

The conversion can then be presented as a function of the dimensionless time:

$$X = 1-\exp(-\tau.(1+\frac{\Psi\tau}{4})) \quad \text{.....(31)}$$

And the time factor ($t_f$) is defined by:

$$t_f = \frac{r_s S_0}{(1-\varepsilon_0)} \quad \text{.....(32)}$$

The conversion can now be described as a function of time and the time factor:

$$X = 1-\exp(-t_f t(1+\frac{\Psi t_f t}{4})) \quad \text{.....(33)}$$

When considering the experimental results, a reduced time ($t/t_x$) is used, with x referring to the conversion considered, usually 50 % or 90 %, as shown in Equation 34. This is done to normalize the experimental data and to obtain reliable results, because as the conversion of the char nears unity, the experimental results display asymptotic behaviour.

$$\frac{t}{t_{90}} = \frac{\sqrt{1-\Psi \ln(1-X)}-1}{\sqrt{1-\Psi \ln(1-0.9)}-1} \quad \text{.....(34)}$$

**Validation Procedure**

The validation procedure for this model requires the structural parameter as well as the time factor as input variables. The structural parameter may be obtained by means of gas adsorption or mercury intrusion measurements as well as from image analysis, which describes the structure of the char particle prior to the reaction (Bhatia and Perlmutter, 1980, Feng and Bhatia, 2003). This method is not favoured, as it does not provide sufficiently accurate results, due to the assumptions and approximations used to describe the non-uniformity of the pore sizes. Instead a method is proposed, which makes use of the regression of experimental data to obtain the structural parameter. The structural parameter is obtained by regressing the normalized time plot with regard to the time required to achieve 90 % conversion for the carbon dioxide gasification, as this reaction is chemical reaction controlled.

The main reason why the calculated and fitted structural parameters do not correspond is because there are a large number of micro-pores that have become blocked during pyrolysis due to recondensation of volatile matter. These pores will rapidly open up as the gasification reaction commences, and by experimentally estimating the structural parameter at the point where the carbon conversion is approximately 15 %, it will result in a more accurate estimation of the structural parameter (Feng and Bhatia, 2003).

The real time conversion as described by Equation 33 can be developed by first defining the reaction rate equation:

$$r_{s0} = k_{s0} \exp(\frac{-E_{act}}{RT}).{P_{CO2}}^{n} \quad \text{.....(35)}$$

Now by plugging this equation for the reaction rate into Equation 32, the time factor can be described as:

$$t_f = \frac{k_{s0} \exp(\frac{-E_{act}}{RT}) P_{CO2}{}^{n} S_0}{(1-\varepsilon_0)} \quad \text{.....(36)}$$

And by defining the lumped pre-exponential factor as:

$$k_{s0}' = \frac{k_{s0} S_0}{(1-\varepsilon_0)} \quad \text{.....(37)}$$

It follows that the equation presenting the time factor (36) can be simplified to:

$$t_f = k_{s0}' \exp(\frac{-E_{act}}{RT}) P_{CO2}{}^{n} \quad \text{.....(38)}$$

And by linearising this equation it follows that:

$$\ln t_f = \ln k_{s0}' + n \ln P_{CO2} + (\frac{-E_{act}}{R})(\frac{1}{T}) \quad \text{.....(39)}$$

This equation can then be used to calculate the kinetic parameters applicable to the gasification of the specific char. By plotting $\ln(t_f)$ as a function of $\ln(P_{CO2})$ at a constant temperature, the carbon dioxide dependence may be determined from the slope. By then plotting $\ln(t_f)$ against (1/T) at a constant carbon dioxide composition, the activation energy may be calculated from the slope, and the lumped pre-exponential factor from the intercept.

## 2.6 Studies on density separated coals

In the past, much work has been done on the gasification and combustion of coal (Richard et al., 1993; Hurt and Gibbins, 1995; Chen and Kojima, 1996; Joutsenoja et al., 1999; Alonso et al., 2001; Homma et al., 2005). The influence of the minerals on coal gasification has also been the topic of many research papers (Liu et al., 2003; Kosminski et al., 2006; Matsuoka et al., 2008; Wagner et al., 2008). In contrast, the

influence of particle density on gasification of South African coals has not been studied in detail as of yet.

Gilfillan et al. (1999) conducted a study on the structure and reactivity of density separated coal fractions. This study involved six coals, with the particles studied in the size range of (38 µm – 20 µm) which were separated into narrow density fractions of approximately 0.02 $g.cm^{-3}$ by means of heavy liquid sink-float experiments. The manual maceral analysis of each fraction was done as well as a new image analysis technique known as the Reactivity Assessment Program. The main focus of the study was to evaluate the reaction of the char fractions in a drop-tube furnace with temperatures ranging up to 1300 ºC in a gas atmosphere containing 1 % oxygen. The main finding of this study was that high density, unreacted material produced thick walled chars that undergo minimal transformation during pyrolysis.

Strezof et al. (2005) studied the effect of pressure on the swelling of density separated coal particles. The different density fractions were obtained by means of heavy liquid sink-float experiments in order to obtain homogenous particle properties. The pressure range used in this study was between 0.1 MPa – 5.0 MPa. The main finding from this study was that increased pressure increased the time with which the coal remained fluidized, and that the degree of swelling decreased with increasing density.

Kawashima et al. (2000) conducted a study on the structural changes of density separated coal fractions during pyrolysis. Different density fractions from four different coals were studied by means of $^{13}C$ ssNMR solid state spectra in order to determine what structural changes have taken place in the maceral groups during pyrolysis. The different density fractions were produced by means of heavy liquid sink-float experiments. Pyrolysis experiments were conducted in the temperature range of 573 K – 973 K, and a heating rate of 3 $K.min^{-1}$ was used. The main finding from this study was that the content of aliphatic groups in each maceral group determines the reactivity of that coal, and that the aliphatic content decreases with increasing density.

Wagner et al. (2008) stated that based on the mode of operation of a fixed bed gasifier as well as the quality of the feedstock, which was a blend of South African low grade

Highveld coals in this case, that varying amounts of discrete carbon particles can be identified in course gasification ash from these gasifiers. In an attempt to understand the reason for this carbon in ash observation, the ash was sampled from a gasifier shutdown and then screened as to obtain the following size fractions:

- 26 mm – 13 mm.
- 13 mm – 4 mm.
- < 4 mm.

From these ash samples the following unconverted carbon groups were identified:

- Unburned carbon.
- Carbonaceous scale.
- Shrinking core particles (carbon enclosed in a hardened ash layer).

From this study, it was concluded that the unconverted carbon can be ascribed to the following factors:

- Cooler channels formed in the gasifier.
- Top size coal particles are not allowed sufficient residence time in the reactor for complete conversion.
- Potential energy of the exothermic reaction in the ash-zone is lower than the cooling effect of the gasifying agent which enters at 340 ºC.

Mèndez et al. (2003) performed a study regarding the influence of the petrographic and mineral matter composition of coal particles on their combustion reactivity. Five different coals were used in this study. These coals were separated into density fractions by means of sink-float experiments. The different density fractions were analyzed in terms of mineral matter and the petrographic composition. Then 12 mg from each of the density fractions was used for thermo gravimetric analysis. The main finding from this study was that there is no clear trend explaining the catalytic effect of minerals on the combustion reaction. Although it was found that the amount and thickness of the clays present in the coal plays an important role in the reactivity of the coal, as the diffusion of reaction gas between the macerals and minerals promotes the reactivity of the coal. The inertinite macerals decrease the reactivity of the coal to a lesser degree compared to the enhancing effect of the minerals up to a density of 1.6

$g.cm^{-3}$ – 1.8 $g.cm^{-3}$, after which the reactivity decreases because of the effect of the low reaction rate of the inertinite macerals segregated into these density fractions being greater than the enhancing effect of the minerals.

## 2.7 Conclusion

From the above it is clear that many researchers have studied the gasification reaction of coal either from a mineral matter perspective or from the basis of gasification reactivity on coal rank. Research has also been conducted based on the petrographic composition of the coal, however inconsistent conclusions are evident which is probably due to the relatively low purity of the macerals tested and the fact that the interactions between the different macerals could not be quantified. Moreover, most previous work did not consider the catalytic effect of the minerals in the maceral chars. Considering the drawbacks in maceral gasification to date, the relatively recent research area of high-ash inertinite-rich gasification of South African coal on the basis of particle density was examined.

# Chapter 3: Sample Preparation

This chapter will describe the origin of the seven coal samples as well as the handling and preparation of these coals for experimental work. The preparation procedures that will be described include:

- Mechanical size reduction by means of crushing and milling.
- Obtaining a specific size range by means of screening.
- Obtaining specific density cuts by means of heavy liquid density separation.

## 3.1 Origin of the coals

The coals used in this study all originate from the Highveld coal field. This coal field is utilized as a coal source for power generation at the Matla and Kriel power stations, and by the synthetic petroleum giant, Sasol. Sasol has six collieries which provide the feed to the gasifiers at the Sasol II and III chemical workup facilities where the coal is used in the coal to liquids (CTL) process to produce liquid fuels as well as other chemicals (Barker, 1999).

The Highveld coal field consists of five coal seams, which are numbered from the bottom upwards. The number one seam lies at the bottom of the field, followed by the number two seam. Then the number three seam is observed as an intermittently developed, very thin coal seam. The number four coal seam is divided into an upper and lower seam. The number five seam is sufficiently developed throughout the entire coal field. The coal samples used in this study were mined from the number four coal seam, except for coal F which was taken from the number three coal seam (Barker, 1999).

## 3.2 Preparation procedures

This section will describe the preparation of the seven coals as required for various experimental analyses. This will include the mechanical size reduction, obtaining a specific particle size range and obtaining specific density fractions. After preparation all of the coal samples were stored under vacuum conditions.

### 3.2.1 Mechanical size reduction

Initially all seven coals were received as (9.5 mm - 6.70 mm) particles in large sealed containers. The first step in the size reduction process was to reduce the particle size to between 1.7 mm and 1 mm. This was done by using an adjustable jaw crusher in conjunction with 1.7 mm and 1 mm screens. In order to gradually reduce the particle size, the jaw crusher was set to its maximum jaw opening, and 250 g of coal was passed through. The crushed sample was screened; then the jaw opening was decreased slightly and the top-size coal particles from the 1.7 mm screen were passed through again. This process was repeated until the entire 250 g sample passes through the 1.7 mm screen. A total of 2 kg of each of the seven coal sources was crushed and screened to the -1.7 mm +1 mm size range. The sub-samples required for the various characterization experiments were taken from this "master sample" and the particle diameter was further reduced and screened as required for the respective analyses (Section 3.2.2).

To further reduce the particle size, a Fritch P-14 rotor mill was used. The speed setting used was 6000 rpm with either the 1 mm or the 200 µm screen. The sample mass used was batches of 30 g of coal.

### 3.2.2 Obtaining a specific size range for characterization purposes

After the mechanical size reduction, the particle size of the resultant coal varies, and in order to obtain a specific size range these coals were screened. This is specifically required to prepare the coals according to specifications shown in Table 3.1 for each analysis.

Table 3. 1: Size requirements for coal analyses.

| Analysis | Size requirement (µm) | Screens used (µm) |
|---|---|---|
| TGA | $1000<d_p<1140$ | 1700; 1140; 1000 |
| MIP | $1000<d_p<1140$ | 1700; 1140; 1000 |
| Gas adsorption | $212<d_p<250$ | 1000; 250; 212 |
| SEM | $125<d_p<150$ | 212; 150; 125 |
| Petrographic | $40<d_p<1000$ | 1000; 250; 120; 40 |

TGA: Thermogravimetric analysis, MIP: Mercury intrusion porosimetry, SEM: Scanning electron microscope.

The sample for the pyrolysis test-rig experiments was also crushed and screened to achieve a specific particle size distribution (PSD) as described in Table 3.2.

Table 3. 2: Standard PSD for pyrolysis experiments.

| Size range (mm) | Mass (g) |
|---|---|
| -19.0 +13.2 | 350 |
| -13.2 +9.5 | 320 |
| -9.5 +6.7 | 290 |
| -6.7 +4.75 | 150 |
| -4.75 +3.35 | 70 |
| -3.35 +2.36 | 20 |
| **Total** | 1200 |

### 3.2.3 Density separation

The setup used for the density separation of the two coal sources (coals B and G) consisted of the following:

- 4 x 500ml glass beakers filled with the dense organic liquid mixtures.
- 4 x 500ml empty glass beakers.
- 8 x wire mesh strainers.
- Wash bottle filled with distilled water.

The densities of the organic liquid mixtures were varied from 1.4 g.cm$^{-3}$ to 2 g.cm$^{-3}$ in increments of 0.2 g.cm$^{-3}$. The required volume of each of the constituting organic liquids was calculated according to the following equation (ISO 7936, 1992):

$$V_m = V_t \frac{\rho_t - \rho_m}{\rho_m - \rho_p} \quad \text{.....(40)}$$

The density of each of the separation solutions was checked with a hydrometer before the experiments were commenced. Table 3.3 illustrates the relative volume of organic liquids used in the make-up of the separation solutions. The dense liquids were chosen, as it has been proven previously (Gilfillan et al., 1999; Kawashima et al., 2000; Wagner et al., 2003; Strezof et al., 2005; Mèndez et al., 2008) that these liquids provide adequate separation on the basis of particle density on laboratory scale.

Table 3. 3: Volume of organic liquids used in density separation.

| Density ($g.cm^{-3}$) | Volume toluene (ml) | Volume TBE (ml) | Volume total (ml) |
|---|---|---|---|
| 1.4 | 298.56 | 101.44 | 400 |
| 1.6 | 260.29 | 139.71 | 400 |
| 1.8 | 222.00 | 178.00 | 400 |
| 2.0 | 183.73 | 216.27 | 400 |

TBE: Tetrabromoethane

The particle size of the coal used in the density separation experiments varied from 1 mm to 1.7 mm. Firstly a batch of 25 g of coal particles is added to the first beaker containing the heaviest (SG: 2.0 $g.cm^{-3}$) organic solution; this is then stirred for 30 seconds and allowed to settle for 5 minutes. Then the beaker is tilted to allow the floating coal particles to be decanted into the first wire mesh strainer, while the organic liquid passes through the wire mesh strainer into an empty glass beaker. After the float fraction has been removed, the sink fraction is then scooped from the bottom of the glass beaker into another wire mesh strainer. These particles in the sink fraction are then washed with distilled water and placed in a vacuum furnace at 60 ºC for two hours to dry. The wire mesh strainer containing the float fraction is placed on a piece of laboratory paper to drain the organic liquid left on the coal. The float fraction is then passed onto the second beaker containing the less-dense (SG: 1.8 $g.cm^{-3}$) organic solution. Here the same procedure is applied, again the sink fraction is removed, washed and dried; while the float fraction is drained and passed onto the next, lower density liquid (SG: 1.6 $g.cm^{-3}$) and so on. This procedure yielded five density fractions; each of which was weighed and the yield is presented in Table 3.4 for both of the coal samples used.

Table 3. 4: Yield of coal obtained for each density fraction.

| Density range ($g.cm^{-3}$) | Coal B | Yield of coal (wt %) | Coal G | Yield of coal (wt %) |
|---|---|---|---|---|
| -1.40 | B1 | 17.4 | G1 | 32.1 |
| 1.40 – 1.60 | B2 | 41.0 | G2 | 37.1 |
| 1.60 – 1.80 | B3 | 17.9 | G3 | 13.6 |
| 1.80 – 2.00 | B4 | 8.1 | G4 | 7.0 |
| +2.00 | B5 | 15.6 | G5 | 10.2 |
| **Total** | | 100 | | 100 |

From Table 3.4 it is clear that coal B contains more, dense material, with the difference most prominent in the +2.0 $g.cm^{-3}$ fraction. Coal B also contains significantly less material in the -1.4 $g.cm^{-3}$ density fraction. It can therefore be seen that coal B contains significantly more liberated mineral phases compared to coal G (Oki et al., 2004). The density distribution as observed for coals B and G is similar to Witbank seam 4 coals (Barker, 1999).

The efficiency of the washing procedure was confirmed by conducting a SEM (Scanning Electron Microscope) analysis on each of the separated fractions to check for the presence of bromine associated with the dense media (TBE). No bromine was detected in any of the samples.

# Chapter 4: Characterization

In this chapter the characterization equipment, procedures, and the results obtained from the coal samples are discussed. Section 4.1 will describe the characterization procedures, while Section 4.2 will describe the characterization results of the parent coals, and Section 4.3 refers to the characterization results of the density fractions obtained from coals B and G.

## 4.1 Characterization procedures

In this section, the experimental equipment and procedures used in the characterization of the relevant coal samples will be described. This will include:

- Chemical analysis.
- Petrographic analysis.
- Structural analysis.
- Scanning Electron Microscope (SEM).
- Mineral analysis.
- Calorific value analysis.
- Ash fusion tests.
- Carbon dioxide reactivity.
- Pyrolysis experiments.

All of the coal samples were prepared for characterization as described in Chapter 3.

### 4.1.1 Chemical and petrographic analyses

As the coal samples for chemical and petrographic analyses were outsourced to other laboratories, and the procedures were performed according to ISO standards, these analyses will not be described in detail. Table 4.1 gives a summary of the chemical and petrographic analyses, including the type of analysis, ISO standard used, and the laboratory responsible for the characterization.

Table 4. 1: Chemical and petrographic analyses.

| Analysis | ISO standard | Laboratory responsible. |
|---|---|---|
| | **Chemical**[a] | |
| **Proximate** | | |
| Moisture | SABS. SM 924 (1978) | SABS Secunda / Eskom |
| Volatile matter | ISO 562 (1998) | SABS Secunda / Eskom |
| Ash content | ISO 1171 (1997) | SABS Secunda / Eskom |
| Fixed carbon | By difference | SABS Secunda / Eskom |
| **Ultimate** | | |
| Carbon/hydrogen/nitrogen | ISO/TS 12902 (2001) | SABS Secunda / Eskom |
| Total sulphur | ISO 351 (1984) | SABS Secunda / Eskom |
| Oxygen | By difference | SABS Secunda / Eskom |
| **Fischer Tar** | SABS SM 1073 (1984) | Sasol Research and Development. |
| | **Petrographic**[b] | |
| Rank | ISO 7404-5 (1985) | Petrographics SA |
| Maceral content | ISO 7404-3 (1985) | Petrographics SA / WITS |
| Microlithotype | ISO 7404-4 (1985) | Petrographics SA / WITS |

a: Chemical analysis for parent coals done by SABS Secunda, for density fractions done at Eskom Sustainability and Innovation Fuels.

b: Petrographic analysis for parent coals done by Petrographics SA, for density fractions at University of the Witwatersrand.

### 4.1.2 Mineral analysis

The mineral analysis includes X-ray diffraction (XRD), QEMSCAN and X-ray fluorescence (XRF) analyses. These analyses give a more accurate indication of the mineralogical and elemental content of the minerals compared to the qualitative SEM analysis. The crystalline minerals are measured by means of XRD analysis, while the QEMSCAN analysis detects the total mineral make-up of the coals. The elemental composition of the ash formed from the mineral phases is detected by means of the XRF analysis. The parent coals were analyzed according to XRD and XRF, while the density fractions were investigated according to QEMSCAN and XRF to obtain the mineralogical and elemental ash make-up respectively.

**XRD Analysis**

The samples for XRD were outsourced to the Geology Department of the University of Pretoria for analysis. In this analysis the coal samples were analyzed using a PANalytical X'Pert Pro powder diffractometer. This analyzer is equipped with

X'Celerator detector and variable divergence-and receiving slits with Fe-filtered Co-Kα radiation. The different phases were identified using X'Pert Highscore Plus software, while the relative amounts of each mineral was estimated by means of the Rietveld method.

**QEMSCAN analysis**

The coal samples for the QEMSCAN analysis were outsourced to the laboratories at the Research and Development Department of Eskom. The sample is prepared by first mixing the coal with molten carnauba wax in a 30 mm mould and allowing this to cure. This solid wax block is then polished, exposing individual particles in the cross-section.

The polished blocks are analyzed by positioning the scanning electron beam at predefined points across a particle. At each point a 7 millisecond, 1000 count X-ray spectrum is acquired. The elemental proportions are then used to identify the mineral phases at each point.

**XRF Analysis**

The samples for XRF were outsourced to the Geology Department of the University of Pretoria for analysis. The method used for this analysis includes fine grinding of the coal to < 75 µm and then drying this fine coal sample at a temperature of 110 ºC. The dried coal sample is then ashed under an air atmosphere at a temperature of 500 ºC for one hour, and at 815 ºC for four hours, in order to determine the Loss On Ignition value. The sample for major element analysis was prepared by adding one gram of the ash to nine grams of $Li_2B_4O_7$ and fusing this into a glass bead. This glass bead is then analyzed in the ARL 9400XP+ spectrometer. A sample for minor and trace element analysis is prepared by pressing an aliquot of the ash into a powder briquette. This briquette is then analyzed by using UniQuant software.

### 4.1.3 Structural analysis

The structural properties of the coal samples were obtained by means of gas adsorption and mercury intrusion experiments.

## Gas Adsorption

The Micrometrics ASAP 2010 Analyzer was used to perform the analysis and both carbon dioxide and nitrogen were used as adsorbent gases in the analyzer. Figure 4.1 illustrates the Micrometrics ASAP 2010 Analyzer as it was used.

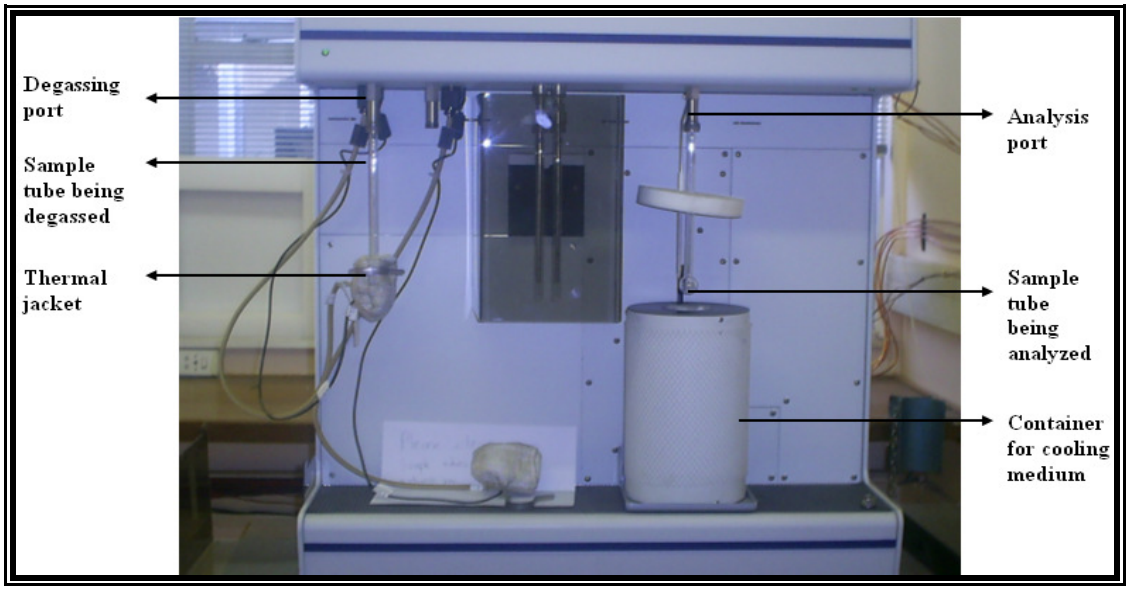


Figure 4. 1: Micrometrics ASAP 2010 analyzer.

Initially the coal samples are degassed at 25 ºC for a period of 48 hours. After degassing, the coal is analyzed by means of gas adsorption to determine the specific surface area, pore volume and pore diameter of the given coal samples. The saturation pressure used in the adsorption experiments was 660 mm Hg. Table 4.2 gives a summary of the experimental conditions used in the gas adsorption experiments.

Table 4. 2: Gas adsorption experimental conditions.

| $T_{degas}$ (ºC) | $P_{final}$(µm Hg) | Coal sample | Analysis gas | $T_{analysis}$ (ºC) | Cooling medium |
|---|---|---|---|---|---|
| 25 | < 4 | Raw coal | $CO_2$ | 0 | Ice water |
| 25 | < 4 | Raw coal | $N_2$ | -197 | Liquid $N_2$ |

$T_{degas}$: Degassing temperature, $P_{final}$: Final degassing pressure, $T_{analysis}$: Analysis temperature.

## Mercury Intrusion

The mercury intrusion experiments were performed using a Micrometrics Autopore IV Analyzer. Figure 4.2 shows this Micrometrics Autopore IV Analyzer as it was used.

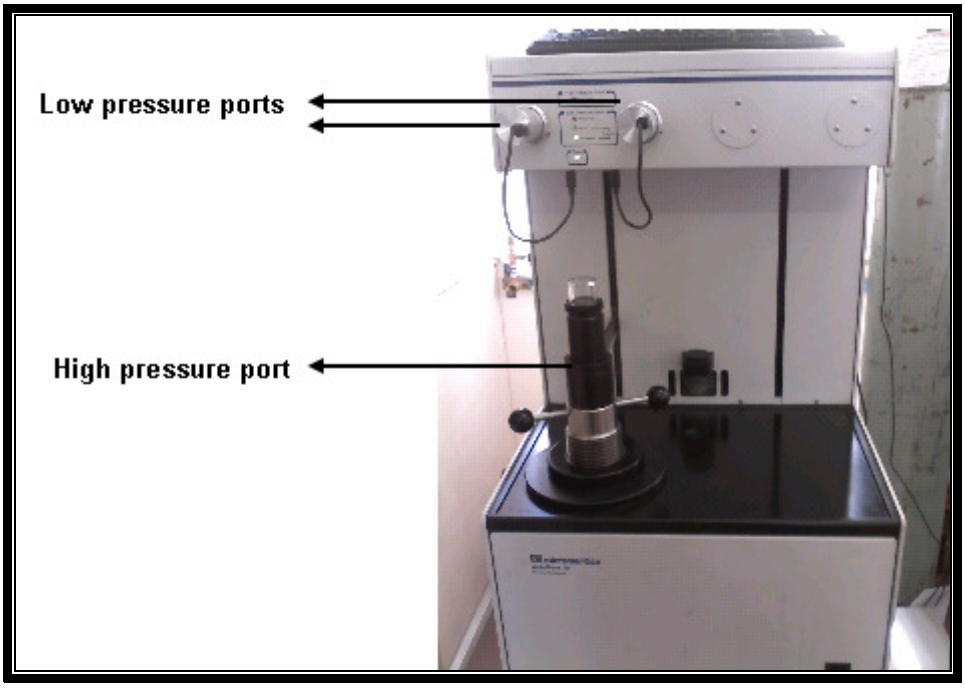


Figure 4. 2: Micrometrics Autopore IV Analyzer.

The coal particles are loaded into a pre-calibrated nr 14 glass analysis tube. This tube is inserted into the low-pressure port, where analysis is done for 45 minutes as to introduce mercury into the tube. Then the tube containing a known amount of mercury is moved to the high pressure port. The pressure applied to the sample as to intrude mercury into the porous coal particles is incrementally varied from 3.6 kPa to 413 MPa, with each pressure being held constant until the amount of mercury intruded is equilibrated. This mercury intrusion data then allows the calculation of the macro-porosity of the coals. Table 4.3 gives a summary of the experimental conditions used in the mercury intrusion experiments.

Table 4. 3: Mercury intrusion experimental conditions.

| $T_{LP}$ (°C) | $T_{HP}$ (°C) | Coal sample | Analysis tube |
|---|---|---|---|
| 25 | 25 | Raw coal | Number 14 |

$T_{LP}$: Low pressure analysis temperature, $T_{HP}$: High pressure analysis temperature.

### 4.1.4 Scanning electron microscope

The Scanning Electron Microscope (SEM) analysis was done using a FEI Quanta 200 ESEM microscope with an integrated Inca 400 EDS system as shown in Figure 4.3.

This analysis was done qualitatively for the parent coals, and was not done on the density fractions.

Figure 4. 3: FEI Quanta 200 ESEM microscope.

The EDS (Energy Dispersive Spectrometry) analysis gives a qualitative elemental analysis of the coal sample. The SEM analysis is done by preparing the coal samples as follows:

- Fine grind raw coal to a particle size of 125 μm by making use of a rotor-mill.
- Prepare a sample frame by applying double sided carbon tape to it.
- Press sample frame into finely ground coal, adhering a single layer of particles on the carbon tape, which is attached to the sample frame.

The SEM analysis can be summarized as follows:
The prepared sample frames, as mentioned above are mounted on a microscope plate. Then, based on the particle size, an appropriate degree of magnification must be selected. This is followed by obtaining a Backscattered Electron Image (BSI). This BSI is an atomic-weight contrast image, which allows for the elemental composition of the coal to be evaluated by means of image processing procedures; as the high molecular-weight elements appear brighter compared to the low molecular-weight elements. This also allows distinguishing between the association of minerals and macerals, as the minerals are observed as bright areas on the SEM micro-photographs, while the carbon-rich macerals are seen as dull areas.

### 4.1.5 Calorific value analysis

The calorific value analysis gives an indication of the amount of energy that can be obtained per kilogram from the given coal sample. This analysis was done by making use of the MC-1000, Mk 2 Modular Calorimeter as shown in Figure 4.4.

Figure 4. 4: MC-1000, MK 2 Modular Calorimeter.

A sample consisting of one gram of the coal, crushed to a particle diameter of -1 mm, is weighed on the laboratory balance and is then loaded into the calorific meter, where the chamber is pressurized with oxygen. The sample is ignited and the temperature increase is measured. This increase in temperature is converted via the relevant software built into the calorific meter to the amount of energy that can be obtained per kilogram of coal. The experiment was performed 3 times for each of the coals to ensure reproducibility.

### 4.1.6 Ash fusion analysis

The coals were outsourced to SABS for ash fusion tests. This was done according to standard procedure: ISO 540: 1995 making use of a reducing gas atmosphere. The ash fusion tests were only done for the density fractions.

### 4.1.7 Pyrolysis behaviour

The pyrolysis experiments were performed by making use of the pyrolysis test-rig belonging to Sasol Technology in Sasolburg, and employing a standard pyrolysis procedure. Only the parent coals were analyzed in terms of the pyrolysis experiments. This section will describe the pyrolysis test-rig setup and procedure.

The pyrolysis test-rig consists of the following (as shown in Figure 4.5):

- Furnace.
- Two cold traps.
- Round bottom flask and ice bath.
- Backpressure regulator.
- Two gas traps.
- Associated gas piping (Both for nitrogen gas feed and pyrolysis product gases).

The first step in this procedure is to crush and screen the coal samples in order to achieve the correct particle size distribution (PSD) as required by the standard pyrolysis procedure. This PSD is described in Section 3.2.2 .

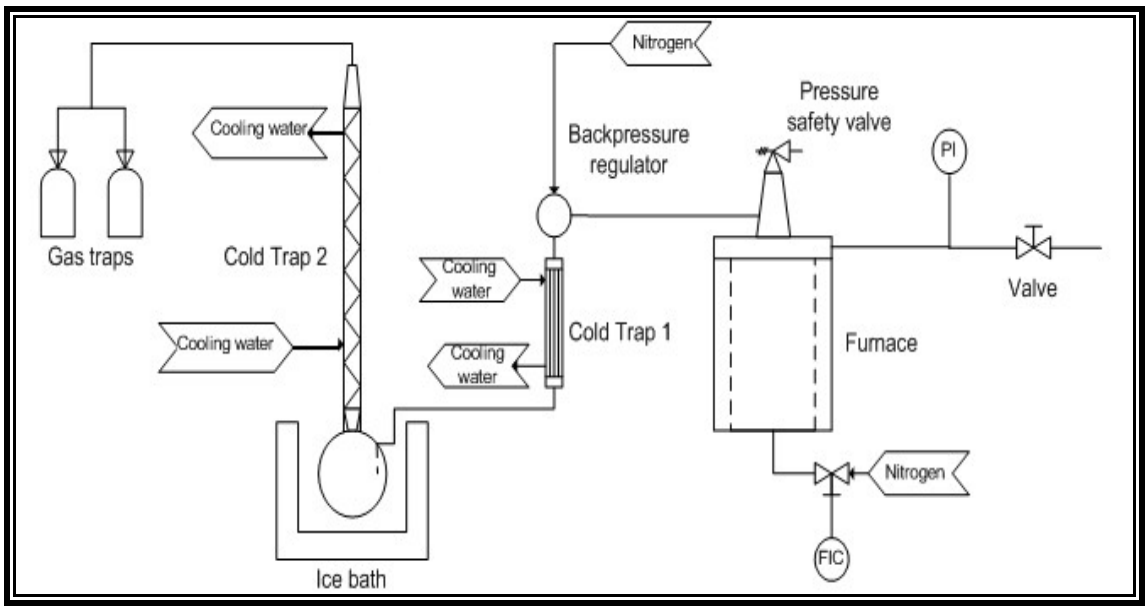


Figure 4. 5: Schematic representation of the pyrolysis test-rig.

The furnace is heated electronically, and the heating rate is limited to 10 ºC.min$^{-1}$. The temperature inside the furnace is measured with an S-type thermocouple connected to a temperature controller which adjusts the power input to the furnace accordingly. At the bottom of the furnace there is a gas inlet port, where nitrogen is constantly fed into the furnace to maintain an inert atmosphere. Initially the system is pressurized to 26 bar with nitrogen at a flow rate of 200 ml.min$^{-1}$. Once the system is pressurized, the nitrogen flow, as regulated by a Brooks 5850 mass flow controller, is reduced to 30 ml.min$^{-1}$. The pressure relief valve automatically opens when the pressure inside the furnace exceeds 40 bar.

The backpressure regulator assists in maintaining an elevated pressure inside the furnace while reducing the pressure in the downstream piping to atmospheric pressure as to prevent damage to this equipment. The first of the two cold traps is similar to a shell-and-tube heat exchanger, with the cooling water at a temperature of 3 ºC flowing in the shell side, and the pyrolysis product gases flowing in the tube side. This heat exchanger assists in condensing most of the tars, heavy hydrocarbons and water which is then collected in a round bottom flask submerged in an ice bath. The second cold trap is a liebich cooler, with cooling water at a temperature of 3 ºC flowing on the inside, while the pyrolysis product gases flow through the outer tube. This second cold trap allows for any remaining tars, water or heavy hydrocarbons to be condensed and collected in the round bottom flask. Finally the remaining lighter gases obtained from the pyrolysis of the coal samples are collected in the two gas traps. Industrial plastic bags are used for collecting the gases. These gases are then taken for analysis in a Gas Chromatograph (GC).

The furnace is allowed to cool down with the nitrogen gas still flowing through the system thereby maintaining an inert atmosphere as to prevent any combustion or gasification reactions from taking place. When the furnace has cooled to below 100ºC, the cold traps and the round bottom flask containing the tars, heavy hydrocarbons and water are removed from the system, and are used in the Fischer tar analysis. When the furnace has reached ambient temperature, the nitrogen gas flow to the furnace is closed and the vessel is depressurized. The furnace may now be opened and the char emptied into a bucket. These chars are weighed as to determine the percentage of char obtained from the given coal samples. Now by knowing the

percentage char, water and tar obtained for each coal sample, the percentage of gas can be calculated by the difference in mass as seen in Equation 41.

$$Gas\ and\ errors\,(\%) = 100\% - \%(Char + Water + Tar) \quad \ldots\ldots (41)$$

## 4.2 Characterization results and discussion: Parent coals

In this section the results obtained from the abovementioned experiments will be discussed for the parent coals.

### 4.2.1 Chemical analysis

The following paragraphs contain the results from the proximate and ultimate analyses of the seven parent coal samples.

**Proximate analysis**

The proximate analysis gives the compositions of volatile matter, fixed carbon and ash contained in the coal when considering a dry base, and includes the amount of moisture in the coal when considering an air dry base. The proximate analysis gives a good indication of the suitability of coal for industrial gasifiers (Van Dyk et al., 2001). The results are displayed in Table 4.4 on air dry base.

Table 4. 4: Proximate analysis of parent coals (Air dry base, based on weight %).

| Composition | A | B | C | D | E | F | G |
|---|---|---|---|---|---|---|---|
| Moisture | 6.4 | 4.8 | 4.4 | 4.2 | 3.7 | 4.5 | 5.3 |
| Volatiles | 22.2 | 20.3 | 23.1 | 19.3 | 18.7 | 23.5 | 21.1 |
| Fixed Carbon | 49.8 | 48.1 | 49.9 | 42.5 | 38.8 | 53.4 | 49.5 |
| Ash | 21.6 | 26.8 | 22.6 | 34.0 | 38.8 | 18.6 | 24.1 |

From this table it can be seen that there is no significant difference in the moisture content or the volatile content of the coals. The fixed carbon shows a variation from 38.8 % (wt) (coal E) to 53.4 % (wt) (coal F). This can be associated with the variation observed in the ash content, where an inverse trend can be seen for coal E having the highest ash content, and coal F the lowest ash content.

**Ultimate analysis.**

The ultimate analysis gives the chemical composition of coal including the amounts of carbon, hydrogen, nitrogen, sulphur and oxygen (by difference) contained in the coal. The results for this analysis can be seen in Table 4.5.

Table 4. 5: Ultimate analysis of parent coals (Dry-ash free, based on weight %).

| Element | A | B | C | D | E | F | G |
|---|---|---|---|---|---|---|---|
| Carbon | 80.3 | 79.9 | 82.1 | 81.0 | 80.4 | 83.2 | 80.7 |
| Hydrogen | 4.8 | 4.8 | 5.3 | 5.0 | 5.3 | 5.0 | 4.9 |
| Nitrogen | 2.1 | 2.1 | 2.3 | 2.0 | 1.9 | 2.2 | 2.1 |
| Sulphur | 1.2 | 1.3 | 1.2 | 3.5 | 1.8 | 1.1 | 1.1 |
| Oxygen | 11.6 | 11.9 | 9.2 | 8.5 | 10.6 | 8.5 | 11.1 |

From the ultimate analysis it was found that the coals are very similar in terms of organic composition, as the carbon, hydrogen and nitrogen contents do not vary significantly. Coal D has a very large amount of sulphur compared to the other coals.

### 4.2.2 Petrographic analysis

This results obtained for the petrographic analysis of the parent coals are discussed in this section; including the vitrinite reflectance, maceral content, microlithotype content, and carbominerite/minerite content of the given coal samples.

**Vitrinite reflectance**

The random vitrinite reflectance of coal gives a good indication of the rank of the coal, as the reflectance of coal increases with increasing degree of coalification (Berkovitz, 1985). The results for the random vitrinite reflectance measurements, along with the standard deviations observed are shown in Table 4.6, while the vitrinite reflectance histograms can be seen in Appendix A.

Table 4. 6: Random vitrinite reflectance for parent coals.

| Property | A | B | C | D | E | F | G |
|---|---|---|---|---|---|---|---|
| RoV | 0.59 | 0.64 | 0.63 | 0.64 | 0.61 | 0.61 | 0.63 |
| σ | 0.065 | 0.070 | 0.068 | 0.072 | 0.085 | 0.076 | 0.077 |

RoV: Mean random reflectance, σ: Standard deviation.

There is no significant difference in the random vitrinite reflectance as measured for the seven coals. According to ISO 11760 (2005), the gasification coal blend, and all of the single source coals (except for coal A) can be ranked as medium rank C bituminous coals. Coal A is a medium rank D bituminous coal, as it has a random vitrinite reflectance of less than 0.60 %.

According to the Economic Commission for Europe (1988), all of the coal samples are classified as typical single seam, non blend coals, because the standard deviation is less than 0.10 for each of the coal samples. This observation is significant, as it shows how similar the single source coals are, since even the gasification coal blend (coal G) is classified as a single seam, non blend coal; as it is made up of coals from the number 4 coal seam from the Highveld coal field.

**Maceral analysis**

The maceral evaluation gives the organic composition of the coal, specifically looking at the maceral make-up of the coals. The results from this analysis are presented in Table 4.7.

Table 4. 7: Maceral content of parent coals (Mineral matter free, based on volume %).

| Maceral group | A | B | C | D | E | F | G |
|---|---|---|---|---|---|---|---|
| Vitrinite | 23 | 23 | 23 | 14 | 21 | 29 | 22 |
| Liptinite | 5 | 4 | 3 | 2 | 4 | 3 | 4 |
| Reactive SF | 13 | 15 | 13 | 15 | 13 | 9 | 13 |
| Inert SF | 23 | 21 | 20 | 25 | 20 | 17 | 19 |
| Fusinite | 3 | 3 | 4 | 2 | 2 | 2 | 3 |
| Micrinite | 1 | 1 | 2 | 1 | 2 | 2 | 2 |
| Reactive Inerto | 8 | 10 | 11 | 13 | 10 | 12 | 12 |
| Inert Inerto | 24 | 23 | 24 | 28 | 28 | 26 | 25 |
| Total inertinite | 72 | 73 | 74 | 84 | 75 | 68 | 74 |

SF: Semi-fusinite, Inerto: Inertodetrinite.

The coals contain relatively small amounts of vitrinite when compared to Northern Hemisphere coals. Coal D contains less vitrinite compared to the other coals, while coal F contains significantly more vitrinite. Liptinite makes up the smallest contribution to the macerals content of the coals, with the liptinite content below 5 %

(vol) in each case. Coal D contains the smallest amount of liptinite compared to the other coals. It was found that all of the coal samples are inertinite-rich coals. This high inertinite content is typical of the Highveld coal seam in South Africa (Barker, 1999).

It can also be seen that the major components contributing to the inertinite content of the coals is inert semi-fusinite and inert-inertodetrinite. These maceral sub-groups are known to form dense, inert chars during pyrolysis (Falcon and Snyman, 1986). The reactive maceral content of the coal includes the vitrinite, liptinite, reactive inertodetrinite and reactive semi-fusinite contained in the coal, and can thus be described as those macerals which react upon heating. The reactive macerals content does not show much variation, but coal D contains the least amount of reactive macerals due to the low vitrinite and liptinite content of this coal.

**Microlithotype analysis**

As previously mentioned, microlithotypes refer to the microscopic bands of maceral and mineral matter. Table 4.8 shows the results for the microlithotype analysis for all seven coals.

Table 4. 8: Microlithotype content of parent coals (Based on volume %).

| Microlithotype | A | B | C | D | E | F | G |
|---|---|---|---|---|---|---|---|
| Vitrite | 9 | 9 | 5 | 7 | 5 | 10 | 5 |
| Liptite | 0 | 0 | 0 | 0 | 0 | 0 | 0 |
| Inertite | 41 | 36 | 40 | 38 | 32 | 40 | 40 |
| Vitrinertite | 10 | 13 | 10 | 11 | 9 | 12 | 10 |
| Clarite | 2 | 1 | 2 | 2 | 1 | 2 | 1 |
| Durite | 9 | 6 | 6 | 6 | 7 | 5 | 9 |
| Tri-macerite | 9 | 9 | 8 | 7 | 9 | 8 | 6 |
| Total Inter | 30 | 29 | 26 | 26 | 26 | 27 | 26 |
| Carbominerite | 15 | 16 | 17 | 18 | 23 | 17 | 20 |
| Minerite | 5 | 10 | 12 | 11 | 14 | 6 | 9 |

Inter: Intermediates.

From these results it can be concluded that the pure inertinite-containing microlithotype called inertite makes up the bulk of the coal. Small amounts of the pure vitrinite-containing microlithotype known as vitrite was observed, with the vitrite content ranging from 5 % (vol) to 10 % (vol). No pure liptite was observed in any of the coals, which is in-line with the findings from Table 4.7, which shows that the coals contain very little liptinite, which is then possibly associated with the inertinite maceral group as found in durite and trimacerite.

The intermediate microlithotype content does not vary significantly, as it ranges from 26 % (vol) to 30 % (vol) for the various coals. The vitrinite and inertinite containing bi-maceral known as vitrinertinite makes up the bulk of the intermediates. Clarite is observed in the smallest quantities, which is in-line with the results from Table 4.7 which states that liptinite, which makes up part of the clarite bi-maceral along with vitrinite, is scarcely found in any of the coals.

When looking at the mineral part of the coal, there are two groups to consider: the carbominerite group and the minerite group. Minerite refers to the more inorganic microlithotypes, containing more than 60 % (vol) mineral matter. The carbominerite groups contained in the given coal samples make up 15 % (vol) (coal A) to 23 % (vol) (coal E) of the total coal volume. The mineral rich minerite groups make up a less significant volume, with the concentrations of minerite ranging from 5 % (vol) (coal A) to 14 % (vol) (coal E). Here it can be seen that coal E contains the greatest amount of carbominerite and minerite groups compared to the other coal samples; which supports the high ash value predicted for this coal in Table 4.4.

**Carbominerite analysis**

Table 4.9 gives the results from the carbominerite and minerite analyses for each of the seven coals. The carbominerite here refers to the maceral/mineral associated groups, while the minerite refers to mineral rich groups as previously mentioned.

Table 4. 9: Carbominerite and minerite content of parent coals (Based on volume %).

| | A | B | C | D | E | F | G |
|---|---|---|---|---|---|---|---|
| **Carbominerite** | | | | | | | |
| C-Arg & C-Sil | 9 | 9 | 13 | 12 | 16 | 14 | 14 |
| Carbo-pyrite | 2 | 3 | 3 | 2 | 2 | 1 | 2 |
| Carbankerite | 4 | 4 | 1 | 4 | 5 | 2 | 4 |
| Total | 15 | 16 | 17 | 18 | 23 | 17 | 20 |
| **Minerite** | | | | | | | |
| Clay & Quartz | 2 | 7 | 9 | 8 | 12 | 5 | 6 |
| Pyrite | 1 | 1 | 2 | 1 | 1 | 0 | 1 |
| Carbonates | 2 | 2 | 1 | 2 | 1 | 1 | 2 |
| Total | 5 | 10 | 12 | 11 | 14 | 6 | 9 |

C-Arg: Carb-argillite, C-Sil: Carbo-silicate.

The main contribution to the carbominerite content of the coals is from the carb-argillite and carbo-silicate groups, which are the clay and quartz-containing groups, while the second largest contribution is made by the carbonate-containing carb-ankerite group. Coals E and F contain very small amounts of carb-ankerite compared to the other coals.

When looking at the minerite groups, the same trend can be seen as in the carbominerite groups, with the bulk of the minerite content consisting of clay and quartz groups. The carbonate groups have the second most significant contribution to the minerite content of the coals, and again it can be seen that the pyrite group contributes the least amount to the mineral content of the coals.

These observations are typical of South African coals, especially from the Highveld coal field; as Matjie et al. (2008) also found that the clay and quartz groups are the most dominant mineral groups in coals derived from this coal field.

### 4.2.3 Mineral analysis

The mineral analysis gives a detailed look into the incombustible matter contained in coal, as these minerals may impact on the gasification performance of the coal. This section describes the results obtained from the evaluation of the incombustible

materials contained in the given coal samples under the following headings: X-ray diffraction (XRD) analysis and X-ray fluorescence (XRF).

**X-ray diffraction**

The XRD analysis gives the crystalline mineral content of the coal. The limitation of this analysis is that it does not accurately take into account the amorphous minerals contained in the coal. Table 4.10 shows the results obtained from the XRD analysis for each of the seven coals.

Table 4. 10: Mineral composition of parent coals (Mineral matter base, based on weight %).

| Mineral | A | B | C | D | E | F | G |
|---|---|---|---|---|---|---|---|
| Anatase | 4.2 | 4.1 | 4.7 | 4.0 | 3.7 | 3.8 | 4.3 |
| Calcite | 2.4 | 2.5 | 1.2 | 2.0 | 1.8 | 2.6 | 1.7 |
| Dolomite | 14.7 | 11.1 | 7.9 | 11.4 | 8.7 | 12.5 | 12.9 |
| Kaolinite | 55.9 | 53.0 | 49.3 | 55.5 | 48.2 | 50.3 | 55.5 |
| Pyrite | 0.5 | 2.7 | 2.9 | 0.5 | 1.2 | 1.2 | 0.6 |
| Quartz | 20.8 | 25.3 | 32.6 | 25.2 | 22.5 | 17.0 | 23.4 |
| Rutile | 1.6 | 1.3 | 1.5 | 1.4 | 1.0 | 1.3 | 1.6 |
| Muscovite | 0 | 0 | 0 | 0 | 12.9 | 11.2 | 0 |

From Table 4.10, it is clear that the most dominant mineral group contained in the coals is kaolinite, as it represents approximately half of the crystalline mineral matter contained in the coal samples. The other significant mineral groups include quartz and dolomite, with minor contributions from minerals such as anatase, calcite and rutile.

This observation supports the results from the carbominerite and minerite analyses (Table 4.9), as the quartz and clay groups were the most significant minerals observed, followed by the carbonates such as dolomite and calcite.

**X-ray Fluorescence**

The XRF analysis of the coal gives an indication of the chemical composition of the ash left behind after the carbon in coal has been consumed. The ash is composed mainly of metallic oxides such as $SiO_2$, $Al_2O_3$ and $Fe_2O_3$. The results from the XRF analysis is shown in Table 4.11 for the major and minor elements contained in the coal ash, while Table 4.12 gives the trace elements contained in the coal ash.

Table 4. 11: Parent coal ash chemistry. (Mineral matter base, based on weight %).

| Element | A | B | C | D | E | F | G |
|---|---|---|---|---|---|---|---|
| $SiO_2$ | 46.9 | 51.5 | 57.1 | 54.1 | 54.8 | 52.9 | 52.4 |
| $TiO_2$ | 1.5 | 1.5 | 1.3 | 1.6 | 1.5 | 1.2 | 1.6 |
| $Al_2O_3$ | 26.1 | 25.2 | 26.0 | 27.4 | 29.1 | 26.7 | 28.2 |
| $Fe_2O_3$ | 2.0 | 4.8 | 5.0 | 2.0 | 3.0 | 3.7 | 2.5 |
| MnO | 0.1 | 0.0 | 0.0 | 0.0 | 0.1 | 0.1 | 0.0 |
| MgO | 3.1 | 2.0 | 1.6 | 2.1 | 1.9 | 2.1 | 2.4 |
| CaO | 11.9 | 7.0 | 4.3 | 6.9 | 4.4 | 6.8 | 7.4 |
| $Na_2O$ | 0.7 | 0.4 | 0.4 | 0.4 | 0.4 | 0.4 | 0.5 |
| $K_2O$ | 0.3 | 0.6 | 0.7 | 0.7 | 0.9 | 1.0 | 0.8 |
| $P_2O_5$ | 1.4 | 0.5 | 0.2 | 0.7 | 0.7 | 0.9 | 1.0 |

The main ash component is $SiO_2$, which is derived from the quartz and clay minerals which make up the bulk of the mineral content of the coals (Spears, 2000). The other large contribution to the ash is made by $Al_2O_3$. This can be explained by the high clay content of the coals (Spears, 2000), as the XRD analysis (Table 4.10) showed that kaolinite is the most common mineral contained in the coals. The $TiO_2$ observed in the XRF analysis is derived from the anatase and rutile mineral groups, as these are the only titanium-containing mineral groups detected by the XRD analysis.

The $Fe_2O_3$ as detected by the XRF analysis can be related to the pyrite as shown in Table 4.10, where it can be seen that coals B and C contain slightly larger quantities of pyrite which are then associated with a larger $Fe_2O_3$ concentration in the ash. This may subsequently contribute to a lower ash-fusion temperature when associated with clay minerals, which may cause the formation of slag in the gasifiers (Bunt, 2006). The high ratio of $SiO_2$ to $Al_2O_3$ associated with the increased concentration of $Fe_2O_3$ contained in coals B and C may well also contribute to these coals having a lower ash fusion temperature (Waanders and Govender, 2005). This is then a possible reason why gasifying coal blends containing larger amounts of coal B results in more unconverted carbon in the ash removed from the gasifiers.

The CaO as detected by the XRF analysis is related to the calcite and dolomite mineral groups as shown in Table 4.10. This is because calcite and dolomite are the main calcium-containing mineral groups, and that coals A, B and G contain

significant amounts of calcite and dolomite, while also displaying increased CaO concentrations.

The $K_2O$ contained in the coals is derived from muscovite, as this the only potassium-containing mineral detected by the XRD analysis, and it can be seen that coals E and F which contain significant amounts of muscovite, also contain more $K_2O$ than the other coal samples. It can also be seen that coal A contains the least amount of $K_2O$, which is less than half that of the other coal samples. Huttinger and Natterman (1994) stated that elements such as sodium, calcium and potassium may have a catalytic effect on the gasification reaction of coal, which cannot be validated in this part of the study, as the content of these minerals in the coals do not differ significantly.

Table 4. 12: Trace element content of parent coals (Based on parts per million).

| Element | A | B | C | D | E | F | G |
|---|---|---|---|---|---|---|---|
| Sr | 676 | 484 | 301 | 593 | 6010 | 598 | 493 |
| Zr | 74 | 103 | 93 | 115 | 1110 | 101 | 84 |
| Cl | 86 | 115 | 66 | 94 | 555 | 51 | 51 |
| S | 3020 | 4780 | 3570 | 3770 | 25400 | 4200 | 2750 |
| Ba | 399 | 528 | 356 | 590 | 1940 | 482 | 376 |

When considering the trace elements, as shown in Table 4.12, it can be observed that coal E contains relatively large amounts of these elements, including Sr, Zr, Cl, S and Ba. None of these trace elements pose a serious environmental hazard when compared to the elements as mentioned by Clarke and Sloss (1992). The sulphur contained in the ash does not correspond to the sulphur as determined by the ultimate analysis of the coals. This may be because the ultimate analysis includes the organic sulphur which has been driven off during the ashing of the coals prior to the XRF analysis.

### 4.2.4 Structural analysis

The specific surface area of the coals was determined by means of both carbon dioxide and nitrogen gas adsorption, and the results are shown in Table 4.13. These results are given as the specific surface area according to the Dubinin-Radushkevich (DR) method for the carbon dioxide adsorption experiments, and according to the

BET method for the nitrogen adsorption experiments. The nitrogen adsorption experiments also allow the calculation of the total adsorption pore volume as well as the average adsorbed pore diameter.

Table 4. 13: Specific surface area of parent coals.

| Property | A | B | C | D | E | F | G |
|---|---|---|---|---|---|---|---|
| $S_{CO2}$ ($m^2.g^{-1}$) | 152.4 | 117.5 | 120.5 | 137.2 | 123.6 | 146.0 | 154.4 |
| $S_{N2}$ ($m^2.g^{-1}$) | 4.3 | 3.9 | 2.2 | 4.9 | 3.5 | 2.1 | 5.2 |
| $V_{N2}$ ($10^{-3}$ $cm^3.g^{-1}$) | 7.0 | 7.7 | 4.1 | 8.0 | 5.4 | 5.4 | 9.6 |
| $V_{MP}$ ($10^{-3}$ $cm^3.g^{-1}$) | 1.6 | 1.5 | 1.1 | 1.1 | 0.6 | 1.0 | 0.5 |
| $D_{Avg}$ (Å) | 81.6 | 92.7 | 88.5 | 77.1 | 72.4 | 114.7 | 84.0 |

$S_{CO2}$: Applied Dubinin Radushkevich method, $S_{N2}$: Applied Brunauer-Emmett-Teller method, $V_{N2}$: adsorption pore volume, $V_{MP}$: micro-pore volume, $D_{Avg}$: average pore diameter determined by nitrogen adsorption.

From Table 4.13 it is observed that the surface area as detected by carbon dioxide gas adsorption is much larger than the area as detected by nitrogen gas adsorption. This is supported by the findings of several researchers (Catellò et al., 2002; Hurt et al., 1991; Nandi and Walker, 1964; Debelak and Schrodt, 1979), who also found that the carbon dioxide surface area is associated with the micro-pore area of coals, while the nitrogen surface area has the limitation that it diffuses very slowly into micro-pores below 5 Å and is therefore a better indication of the meso-pore surface area. It can then be seen that the surface area detected by carbon dioxide adsorption experiments varies from 117.5 $m^2.g^{-1}$ (coal B) to 154.4 $m^2.g^{-1}$ (coal G). The surface area as obtained by the nitrogen adsorption experiments varies from 2.1 $m^2.g^{-1}$ (coal F) to 5.2 $m^2.g^{-1}$ (coal B). This analysis shows that the coal surface properties do vary for the parent coals, although it is not expected that the coal surface area will influence the reactivity behaviour of the coals, as charring will further develop these properties.

When observing the adsorption pore volume of the coals, it can be concluded coals C, E and F have slightly lower total pore volumes compared to the other coals. It can also be seen that coals E and G have a much lower micro-pore volume compared to the other coals. The average pore diameter measured for these coals vary from 72.4 Å (coal E) to 114.7 Å (coal F). This range of pore diameters refers to the meso-pores; as the pore diameter for meso-pores ranges from 20 Å to 500 Å.

### 4.2.5 Scanning electron microscope

Figure 4.6 shows a typical SEM micro-photograph of a parent coal used in this study. Table 4.14 gives the elemental analysis of each of the points which are included in Figure 4.6. The most prominent elements observed during the SEM analysis include: carbon, oxygen, aluminium, silicon, sulphur, iron and calcium. Figure 4.6 shows the heterogeneous nature of coal as there are several different types of particles observed:

- Organic particles (# 3).
- Discrete mineral particles (# 1, 4, 5, 6).
- Minerals associated with organic material (# 2, 7).

All of the observations are supported by the minerite analysis, as shown in Table 4.9; as this table shows that the main discrete mineral groups are from the clay, quartz, pyrite and carbonate groups. Also the mineral-maceral associations observed are in agreement with the carbominerite analysis (Table 4.9), as clay, pyrite and carbonate groups were found to be in association with the organic groups.

Table 4. 14: Elemental SEM analysis of parent coal (Refer to Figure 4.6, based on atomic %).

| Element | 1 | 2 | 3 | 4 | 5 | 6 | 7 |
|---|---|---|---|---|---|---|---|
| C | 5.8 | 48.5 | 85.6 | 17.3 | 14.7 | 7.5 | 23.0 |
| O | 60.9 | 8.7 | 11.2 | 57.5 | 52.7 | 18.8 | 46.8 |
| Mg | 0 | 0 | 0 | 0 | 0 | 0.4 | 0 |
| Al | 15.4 | 0.6 | 0.5 | 0 | 0.5 | 0 | 3.6 |
| Si | 17.9 | 0.9 | 2.3 | 0.2 | 0.4 | 0.6 | 4.4 |
| S | 0 | 12.1 | 0.4 | 0.2 | 0 | 34.9 | 8.5 |
| Ca | 0 | 0.4 | 0 | 24.2 | 29.1 | 0 | 0 |
| Fe | 0 | 28.9 | 0 | 0.7 | 0 | 37.8 | 13.6 |
| Sr | 0 | 0 | 0 | 0 | 2.6 | 0 | 0 |
| Total | 100 | 100 | 100 | 100 | 100 | 100 | 100 |

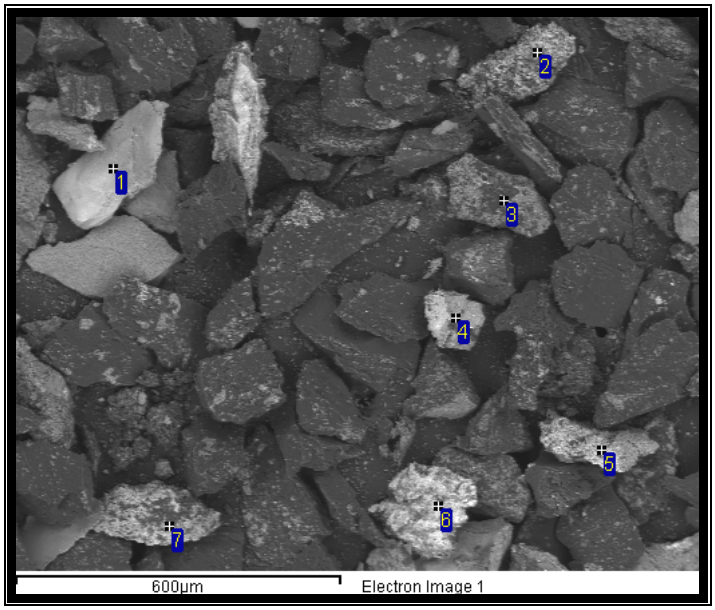


Figure 4. 6: Typical SEM micro-photograph of parent coal.

It can be concluded that coal is very heterogeneous, as even the minerals contained in the coal vary both in composition as well as in the associations in which they occur; which may then alter the behaviour of these minerals during heating under gasification conditions.

### 4.2.6 Calorific value analysis

When coal is gasified, the heat generated from the exothermic combustion reaction of carbon assists the endothermic gasification of the carbon with the various reaction gases. It follows that the calorific value of coal gives an indication of the ability of coal to generate heat to drive the reactions in industrial gasifiers. The results for the calorific values are shown in Table 4.15 for the seven parent coals.

Table 4. 15: Calorific values of parent coals (Gross Calorific value, $MJ.kg^{-1}$, Based on air-dry coal).

| | A | B | C | D | E | F | G |
|---|---|---|---|---|---|---|---|
| **Calorific value** | 21.8 | 17.5 | 20.5 | 19.4 | 17.4 | 23.0 | 21.1 |

Figure 4.7 shows the calorific value as a function of the fixed carbon (air dry base) contained in the coal.

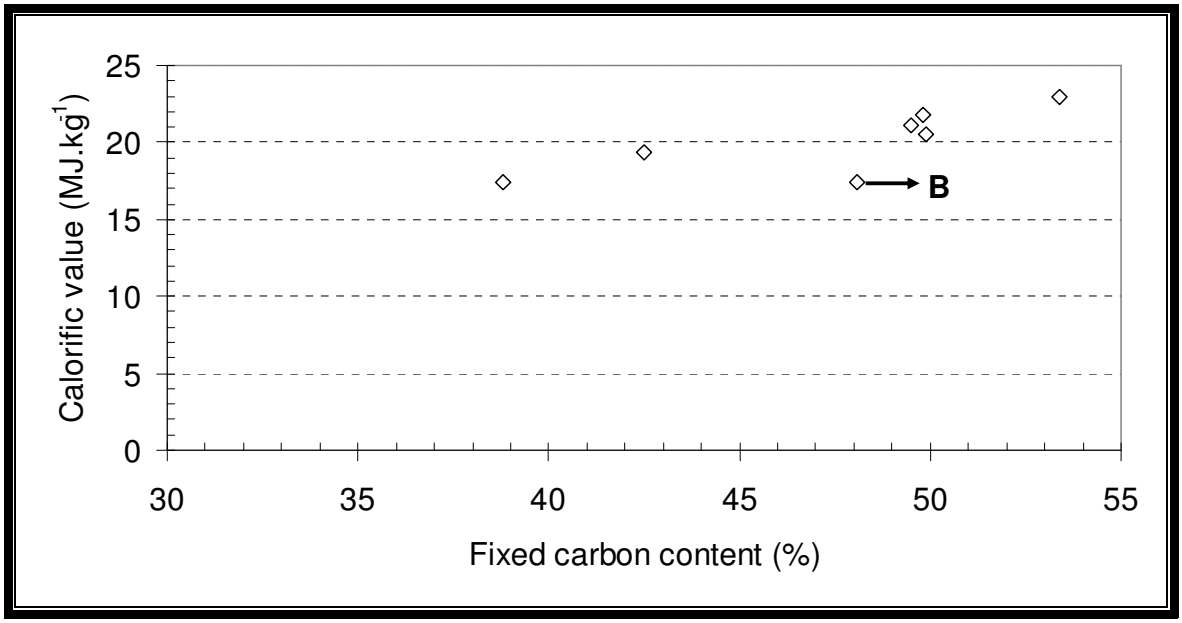


Figure 4. 7: Calorific value as a function of fixed carbon content.

The calorific value increases with an increase in the fixed carbon content, except for one of the coals, coal B which shows a clear deviation from this trend, as it has a calorific value of 17.5 $MJ.kg^{-1}$ and a fixed carbon content of 48.10 % (wt). This calorific value obtained for coal B corresponds to that of coal E which has a much smaller fixed carbon content of 38.8 % (wt) and a calorific value of 17.4 $MJ.kg^{-1}$.

It is hypothesized that the minerals such as kaolinite contained in the carbonaceous shale releases water of crystallization which has a quenching effect on the coal combustion. This effect will be pronounced by the large amount of dense, liberated mineral particles (SG > 2.0 $g.cm^{-3}$) found for coal B compared to coal G as shown in Table 3.3. This motivates further study of coal B, especially the characterization of the density separated fractions as well as the determination of the activation energy associated with the gasification of the density separated fractions obtained from this coal sample.

### 4.2.7 Pyrolysis behaviour

The results obtained for the experiments done on the pyrolysis test-rig are shown in this section. This includes the pyrolysis components as obtained from Fischer analysis as well as an evaluation of the light pyrolysis gases.

**Pyrolysis components**

The Fischer analysis gives the main components that can be obtained from the pyrolysis of coal, including the relative amounts of tar, char, water and gas obtained from this devolatilisation step. The results for the Fischer analysis are presented in Table 4.16.

Table 4. 16: Pyrolysis components of parent coals (Based on weight %).

| Component | A | B | C | D | E | F | G |
|---|---|---|---|---|---|---|---|
| Tar | 2.6 | 2.7 | 2.7 | 2.4 | 4.8 | 5.4 | 2.5 |
| Char | 82.4 | 86.0 | 86.1 | 87.2 | 88.2 | 83.4 | 85.8 |
| Water | 11.6 | 9.0 | 8.3 | 8.4 | 6.0 | 8.9 | 9.5 |
| Gas | 3.4 | 2.3 | 2.9 | 2.0 | 1.0 | 2.3 | 2.2 |

When looking at the amount of tars obtained from the coals, it is clear that coals E and F have a very large tar yield, almost double that of the other coals. The coals are very similar in terms of the char content, although the amount of char as given by the Fischer analysis does not correspond to the combined fixed carbon and ash content as presented by the proximate analysis in Table 4.4. This is due to a lower temperature (600 ºC) used in the pyrolysis experiments compared to that of the proximate analysis (900 ºC). Coal E has the highest char content of 88.2 % (wt); while coal A contains the least amount of char. According to Table 4.8 coal E also contains the largest amount of carbominerite and minerite groups and has the least amount of pure mono-macerals; while coal A has the lowest carbominerite and minerite associations and contains the largest amount of pure mono-macerals. It can be concluded that the amount of char formed increases with increasing carbominerite and minerite associations, and decreases with increasing mono-maceral content. This may be because there is a greater association of the carbon with the minerals as well as a larger content of mineral groups which contributes to the increased char percentage.

It was observed that the largest amount of water is evolved from coal A, and the least amount from coal E. This is in-line with the moisture content of the coal as shown in Table 4.4, as coal A contains the most moisture and coal E contains the least moisture on an air-dried base.

The amount of gas obtained from the coals varies significantly, as coal A has a very large gas yield compared to the other coals, and coal E has the lowest gas yield, which is less than a third compared to coal A.

**Pyrolysis gases**

A detailed analysis of the light gases obtained from the pyrolysis of the seven coal samples was done (on a nitrogen free base) and the results can be seen in Table 4.17. These light gases consist of oxygen, hydrogen as well as the carbon-containing gases: carbon monoxide, carbon dioxide and methane evolved during pyrolysis.

Table 4. 17: Parent coal pyrolysis gas composition (Based on volume %).

| Gas | A | B | C | D | E | F | G |
|---|---|---|---|---|---|---|---|
| $H_2$ | 16.6 | 17.5 | 18.0 | 15.9 | 15.7 | 16.8 | 16.1 |
| $O_2$ | 1.0 | 0.8 | 0.8 | 0.8 | 1.0 | 0.9 | 0.5 |
| CO | 7.3 | 6.0 | 5.9 | 6.6 | 5.9 | 6.5 | 6.9 |
| $CO_2$ | 31.6 | 32.4 | 26.1 | 30.3 | 27.5 | 23.1 | 31.3 |
| $CH_4$ | 43.5 | 43.3 | 49.1 | 46.4 | 49.9 | 52.7 | 45.2 |

The amount of gas obtained from the seven coals does not differ significantly for the different coal samples in terms of hydrogen, oxygen or carbon monoxide evolved. The methane gas yield was observed to make up the bulk of the total pyrolysis gases. Moulijn and Tromp (1985) found that the $C_1 – C_3$ gas yield increases with increasing rank; this trend could not be confirmed in this study as the coals studied in this paper are all of approximately the same rank.

It was observed that the carbon dioxide gas made up the second largest portion of the total pyrolysis gas yield. The carbon dioxide gas yield shows an inversely proportional trend compared to the methane gas yield. Moulijn and Tromp (1985) stated that the yield of oxygen containing groups such as carbon dioxide decreases with an increase in coal rank, which could not be confirmed in the current study.

### 4.2.8 Conclusion

From the analysis of the six single-source coals as well as the gasification coal blend, it was found that all of the coals displayed properties typical of South African coals

derived from the Highveld coal field, being inertinite rich, and high ash coals. The coals were classified as being typical single seam, non-blend coals, varying in rank from Medium rank C bituminous to Medium rank D bituminous coals. Coal G, which is the gasification coal blend, displayed properties typical of coal blends used in the Sasol gasifiers in Secunda (Van Dyk et al., 2001; Wagner et al., 2008). Coal B shows a relatively low calorific value when considering the amount of fixed carbon contained in this coal. This motivates further study into the properties and gasification kinetics of coals B and G, where coal G will represent the benchmark for a typical gasification feed coal.

## 4.3 Characterization results and discussion: Density fractions

The results obtained from the characterization of the density fractions from coals B and G are presented in the following section.

### 4.3.1 Chemical analysis

The proximate and ultimate analyses of the density separated coal fractions are discussed in this section.

**Proximate analysis**

The proximate analysis refers to the relative amounts of moisture, volatile matter, fixed carbon and ash contained in the coal. The results from the proximate analysis of the density fractions derived from coals B and G are shown in Table 4.18.

The range of densities used was between 1.4 $g.cm^{-3}$ and 2.0 $g.cm^{-3}$ and the 5 fractions produced are labelled as follows: floats at 1.4 $g.cm^{-3}$ – B/G 1; sinks at 1.4 $g.cm^{-3}$ floats at 1.6 $g.cm^{-3}$ – B/G 2; sinks at 1.6 $g.cm^{-3}$ floats at 1.8 $g.cm^{-3}$ – B/G 3; sinks at 1.8 $g.cm^{-3}$ floats at 2.0 $g.cm^{-3}$ – B/G 4; and sinks at 2.0 $g.cm^{-3}$ – B/G 5.

Table 4. 18: Proximate analysis of density fractions (Air dry base, based on weight %).

| Composition | B5 | B4 | B3 | B2 | B1 | G5 | G4 | G3 | G2 | G1 |
|---|---|---|---|---|---|---|---|---|---|---|
| Moisture | 2.1 | 3.1 | 3.3 | 3.7 | 4.0 | 1.6 | 2.7 | 3.5 | 4.0 | 4.1 |
| Volatiles | 14.5 | 16.9 | 19.0 | 22.1 | 27.0 | 13.8 | 16.0 | 18.5 | 21.1 | 26.6 |
| Fixed Carbon | 10.4 | 28.0 | 41.5 | 55.2 | 60.1 | 10.7 | 24.6 | 41.2 | 56.3 | 57.5 |
| Ash | 73.0 | 52.0 | 36.2 | 19.0 | 8.9 | 73.9 | 56.7 | 36.8 | 18.6 | 11.8 |

Density separation was able to produce five different coal fractions for both coals, each with varying properties. The two main components in the coal fractions are ash and fixed carbon. The ash is seen to decrease from the densest fraction to the lighter fractions, which is as expected, as more minerals are concentrated in the densest fraction. The fixed carbon increases from the densest to the least dense fractions, and the same trend can be seen for the moisture and volatile matter. This indicates that the volatile matter is more closely associated with the fixed carbon.

**Ultimate analysis**

As previously mentioned, the ultimate analysis refers to the elemental make-up of the coal, including the relative amounts of carbon, hydrogen, nitrogen, sulphur and oxygen (by difference). The results for the ultimate analysis of the density fractions are shown in Table 4.19.

Table 4. 19: Ultimate analysis of density fractions (Dry-ash free, based on weight %).

| Element | B5 | B4 | B3 | B2 | B1 | G5 | G4 | G3 | G2 | G1 |
|---|---|---|---|---|---|---|---|---|---|---|
| Carbon | 47.5 | 68.5 | 77.4 | 83.2 | 85.2 | 43.9 | 64.1 | 76.0 | 82.2 | 82.9 |
| Hydrogen | 4.4 | 4.2 | 3.5 | 3.3 | 3.8 | 4.1 | 3.9 | 3.4 | 3.3 | 3.7 |
| Nitrogen | 0.3 | 1.4 | 1.8 | 2.0 | 2.2 | 0.2 | 1.2 | 1.7 | 2.0 | 2.1 |
| Sulphur | 15.4 | 3.2 | 1.4 | 0.7 | 0.8 | 17.5 | 2.1 | 0.9 | 0.5 | 0.5 |
| Oxygen | 32.4 | 23.1 | 16.0 | 10.7 | 8.1 | 34.3 | 28.7 | 18.1 | 12.1 | 10.8 |

The carbon content shows a decreasing trend with increasing density of coal. This supports the findings from the proximate analysis presented in Table 4.18, as both the fixed carbon and volatile matter contents decrease from the lightest to the heaviest density fractions. The nitrogen content as determined by the ultimate analysis also decreases with increasing density, because the nitrogen is associated with the organic part of the coal; and decreases with increasing density.

When considering the sulphur content of the fractions, it is clear that the heaviest coal fractions contain significantly more sulphur compared to the lighter density fractions. This observation may be due to the increased content of sulphur bearing minerals such as pyrite in the more dense coal fractions. The oxygen content of the coals shows an almost linear increase with increasing coal density. It is also suggested that this observation is due to the increased minerals content of the more dense fractions, especially of the clay, quartz and carbonate-containing mineral groups.

Overall it can be concluded that the chemical properties of the corresponding density fractions for both coals do not show significant differences; again emphasizing the similarity of the coals derived from the number 4 seam of the Highveld coal field.

### 4.3.2 Petrographic analysis

The results obtained from the petrographic analysis of the density separated coal fractions are presented in this section, and includes the maceral, microlithotype and carbominerite compositions.

**Maceral analysis**

Table 4.20 shows the maceral composition of the density fractions. Inertinite makes up the bulk of the maceral groups for each density fraction of coals B and G, and there is no real difference in the inertinite content of the corresponding fractions. Both of these coals show the same trend, as the inertinite content increases from the # 1 to the # 4 fraction, and then decreases in the densest fraction.

Vitrinite is the second most prominent maceral group observed, and shows the opposite trend to that seen in the inertinites, as the vitrinite content decreases from the # 1 to the # 3 fraction, and then increases to the # 5 fraction. Coal G contains more vitrinite in all the fractions compared to coal B. When looking at the liptinite group, it is clear that this makes up the smallest part of the macerals in each case.

Table 4. 20: Maceral content of density fractions (Mineral matter free, based on volume %).

| Maceral group | B5 | B4 | B3 | B2 | B1 | G5 | G4 | G3 | G2 | G1 |
|---|---|---|---|---|---|---|---|---|---|---|
| Vitrinite | 11.1 | 7.8 | 4.6 | 8.8 | 32.3 | 18.2 | 8.4 | 5.2 | 9.4 | 34.7 |
| Liptinite | 2.8 | 0.4 | 3.1 | 7.1 | 4.9 | 0 | 2.3 | 4.3 | 7.0 | 6.3 |
| Reactive SF | 0 | 2.6 | 1.3 | 3.5 | 7.8 | 4.5 | 5.1 | 0.8 | 5.3 | 4.8 |
| Inert SF | 11.1 | 11.2 | 20.3 | 34.7 | 33.5 | 13.6 | 11.2 | 21.7 | 39.2 | 35.8 |
| Fusinite | 0 | 1.9 | 0.5 | 2.6 | 2.7 | 0 | 2.3 | 1.9 | 0.2 | 1.9 |
| Micrinite | 0 | 0 | 0 | 0.9 | 0.6 | 0 | 3.3 | 1.4 | 1.7 | 2.5 |
| Reactive Inerto | 0 | 0 | 0.8 | 2.6 | 2.0 | 0 | 1.9 | 0.8 | 1.7 | 0.6 |
| Inert Inerto | 75.0 | 76.2 | 69.4 | 39.7 | 16.2 | 63.6 | 65.4 | 63.9 | 35.4 | 13.3 |
| Total inertinite | 86.1 | 91.8 | 92.3 | 84.1 | 62.8 | 81.8 | 89.3 | 90.5 | 83.6 | 58.9 |

Inerto: Inertodetrinite, SF: Semi-fusinite.

According to Borrego et al. (1997) the density of maceral groups may vary from heaviest to lightest in the order: inertinite > vitrinite > liptinite. These trends can be seen here as the inertinite macerals tend to concentrate to the densest fraction, while the vitrinite and liptinite concentrates towards the least dense fraction. As the density is influenced by the minerals in the coal; these trends can only be taken as a qualitative indication of the density segregation of the maceral groups. The overall maceral make-up of each fraction is in-line with the petrographic make-up of the parent coals as presented in Table 4.7, as inertinite makes up the bulk, followed by vitrinite and liptinite groups.

**Microlithotype analysis**

The results obtained from the microlithotype evaluation of the density fractions are presented in this section. This includes the mono-macerals, intermediates, carbominerite and minerite groups. Table 4.21 shows the results for both coals.

The inertite mono-maceral group makes up the bulk of the microlithotypes in each fraction, except for the mineral-rich # 5 fraction. The inertite content concentrates towards the heavier density fractions, reaching a peak in the # 3 and 2 fractions.

Table 4. 21: Microlithotype content of density fractions (Mineral matter basis, based on volume %).

| Microlithotype | B5 | B4 | B3 | B2 | B1 | G5 | G4 | G3 | G2 | G1 |
|---|---|---|---|---|---|---|---|---|---|---|
| Vitrite | 0.8 | 3.0 | 2.2 | 4.4 | 19.2 | 1.0 | 1.2 | 1.6 | 4.4 | 22.6 |
| Liptite | 0 | 0 | 0 | 0 | 0.8 | 0 | 0 | 0.4 | 0.6 | 0.4 |
| Semi-Fusite | 1.4 | 4.4 | 9.0 | 26.2 | 30.4 | 1.4 | 4.0 | 10.8 | 29.8 | 25.0 |
| Fusite | 0 | 0 | 0.6 | 1.2 | 0 | 0 | 0.6 | 1.8 | 1.2 | 3.6 |
| Inertodetrite | 4.0 | 42.4 | 63.0 | 40.6 | 16.8 | 2.2 | 35.8 | 61.0 | 43.0 | 22.8 |
| Total Inertite | 5.4 | 46.8 | 72.6 | 68.0 | 47.2 | 3.6 | 40.4 | 73.6 | 74.0 | 51.4 |
| Vitrinertite | 0 | 3.0 | 2.4 | 8.6 | 12.0 | 0.4 | 1.8 | 2.0 | 7.0 | 10.4 |
| Clarite | 0 | 0.4 | 0.2 | 0.4 | 2.2 | 0.2 | 0 | 0 | 0.4 | 1.6 |
| Durite | 0 | 0.4 | 3.2 | 5.8 | 3.8 | 0.2 | 1.4 | 3.4 | 4.6 | 3.0 |
| Tri-macerite | 0.2 | 0.2 | 2.0 | 2.8 | 8.4 | 0 | 0.4 | 1.2 | 1.4 | 5.0 |
| Total Inter | 0.2 | 4.0 | 7.8 | 17.6 | 26.4 | 0.8 | 3.6 | 6.6 | 13.4 | 20.0 |
| Carbominerite | 9.0 | 35.6 | 15.6 | 9.8 | 5.4 | 6.0 | 30.2 | 13.0 | 7.6 | 5.6 |
| Minerite | 84.6 | 10.6 | 1.8 | 0.2 | 1.0 | 88.6 | 24.6 | 4.8 | 0 | 0 |

Inter: Intermediate.

The vitrite mono-maceral is mainly found in the lowest density fraction, with minor inclusions in the other 4 fractions. The liptinite containing mono-maceral known as liptite was observed in very small amounts. For coal B, liptinite was only seen in the # 1 fraction, while for coal G observations of liptite was made in the # 1, 2 and 3 fractions; in each case below 1 % (vol).

The intermediate groups consisting of maceral-maceral associations show a steady decrease from the lightest to the heaviest fraction. On average, coal B contains more intermediate groups compared to coal G. It can also be seen from the proximate analysis in Table 4.18 that the volatile matter content correlates with the intermediates content of the coal fractions; as an increase in the intermediate groups lead to increased volatile matter content. The most prominent intermediate group was found to be the combined vitrinite and inertinite containing group known as vitrinertite.

The carbominerite groups, referring to the maceral-mineral associations (5 % (vol) to 60 % (vol) minerals) show a steady increase from the lightest to the heaviest fraction, but then drops in the most dense fractions. This again shows the tendency of the

mineral groups to concentrate towards the heavy density fractions. The minerite groups increase from the lightest to the heaviest density fractions, with an almost exponential increase observed into these heavy fractions, as most of the mineral matter is concentrated in these fractions.

Overall it can be concluded that there is an increase in mineral-containing groups from the lightest to the heaviest density fractions, while the opposite trend is observed for the mono-maceral and intermediate groups. This shows the effectiveness of density separation to segregate and concentrate mineral and organic matter into separate fractions.

**Carbominerite**

Table 4.22 shows the results obtained from the carbominerite analysis for each of the density fractions.

Table 4. 22: Carbominerite content of density fractions (based on volume %).

| Group | B5 | B4 | B3 | B2 | B1 | G5 | G4 | G3 | G2 | G1 |
|---|---|---|---|---|---|---|---|---|---|---|
| C-Arg & C-Sil | 6.0 | 31.6 | 11.1 | 4.2 | 0.8 | 2.8 | 24.0 | 9.2 | 2.8 | 3.0 |
| Carbo-pyrite | 2.2 | 2.8 | 0.4 | 0.6 | 0.8 | 1.6 | 4.2 | 1.2 | 0.4 | 0.4 |
| Carb-ankerite | 0.8 | 1.2 | 4.1 | 5.0 | 3.8 | 1.6 | 2.0 | 2.6 | 4.4 | 2.2 |
| Total | 9.0 | 35.6 | 15.6 | 9.8 | 5.4 | 6.0 | 30.2 | 13.0 | 7.6 | 5.6 |

C-Arg: carb-argillite, C-Sil: carbo-silicate.

From this table it is clear that similar trends are observed for the carbominerite groups for the corresponding density fractions of both coals. The carb-argillite and carbo-silicate groups make up the bulk of the total carbominerite content for both coals. The combined carb-argillate and carbo-silicate groups increase towards the dense fractions, reaching a peak in the # 4 density fraction. The same trend is observed for carbo-pyrite. Carb-ankerite shows the opposite trend as it increases towards the less dense fractions, reaching a peak in the # 2 fraction.

### 4.3.3 Mineral analysis

The results obtained from the mineral evaluation of the density fractions are discussed in this section. This includes the mineral forms as detected by QEMSCAN, as well as the elemental composition of the ash as determined by X-ray fluorescence.

**QEMSCAN**

QEMSCAN evaluation gives an accurate indication of the different minerals contained in the coal density fractions, making it more applicable compared to the X-ray diffraction characterization. Table 4.23 gives the results from the QEMSCAN analysis for both of the coals.

Table 4. 23: Mineral composition of density fractions (Mineral matter base, based on weight %).

| Mineral | B5 | B4 | B3 | B2 | B1 | G5 | G4 | G3 | G2 | G1 |
|---|---|---|---|---|---|---|---|---|---|---|
| Alunite | 3.8 | 5.1 | 12.0 | 14.0 | 12.0 | 1.0 | 0.9 | 2.5 | 7.9 | 20.9 |
| Pyrite | 8.2 | 3.3 | 1.5 | 0.9 | 0.9 | 12.7 | 3.4 | 1.1 | 2.0 | 0.7 |
| Siderite | 0 | 0 | 0 | 0 | 0.9 | 0 | 0 | 0 | 0.4 | 0 |
| Calcite | 6.0 | 1.8 | 2.4 | 3.1 | 4.3 | 5.6 | 3.2 | 2.3 | 4.7 | 2.7 |
| Dolomite | 2.0 | 2.5 | 10.5 | 32.5 | 31.6 | 1.0 | 3.2 | 9.5 | 23.6 | 22.3 |
| Apatite | 0.2 | 0.1 | 0 | 3.1 | 2.6 | 0 | 0.1 | 0.2 | 1.2 | 2.0 |
| Kaolinite | 50.1 | 57.0 | 40.2 | 23.7 | 23.1 | 48.3 | 53.5 | 53.5 | 39.0 | 22.3 |
| Quartz | 18.9 | 17.2 | 17.1 | 9.2 | 13.7 | 25.1 | 28.3 | 22.6 | 12.6 | 10.8 |
| Illite | 0.7 | 1.9 | 4.1 | 6.6 | 1.7 | 0.1 | 0.5 | 1.5 | 1.6 | 1.4 |
| Muscovite | 5.3 | 6.7 | 7.8 | 2.6 | 1.7 | 2.0 | 3.4 | 3.6 | 2.0 | 2.0 |
| Microline | 1.4 | 0.6 | 1.5 | 1.3 | 0.9 | 1.1 | 0.5 | 0.8 | 0.8 | 1.4 |
| Rutile | 2.8 | 3.1 | 2.0 | 0.9 | 0.9 | 2.7 | 2.6 | 1.7 | 1.2 | 0.7 |
| Other | 0.5 | 0.4 | 1.0 | 2.2 | 5.1 | 0.5 | 0.3 | 0.6 | 3.9 | 13.5 |

From this table it is clear that the bulk of the minerals are made up of kaolinite and quartz, which is in-line with the parent coal mineral analysis as presented in Table 4.10. These two minerals can be seen to concentrate towards the more dense fractions, and is in-line with the results from the carbominerite analysis, which also found the carb-argillite and carbo-silicate groups to increase into the more dense fractions as shown in Table 4.22. Dolomite also contributes significantly to the total minerals content, especially concentrating towards the less dense fractions; corresponding with the results for the calcium-containing carb-ankerite groups as shown in Table 4.22.

This supports the findings of Oki et al. (2004), who stated that dolomite is a low density mineral found in coal.

Alunite is an aluminium-sulphate group which is formed by sulphuric acid (possibly from mine drainage) reacting with microline minerals. This mineral group is concentrated in the least dense fractions. When looking at the illite contained in the density fractions, it can be seen that this mineral shows a spread across the different densities, peaking at a density of 1.4 $g.cm^{-3}$ – 1.6 $g.cm^{-3}$ (sample fraction # 3). Another observation is that coal B contains significantly more illite compared to coal G.

Pyrite is of interest as many researchers (Nishiyama, 1986; Kyotani et al., 1993; Samaras et al., 1996; Liu et al., 2000b; Ochoa et al., 2001; Lemaignen et al., 2002; Yücel et al., 2007) have found that this mineral, along with calcium, may act as catalyst in the gasification of coal. Pyrite tends to increase towards the more dense fractions showing an almost exponential trend. This observation correlates with the results from the carbominerite analysis which found that the carbo-pyrite also increases towards the more dense fractions (Table 4.22). The calcite contained in the density fractions does not show any trend. For both coals the calcite reaches a maximum in the densest fraction.

Muscovite, which is another clay mineral; shows a spread distribution across the density fractions, and reaches a peak in the # 4 fraction for both coals. Rutile is a relatively high density mineral, as seen in its distribution towards the heavier density fractions. Apatite, also a calcium-containing mineral, is rarely observed in any of the fractions, with the largest concentrations seen in the # 2 and # 1 fractions for both coals. Siderite contributes the smallest amount to the total mineral content of the density fractions, as it was only found in the # 1 and # 2 fractions for coals B and G respectively.

In order to evaluate the influence of separate elements on the gasification behaviour of the coals; a mole balance was performed on the mineral make-up as detected by the QEMSCAN analysis and is presented in Table 4.24.

Table 4. 24: Elemental composition of minerals in density fractions (mole %).

| | B1 | B2 | B3 | B4 | B5 | G1 | G2 | G3 | G4 | G5 |
|---|---|---|---|---|---|---|---|---|---|---|
| **Ti** | 0.9 | 1.1 | 2.0 | 3.1 | 2.6 | 0.9 | 1.3 | 1.5 | 2.0 | 2.1 |
| **O** | 43.6 | 45.0 | 42.3 | 42.2 | 40.3 | 43.5 | 44.1 | 42.2 | 40.5 | 38.4 |
| **Ca** | 8.1 | 9.0 | 3.0 | 1.4 | 3.2 | 6.9 | 6.9 | 2.4 | 1.6 | 2.4 |
| **C** | 4.1 | 4.5 | 1.4 | 0.5 | 1.0 | 3.4 | 3.3 | 1.1 | 0.6 | 0.8 |
| **Mg** | 3.3 | 3.9 | 1.0 | 0.2 | 0.2 | 2.8 | 2.5 | 0.8 | 0.2 | 0.1 |
| **Al** | 3.5 | 4.6 | 5.5 | 6.7 | 5.3 | 4.8 | 5.2 | 5.2 | 4.4 | 4.2 |
| **Si** | 33.7 | 28.5 | 41.8 | 42.4 | 41.1 | 33.8 | 33.6 | 45.6 | 48.4 | 44.5 |
| **K** | 0.4 | 0.6 | 0.4 | 0.2 | 0.1 | 0.7 | 0.3 | 0.1 | 0.1 | 0.0 |
| **H** | 0.3 | 0.3 | 0.4 | 0.5 | 0.4 | 0.3 | 0.4 | 0.4 | 0.3 | 0.3 |
| **Fe** | 0.7 | 0.3 | 0.4 | 0.8 | 1.7 | 0.2 | 0.7 | 0.2 | 0.6 | 2.3 |
| **S** | 1.4 | 1.9 | 1.7 | 2.1 | 4.1 | 2.5 | 1.7 | 0.6 | 1.4 | 5.1 |
| **P** | 0.2 | 0.2 | 0.0 | 0.0 | 0.0 | 0.1 | 0.1 | 0.0 | 0.0 | 0.0 |

The elemental make-up of the density fractions of these two coals do not differ significantly, although coal B contains slightly more calcium than coal G, especially in the least dense fractions.

### X-ray Fluorescence

The XRF analysis is used to determine the elemental composition of the ash. The ash is mainly made-up of metallic oxides. The results from the XRF analysis are shown in Table 4.25.

Table 4. 25: Density fractions ash chemistry. (Mineral matter basis, based on weight %).

| Element | B5 | B4 | B3 | B2 | B1 | G5 | G4 | G3 | G2 | G1 |
|---|---|---|---|---|---|---|---|---|---|---|
| $SiO_2$ | 57.4 | 54.4 | 51.1 | 42.7 | 58.0 | 60.6 | 57.3 | 56.9 | 48.9 | 44.1 |
| $Al_2O_3$ | 23.8 | 31.0 | 31.7 | 31.1 | 20.9 | 28.5 | 29.1 | 29.9 | 28.7 | 30.8 |
| $Fe_2O_3$ | 5.8 | 2.3 | 1.7 | 1.7 | 6.3 | 1.6 | 1.5 | 1.5 | 1.1 | 1.2 |
| $TiO_2$ | 1.3 | 1.7 | 1.6 | 1.4 | 1.2 | 1.4 | 1.6 | 1.5 | 1.5 | 1.8 |
| $P_2O_5$ | 0.5 | 0.7 | 0.9 | 1.9 | 0.4 | 0.4 | 0.5 | 0.5 | 1.4 | 2.2 |
| CaO | 4.0 | 3.7 | 5.8 | 11.1 | 5.5 | 3.3 | 5.2 | 5.0 | 9.5 | 10.1 |
| MgO | 0.8 | 1.5 | 2.5 | 5.0 | 0.7 | 1.1 | 2.2 | 2.2 | 4.0 | 4.0 |
| $K_2O$ | 0.8 | 0.8 | 1.0 | 0.6 | 0.6 | 0.5 | 0.4 | 0.4 | 0.2 | 0.3 |
| $SO_3$ | 5.6 | 3.9 | 3.6 | 4.5 | 6.4 | 2.4 | 2.3 | 1.9 | 4.6 | 5.4 |
| MnO | 0.0 | 0.0 | 0.0 | 0.1 | 0.0 | 0.0 | 0.0 | 0.0 | 0.1 | 0.1 |

The main contribution to the chemical make-up of the ash is made by $SiO_2$ and $Al_2O_3$. This observation is in-line with the large amount of clay and quartz minerals, as well as alunite contained in the coal fractions as shown in Table 4.23. The third most prominent species detected is CaO, as it contributes to between 3.3 % (wt) and 11.1 % (wt) to the total ash content. This is associated with the calcite and dolomite mineral groups, as these are the main calcium-bearing minerals contained in coal. Magnesium oxide was detected in various quantities in the different density fractions; where the main source of MgO in the coal ash is the mineral group known as dolomite.

The $Fe_2O_3$ as detected by the XRF analysis is associated with the pyrite mineral group as shown in Table 4.23. Coal B contains significantly more iron compared to coal G, especially when looking at the most and least dense fractions. The $SO_3$ found in the coal ash is associated with the pyrite mineral group; as this mineral consists of iron and sulphur, where the iron is converted to iron oxides and the sulphur is driven off as $SO_2$, which may be captured by the calcium bearing minerals as $CaSO_4$

### 4.3.4 Ash fusion analysis

Ash fusion tests are done as to determine the different melting temperatures associated with ash transformation. The results from the ash fusion tests, done in a reducing gas atmosphere, are shown in Table 4.26 and include the deformation, sphere, hemisphere and flow temperatures associated with the ash samples. When considering the ash fusion tests, the most important parameter to consider is the ash flow temperature, as this is the temperature at which non-slagging gasifiers start to experience problems due to ash clinker formation and channel burning (Van Dyk and Waanders, 2007).

Table 4. 26: Ash fusion temperatures of density fractions (Specified in ºC).

| Temperature | B5 | B4 | B3 | B2 | B1 | G5 | G4 | G3 | G2 | G1 |
|---|---|---|---|---|---|---|---|---|---|---|
| Deformation | 1300 | 1280 | 1510 | 1450 | 1320 | 1300 | 1520 | 1440 | 1300 | 1320 |
| Sphere | 1320 | 1300 | 1530 | 1460 | 1330 | 1330 | 1550 | 1470 | 1310 | 1330 |
| Hemisphere | 1320 | 1320 | 1550 | 1470 | 1340 | 1360 | 1580 | 1500 | 1320 | 1340 |
| Flow | 1340 | 1340 | 1570 | 1480 | 1350 | 1410 | 1600 | 1540 | 1340 | 1350 |

The flow temperatures range from 1340 ºC to 1600 ºC for both coals. It follows that coal B has a much lower ash flow temperature in the two densest fractions (fractions # 4 and # 5) compared to coal G. This can be associated with the ash chemistry, as coal B contains significantly more $Fe_2O_3$ compared to coal G, with the differences more pronounced in the densest fraction as shown in Table 4.25. Waanders and Govender (2005) stated that pyrite acts as a fluxing mineral and contributes to lowering the ash flow temperature. This can be seen in this study, as the coal fractions containing more $Fe_2O_3$ have lower ash flow temperatures.

This difference in ash-flow temperatures might be an explanation to the problem experienced with coal blends containing larger portions of coal B, because if the ash were to melt, it will encapsulate the carbon particles preventing the gasification reactions from taking place and in turn lead to decreased carbon efficiency in the gasifier. This effect will be more pronounced in coal B, as coal B contains significantly more material in the # 4 and # 5 fractions compared to coal G, as seen in Table 3.3.

### 4.3.5 Structural analysis

The specific surface area of the density fractions was obtained by means of carbon dioxide gas adsorption experiments for the raw coals, as well as the chars prepared at 1000 ºC; the results are shown in Table 4.27. Also shown in this table is the surface area as detected by nitrogen gas adsorption as well as the porosity of the samples as calculated from mercury intrusion data.

As previously mentioned, several researchers (Castellò et al., 2002; Hurt et al., 1991; Nandi and Walker, 1964; Debelak and Schrodt, 1979) have stated that the use of carbon dioxide as adsorbent gas gives a good indication of the micro-pore surface area of coals, while the nitrogen gas adsorption indicates the meso-pore surface area of these coals. From Table 4.27 it is clear that the micro-pore surface area increases with decreasing density.

Table 4. 27: Specific surface area of density fractions.

| Property | B5 | B4 | B3 | B2 | B1 | G5 | G4 | G3 | G2 | G1 |
|---|---|---|---|---|---|---|---|---|---|---|
| $S_{CO2}$ ($m^2.g^{-1}$) | 38.0 | 65.9 | 102.6 | 138.9 | 142.6 | 35.4 | 56.7 | 88.8 | 123.6 | 132.3 |
| $S_{CHAR}$ ($m^2.g^{-1}$) | 39.3 | 74.7 | 53.0 | 34.3 | 31.8 | 36.1 | 59.3 | 52.5 | 40.5 | 35.5 |
| $S_{N2}$ ($m^2.g^{-1}$) | 4.1 | 6.0 | 3.5 | 0.5 | 0.2 | 3.6 | 3.8 | 2.6 | 1.1 | 0.8 |
| $V_{N2}$ ($10^{-3}$ $cm^3.g^{-1}$) | 9.2 | 13.8 | 8.9 | 2.7 | 0.5 | 8.9 | 9.1 | 12.1 | 3.4 | 3.1 |
| $V_{MP}$ ($10^{-3}$ $cm^3.g^{-1}$) | 1.3 | 0.7 | 0.8 | 2.4 | 0.1 | 0.9 | 1.8 | 1.8 | 1.4 | 1.0 |
| $D_{avg}$ (Å) | 101.8 | 100.2 | 110.6 | 274.5 | 244.8 | 108.2 | 109.1 | 202.6 | 138.5 | 154.6 |
| Porosity (%) | 12.3 | 17.6 | 11.3 | 15.0 | 14.7 | 12.1 | 14.1 | 17.5 | 14.6 | 19.5 |

$S_{CO2}$ : Applies Dubinin Radushkevich method, $S_{N2}$: Applies Brunauer-Emmett-Teller method, $V_{N2}$: adsorption pore volume determined by nitrogen adsorption, $V_{MP}$: micro-pore volume, $D_{Avg}$: average pore diameter determined by nitrogen adsorption.

This is expected, as the lighter fractions contain more fixed carbon as well as greater amounts of vitrinite, and therefore has more micro-pores compared to the mineral-rich fractions. It can also be seen from Table 4.18 that the moisture content increases with increasing micro-pore surface area, which supports the findings of Takarada et al. (1985), which stated that the moisture content gives an indication of the porosity of the coal. It is clear that there is no significant difference between the $CO_2$ surface areas of the corresponding density fractions obtained from coals B and G.

From Table 4.27 it is seen that the coal pyrolysis at 1000 ºC for 1 hour has altered the coals structurally, with the effects more pronounced for coal fractions having densities of less than 1.8 $g.cm^{-3}$ (fractions # 1 - # 3) as observed for both coals. There is a clear decrease in the micro-pore surface area seen in the # 1 - # 3 fractions, while the # 4 and # 5 fractions do not show significant change. This decrease in surface area can be explained by the fact that heating bituminous coals leads to a poor pore structure due to pore closure, increased graphitic nature of the coal, and the alignment of poly-condensed aromatic molecules (Liu et al., 2006; Liu et al., 2004; Centeno et al., 2001). This behaviour is more enhanced in coals with thermoplastic properties and in high volatile-containing coals (Yücel et al., 2007; Liu et al., 2004; Centeno et al., 2001; Liu et al., 2000a; Tsai and Scaroni, 1987). The sharp decrease in the micro-pore surface area for the # 1 - # 3 fractions is evidence of this, as these fractions contain more volatile matter and fixed carbon (Table 4.18) compared to the # 4 and 5 fractions. Similar observations were made by Salatino and Senecca (1998) who found

that micro-porosity decreases during pyrolysis, especially with pyrolysis times in excess of one hour. There is a trend between the inert inertodetrinite (Table 4.20) and the degree to which the surface area decreases. This is because inert inertodetrinite is known to form dense chars during pyrolysis (Falcon and Snyman, 1986).

It is observed that the surface area detected by carbon dioxide gas adsorption is much larger than the surface area detected by nitrogen gas adsorption, which is due to slow diffusion of nitrogen into pores with diameters of less than 5 Å (Nandi and Walker, 1964). The surface area as determined by nitrogen gas adsorption shows the opposite trend as that observed for the carbon dioxide gas adsorption. This observation may be due to the more dense fractions containing more meso-pores as a result of increased mineral-organic associations. This indicates the presence of more feeder pores in these mineral-rich fractions compared to the lighter fractions.

The average pore diameter for each of the fractions fall within the limits for meso-pores (20 Å – 500 Å). Fractions B2 and B1 have significantly larger pore diameters compared to the other fractions. The porosity of the coal fractions is seen to vary from 11.3 % to 19.5 %. There are no trends between density and the porosity of the samples; and the surface properties of the coals as measured by gas adsorption do not correlate with the porosity as detected by mercury intrusion. This is because the mercury intrusion gives an indication of the macro-porous nature of coal, while gas adsorption detects micro-pores (carbon dioxide adsorption) and meso-pores (nitrogen adsorption) (Wildman and Derbyshire, 1991). According to Friesen and Mikula (1988) mercury porosimetry is subject to simultaneous pore filling and compression of the coal sample, and can only be taken as a qualitative indication of the macro-porous nature of coal.

### 4.3.6 Calorific value analysis

The results obtained for the calorific values of the various density fractions is shown in Table 4.28 for both coals. The results are presented as the gross calorific value.

Table 4. 28: Calorific values of density fractions (Gross calorific value, $MJ.kg^{-1}$, Based on air-dry coal).

| | B5 | B4 | B3 | B2 | B1 | G5 | G4 | G3 | G2 | G1 |
|---|---|---|---|---|---|---|---|---|---|---|
| **Calorific Value** | 3.3 | 9.8 | 16.6 | 23.5 | 28.3 | 3.5 | 8.5 | 15.8 | 23.2 | 26.4 |

From this table it can be observed that the calorific value increases with decreasing density. The corresponding fractions from the two coals have similar calorific values, and in each case the heat that can be obtained from the least dense fraction is approximately ten times larger than the densest fraction. These results can be correlated with the fixed carbon contained in the fractions, as the calorific value increases with increasing fixed carbon content in Figure 4.8. Also shown in this figure is the calorific value of the parent coals as a function of fixed carbon content.

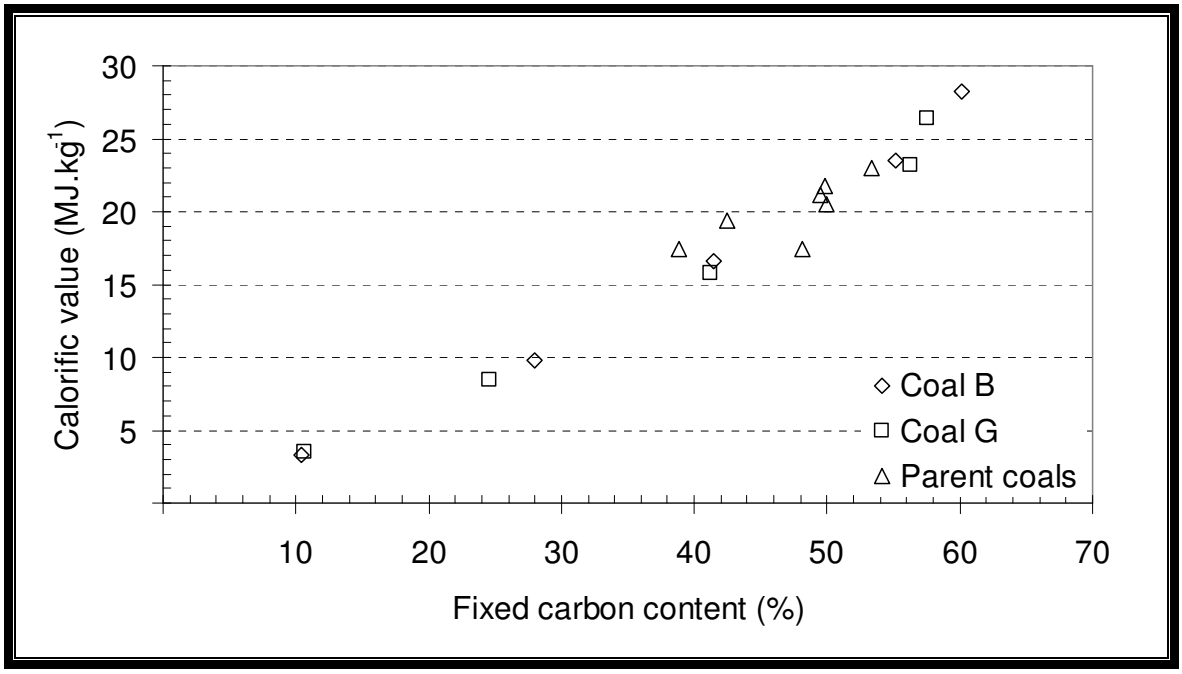


Figure 4. 8: Calorific value as a function of fixed carbon content after density separation.

It can be seen that the amount of heat that can be obtained increases with increasing fixed carbon content, which is due to the ash content of the coals having an inversely proportional trend compared to the fixed carbon (Table 4.18). This results in the high density coals containing less fuel (carbon) to generate heat in the combustion reaction.

In Section 4.2.6 it was hypothesized that coal B has a lower calorific value due to minerals such as kaolinite and carbonaceous shale releases water of crystallization, which has a quenching effect on the coal combustion. This is true, as Table 3.3 and

Table 4.28 shows that coal B contains significantly more material in the high density, low energy fraction (SG > 2.0 g.cm$^{-3}$) compared to coal G. Coal B also contains less material in the less dense, high energy fractions (SG < 1.6 g.cm$^{-3}$). It can therefore be said that it is not so much what is in the coal fractions, but rather the contribution of each fraction to the behaviour of the parent coals that affect the gasification behaviour of coals in industrial gasification processes.

### 4.3.7. Conclusion

Characterization of the density separated fractions showed several trends relating coal properties to coal density as shown in a summary in Table 4.29. In the chemical analysis it was found that the ash increases and fixed carbon decreases with increasing particle density. It is concluded that the volatile matter is associated with the fixed carbon as well as total carbon, as these constituents follow similar trends, increasing towards the less dense fractions. Nitrogen is also related to the volatile/organic part of the coals, as this element is concentrated towards the less dense coal fractions. The bulk of the sulphur and oxygen detected in the samples are associated with minerals such as pyrite, clay and quartz groups respectively.

From the petrographic analysis, it was found that the main maceral group is inertinite, followed by vitrinite and then liptinite. This separation qualitatively indicates the degree of maceral segregation as a function of particle density. An evaluation of the microlithotypes supported the maceral analysis, as the inertinite-containing inertite group made up the bulk of the microlithotypes, except in the +2 g.cm$^{-3}$ fraction, where minerite is the main microlithotype.

The bi-and-tri maceral groups increase towards the less dense fractions, and consist mainly of the vitrinertinite bi-maceral group. Carbominerite and minerite groups increase with increasing particle density, with carbominerite reaching a peak in the 1.8 g.cm$^{-3}$ – 2.0 g.cm$^{-3}$ fraction. The mineral component consists mainly of clay and quartz groups, which are related to the kaolinite and quartz minerals, with significant observations of carbonate groups related to dolomite in the less dense coal fractions. The two densest fractions of coal B have significantly lower ash flow temperatures compared to the corresponding fractions of coal G.

Table 4. 29: Summary of density separated coal properties.

| | B5 | B4 | B3 | B2 | B1 | G5 | G4 | G3 | G2 | G1 |
|---|---|---|---|---|---|---|---|---|---|---|
| **Yield (wt %)** | 15.6 | 8.1 | 17.9 | 41.0 | 17.4 | 10.2 | 7.0 | 13.6 | 37.1 | 32.1 |
| **Proximate analysis (wt %, dry base)** | | | | | | | | | | |
| **Moisture** | 2.1 | 3.1 | 3.3 | 3.7 | 4.0 | 1.6 | 2.7 | 3.5 | 4.0 | 4.1 |
| **Volatiles** | 14.5 | 16.9 | 19.0 | 22.1 | 27.0 | 13.8 | 16.0 | 18.5 | 21.1 | 26.6 |
| **Fixed Carbon** | 10.4 | 28.0 | 41.5 | 55.2 | 60.1 | 10.7 | 24.6 | 41.2 | 56.3 | 57.5 |
| **Ash** | 73.0 | 52.0 | 36.2 | 19.0 | 8.9 | 73.9 | 56.7 | 36.8 | 18.6 | 11.8 |
| **Gross calorific value (MJ/kg)** | 3.3 | 9.8 | 16.6 | 23.5 | 28.3 | 3.5 | 8.5 | 15.8 | 23.2 | 26.4 |
| **Ultimate analysis (wt %, daf)** | | | | | | | | | | |
| **Carbon** | 47.5 | 68.5 | 77.4 | 83.2 | 85.2 | 43.9 | 64.1 | 76.0 | 82.2 | 82.9 |
| **Hydrogen** | 4.4 | 4.2 | 3.5 | 3.3 | 3.8 | 4.1 | 3.9 | 3.4 | 3.3 | 3.7 |
| **Nitrogen** | 0.3 | 1.4 | 1.8 | 2.0 | 2.2 | 0.2 | 1.2 | 1.7 | 2.0 | 2.1 |
| **Sulphur** | 15.4 | 3.2 | 1.4 | 0.7 | 0.8 | 17.5 | 2.1 | 0.9 | 0.5 | 0.5 |
| **Oxygen** | 32.4 | 23.1 | 16.0 | 10.7 | 8.1 | 34.3 | 28.7 | 18.1 | 12.1 | 10.8 |
| **Maceral analysis (vol %, mmf)** | | | | | | | | | | |
| **Vitrinite** | 11.1 | 7.8 | 4.6 | 8.8 | 32.3 | 18.2 | 8.4 | 5.2 | 9.4 | 34.7 |
| **Liptinite** | 2.8 | 0.4 | 3.1 | 7.1 | 4.9 | 0 | 2.3 | 4.3 | 7.0 | 6.3 |
| **Inertinite** | 86.1 | 91.8 | 92.3 | 84.1 | 62.8 | 81.8 | 89.3 | 90.5 | 83.6 | 58.9 |

| (Table 4.29 Continued) | B5 | B4 | B3 | B2 | B1 | G5 | G4 | G3 | G2 | G1 |
|---|---|---|---|---|---|---|---|---|---|---|
| **Microlithotype analysis (vol %, mmb)** | | | | | | | | | | |
| **Vitrite** | 0.8 | 3.0 | 2.2 | 4.4 | 19.2 | 1.0 | 1.2 | 1.6 | 4.4 | 22.6 |
| **Liptite** | 0 | 0 | 0 | 0 | 0.8 | 0 | 0 | 0.4 | 0.6 | 0.4 |
| **Inertite** | 5.4 | 46.8 | 72.6 | 68.0 | 47.2 | 3.6 | 40.4 | 73.6 | 74.0 | 51.4 |
| **Intermediate** | 0.2 | 4.0 | 7.8 | 17.6 | 26.4 | 0.8 | 3.6 | 6.6 | 13.4 | 20.0 |
| **Carbominerite** | 9.0 | 35.6 | 15.6 | 9.8 | 5.4 | 6.0 | 30.2 | 13.0 | 7.6 | 5.6 |
| **Minerite** | 84.6 | 10.6 | 1.8 | 0.2 | 1.0 | 88.6 | 24.6 | 4.8 | 0 | 0 |
| **Carbominerite (vol %)** | | | | | | | | | | |
| **Carb-Argillate & Carb-Silicate** | 6.0 | 31.6 | 11.1 | 4.2 | 0.8 | 2.8 | 24.0 | 9.2 | 2.8 | 3.0 |
| **Carbo-Pyrite** | 2.2 | 2.8 | 0.4 | 0.6 | 0.8 | 1.6 | 4.2 | 1.2 | 0.4 | 0.4 |
| **Carb-Ankerite** | 0.8 | 1.2 | 4.1 | 5.0 | 3.8 | 1.6 | 2.0 | 2.6 | 4.4 | 2.2 |
| **Ash flow temperature (ºC)** | 1340 | 1340 | 1570 | 1480 | 1350 | 1410 | 1600 | 1540 | 1340 | 1350 |
| **$S_{COAL}$ ($m^2.g^{-1}$)** | 38.0 | 65.9 | 102.6 | 138.9 | 142.6 | 35.4 | 56.7 | 88.8 | 123.6 | 132.3 |
| **$S_{CHAR}$ ($m^2.g^{-1}$)** | 39.3 | 74.7 | 53.0 | 34.3 | 31.8 | 36.1 | 59.3 | 52.5 | 40.5 | 35.5 |

This is associated with the $Fe_2O_3$ which acts as a fluxing agent as to lower the ash flow temperature. This lower ash flow temperature causes molten mineral phases to form, which may then encapsulate the carbon sites and limit the reactant gas access to these sites leading to more carbon in the ash.

The corresponding fractions have similar surface properties, and it was found that the micro-pore surface area is associated with the fixed carbon and vitrinite content, as these constituents are more porous compared to the mineral and inertinite components. It is concluded that pyrolysis leads to a decrease in surface area, especially in coal fractions containing more volatile matter, due to pore closure, increased graphitic nature, thermal annealing and alignment of poly-condensed aromatic molecules. Inert inertodetrinite is associated with the decrease in micro-pore surface area.

Calorific value increases with increasing fixed carbon, and decreases with increasing ash content, showing a linear relationship in each case. In Section 4.2.6 it was found that coal B does not show a linear relationship with ash or fixed carbon. This is because coal B contains more high density (SG > 2.0 $g.cm^{-3}$), low energy coal particles and less low density (SG < 1.6 $g.cm^{-3}$), high energy coal particles compared to coal G.

# Chapter 5: Gasification and Kinetic Evaluation

The focus of this study is to quantify the relationship between density and kinetics of char gasification. This is done by gasifying char particles of different densities in a Thermo-Gravimetric Analyzer (TGA). In this chapter the experimental equipment and procedures (Section 5.1) as well as the gasification results (Section 5.2) are presented.

## 5.1 Gasification: Experimental

The evaluation of the kinetics of char gasification in a $CO_2$ atmosphere was done in a TGA, as this equipment allows the accurate control of temperature and gas atmosphere around the coal sample. This chapter addresses the equipment and procedures used in these gasification experiments and will include:

- Experimental equipment.
- Experimental procedures.
- Chemicals.
- Experimental program.

### 5.1.1 Equipment

The TGA used in this study for the carbon dioxide reactivity experiments on the given density cuts of coal B and G, is the Thermax 700 Thermo-Gravimetric Analyzer supplied by the Cahn Company. The TGA measures the temperature and weight of the coal sample as a function of time. This time/temperature/weight data can then be exported to software programs such as Microsoft Excel or Polymath for further data analysis.

The balance of this TGA incorporates a closed loop servo network, which automatically compensates for the weight changes in the sample. The balance functions electronically, and the electric current required to return the balance to the null position is directly proportional to the weight measured by the balance. The balance is able to measure a maximum weight of 100 g with a sensitivity of 1.0 mg which provides very accurate experimental data for analysis. The reactor furnace is capable of operating at a maximum temperature of 1700 ºC and is controlled

electronically via the Cahn Thermax software suite installed on the connected computer. This furnace has a maximum heating rate of 100 ºC.min$^{-1}$.

The TGA has a plastic feed gas tube, which allows reactant or inert gases to be fed to the reactor. The flow of these gases is regulated via 2 Brooks 5850 mass flow controllers in order to control the gaseous environment in which the reaction takes place. These mass flow controllers were calibrated prior to the gasification experiments and the calibration curves can be seen in Appendix B. Table 5.1 illustrates the specifications of the TGA.

Table 5. 1: Thermax 700 TGA specifications.

| **Balance** | |
|---|---|
| Capacity | 100 g |
| Weighing range | ±10 g |
| Readability | 1 µg |
| Temperature drift | 10 µg.ºC$^{-1}$ |
| Full range zeroing | Yes |
| **Furnace** | |
| Maximum temperature | 1700 ºC |
| Maximum heating rate | 100 ºC.min$^{-1}$ |
| Maximum cooling rate | 50 ºC.min$^{-1}$ |
| Temperature repeatability | ±3 ºC |
| **Reaction chamber** | |
| Sample volume | 29 cm$^3$ |
| Reactor tube volume | 350 cm$^3$ |
| Oxygen free environment | Yes |
| Reducing gases | Yes |
| Oxidizing gases | Yes |
| Corrosive gases | Yes |

This TGA is suitable to be used with reducing gases, oxidizing gases, as well as corrosive gases. It is important to note that because of the differential operation of the TGA, the concentration of the gas atmosphere at the surface of the coal particle is very close to the feed gas concentration and can thus be easily regulated. A schematic representation of the Thermax 700 TGA is shown in Figure 5.1, while Figure 5.2 shows a photo of the Thermax 700 TGA as it is set up in the laboratory.

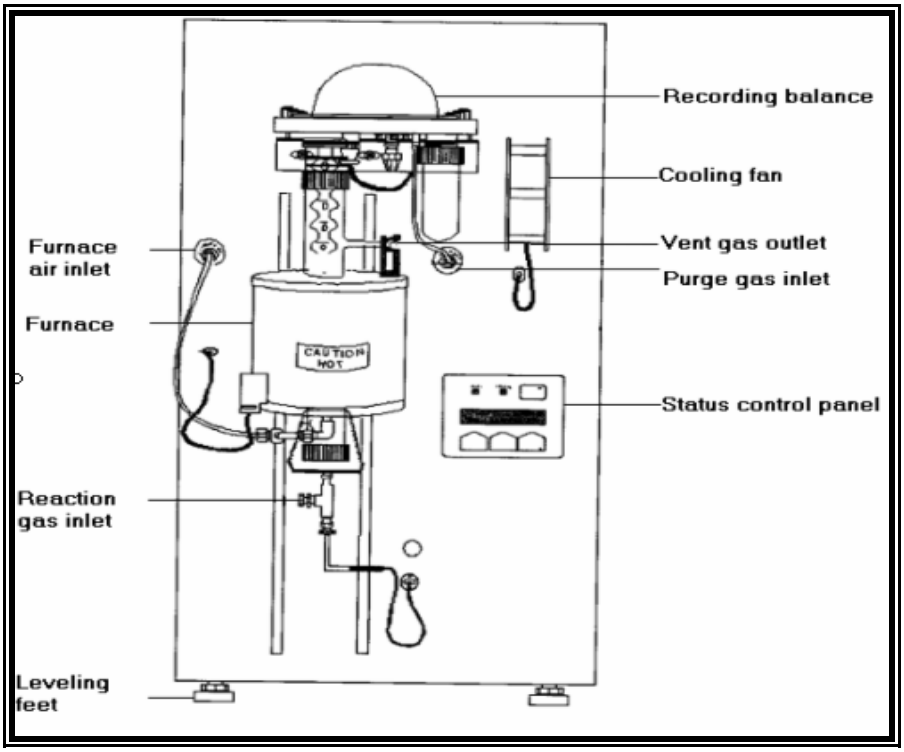


Figure 5. 1: Schematic representation of the Thermax 700 TGA.

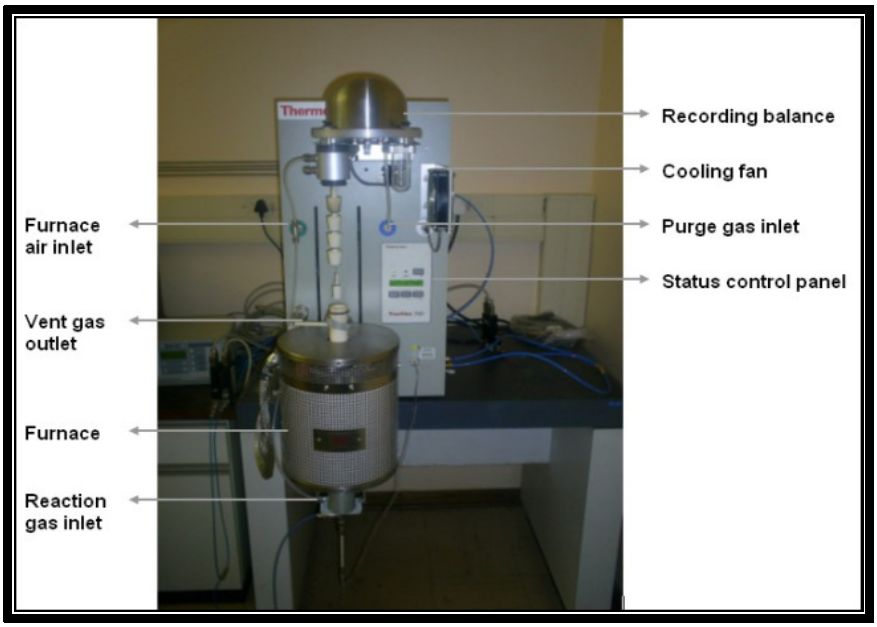


Figure 5. 2: Thermax 700 TGA.

### 5.1.2 Procedures

The density fractions used in the gasification experiments were prepared from the parent coals B and G as explained in Section 3.2.3. These samples were screened as described in Section 3.2.2 in order to obtain (-1140 µm +1000 µm) coal particles for use in the gasification experiments. From these coal particles, 500 mg (± 5 mg) coal samples were taken for each of the gasification experiments.

Initially the gas flow to the TGA was set to 200 $ml.min^{-1}$ consisting only of nitrogen, as to create an inert gas atmosphere. Next the coal sample is loaded into the porous platinum basket which is then connected to the TGA balance. The TGA is closed and the nitrogen is passed through the furnace for 30 minutes before the heating is commenced. The furnace is set to a heating rate of 20 ºC.$min^{-1}$ until a temperature of 1000 ºC is reached. This temperature is kept constant for 1 hour before a rapid heating rate of 30 ºC.$min^{-1}$ is employed until the reaction temperature is reached. At this point the inert nitrogen gas feed is switched to carbon dioxide; still at a total gas flow rate of 200 $ml.min^{-1}$. This reaction temperature is kept constant until no further mass loss is observed. The heating is stopped, the gas flow is closed and the furnace is allowed to cool down before the basket is removed. Finally the ash is weighed and the basket is burnt clean in a Bunsen flame. The experimental error is calculated as shown in Appendix I, and was found to be 1.6 %.

### 5.1.3 Chemicals

The chemicals used include the coal samples as well as the gases used in the gasification experiments. The coals were supplied by six collieries (Section 3.1), and a detailed characterization of the parent coals is given in Section 4.2. The density fractions of coals B and G that are used in the gasification experiments were prepared as described in Section 3.2.3, and the characterization results of these fractions are given in Section 4.3.

The gases used in the gasification experiments are of high purity and were supplied by African Oxygen (Afrox) limited South Africa. A summary of these gases including the type of gas, grade and purity is given in Table 5.2.

Table 5. 2: Gas grade and purity used for gasification experiments.

| Gas | Grade | Purity |
|---|---|---|
| Carbon dioxide | Medical purity grade | >99.99 % |
| Nitrogen | Ultra high purity grade | >99.999 % |

### 5.1.4 Experimental program

A detailed evaluation of the coal conversion versus time data obtained from the $CO_2/N_2$ experiments will be done as to evaluate the kinetics associated with coal gasification as well as to determine the activation energy of each coal fraction; and will be presented in Section 5.2. Table 5.3 gives a summary of the different experimental conditions used. The main experimental parameters include the reaction temperature and the density of the coal. Selected experiments were repeated as to confirm the reproducibility of the experiments.

Table 5. 3: Reaction conditions for gasification experiments.

| Variable | Ranges and compositions |
|---|---|
| Temperature | 1000 ºC, 1015 ºC, 1030 ºC, 1070 ºC |
| Pressure | 0.875 bar |
| Reaction mixtures (% $CO_2$) | 100 % |
| Particle size | 1 mm |
| Density fractions | < 1.4 $g.cm^{-3}$ |
| | 1.4 $g.cm^{-3}$ - 1.6 $g.cm^{-3}$ |
| | 1.6 $g.cm^{-3}$ – 1.8 $g.cm^{-3}$ |
| | 1.8 $g.cm^{-3}$ – 2 $g.cm^{-3}$ |
| | > 2$g.cm^{-3}$ |
| Coal samples | Coals B and G |

# 5.2 Gasification: Results and discussion

In this section the focus is on the results obtained from the $CO_2$ gasification experiments for each of the density fractions for both coals according to the procedures as described in Section 5.1. This is done as to establish a link between the coal properties and the intrinsic reaction rate, as well as to present a model describing the kinetics of $CO_2$ gasification. In Section 5.2.1 it is shown how the raw data is obtained and normalized, Section 5.2.2 includes the influence of temperature on the gasification reaction; and Section 5.2.3 describes the effect of density on the $CO_2$ gasification reaction. Section 5.2.4 describes the intrinsic reactivity of the fractions as a function of temperature and coal properties, while Section 5.2.5 includes the results pertaining to the modelling of the experimental data with the random pore model.

### 5.2.1 Experimental results

Figure 5.3 shows a typical TGA curve obtained for the $CO_2$ gasification of coal (fraction B1) at 1000 ºC and atmospheric pressure (87.5 kPa).

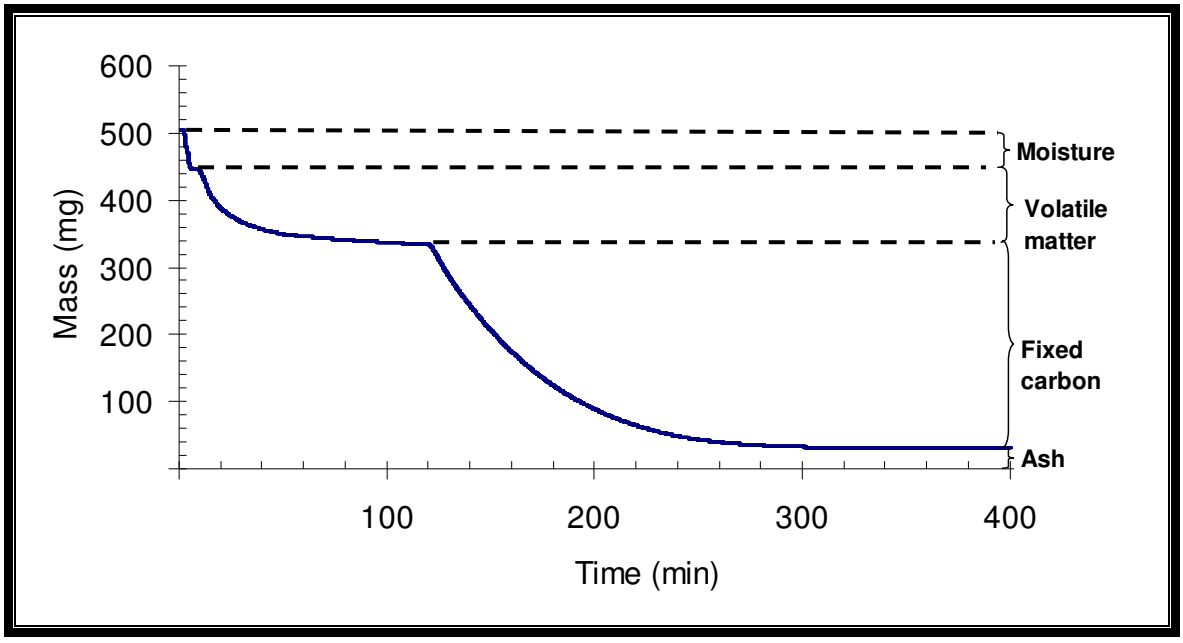


Figure 5. 3: Typical TGA curve for coal B1.

The curves obtained for the other fractions are presented in Appendix C. The experimental procedure (as described in Section 5.1.2) allows for the relative amounts

of moisture, volatile matter, fixed carbon and ash to be obtained from these experiments; because initially under an inert nitrogen atmosphere, only moisture and volatile matter is evolved, and when carbon dioxide is introduced the fixed carbon is consumed in the gasification reaction. The mass-time curve reaches a plateau value, indicating that all of the carbon is depleted, and this final mass can be taken as the ash value of that specific fraction. The percentage ash as calculated from the TGA curves agrees to within 5 % (relative) with the ash content obtained by the proximate analysis, as shown in Table 4.18.

Figure 5.3 can be normalized to a conversion-time plot, where the data is presented on a dry, ash-free, volatile-free basis, thus only looking at the conversion of fixed carbon. This normalization is done according to Equation 42:

$$X = \frac{M_0 - M_t}{M_0 - M_{ASH}} \quad \text{..... (42)}$$

Here $M_0$ refers to the sample mass at the start of gasification (when carbon dioxide is introduced), $M_t$ is the sample mass as a function of time and $M_{ASH}$ is the mass of the ash left behind after the reaction. From here 20 data points were used throughout the range of carbon conversion.

Figure 5.4 shows such a conversion versus time plot for coal B1 at 1000 ºC. The other conversion versus time graphs can be seen in Appendix D. From the dotted lines (indicating the rate of the reaction), it is concluded that initially there is a very rapid reaction rate, which then slows as conversion nears unity.

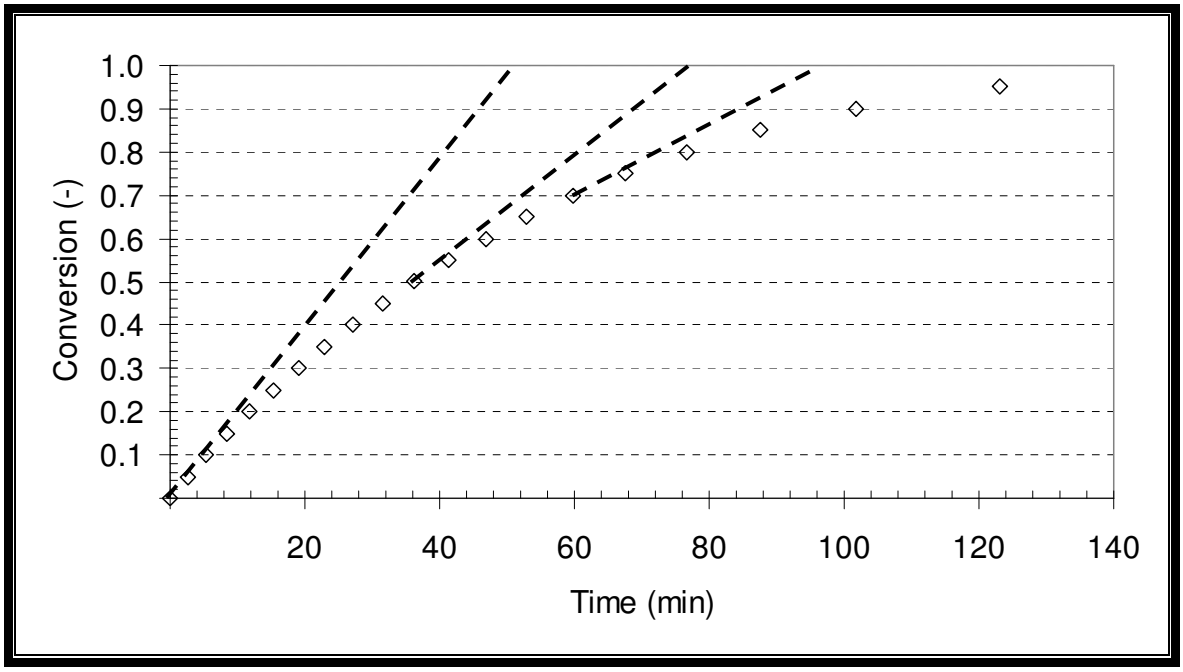


Figure 5. 4: Carbon conversion as a function of time for coal B1 (dotted lines indicate reaction rate).

### 5.2.2 Temperature effect

The influence of temperature on the carbon conversion rate for coal B1 is presented in Figure 5.5, while Figure 5.6 shows the effect of temperature on coal G1. The temperature dependence of the other fractions is given in Appendix E.

In each case, an increase in temperature leads to an increase in the gasification rate. Several other researchers (Ye et al., 1998; Ochoa et al., 2001; Everson et al., 2008; Liu et al., 2004; Liu et al., 2006) found the same trends for carbon dioxide gasification of various coal samples. It is clear that there is a significant increase in the conversion rate from 1000 ºC to 1015 ºC. As the temperature is increased further, the increase in the gasification rate is less significant, as seen from the difference between 1015 ºC and 1030 ºC as well as between 1030 ºC and 1070 ºC.

It was assumed that the intrinsic pore diffusion does not significantly affect the reaction rate, and this assumption was validated by evaluating the Wagner-Weisz-Wheeler modulus as shown in Appendix J. The value of this modulus for each of the coals at the highest reaction temperature (1070ºC), was several orders of magnitude smaller than 0.15, which signifies that internal pore diffusion does not have a real impact on the gasification reaction rate in this temperature range.

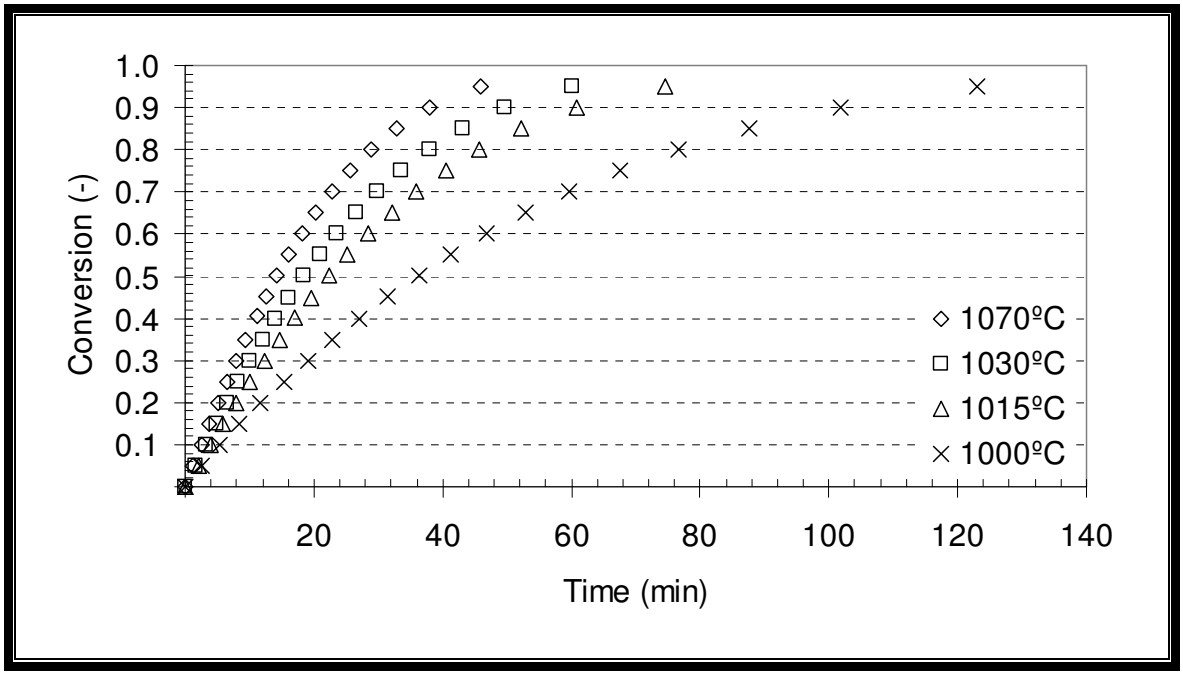


Figure 5. 5: Influence of temperature on gasification rate for coal B1.

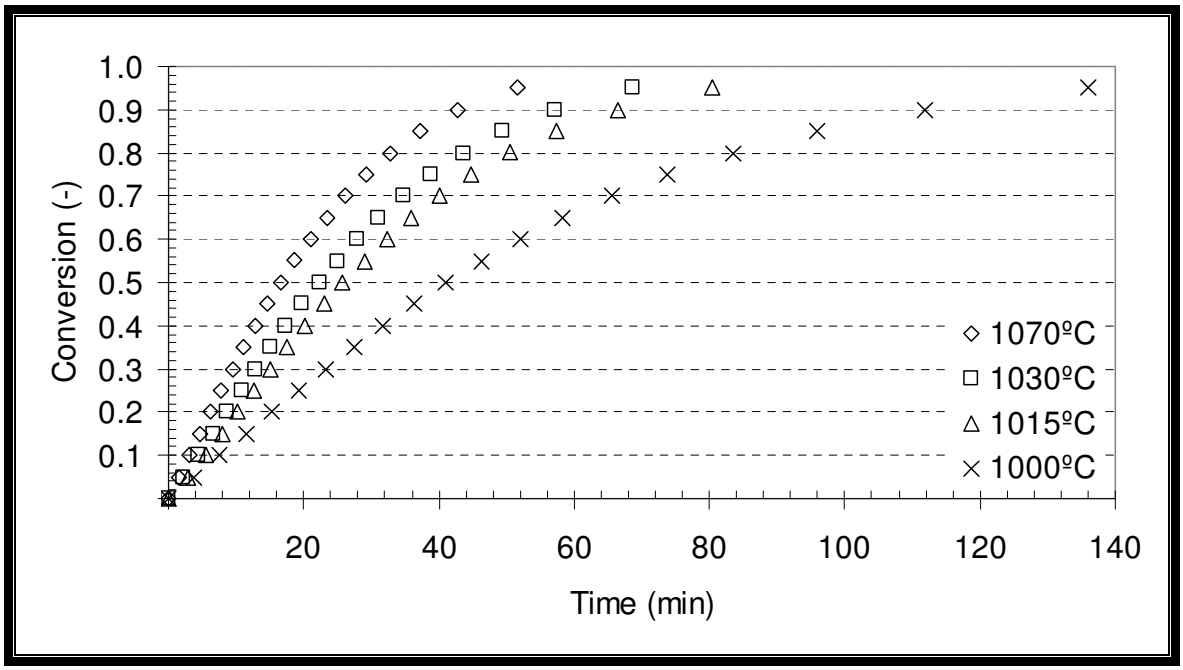


Figure 5. 6: Influence of temperature on gasification rate for coal G1.

### 5.2.3 Density effect

The influence of particle density on the gasification rate of coal B at 1000 ºC is shown in Figure 5.7, while Figure 5.8 presents the influence of density on the gasification

rate of coal G, also at 1000 ºC. The reaction at other temperatures shows similar trends, and these figures are given in Appendix F.

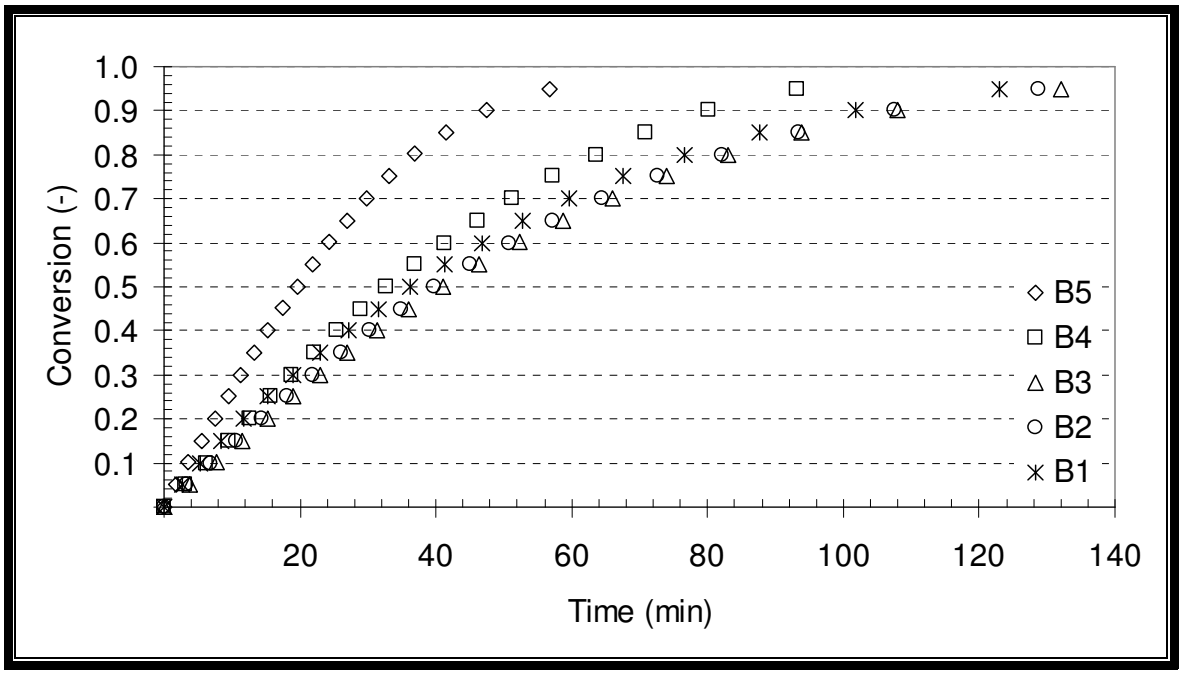


Figure 5. 7: Influence of density on gasification rate for coal B.

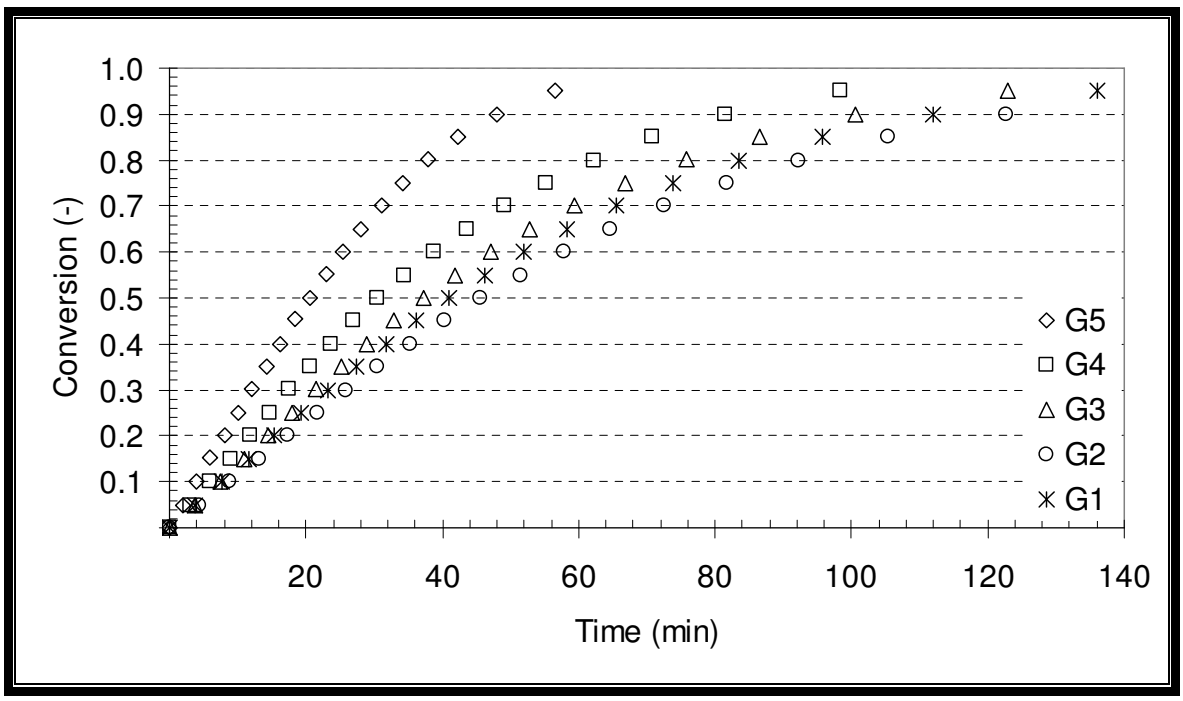


Figure 5. 8: Influence of density on gasification rate for coal G.

It was observed that the density has an effect on the gasification rate of coal. From Figure 5.7 and Figure 5.8 it is clear that the +2.0 $g.cm^{-3}$ fraction reacts the fastest,

followed by the 1.8 g.cm$^{-3}$ - 2.0 g.cm$^{-3}$ fraction. The fractions having a density of less than 1.8 g.cm$^{-3}$ are grouped close together, and it follows for coal B that fraction B1 is slightly faster than B2 and B3 which lie on the same line. For coal G, fraction G3 is faster than G1, which is in-turn faster than G2. It can therefore be concluded that at relatively low densities (up to 1.8 g.cm$^{-3}$), density does not have such a significant influence on the gasification rate. For higher density coal (> 1.8 g.cm$^{-3}$), density has a noteworthy influence on the gasification rate, as the gasification rate increases with increasing coal density. The influence of coal properties associated with the density separation of coal particles on the reaction rate, specifically the initial intrinsic reactivity is discussed further in Section 5.2.4.

### 5.2.4 Intrinsic reactivity

The carbon dioxide surface area as discussed in Section 4.3.5 is important, as previous research found that $CO_2$ gasification activates the narrow micro-pores, and that the gasification reaction preferably takes place in these micro-pores (Yücel et al., 2007; Salatino and Senneca, 1998). The micro-pore surface area of the chars is used in the calculation of the initial intrinsic reactivity according to (Samaras et al., 1996; Liu et al., 2000b):

$$R_I = \frac{R_A}{S_{CO_2}} \quad \text{.....(43)}$$

With the initial apparent reactivity defined according to (Samaras et al., 1996; Yücel et al., 2007):

$$R_A = \frac{1}{w_0}\frac{dw_0}{dt} \quad \text{.....(44)}$$

The initial intrinsic reactivity allows a better estimation of how the reactivity of coal depends on the various coal properties, especially the mineral components, which may act as catalysts during the gasification reaction, as it does not take into account the structural properties of the coals. Therefore the initial intrinsic reactivity is the

only reactivity parameter considered in this study. Table 5.4 shows a summary of the initial intrinsic reaction rate for both coals at the various reaction temperatures.

Table 5. 4: Initial intrinsic reaction rate ($10^{-4}$g.m$^{-2}$.min$^{-1}$).

| Temperature | B1 | B2 | B3 | B4 | B5 | G1 | G2 | G3 | G4 | G5 |
|---|---|---|---|---|---|---|---|---|---|---|
| **1000 ºC** | 5.5 | 4.6 | 2.8 | 2.2 | 8.9 | 3.8 | 3.2 | 3.0 | 3.0 | 9.0 |
| **1015 ºC** | 8.7 | 7.9 | 4.9 | 3.5 | 10.6 | 5.6 | 5.6 | 5.0 | 5.3 | 10.6 |
| **1030 ºC** | 10.9 | 8.3 | 5.2 | 4.1 | 12.0 | 6.6 | 6.2 | 5.9 | 6.8 | 21.5 |
| **1070 ºC** | 13.2 | 10.9 | 7.4 | 6.7 | 21.5 | 9.7 | 8.1 | 8.2 | 9.9 | 30.7 |

There is a general trend for the initial intrinsic reactivity values at the different temperatures, which is different for coal G compared to coal B. For coal B, the initial intrinsic reactivity decreases with increasing density up to the B4 fraction, and then increases in the densest fraction. For coal G it is seen that the initial intrinsic reactivity also decreases with increasing density up to the G3 fraction, then slightly increases to the G4 fraction and finally increases significantly in the G5 fraction. For both coals it is clear that the densest fraction has the highest initial intrinsic reactivity at each of the temperatures studied. These results are significant, as the variations observed are greater than the experimental error of 1.6 % as calculated in Appendix I.

The coal fractions have similar initial intrinsic reactivity values at 1000 ºC, except for the two lightest fractions, where coal B shows a higher reactivity. When considering the initial intrinsic reactivity calculated at each of the temperatures, it can be concluded that coal G has a higher reactivity in the denser fractions (> 1.8 g.cm$^{-3}$), with this observation becoming more pronounced at reaction temperatures of 1030 ºC and 1070 ºC. The large difference observed in the initial intrinsic reactivity between the denser fractions of coals B and G onwards from a reaction temperature of 1030 ºC may be attributed to the relatively low ash fusion temperature of coal fractions B4 and B5 compared to fractions G4 and G5 (Table 4.26). It is suggested by Van Dyk et al. (2009) that even though ash fusion analysis gives an indication of the ash transition points, that there are some ash forming minerals which will melt and transform at lower temperatures. These molten minerals may then encapsulate the carbon particles causing diffusion limitations of the reactant gas to the carbon sites, and this limits the

degree to which the initial intrinsic reactivity increases from a reaction temperature of 1015 ºC to 1030 ºC.

The influence of the organic make-up of the coal on the initial intrinsic reactivity is observed to a lesser degree. It is seen that the inert inertodetrinite (Table 4.20) acts as to decrease the reactivity as shown in Figure 5.9 for coal B and Figure 5.10 for coal G. This decrease in reactivity associated with the increase in inert inertodetrinite content is due to this maceral sub-group forming dense, inert chars during pyrolysis (Falcon and Snyman, 1986).

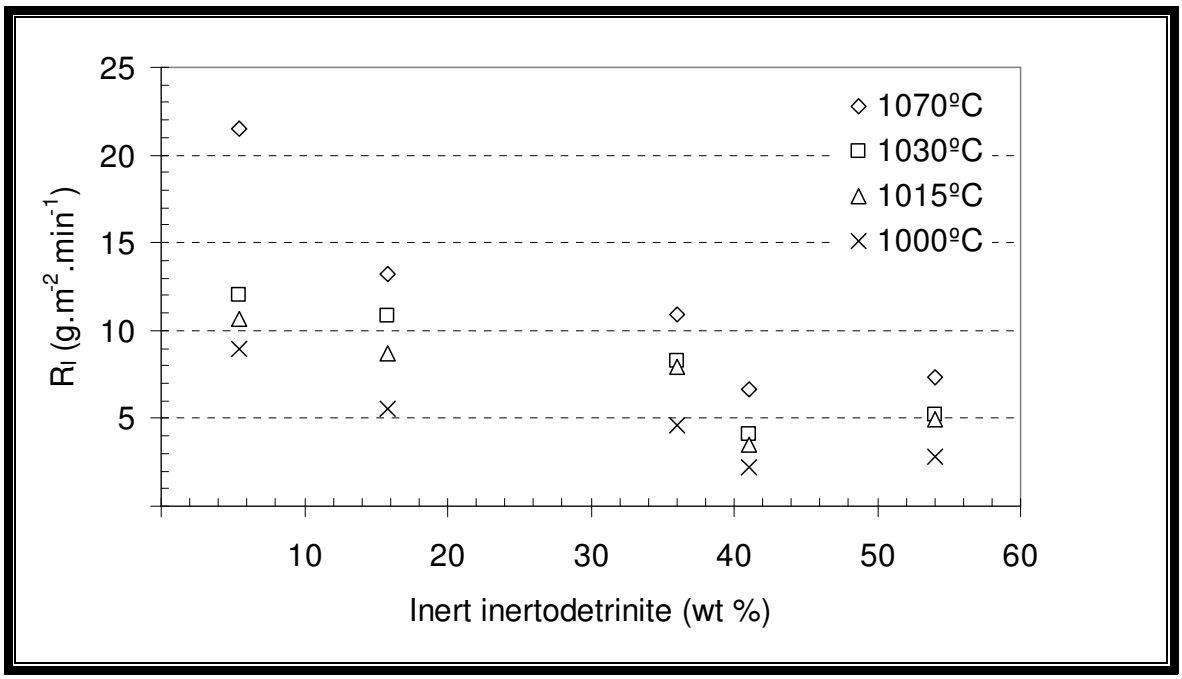


Figure 5. 9: Influence of inert inertodetrinite on initial intrinsic reactivity for coal B.

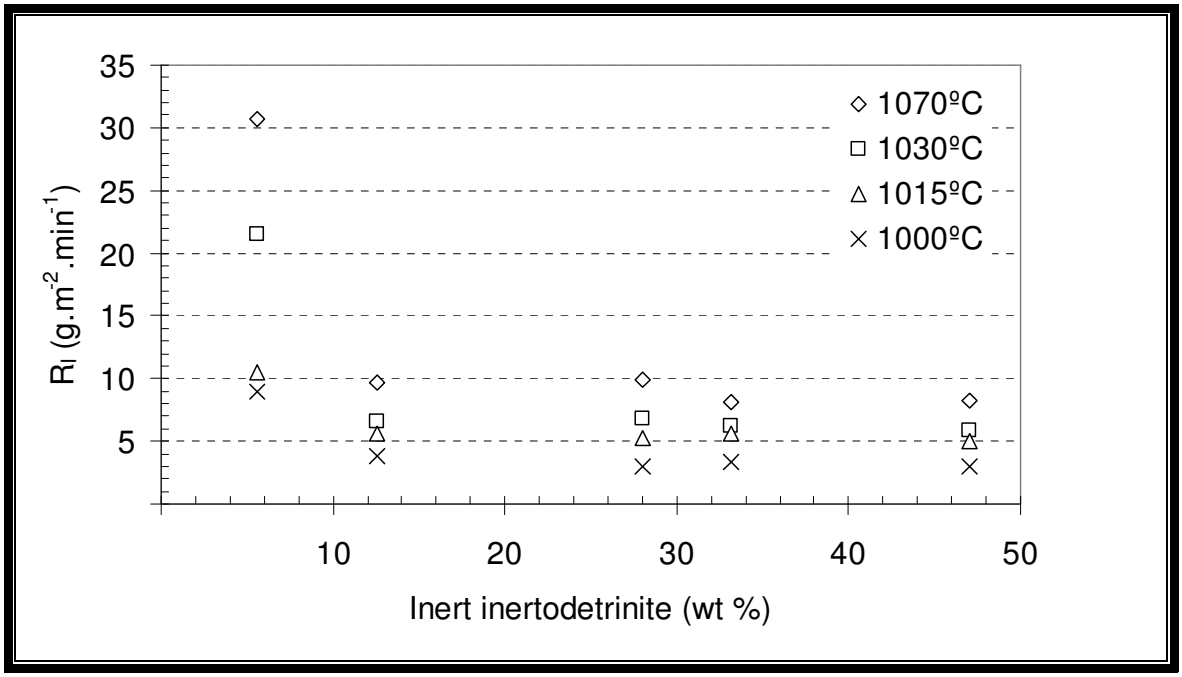


Figure 5. 10: Influence of inert inertodetrinite on initial intrinsic reactivity for coal G.

### 5.2.5 Modelling

The focus of this section is on the application of the random pore model to the experimental data, and the subsequent evaluation of the activation energy values associated with each of the coals.

**Random pore model**

There are various models available to describe carbon conversion in the $CO_2$ gasification reaction. In this study the random pore model (RPM) as developed by Bhatia and Perlmutter (1980) is applied to the experimental data. This model has been applied effectively in several other studies concerning the $CO_2$ gasification of coal (Ochoa et al., 2001; Liu et al., 2004; Liu et al., 2006; Everson et al., 2008). The model equations are discussed in detail in Section 2.5.3 (Equations 26 – 39).

As described in Equation 34, the reduced time to 90 % carbon conversion is used to determine the structural parameter for each of the experiments by means of regression. Figure 5.11 presents the conversion as a function of this reduced time parameter for coal B1 at all of the reaction temperatures; with the conversion reduced-time graphs for the other fractions being shown in Appendix G.

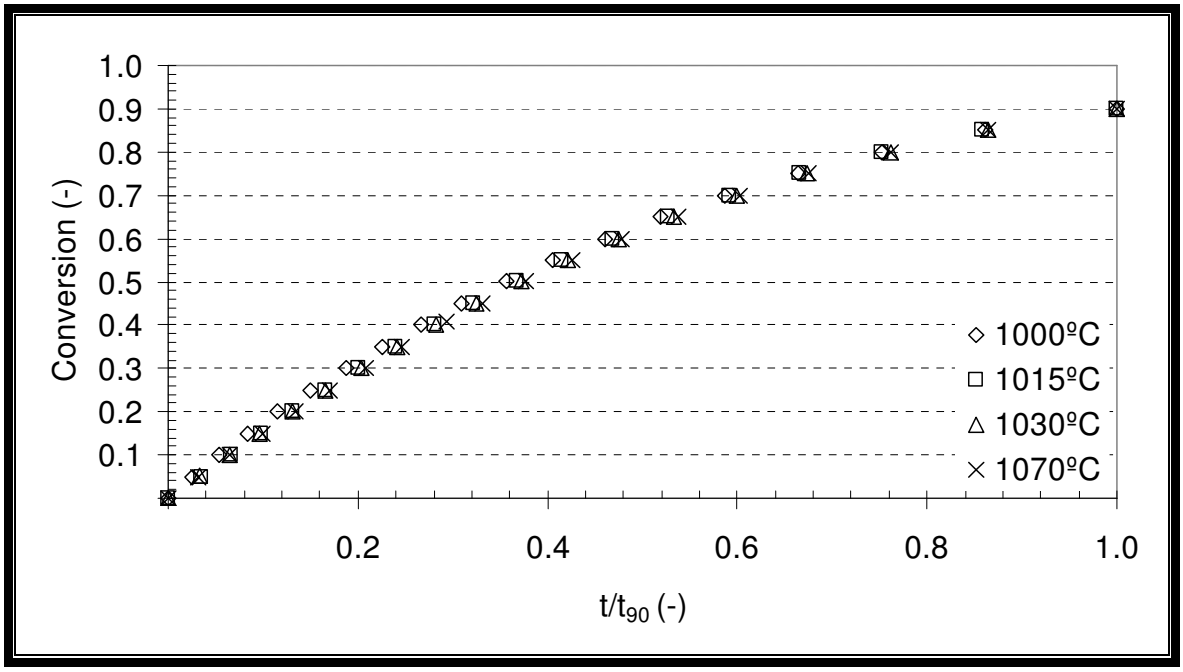


Figure 5. 11: Determination of the structural parameter for coal B1.

Figure 5.11 illustrates that the conversion curves tend to converge to a uniform curve; and therefore the average structural parameter is calculated from the values obtained from each of the temperatures; and this value is used for further calculations and the determination of $t_f$. Equation 34 is used to calculate $t_f$ from conversion-time data by using the structural parameter as previously determined.

Figure 5.12 shows the fit of the random pore model to the experimental conversion data obtained for coal B at 1000 ºC with model parameters as presented in Table 5.5. The fit of the random pore model at the other temperatures and for the other coal fractions is shown in Appendix H.

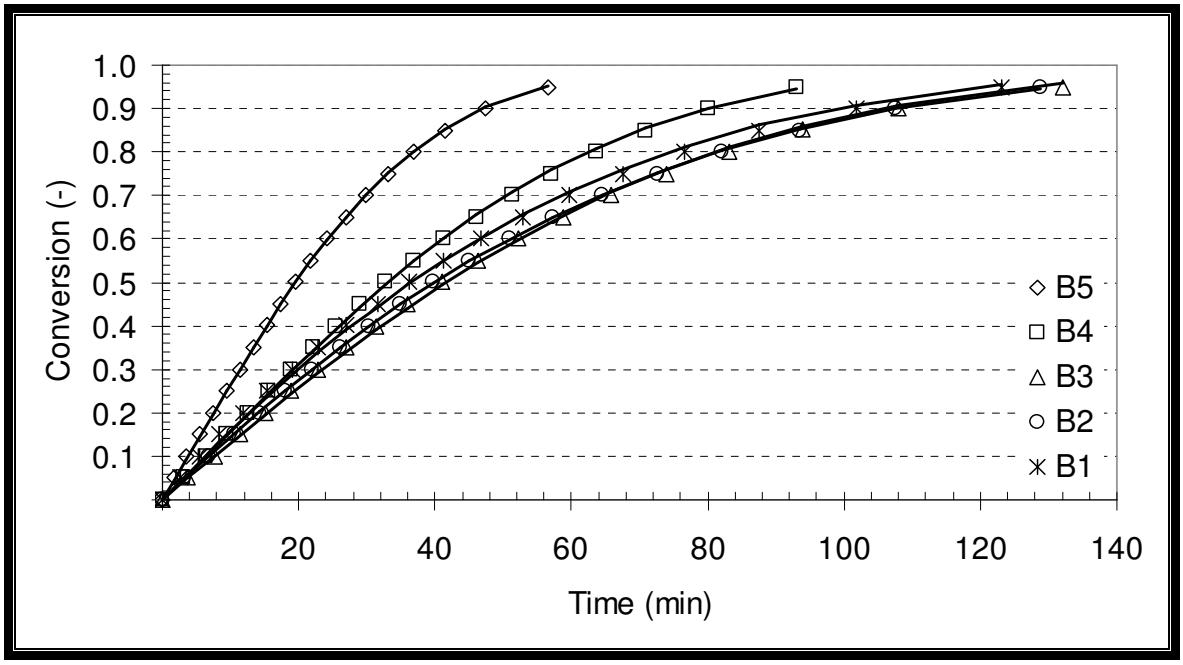


Figure 5. 12: Fit of random pore model to experimental data for coal B at 1000ºC (lines indicate modelled data).

The model parameters calculated for the RPM fit to the data are shown in Table 5.5 for both coals. This includes the structural parameter (ψ) which gives an indication of the char surface area development during reaction, as well as the fitted $t_f$ values at each temperature. The value of $t_f$ is analogous to the initial apparent reactivity of the coals. The variations observed here are significant, as they greater than the experimental error of 1.6 % as calculated in Appendix I

Table 5. 5: Random pore model parameters.

| | B1 | B2 | B3 | B4 | B5 | G1 | G2 | G3 | G4 | G5 |
|---|---|---|---|---|---|---|---|---|---|---|
| $\psi$ | 1.0 | 1.0 | 1.9 | 2.9 | 2.9 | 1.5 | 1.2 | 1.3 | 2.4 | 2.5 |
| $t_{f\text{-}1000\,^{\circ}C}$ ($10^{-3}$ min$^{-1}$) | 1.7 | 1.5 | 1.4 | 1.5 | 2.7 | 1.5 | 1.3 | 1.6 | 1.9 | 2.3 |
| $t_{f\text{-}1015\,^{\circ}C}$ ($10^{-3}$ min$^{-1}$) | 2.7 | 2.7 | 2.5 | 2.5 | 4.5 | 2.2 | 2.2 | 2.6 | 2.8 | 4.9 |
| $t_{f\text{-}1030\,^{\circ}C}$ ($10^{-3}$ min$^{-1}$) | 3.2 | 2.8 | 2.6 | 3.1 | 4.8 | 2.5 | 2.5 | 3.0 | 3.7 | 5.9 |
| $t_{f\text{-}1070\,^{\circ}C}$ ($10^{-3}$ min$^{-1}$) | 4.1 | 3.6 | 3.7 | 4.7 | 8.4 | 3.4 | 3.2 | 4.2 | 5.8 | 10.1 |

The structural parameter increases with increasing density, as observed for both coals. According to Bhatia and Perlmutter (1980), it follows that for larger values of the structural parameter, the process of pore coalescence is delayed. This indicates that for larger values of the structural parameter associated with higher particle densities,

the overall gasification process is more affected by pore growth than by pore collapse. The organic make-up of the coal fractions also affects the pore development, and therefore also the structural parameter. Figure 5.13 and Figure 5.14 show the observed effect that liptinite content has on the structural parameter of coals B and G respectively.

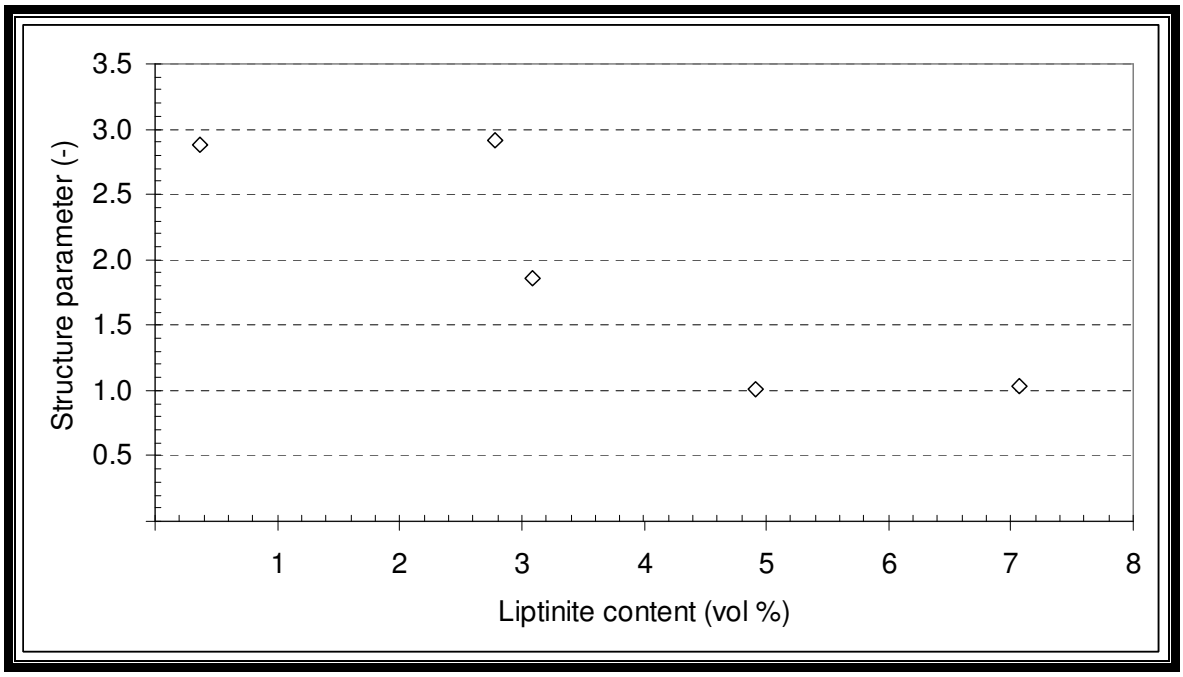


Figure 5. 13: Structural parameter as function of liptinite content for coal B.

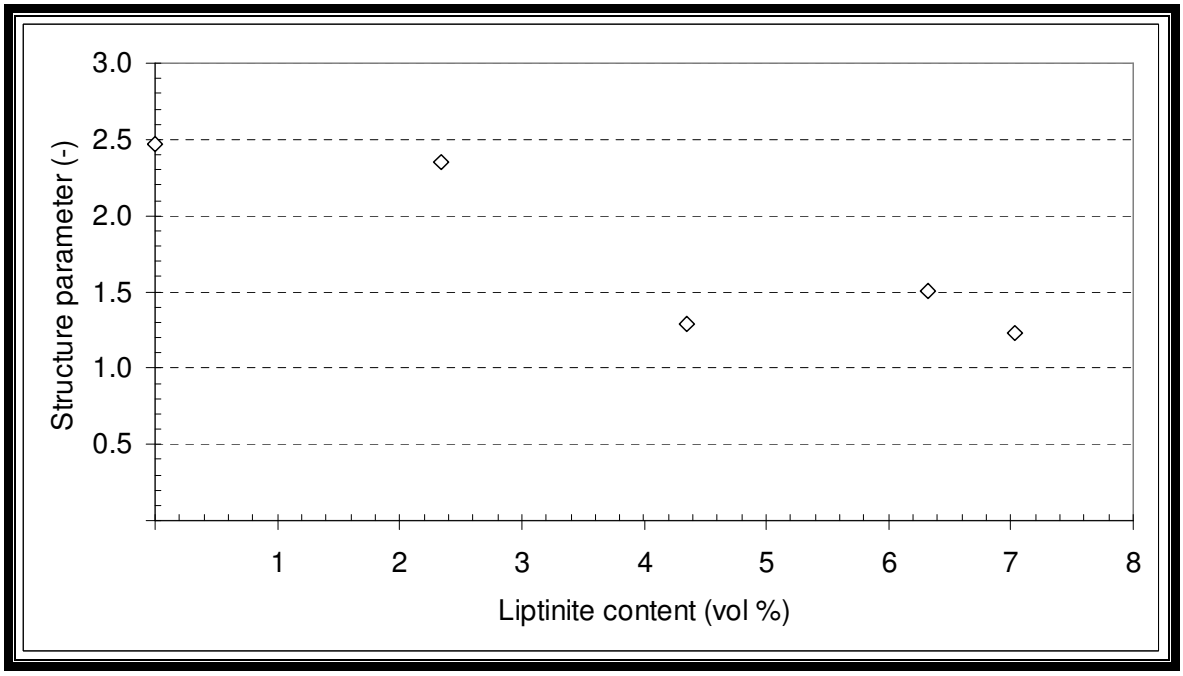


Figure 5. 14: Structural parameter as function of liptinite content for coal G.

Coal fractions containing more liptinite have lower values of the structural parameter. This is because liptinite is known to swell during pyrolysis, leading to pore development (Neavel, 1982; Grainger and Gibson, 1981; Borrego et al., 1997).

**Kinetic evaluation**

As described in Section 2.5.3, it is possible to calculate the kinetic parameters from modelled carbon conversion data. In this study only the activation energy is considered. The Arrhenius plot for coal B is shown in Figure 5.15, and the corresponding plot for coal G is presented in Figure 5.16. This type of plot allows the calculation of the activation energy from the slope of the data points as mentioned in Section 2.5.3 (using Equation 39).

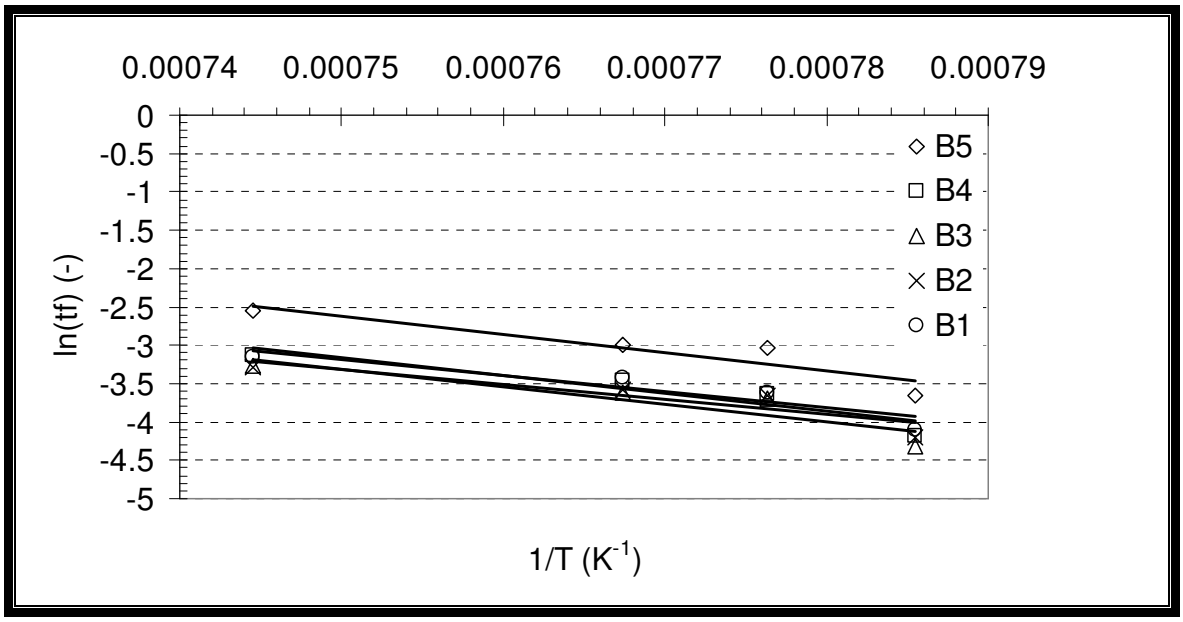


Figure 5. 15: Arrhenius plot for coal B.

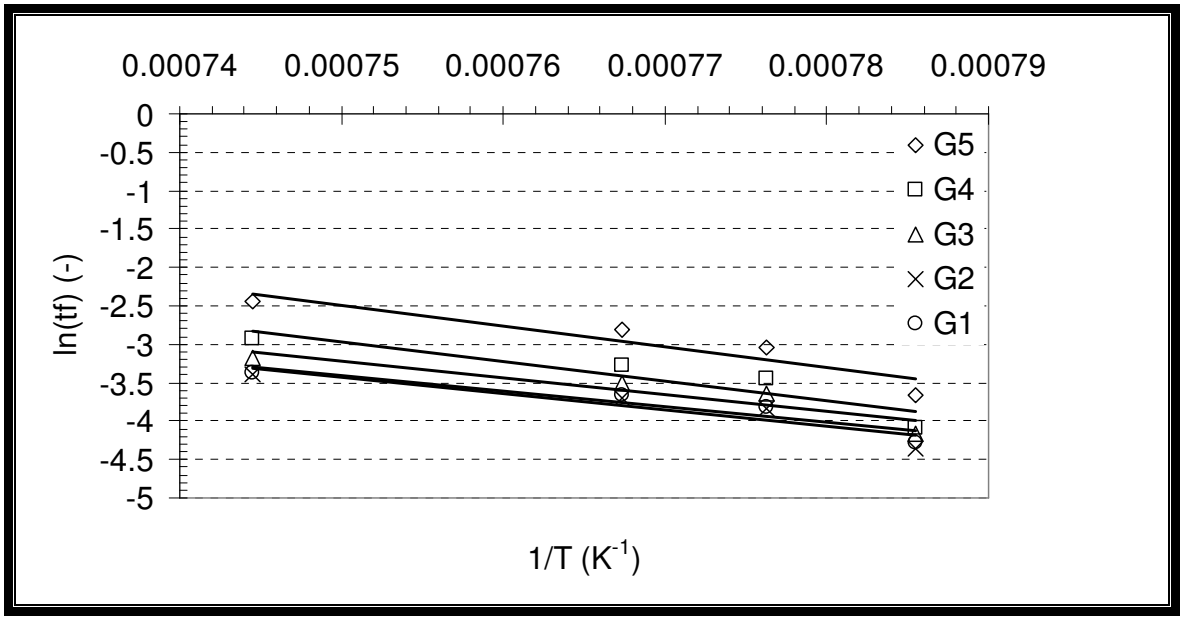


Figure 5. 16: Arrhenius plot for coal G.

The values obtained for the activation energy of both coals is presented in Table 5.6.

Table 5. 6: Calculated activation energies.

| | B1 | B2 | B3 | B4 | B5 | G1 | G2 | G3 | G4 | G5 |
|---|---|---|---|---|---|---|---|---|---|---|
| $E_{activation}$ (kJ.mole$^{-1}$) | 174 | 163 | 190 | 194 | 199 | 169 | 176 | 184 | 211 | 225 |

The activation energy values vary from 163 kJ.mole$^{-1}$ to 225 kJ.mole$^{-1}$. This is in the range as observed by Everson et al. (2008) who found the activation energy to vary from 192 kJ.mole$^{-1}$ to 247 kJ.mole$^{-1}$, as well as Kajitani and Matsuda (2006) who observed the activation energy to vary from 240 kJ.mole$^{-1}$ to 280 kJ.mole$^{-1}$. For coal B, the activation energy decreases with decreasing density up to the 1.4 g.cm$^{-3}$ – 1.6 g.cm$^{-3}$ fraction and then slightly increases to the least dense fraction. The activation energy values for coal G show a steady increase with increasing density. These activation energy values are statistically significant, as the variations observed are greater than the experimental error of 1.6 %, as calculated in Appendix I.

Evaluation of the activation energy values allows a good estimation of the catalytic effect of the mineral components in the coal, as a catalyst is defined as to lower the activation energy of a specific reaction (Levenspiel, 1972). Figure 5.17 shows the influence of ash content (Table 4.18) on the activation energy of coal B, while Figure 5.18 shows this relationship for coal G.

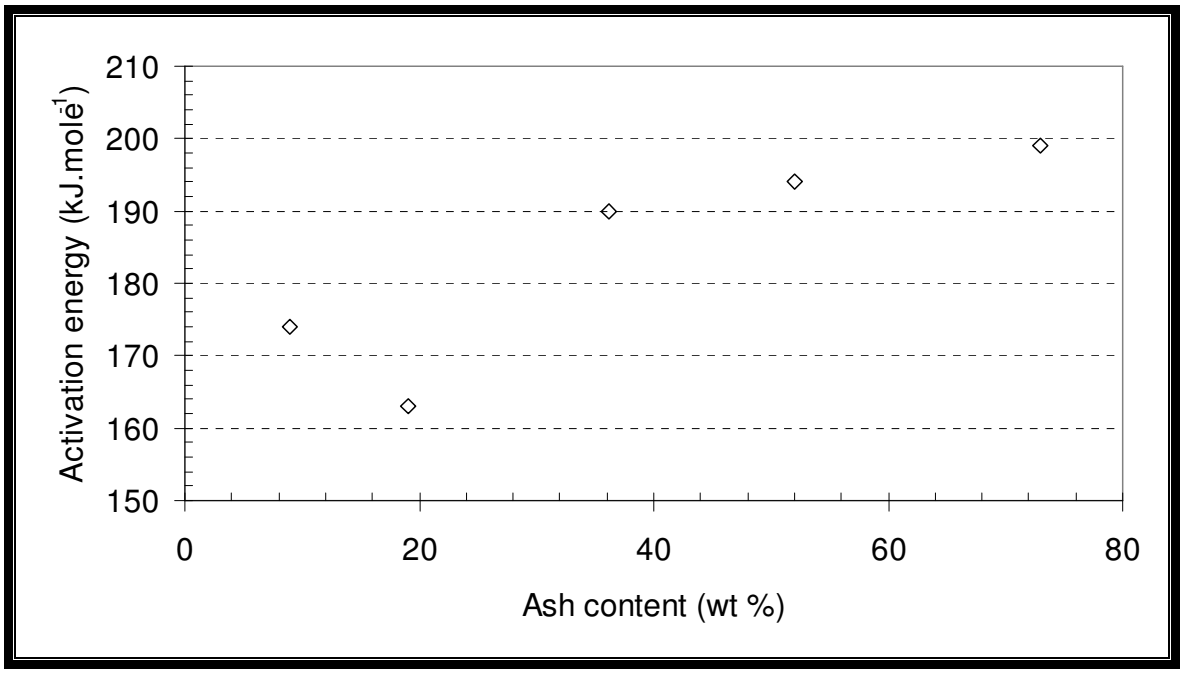


Figure 5. 17: Influence of ash content on activation energy for coal B.

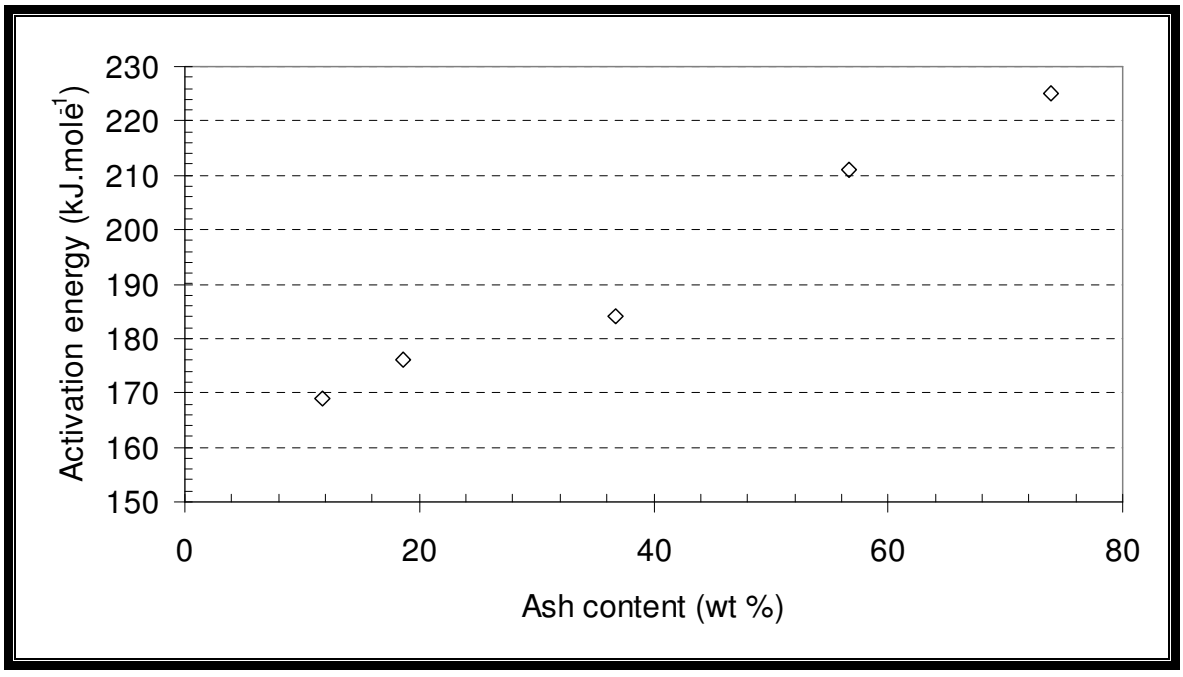


Figure 5. 18: Influence of ash content on activation energy for coal G.

From Figure 5.17 and Figure 5.18 above it is clear that the activation energy increases with increasing ash content. It is therefore clear that the ash cannot be considered as a catalyst, but rather that certain inorganic constituents in the coals may be catalytically active during the reaction, and this will be discussed in the following paragraphs.

When considering the elemental make up of the mineral fractions (Table 4.24); several elements can be considered as catalysts for the $CO_2$ gasification reaction. Figure 5.19 and Figure 5.20 show the effect that calcium has on the activation energy of coals B and G respectively.

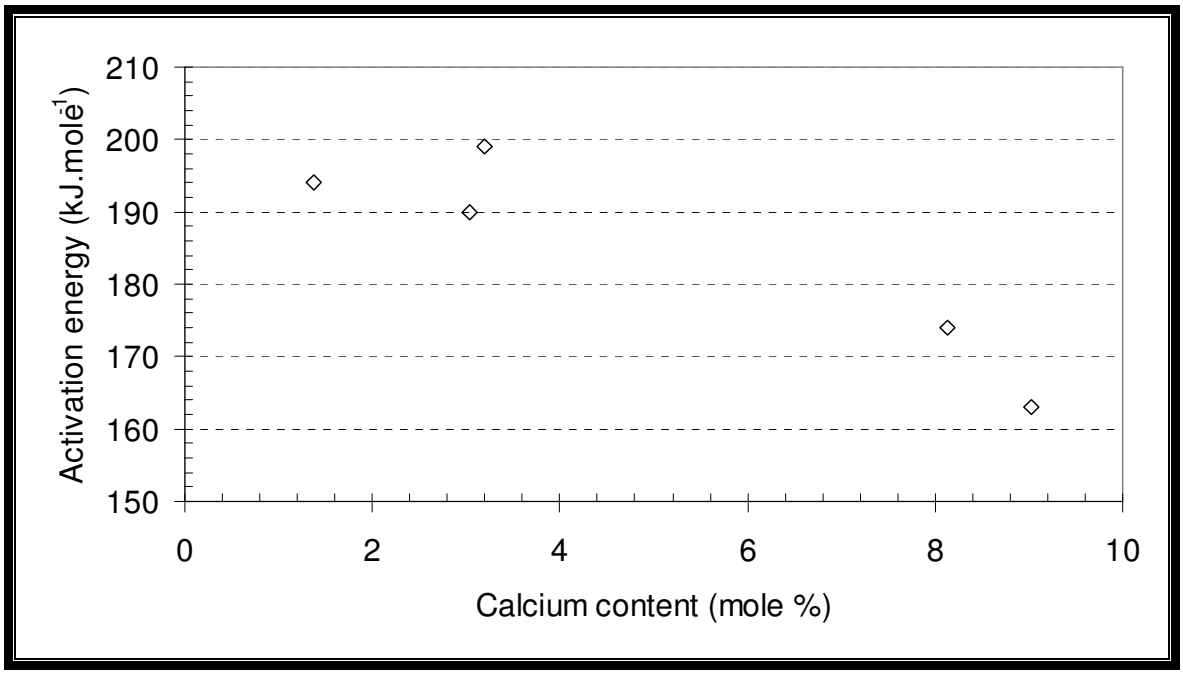


Figure 5. 19: Influence of calcium content on activation energy for coal B.

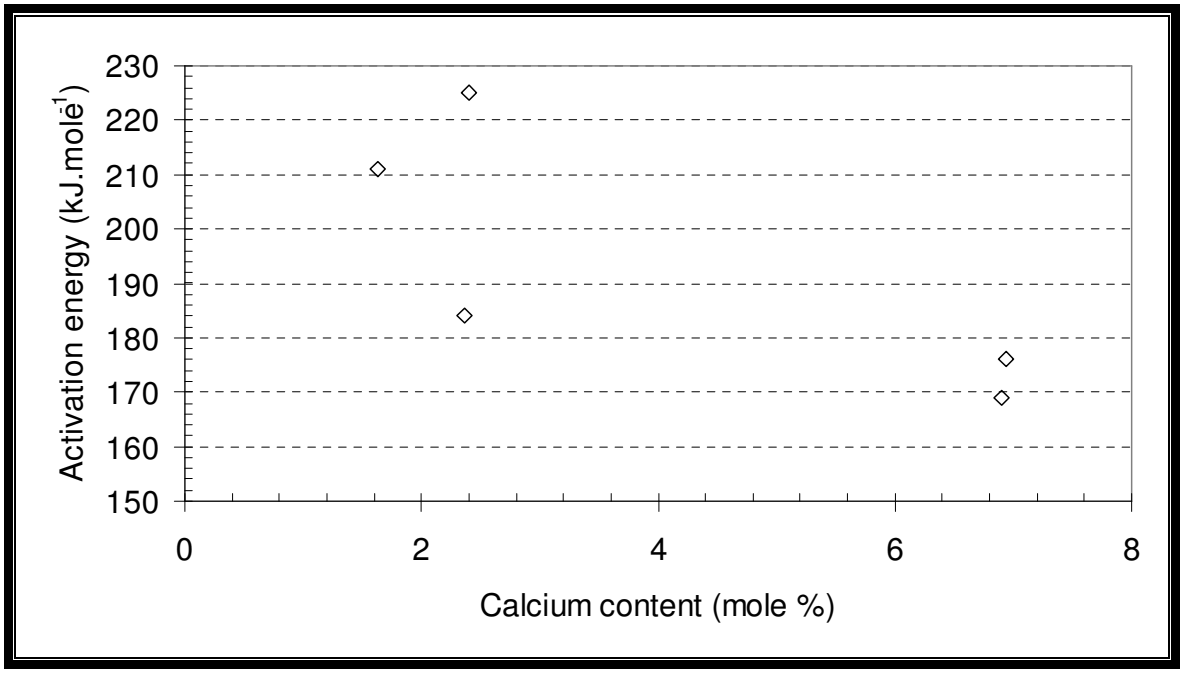


Figure 5. 20: Influence of calcium content on activation energy for coal G.

It can be observed that coal fractions containing more calcium have lower activation energies, indicating catalytic activity of calcium in the $CO_2$ gasification reaction, even though the trend is not that pronounced for coal G. Other researchers also made similar observations (Samaras et al., 1996; Liu et al., 2000b; Ochoa et al., 2001; Köpsel and Zabawski, 1990; Herman et al., 1984).

Magnesium was also seen to be associated with lower activation energy values as shown in Figure 5.21 for coal B and Figure 5.22 for coal G.

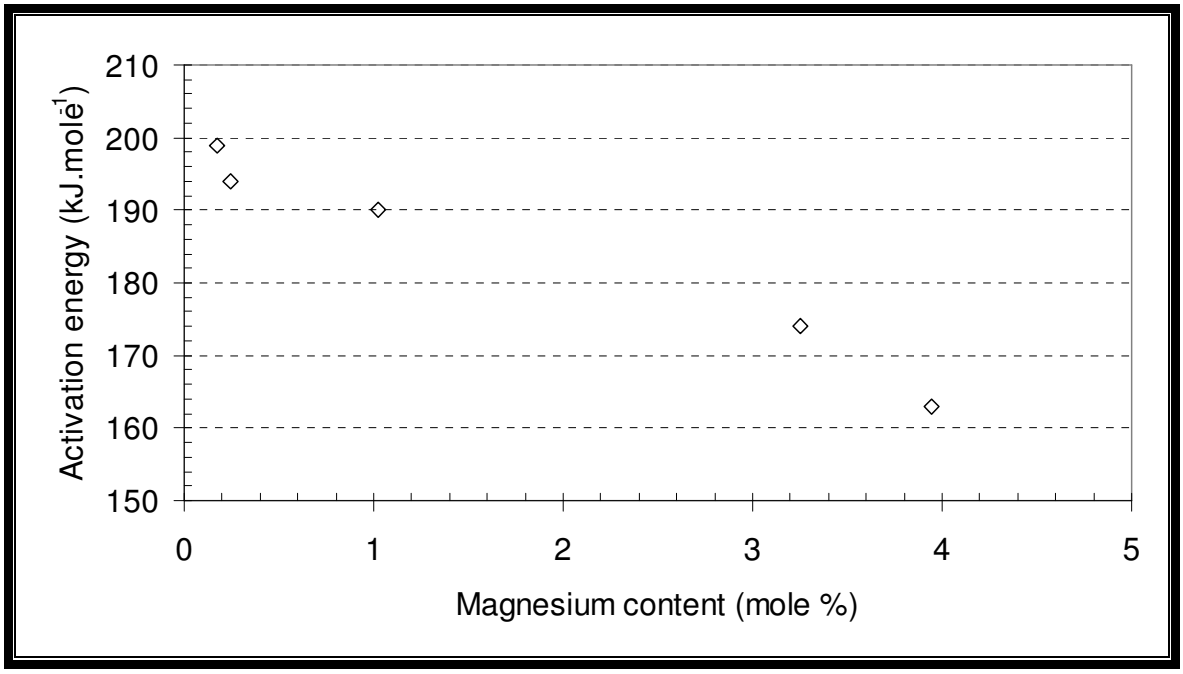


Figure 5. 21: Influence of magnesium content on activation energy for coal B

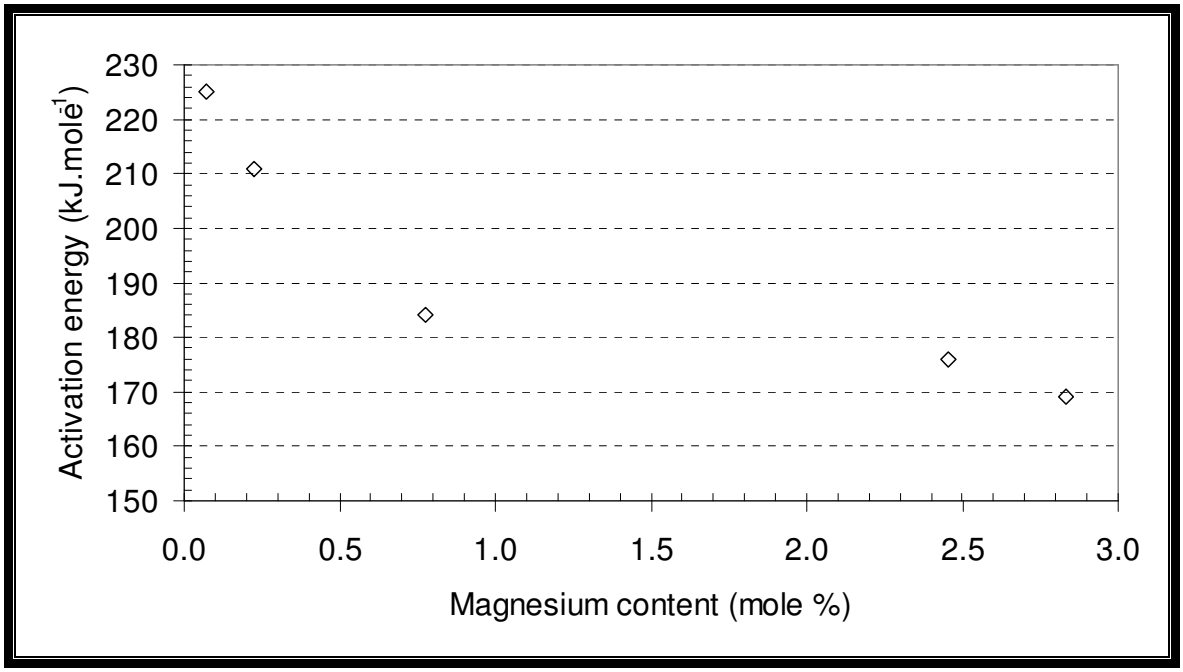


Figure 5. 22: Influence of magnesium content on activation energy for coal G

Again this trend of decreasing activation energy associated with increasing magnesium content indicates catalytic activity of magnesium in the gasification reaction. Although magnesium has not been investigated to such an extent as being a catalyst in $CO_2$ gasification, it is seen here to have the same effect as other alkaline earth metals.

For both coals B and G it was observed that fractions containing more potassium have lower activation energy values as shown in Figure 5.23 for coal B and Figure 5.24 for coal G.

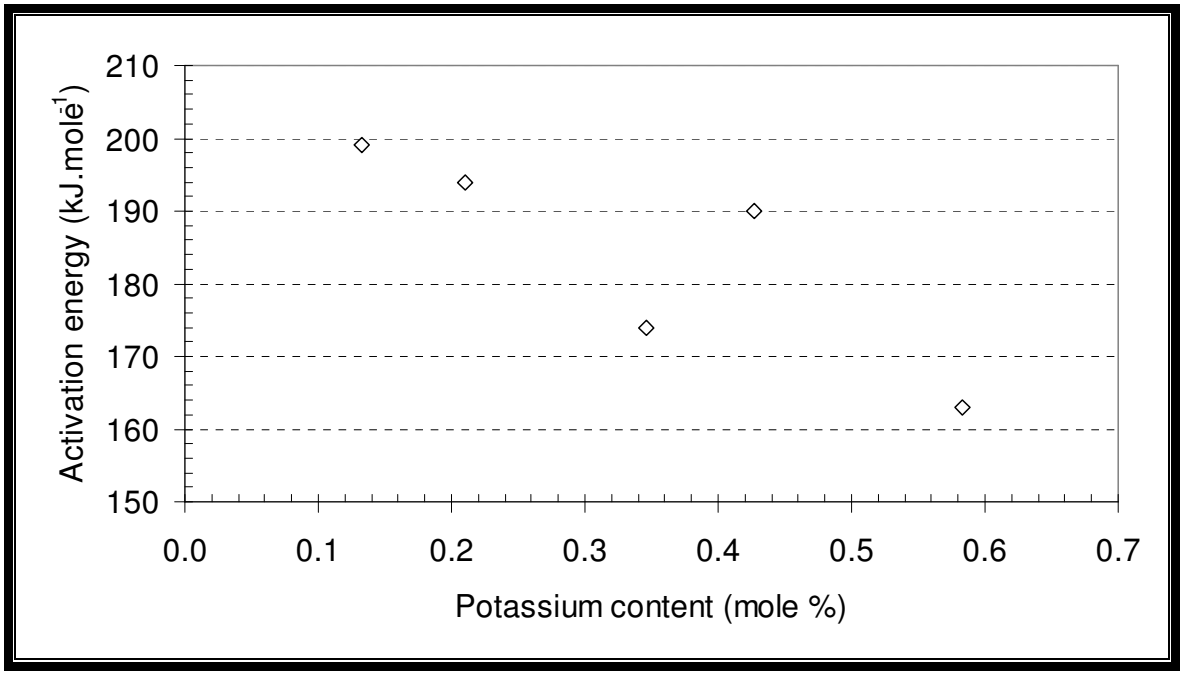


Figure 5. 23: Influence of potassium content on activation energy for coal B.

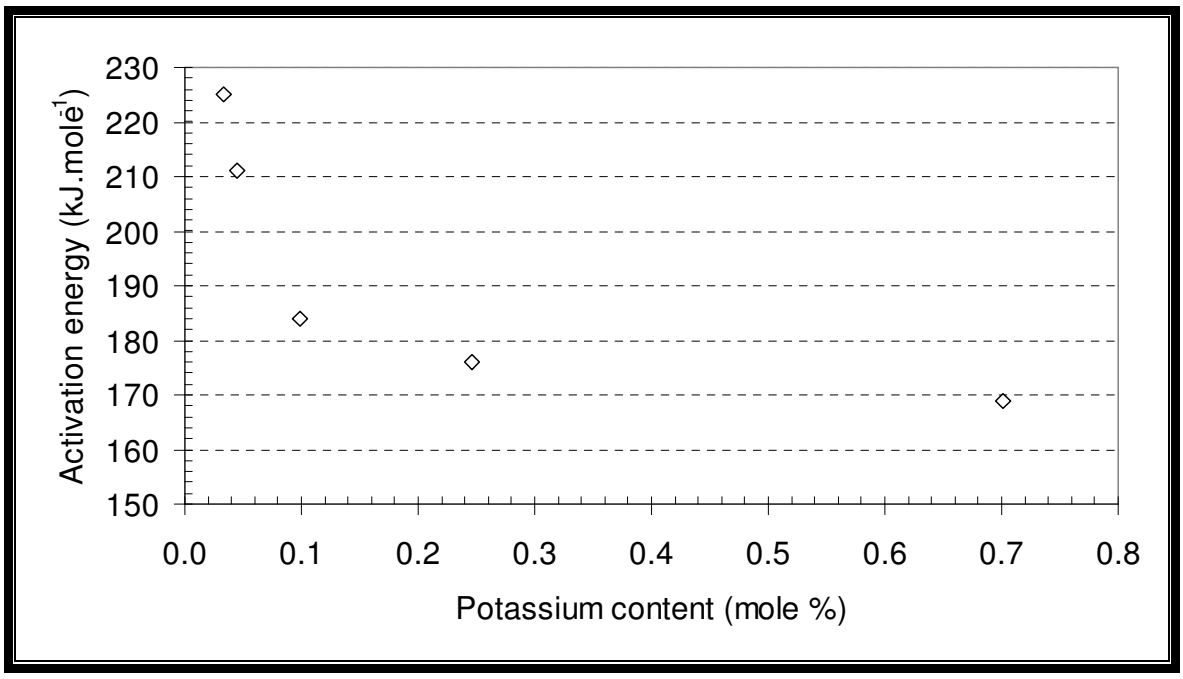


Figure 5. 24: Influence of potassium content on activation energy for coal G.

Several other researchers found that potassium is active as catalyst in the $CO_2$ gasification reaction confirming this result (Köpsel and Zabawski, 1990; Hamilton et al., 1984; Audley, 1987).

### 5.2.6 Conclusion

It was found that a lab-scale TGA is an efficient tool in evaluating the $CO_2$ gasification of coal, especially considering the kinetic evaluation and modelling data associated with the conversion of carbon in this reaction. It was observed that the conversion rate of carbon increases with increasing reaction temperature, but tends to level off at higher temperatures (T > 1030 ºC). It was also seen that increasing particle density has no significant effect on the rate of carbon conversion at relatively low density cuts (up to 1.8 $g.cm^{-3}$), but further increase in particle density results in a relatively large increase in the carbon conversion rate. The initial intrinsic reactivity was taken as a measure of the coal reactivity based on the make-up of the coal independent of the surface area. For both coals this initial intrinsic reactivity decreases with increasing density, but then shows a sharp increase in the densest fraction. The dense fractions of coal G (particle density > 1.8 $g.cm^{-3}$) is more reactive than the corresponding fractions of coal B, and this is more pronounced from a reaction temperature of 1030 ºC. This is ascribed to the low ash fusion temperature of the dense fractions of coal B compared to coal G. The initial intrinsic reactivity is related to several coal properties, as it is observed that fractions containing more inert inertodetrinite have a lower initial intrinsic reactivity. The random pore model was effectively applied to the experimental data. It was found that the structural parameter increases with increasing particle density; which signifies that the gasification reaction is more influenced by pore growth compared to pore collapse. Liptinite was also found to be associated with lower values of the structural parameter due to the swelling properties of this maceral group. Experimental and modelled data were used to calculate the activation energy of the different coal fractions. The activation energy tends to increase with increasing density and the values are in-line with previous research (163 $kJ.mole^{-1}$ - 225 $kJ.mole^{-1}$). It was seen from an elemental mole balance done on the mineral groups as detected by QEMSCAN analysis that the calcium, magnesium and potassium are associated with lower activation energy values of the coal fractions, possibly due to these elements being catalytically active in the gasification reaction.

# Chapter 6: Conclusions and Recommendations

This chapter summarizes the main findings of this study for each of the sub-categories. Section 6.1 includes the characterization of the parent coals, characterization of the density separated coal fractions, $CO_2$ gasification experiments, as well as the kinetic evaluation and modelling of the gasification reaction. Section 6.2 presents the recommendations arising from these conclusions.

## 6.1 Conclusions

### 6.1.1 Characterization: Parent coals

From the analysis of the six single-source coals as well as the gasification coal blend, it was found that all of the coals displayed properties typical of South African coals derived from the Highveld coal field, being inertinite rich, and high ash coals. The coals were classified as being typical single seam, non-blend coals, varying in rank from Medium rank C bituminous to Medium rank D bituminous coals. Coal B shows a relatively low calorific value when considering the amount of fixed carbon contained in this coal. This low calorific value of coal B is due to this coal having a significantly higher yield in the high density, low energy fractions (SG > 2.0g.cm$^{-3}$), and a lower yield in the low density, high energy fractions (SG < 1.6 g.cm$^{-3}$) compared to coal G. From the evaluation of pyrolysis gases, it was found that the total gas yield varied significantly with coal A having the highest gas yield and coal E the lowest gas yield. This variation could not be correlated to any coal properties. The pyrolysis gas composition did not show significant variation, and it was seen that $CH_4$ and $CO_2$ makes up the bulk of the pyrolysis gases followed to a lesser degree by $H_2$. These gas compositions could not be linked to any of the coal properties, especially as there were no significant variation in the coal properties and the rank of the coals.

### 6.1.2 Characterization: Density separated coal fractions

Density separation and characterization of the density separated fractions prepared from coals B and G showed that 5 coal fractions with uniquely varying properties can be prepared by this procedure.

From this characterization several significant trends were observed relating coal properties to particle density such as:

- The ash content increased with increasing particle density, while the fixed carbon content decreased with increasing particle density.
- Nitrogen in the coals is associated with the organic/volatile part of the coals, as it also increases towards the lighter fractions.
- The oxygen and sulphur can be linked to the mineral component of the coals, as it was observed that these elements increase with increasing particle density.
- The maceral analysis of the coals qualitatively showed that there is maceral segregation taking place due to maceral groups being associated with different particle densities; as inertinite reached a peak in the 1.8 $g.cm^{-3}$ – 2.0 $g.cm^{-3}$ fractions, while the vitrinite and liptinite contents increased towards the least dense coal fractions.
- Ash fusion temperature tests showed that the denser fractions of coal B have significantly lower ash flow temperatures compared to coal G. This lower ash melting temperature is possibly one of the reasons for the deviation of coal B from the other Highveld coals in terms of calorific value.
- Pyrolysis of the density separated fractions at 1000 ºC for 1 hour results in decreasing surface area from the parent coal to the char. Especially the low density, high volatile-containing fractions were affected.
- Calorific value analysis of the density separated fractions showed that the gross calorific value increases with increasing fixed carbon content associated with decreasing particle density and decreasing ash content.

### 6.1.3 Gasification: General

The $CO_2$ gasification behaviour of the various density separated fractions was reviewed; with the focus on relating coal properties to the intrinsic reactivity as well as the activation energy of the coal particles in the $CO_2$ gasification reaction. It was found that the reaction rate stays approximately constant with increasing particle density up to a density of 1.8 $g.cm^{-3}$. A further increase in particle density results in a significant increase in the reaction rate.

Initial intrinsic reactivity was used as the parameter according to which the reactivity of the various coal fractions was compared. It was observed for both coals that the densest fraction has the highest initial intrinsic reactivity. It was also concluded that the ash flow temperature influenced the initial intrinsic reactivity, especially at gasification temperatures above 1030 ºC. It was found that the inert inertodetrinite in the raw coals act as to decrease the initial intrinsic reactivity.

### 6.1.4 Gasification: Modelling and activation energy

The random pore model was found to give an adequate fit to the experimental conversion-time data. The structural parameter was seen to increase with increasing particle density. Increased liptinite contents in the raw coal fractions are associated with lower values for the structural parameter.

The activation energy for the $CO_2$ gasification reaction was calculated to vary from 163 kJ.mole$^{-1}$ to 225 kJ.mole$^{-1}$ for the various coal fractions. These values of the activation energy allow the evaluation of catalytic activity of the inorganic components. It was concluded that Ca, Mg and K catalyze the $CO_2$ gasification reaction, as increased amounts of these elements are associated with decreased activation energy values.

### 6.1.5 Prospects

Although density separation is a useful beneficiation process, it is still mostly applied in preparing coals for the export market, and not so much to prepare coal feedstocks for South African gasification processes. Beneficiation is not required in most cases as the moving-bed gasifiers in South Africa can be operated with a varying quality of coal; as the design and operation of these process units are very robust (Horsfall, 1993).

This study allowed a detailed snapshot into how coal properties vary with density. Even though it could not give a definite answer to why gasifying Highveld coal blends containing more of coal B lead to more carbon in ash, this study did however contribute to the understanding of why this inefficient gasifier operation is observed. This is related to coal B containing more high density material compared to coal G.

These high density coal particles are associated with having lower heating values as well as lower ash fusion temperatures, which may lead to lower carbon efficiencies. To limit the amount of carbon in ash will result in increased gas production, as more carbon is consumed in the gasification reaction. The following recommendations are made towards optimizing gasifier performance, especially those operating with a Highveld coal blend as feed.

## 6.2 Recommendations

Advanced characterization of the structure of the Highveld coals is recommended as to confirm the reason why coal B behaves differently from the other coals, as these coals have very similar properties.

It is recommended to do char-form analysis on density separated coal fractions, as to confirm the observations made regarding dense char formation from the inert maceral groups, as well as to evaluate the reactivity of different char forms under $CO_2$ gasification conditions.

Demineralization of the density separated coal fractions is recommended in order to isolate the maceral components. This will allow the evaluation of intrinsic gasification kinetics of maceral groups, and give insight into the properties of these groups. Further research must also be done with these density separated, demineralised coals by dosing them with alkali metals such as sodium, potassium, magnesium and calcium as to confirm the catalytic activity of these inorganic elements.

A detailed study of the ash fusion temperatures as well as mineral transformations in coal is recommended. This may involve reconstituting a coal blend from density separated coal fractions, with the coal fractions having a density of more than 1.8 $g.cm^{-3}$ removed. This is recommended as the dense coal fractions has low ash flow temperatures, and leads to more carbon encapsulated in ash. This also validates an economic feasibility study for potential beneficiation of coal B before blending, as to remove the coal fractions having a density of more than 1.8 $g.cm^{-3}$ in an attempt to lower the amount of carbon in ash obtained form the gasifiers operating with coal blends from the Highveld coal field.

Another recommendation is to include larger coal particles (> 25 mm) in kinetic gasification research. This is to confirm trends observed in fine coal research as well as to create a link between lab-scale experiments and pilot-plant experiments. This will eventually lead to lab-scale research on the kinetics of coal to be up-scaled to industrial gasifier operation.

# References

AARNA, I. AND SUUBERG, E.M. 1998. Changes in reactive surface area and porosity during char oxidation. Twentieth Symposium on Combustion. The Combustion Institute (1998): 2933 – 2939.

ALONSO, M.J.G., BORREGO, A.G., ALVAREZ, D., KALKREUTH, W. AND MENENDÉZ, R. 2001. Physiochemical transformations of coal particles during pyrolysis and combustion. Fuel, 73(2001): 485-491.

ALPERN, B., NAHUYS, J. AND MARTINEZ, L. 1984. Mineral matter in ashy and non-washable coals - Its influence on chemical properties. Symposium on Godwana coals, Lisbon – Proceedings and Papers, 70(2): 299-317.

ARENDT, P. AND VAN HEEK, K.H. 1981. Comparative investigations of coal pyrolysis under inert gas and $H_2$ at low and high heating rates and pressures up to 10MPa. Fuel, 60(9): 779-787.

AUDLEY, G.J. 1987. An evaluation of methods for enhancing the $CO_2$-reactivity of a caking bituminous coal. Fuel, 66(1987): 1635.

BAILY, J.G., TATE, A.G., DIESSEL, C.F.K. AND WALL, T.F. 1990. A char morphology system with applications to coal combustion. Fuel, 69(1990): 224.

BARKER, O.B. 1999. A techno-economic and historical overview of the South African coal industry in the 19$^{th}$ and 20$^{th}$ centuries, in Bulletin 113. ed. Pinheiro, H.J. (South African Bureau of Standards), pp. 1-63.

BERKOWITZ, N. 1985. The chemistry of coal. Amsterdam: New York.

BERMENJO, M.D., COCERO, M.J. AND FERNANDEZ-POLANCO, F. 2003. Process for generating power from the oxidation of coal in supercritical water. Fuel, 83(2003): 195-204.

BHATIA, S.K. AND GUPTA, G.R. 1992. Mathematical modelling of gas-solid reactions: Effect of pore structure. Reviews Chemical Engineering, 8(1992):177-258.

BHATIA, S.K. AND PERLMUTTER, D.D. 1980. A random pore model for fluid-solid reactions: I Isothermal kinetic control. American Institute of Chemical Engineering Journal, 26(3): 379:385.

BHATIA, S.K. AND PERLMUTTER, D.D. 1981. A random pore model for fluid-solid reactions: II Diffusion and transport effects. American Institute of Chemical Engineering Journal, 27(2): 247.

BORREGO, A.G., ALVAREZ, D. AND MENENDEZ, R. 1997. Effects of inertinite content in coal on char structure and combustion. Energy and Fuels, 43(1997): 702-761.

BROWN, R.C. AND DYKSTRA, J. 1995. Systematic errors in the use of loss-on-ignition to measure unburned carbon in fly-ash. Fuel, 74(4): 570-574.

BUNT, J.R. 2006. A new dissection methodology and investigation into coal property transformational behaviour impacting on a commercial-scale Sasol-Lurgi MK IV Fixed-Bed gasifier. Potchefstroom: NWU. (Thesis-PhD) 156p.

BUNT, J.R. 2008. Verbal communication with the author. Potchefstroom.

CAI, H.Y., GUELL, A.J., CHATZAKIS, I.N., LIM, L.Y., DUGWELL, D.R. AND KANDIYOTI, R. 1996. Combustion reactivity and morphology changes in coal chars: Effect of pyrolysis temperature, heating rate and pressure. Fuel, 75(1996): 15-24.

CAMPBELL, C.J. 2002. Peak Oil: an outlook on crude oil depletion. http//www.mbendi.com/indy/oilg/p0070.htm Date of access: 02 Mar. 2008.

CASTELLÓ, D.L., AMORÓS, D.C. AND SOLANO, A.L. 2002. Can highly activated carbons be prepared with a homogeneous micropore size distribution. Fuel Processing Technology, 77-78 (2002): 325 – 330.

CENTENO, T.A., PIS, J.J., PAJARES, J.A. AND FUERTES, A.B. 2001. Microporous structure of chars produced by pyrolysis of preoxidized coals. Journal of Analytical and Applied Pyrolysis, 58(2001): 873.

CHEN, C. AND KOJIMA, T. 1996. Single char particle combustion at moderate temperature: Effects of ash. Fuel Processing Technology, 47(1996): 215-232.

CHERMIN, H.A.G. AND VAN KREVELEN, D.W. 1956. Calculation of the free enthalpy of formation of hydrocarbons from group contributions. Fuel, 36(1956): 85.

CLARKE, L.B. AND SLOSS, L.L. 1992. Trace elements – emission from coal combustion and gasification. IEACR/49. London, UK, IEA Coal Research.

CLOKE, M. AND LESTER, E. 1994. Characterization of coals for combustion using petrographic analysis, A review. Fuel, 73(1994): 315-320.

DAS, T.K. 2001. Evolution characteristics of gases during pyrolysis of maceral concentrates of Russian coking coals. Fuel, 80(2001): 489-500.

DEBELAK, K.A. AND SCHRODT, J.T. 1979. Diffusion and adsorption in microporous solids: Measurement and effective diffusivities in coal. Journal of colloid and interface science, 70(1979): 67-73.

DEVORE, J. AND FARNUM, N. 2005. Applied statistics for engineers and scientists. Thompson-Brooks/Cole. pp. 100-127.

DU CANN, V.M. 2002. Special report: Analysis of coal product samples of South African collieries. South African Bureau of Standards.

DUTTA, S., WEN, C.Y. AND BELT, R.J.J. 1977. Reactivity of coals and char in carbon dioxide atmosphere. Ind. Eng. Chem. Process, 16(1): 20-30.

DYRCACZ, G.R., BLOOMQUIST, C.A. AND SOLOMON, P.R. 1984. Fourier transform infrared study of high purity macerals. Fuel, 63(1984): 536-542.

ECONOMIC COMMISSION FOR EUROPE. 1988. International Codification System for Medium and High Rank Coals. New York. United Nations Publication. 26p. (E.88.11.E.15).

EDDINGER, R.T. 1974. Coal – Nature's black diamond. Prepared for the American Chemical Society, Division of Fuel Chemistry, 19(1974): 5.

ERGUN, S. 1962. Kinetics of the reactions of carbon dioxide and steam with coke. U.S Bureau of Mines Bulletin. 37p.

ERICSSON, K. 2007. Co-firing - A strategy for bioenergy in Poland? Energy, 32(2007): 1838-1847.

ESSENHIGH, R.H. 1981. Fundamentals of coal combustion, in Chemistry of Coal Utilization: Second Supplementary Volume, ed. Elliot, M.A. (Wiley and Sons: New York), pp. 1153-1313.

EVERSON, R.C., NEOMAGUS, H.W.J.P., KASAINI, H. AND NJAPHA, D. 2006. Reaction kinetics of pulverized coal-chars derived from inertinite-rich coal discards: Gasification with carbon dioxide and steam. Fuel, 85(2006): 1076-1082.

EVERSON, R.C., NEOMAGUS, H.W.J.P., KAITANO, R., FALCON, R. AND DU CANN, V.M. 2008. Properties of high ash coal-char particles derived from inertinite-rich coal II: Gasification with carbon dioxide. Fuel, 87(2008): 3403-3408.

FALCON, R.M.S. 1981. The petrographic components of coal. R. Falcon Research Laboratory (Pty.)Ltd., Johannesburg, RSA.

FALCON, L.M. AND FALCON, R.M.S. 1983. The application of coal petrography to certain beneficiation technologies on South African coal. The Geological Society of South Africa., Johannesburg, RSA.

FALCON, L.M. AND FALCON, R,M.S. 1987. The petrographic composition of Southern African coals in relation to friability, hardness and abrasive indices. Journal of the South African Institute of Mining and Metallurgy, 87(10): 323-336.

FALCON, R.M.S. AND SNYMAN, C.P. 1986. An introduction to coal petrography: Atlas of petrographic constituents in the bituminous coals of Southern Africa. The Geological Society of South Africa., Johannesburg, RSA.

FENG, B. AND BHATIA, S.K. 2003. Variation of the pore structure of coal chars during gasification. Carbon(2003): 507-523.

FREIHAUT, J.D., ZABIELSKI, M.F. AND SEERY, J.D. 1982. A parametric investigation of tar release in coal devolatilisation, in Nineteenth Symposium (Int.) on Combustion. (The Combustion Institute: Pittsburg), pp. 1159-1168.

FRIESEN, W.I. AND MIKULA, R.J. 1988. Mercury porosimetry of coals. Fuel, 67(1988): 1516-1520.

GILFILLAN, A., LESTER, E., CLOKE, M. AND SNAPE, C. 1999. The structure and reactivity of density separated coal fractions. Fuel, 78(1999):1639-1644.

GÖNENÇ, Z.S. AND SUNOL, A.K. 1994. Pyrolysis of coal, in Coal Resources, Properties, Utilization, Pollution. ed. Kural, O. (Istanbul Technical University: Istanbul), pp. 337-351.

GOYAL, A., ZABRANSKY, R.F AND REHMAT, A. 1989. Gasification kinetics of Western Kentucky bituminous coal char. Industrial Engineering Chemistry, 28(1989): 1767-1778.

GRAINGER, L. AND GIBSON, J. 1981. Coal utilization: Technology, Economics and Policy. Graham and Trotman. pp.1-30.

GRIFFIN, L.P., HOWARD, J.B. AND PETERS, W.A. 1994. Pressure and temperature effects in bituminous coal pyrolysis: Experimental observations and a transient lumped parameter model. Fuel, 73(1994): 591.

GURURAJAN, V.S., AGARWAL, P.K. AND AGNEW, J.B. 1992. Mathematical modelling of fluidized-bed coal gasifiers. Trans IchemE, 70(1992): 211-237.

HAMILTON, R.T., SAMS, D.A. AND SHADMAN, F. 1984. Variation of rate during potassium-catalysed $CO_2$ gasification of coal char. Fuel, 63(1984): 1008

HASHIMOTO, K., MIURA, K. AND UEDA, T. 1986. Correlation of gasification rates of various coals measured by rapid heating method in a steam atmosphere at relatively low temperature. Fuel, 65(1986): 1516.

HERMAN, R.G., SIMMONS, G.W., COLE, D.A., KUZMICZ, V AND KLIER, K. 1984. Catalytic action of minerals in the low temperature oxidation of coal. Fuel, 63(1984): 673-678.

HODGE, E.M., ROBERTS, D.G., HARRIS, D.J. AND STUBINGTON, J.F. The significance of char morphology to the analysis of high – temperature char – $CO_2$ reaction rates. Energy and Fuels, 24(2010): 100-107.

HOMMA, S., OGATA, S., KOGA, J. AND MATSUMOTO, S. 2005. Gas-solid reaction model for a shrinking core spherical particle with unreacted shrinking core. Chemical Engineering Science, 60(2005): 4971-4980.

HORSFALL, D.W. 1993. Coal preparation and usage - Volume 1. Coal Publications (Pty) Ltd.

HSU, G.C., KALVINSKAS, J.J., GANGULI, P.S. AND GAVALAS, G.R. 1977. Coal desulphurization by low temperature chlorinolysis, in Coal Desulphurization: Chemical and Physical methods. pp. 311-358.

HURT, R.H., SAROFIM, A.F. AND LONGWELL, J.P. 1991. The role of microporous surface area in the gasification of chars from sub-bituminous coal. Fuel, 70(1991): 1079-1082.

HURT, R.J. AND GIBBINS, J.R. 1995. Residual carbon from pulverized coal fired boilers: Size distribution and combustion reactivity. Fuel, 74(1995): 471-480.

HUTTINGER, K.J. AND NATTERMAN, C. 1994. Correlation between coal reactivity and inorganic matter content for pressure gasification with steam and carbon dioxide. Fuel, 73(1994): 1682.

ISO 351 (International Standards Organization). 1984 . Solid mineral fuels – Determination of total sulphur – High temperature combustion method. Standards South Africa.

ISO 7404 – 2 (International Standards Organization). 1985. Methods for the petrographic analysis of bituminous coal and anthracite. Part 2: Method of preparing coal samples. Standards South Africa.

ISO 7404 – 3 (International Standards Organization). 1985. Methods for the petrographic analysis of bituminous coal and anthracite. Part 3: Method of determining maceral group composition. Standards South Africa.

ISO 7404 – 4 (International Standards Organization). 1985. Methods for the petrographic analysis of bituminous coal and anthracite. Part 4: Method of determining microlithotype, carbominerite and minerite composition. Standards South Africa.

ISO 7404 – 5 (International Standards Organization). 1985. Methods for the petrographic analysis of bituminous coal and anthracite. Part 5: Method of determining microscopically the reflectance of vitrinite . Standards South Africa.

ISO 7936 (International Standards Organization). 1992. Hard coal – Determination and presentation of float and sink characteristics: General directions for apparatus and procedures. Standards South Africa.

ISO 1213 (International Standards Organization). 1992. Solid mineral fuels – Vocabulary. Part 2: Terms relating to sampling, testing and analysis. Standards South Africa.

ISO 540 (International Standards Organization). 1995. Solid mineral fuels – Determination of fusibility of ash – High temperature tube method. Standards South Africa.

ISO 1171 (International Standards Organization). 1997. Solid mineral fuels – Determination of ash content. Standards South Africa.

ISO 562 (International Standards Organization). 1998. Hard coal and coke – Determination of volatile matter. Standards South Africa.

ISO/TS 12902 (International Standards Organization). 2001. Solid mineral fuel – Determination of total carbon, hydrogen and nitrogen – Instrumental methods. Standards South Africa.

ISO 11760 (International Standards Organization). 2005. Classification of coals. Standards South Africa.

JOHNSON, J.L. 1979. Kinetics of gasification. New York: Wiley and Sons. 283p.

JONES, R.B., McCOURT, C.B., MARLEY, C. AND KING, K. 1985. Macerals and rank influence on the morphology of coal char. Fuel, 64(1985): 640.

JOUTSENOJA, T., SAASTAMOINEN, J., AHO, M. AND HERNBERG, R. 1999. Effects of pressure and oxygen concentration on the combustion of different coals. Energy and Fuels, 13(1999): 130-145.

KAJITANI, S., SUZUKI, W., ASHIZAWA, M. AND HARA, S. 2006. $CO_2$ gasification rate analysis of coal char in entrained flow coal gasifier. Fuel, 85(2006): 163-169.

KAJITANI, S. AND MATSUDA, S.H.H. 2002. Gasification rate analysis of coal char with a pressurized drop tube furnace. Fuel, 81(2002): 539-546.

KAWASHIMA, H., YAMASHITA, Y. AND SAITO, I. 2000. Studies on the structural changes of coal density-separated components during pyrolysis by means of solid-state C NMR spectra. Journal of Analytical and Applied Pyrolysis, 53(2000): 35-50.

KHAN, M.R. 1989. A literature survey and an experimental study of coal devolatilisation at mild and severe conditions: Influences of heating rate, temperature and reactor type on product yield and composition. Fuel, 68(12): 1513-1522.

KÖPSEL, R. AND ZABAWSKI, H. 1990. Catalytic effects of ash components in low rank coal gasification. Part 1: Gasification with carbon dioxide. Fuel, 69(1990): 275.

KOSMINSKI, A., ROSS, D.P. AND AGNEW, J.B. 2006. Influence of gas environment on reaction between sodium and silicon minerals during gasification of low-rank coal. Fuel Processing Technology, 87(2006): 953-962.

KYOTANI, T., KUBOTA, K., CAO, J., YAMASHITA, H. AND TOMITA, A. 1993. Combustion and $CO_2$ gasification of coals in a wide temperature range. Fuel Processing Technology, 36(1993): 209-217.

LAINE, N.R., VASTOLA, F.J. AND WALKER, P.L. 1963. The importance of active surface area in the carbon-oxygen reaction. Journal of Physical Chemistry, 67(1963): 2030-2034.

LAURENDEAU, N.M. 1978. Heterogeneous kinetics of coal char gasification and combustion. Progress in Energy and Combustion Science, 4(1978): 221.

LEMAIGNEN, L., ZHAO, Y., REED, G.P., DUGWELL, D.R. AND KANDIYOTI, R. 2002. Factors governing reactivity in low temperature coal gasification. Part II: An attempt to correlate conversions with inorganic and mineral constituents. Fuel, 81(2002): 315-326.

LEVENSPIEL, O. 1972. Chemical reaction engineering, 2nd ed. New York: Wiley and Sons.

LIU, G.S. 1999. Mathematical modelling of coal char reactivity in a pressurized entrained flow gasifier. Australia: University of Newcastle. (Thesis – PhD).

LIU, G., BENYON, P., BENFELL, K.E., BRYANT, G.W., TATE, A.G., BOYD, R.K., HARRIS, D.J. AND WALL, T.F. 2000a. The porous structure of bituminous coal chars and its influence on combustion and gasification under chemically controlled conditions. Fuel, 79(2000): 617-626.

LIU, G., TATE, A.G., BRYANT, G.W. AND WALL, T.F. 2000b. Mathematic modelling of coal char reactivity with $CO_2$ at high pressures and temperatures. Fuel, 79(2000): 1145-1154.

LIU, H., LUO, C., TOYOTA, M., KATO, S., UEMIYA, S., KOJIMA, T. AND TOMINAGA, H. 2003. Mineral reaction and morphology change during gasification of coal in $CO_2$ at elevated temperatures. Fuel, 82(2003): 523-530.

LIU, H., KANEKO, M., LUO, C., KATO, S. AND KOJIMA, T. 2004. Effect of pyrolysis time on gasification reactivity of char with CO2 at elevated temperatures. Fuel, 83(2004): 1055-1061.

LIU, H., LUO, C., KATO, S., UEMIYA, S., KANEKO, M. AND KOJIMA, T. 2006. Kinetics of $CO_2$/Char gasification at elevated temperatures: Part 1: Experimental results. Fuel Processing Technology, 87(2006): 775.

LU, G.Q. AND DO, D.D. 1992. A kinetic study of coal reject-derived char activation with $CO_2$, $H_2O$ and air. Carbon, 30(1): 21-29.

LU, G.Q. AND DO, D.D. 1994. Comparison of structural models for high-ash char gasification. Carbon, 32(2): 247-263.

LU, L., SAHAJWALLA, D. AND HARRIS, D. 2000. Characteristics of chars prepared from various pulverized coals at different temperatures using a drop-tube furnace. Energy and Fuels, 14(2000): 869-876.

LYNCH, L.J., WEBSTER, D.S., SAKUROVS, R., BARTON, W.A. AND MAHER, T.P. 1988. The molecular basis of coal thermoplasticity. Fuel, 67(1988): 579-583.

MACHNIKOWSKA, H., KRZTON, A. AND MACHNIKOWSKI, J. 2002. The characterization of coal macerals by diffuse reflectance infrared spectroscopy. Fuel, 81(2002): 245-252.

MANOVIC, V., GRUBOR, B. AND LANCAREVIC, D. 2006. Modelling of inherent $SO_2$ capture in coal particles during combustion in fluidized bed. Chemical Engineering Science, 61(2006): 1676-1685.

MARQUEZ - MONTESINOS, F., CORDERO, T., RODRÍGUEZ – MIRASOL, J. AND RODRÍGUEZ, J.J. 2002. $CO_2$ and steam gasification of grapefruit skin char. Fuel, 81(2002): 423-429.

MATJIE, R.H. AND VAN ALPHEN, C. 2008. Mineralogical features of size and density fractions in Sasol coal gasification ash, South Africa and potential by-products. Fuel, 87(2008): 1439-1445.

MATJIE, R.H., ZHONGSHENG, L. AND WARD, C.R. 2008. Determination of mineral matter and elemental composition of individual macerals in coals from Highveld mines. Sasol Technology R&D Internal Report.

MATSUOKA, K., YAMASHITA, T., KURAMOTO, K., SUZUKI, Y., TAKAYA, A. AND TOMITA, A. 2008. Transformation of alkali and alkaline earth metals in low rank coal during gasification. Fuel, 87(2008): 885-893.

MEGARITIS, A., MESSENBÖCK, R.C., CHATZAKIS, I.N., DUGWELL, D.R. AND KANDIYOTI, R. 1999. High pressure pyrolysis and $CO_2$-gasification of coal maceral concentrates: Conversions and char combustion reactivities. Fuel, 78(1999): 871-882.

MÉNDEZ, L.B., BORREGO, A.G., MARTINEZ-TARAZONA, M.R. AND MENENDEZ, R. 2003. Influence of petrographic and mineral matter composition of coal particles on their combustion reactivity. Fuel, 82(2003): 1875-1882.

MIURA, K., HASHIMOTO, K. AND SILVESTON, P.L. 1989. Factors affecting the reactivity of coal chars during gasification and indices representing reactivity. Fuel, 68(1989): 1416.

MOULIJN, J.A. AND TROMP, P.J.J. 1985. Coal pyrolysis, in Carbon and Coal Gasification- Science and Technology. (Martinus Nijhoff Publishers: Dordrecht). pp.455-484.

NANDI, S.P. AND WALKER, P.L. 1964. The diffusion of nitrogen and carbon dioxide from coals of various rank. Fuel, 43(1964): 385-393.

NEAVEL, R.C. 1982. Origin, petrography and classification of coal, in Chemistry of Coal Utilization: Second Supplementary Volume, ed. Elliot, M.A. (Wiley and Sons: New York), pp. 91-158.

NISHIYAMA, Y. 1986. Catalytic behaviour of iron and nickel in coal gasification. Fuel, 65(10): 1404-1409.

NOWAKII, P. 1981. Coal gasification processes. Energy Technology Review, 70(1981): 77-137.

O'BRIEN, W.S., WU, R.C.R., MOSLEHI, A. AND CHEN, J.W. 1990. Modelling of coal in a mild-temperature gasifier, in Processing and Utilization of High-Sulphur Coals III. (Elsevier: Amsterdam), pp. 675-685.

OCHOA, J., CASSANELLO, M.C., BONELLI, P.R. AND CUKIERMAN, A.L. 2001. $CO_2$ gasification of Argentinean coal chars: A kinetic characterization. Fuel, 74(2001): 161-176.

OKI, T., YOTSUMOTO, H. AND OWADA, S. 2004. Calculation of degree of mineral matter liberation in coal from sink-float separation data. Minerals Engineering, 17(2004): 39-51.

OSBORNE, D.G. 1988. Coal preparation technology: Volume 1. (Graham and Trotham: Oxford), pp. 153-199.

PARK, W.H., PARK, K.W., BOIK, N.J. AND PARK, D. 1989. Low temperature pyrolysis of high volatile coals in a fluidized bed, in Sixth Korea-USA joint workshop on Coal Utilization Technology, Seoul, Korea, 17-18Oct 1989. Daejon, Korea, Korea Institute of Energy and Resources. Energy and Environmental Research Division. pp. IV59-IV72.

PARKS, B. 1963. Origin and petrography and classification of coal, in Chemistry of Coal Utilization: Second Supplementary Volume, ed. Lawry, H.H. (Wiley and Sons: New York), pp. 1-34.

PETERSON, E.E. 1957. Reaction of porous solids. American Institute of Chemical Engineering Journal, 3(1957): 443-448.

PLUMSTEAD, E.P. 1966. The story of South Africa's coal. Optima, (16): 186-202.

RICHARD, J.R., AL MAIJTHOUB, M., AHO, M.J. AND PIRKONEN, P.M. 1993. Separate effects of pressure and some other variables on char combustion under fixed bed conditions. Fuel, 73(4): 485-491.

ROBERTS, D.G. AND HARRIS, D.J. Char gasification with $O_2$ $CO_2$ and $H_2O$: Effects of pressure on intrinsic reaction kinetics. Energy and Fuels, 14(2000): 483-489.

ROSENBURG, P., PETERSEN, H.I. AND THOMSEN, E. 1996. Combustion char morphology related to combustion temperature and coal petrography. Fuel, 9(1996): 739.

RUSSEL, N.V., BEELY, T.J., MAN, C.K., GIBBINS, J.R. AND WILLIAMSON, J. 1998. Development of TG measurements of intrinsic char combustion reactivity for industrial and research purposes. Fuel Processing Technology, 57: 113-130.

SABS SM 924 (South African Bureau of Standards). 1978. Moisture content of coal samples intended for general analysis: Vacuum oven method. Council of the South African Bureau of Standards.

SABS SM 1073 (South African Bureau of Standards). 1984. Yields of tar, water, gas and coke residue from coal by low temperature distillation. Council of the South African Bureau of Standards.

SALATINO, P. AND SENNECA, O. 1998. Loss of gasification reactivity of chars upon thermal annealing. International Conference on ash behaviour control in energy conversion systems. Pacifico Yokohama, Japan.

SAMARAS, P., DIAMADOPOULOS, E. AND SAKELLAROPOULOS, G. 1996. The effect of mineral matter and pyrolysis conditions on the gasification of Greek lignite by carbon dioxide. Fuel, 75(1996): 1108-1114.

SANDERS, D. 1996. Coal characterization in marketing – An elementary approach, Workshop on coal characterization – for existing and emerging technologies. CRC for Black Coal Utilization. Newcastle, Australia.

SASOL. 2007. SSL Annual and Transitional Report. 125p.

SASOL. 2007. Sasol Facts. http://Sasol.investoreports.com/Sasol_sf_2007/ downloads/segmented/Sasol_facts_introdcing_sasol.pdf Date of access: 02 Mar. 2008.

SCARONI, A.W., WALKER, P.L. AND ESSENHIGH, R.H. 1981. Kinetics of lignite pyrolysis in an entrained flow, isothermal furnace. Fuel, 60(1981):71-66.

SHILLING, H.D., BONN, B. AND KRAUSS, U. 1981. Coal gasification: Existing processes and new developments. Graham and Trotman: London. 330p.

SHIRAZI, A.R., BÖRTIN, O., EKLUND, L. AND LINDQVIST, O. 1995. The impact of mineral matter in coal on its combustion, and a new approach to the determination of the calorific value of coal. Fuel, 74(1995): 247-251.

SIMBECK, D.R., KORENS, N., BIASCA, F.E., VEJATASA, S. AND DICKENSON, R.L. 1993. Coal gasification guidebook: Status, applications and technologies.

SIMON, G.A. 1983. The role of pore structure in coal pyrolysis and gasification. Progress in Energy Combustion Science, 9(1983): 227.

SMOOT, L.D. AND SMITH, P.J. 1985. Coal gasification and combustion. New York and London: Plenum Press.

SOLOMON, P.R., SERGIO, M.A. AND SUUBERG, E.M. 1992. Coal pyrolysis: Experiments, kinetic rates and mechanisms. Progress in Energy and Combustion Science, 18(2): 133-220.

SOLOMON, P.R., SERGIO, M.A., DESPONDE, G.V. AND KROO, E. 1990. Cross-linking reactions during coal conversion. Energy and Fuels, 4(1): 42-54.

SOUTH AFRICA. Department of Minerals and Energy. 2007. Coal. http://www.dme.gov.za/energy/coal.stm Date of access: 02 Mar. 2008.

SPEARS, D.A. 2000. Role of clay minerals in UK coal combustion. Applied Clay Science, 16(2000): 87-95.

STANDISH, N. AND TANJUNG, A.F.A. Gasification of single wood charcoal particles in $CO_2$. Fuel, 67(1988): 666-672.

STREZOV, V., LUCAS, J.A. AND WALL, T.F. 2005. Effect of pressure on the swelling of density-separated coal particles. Fuel, 84(2005): 1238-1245.

STUBINGTON, J.F. AND LINJEWILE, T.M. 1989. The effects of fragmentation on devolatalisation of large coal particles. Fuel, 68(1989): 155-160.

SUUBERG, E.M., PETERS, W.A. AND HOWARD, J.B. 1978. Product composition and kinetics of lignite pyrolysis. Industrial Engineering Process Design and Development, 17(1): 37-46.

TAKARADA, T., TAMAI, Y. AND TOMITA, A. 1985. Reactivities of 34 coals under steam gasification. Fuel, 64(1985): 1438-1442.

TONGE, J. 1907. Coal. London: Archibald Constable and Company. pp.1-4.

TSAI, S.C. 1982. Fundamentals of coal beneficiation and utilization. Amsterdam: Elsevier. 292p.

TSAI, C.Y. AND SCARONI, A.W. 1987. The structural changes of bituminous coal particles during the initial stages of pulverized-coal combustion. Fuel, 66(1987): p. 200.

VAN DYK, J.C., KEYSER, M.J. AND VAN ZYL, J.W. 2001. Suitability of feedstocks for the Sasol-Lurgi Fixed Bed Dry Bottom gasification process. GTC Conference, San Fracisco, USA.

VAN DYK, J.C. AND WAANDERS, F.B. 2007. Manipulation of gasification coal in order to increase the ash fusion temperature of the coal enabling the gasifiers to operate at higher temperatures. Fuel, 86(2007): 2728-2735.

VAN DYK, J.C., BENSON, S.A., LAUMB, M.L. AND WAANDERS, B. 2009. Coal and coal ash characteristics to understand mineral transformations and slag formation. Fuel, 88(2009): 1057-1063.

WAANDERS, F.B. AND GOVENDER, A. 2005. Mineral associations in coal and their transformation during gasification. Hyperfine Interactions, 166(2005): 687-691.

WAGNER, N.J. 1998. The effect of weathering on stored discard coals and the impact on combustion. Johannesburg: University of the Witwatersrand. (Thesis – PhD).

WAGNER, N.J., MATJIE, R.H., SLAGHUIS, J.H. AND VAN HEERDEN, J.H.P. 2008. Characterization of unburned carbon present in coarse gasification ash. Fuel, 87(2008): 683-691.

WALKER, P.L. 1977. The scientific base of coal gasification. Industrial Heating, 44(11): 16-20.

WALKER, P.L., RUSINKO, F. AND AUSTIN, L.G. 1959. Gas reactions of carbon. Advanced Catalysis, 11(1959): 133-221.

WCI. 2007. Coal Facts: 2007 Edition with 2006 data. http://www.worldcoal.org/assets_cm/files/pdf/fact_card07.pdf Date of access: 02 Mar. 2008.

WICKE, E. 1955. Contributions to the combustion mechanism of carbon. Procured 5th Symposium (Int) Combustion. New York: Reinhold Publishing Corp. pp245-252.

WIGMANS, T., GEBEL, J.C., AND MOULIJN, J.A. The influence of pre-treatment on the activity and stability of sodium and potassium catalysts in carbon-steam reactions. Carbon, 21(1983): 295-301.

WILDMAN, J. AND DERBYSHIRE, F. 1991. Origins and functions of macroporosity in activated carbons from coal and wood precursors. Fuel, 70(1991): 655-661.

XU, W.C. AND TOMITA, A. 1987. Effect of coal type on the flash pyrolysis of various coals. Fuel, 66(5): 627-631.

YE, D.P., AGNEW, J.B. AND ZHANG, D.K. 1998. Gasification of South Australian low rank coal with carbon dioxide and steam: Kinetics and reactivity studies. Fuel, 77(11): 1209-1219.

YU, J.L., STREZOV, V., LUCAS, J., LIU, G.S. AND WALL, T. 2002. A mechanistic study on char structure evolution during coal devolatilisation-Experiments and model predictions. Proceedings of the Combustion Institute, 29(2002): 467-473.

YÜCEL, H., CAKAL, G.Ö. AND GÜRÜZ, A.G. 2007. Physical and chemical properties of Turkish lignites and their pyrolysis and gasification rates determined by thermogravimetric analysis. Journal of Analytical and Applied Pyrolysis, 80(2007): 262-268.

ZONG, Z.M., ZHANG, J.W., WANG, T.X., XIE, R.L., DING, M.J., CAI, K.Y., HUANG, Y.G., GAO, J.S., WU, Y.Q. AND WEI, X.Y. 2007. Reactivities of Shenfu chars towards gasification with carbon dioxide. Journal of China University of Mining and Technology, 17(2): 197-200.

# Appendices

## Appendix A: Parent coal reflectance histograms

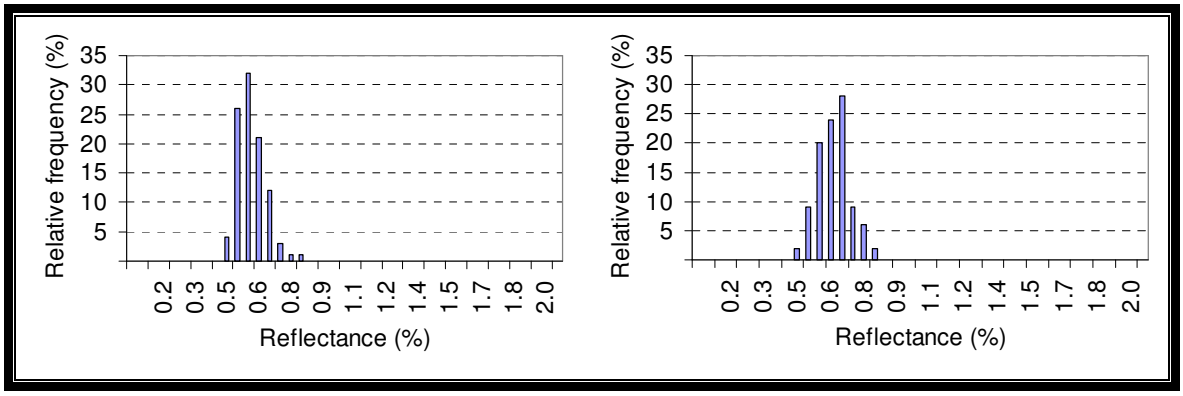


Figure A. 1: Reflectance histograms: coal A and coal B.

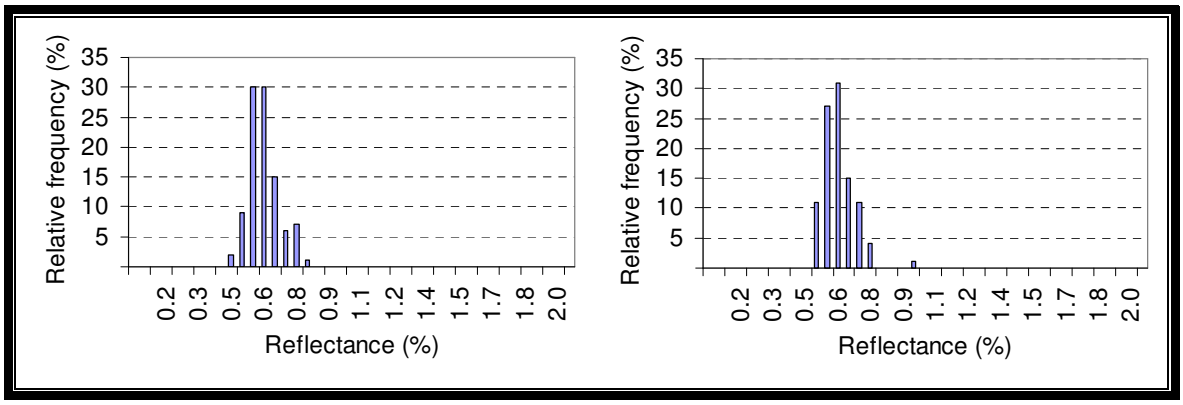


Figure A. 2: Reflectance histograms: coal C and coal D.

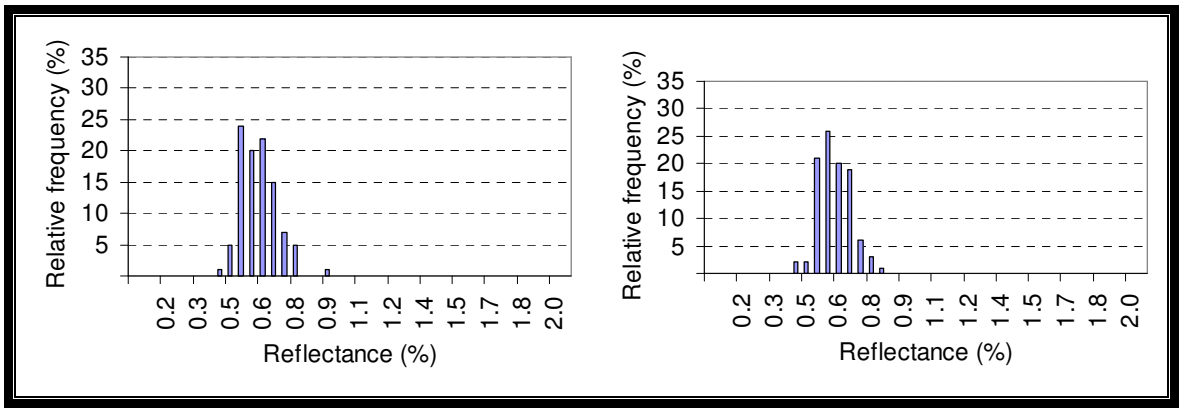


Figure A. 3: Reflectance histograms: coal E and coal F.

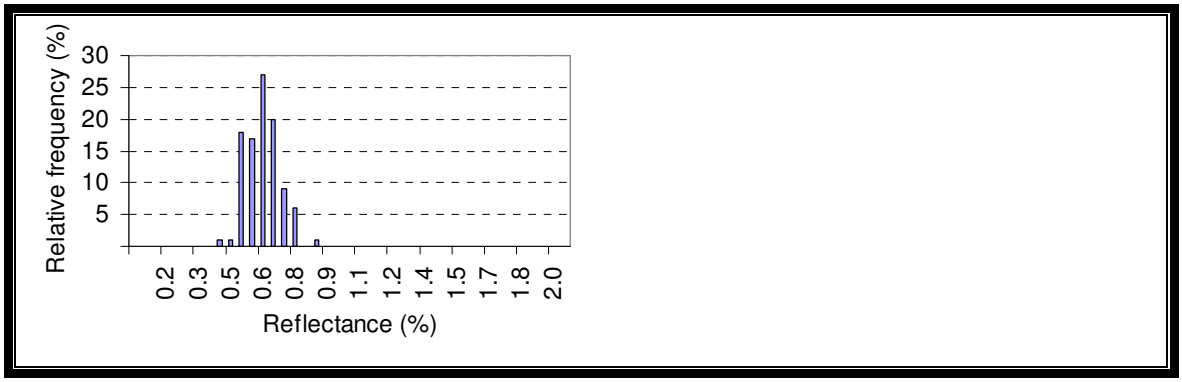


Figure A. 4: Reflectance histograms: coal G.

# Appendix B: Flow controller calibration curves

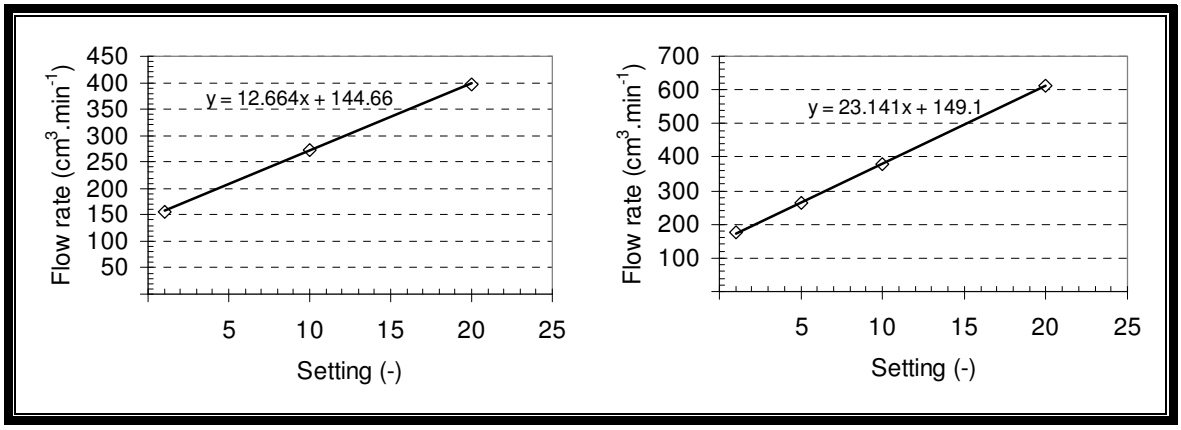


Figure B. 1: Calibration curves for nitrogen gas to purge and furnace.

The characteristic equation describing the flow rate as a function of the flow meter setting for the nitrogen purge gas is given by:

$$y = 12.66x + 144.66 \quad \text{(B.1)}$$

The characteristic equation giving the relation between flow rate and flow meter setting for the nitrogen to the furnace is given by:

$$y = 23.14x + 149.1 \quad \text{(B.2)}$$

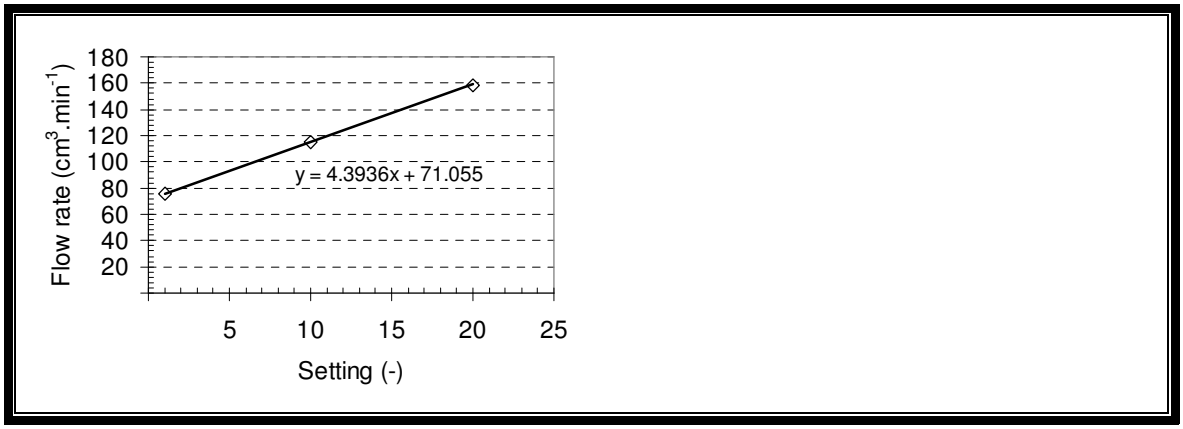


Figure B. 2: Calibration curve for carbon dioxide gas to furnace.

The characteristic equation describing the flow rate of carbon dioxide to the furnace as a function of flow meter setting is given by:

$$y = 4.40x + 71.06 \quad \text{(B.3)}$$

# Appendix C: TGA curves

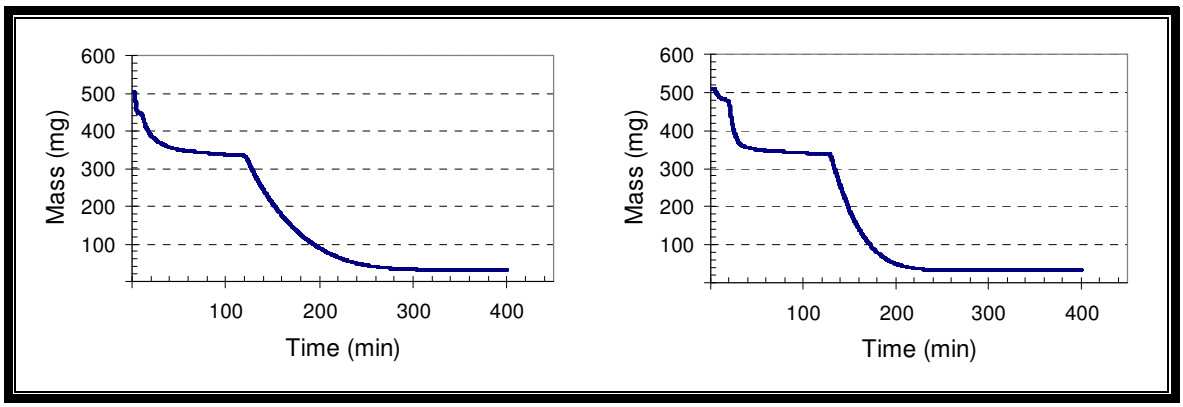


Figure C. 1: TGA curves for coal B1 at 1000ºC and 1015ºC.

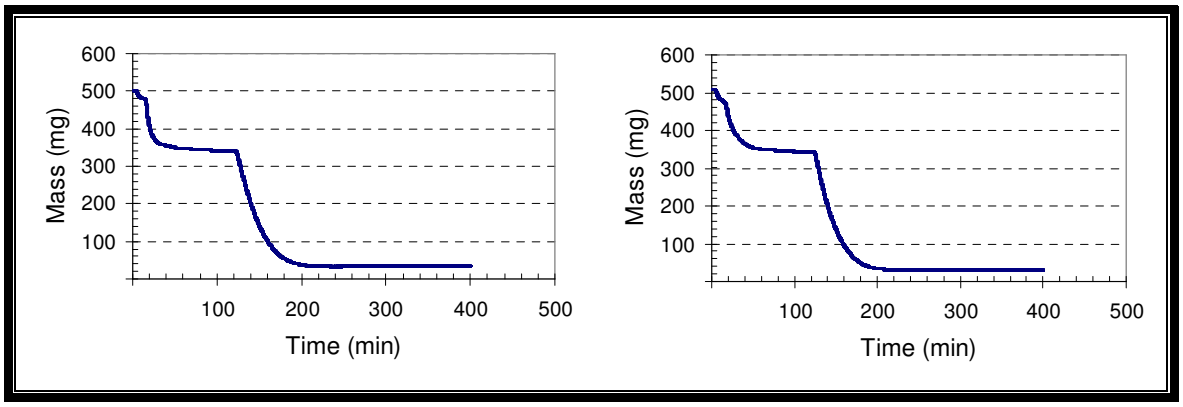


Figure C. 2: TGA curves for coal B1 at 1030ºC and 1070ºC.

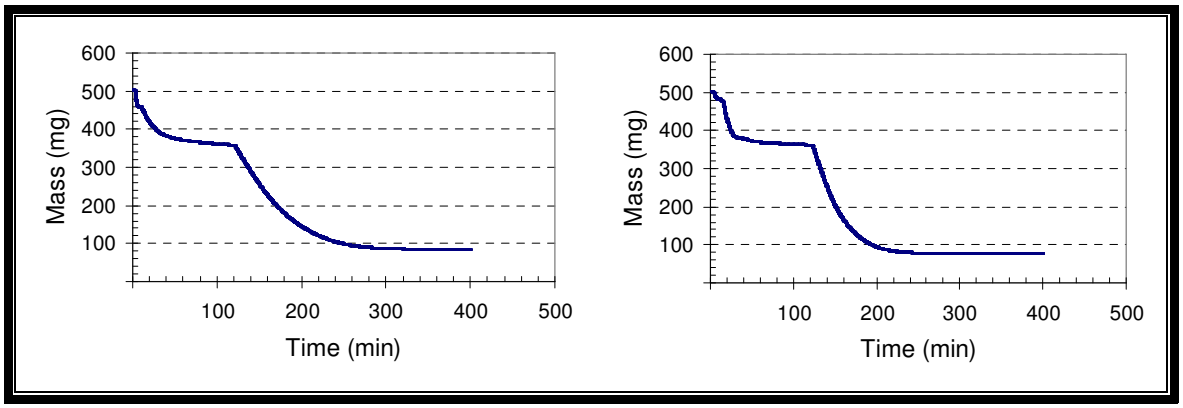


Figure C. 3: TGA curves for coal B2 at 1000ºC and 1015ºC.

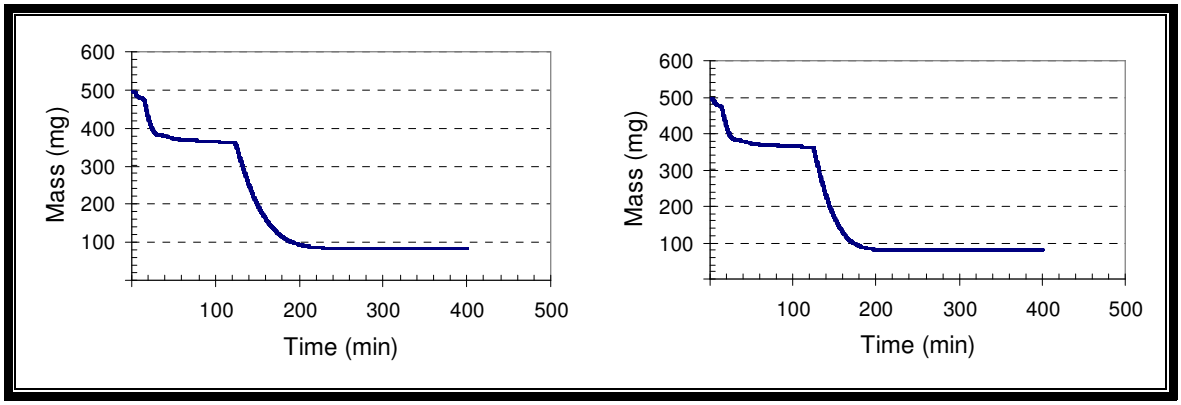


Figure C. 4: TGA curves for coal B2 at 1030ºC and 1070ºC.

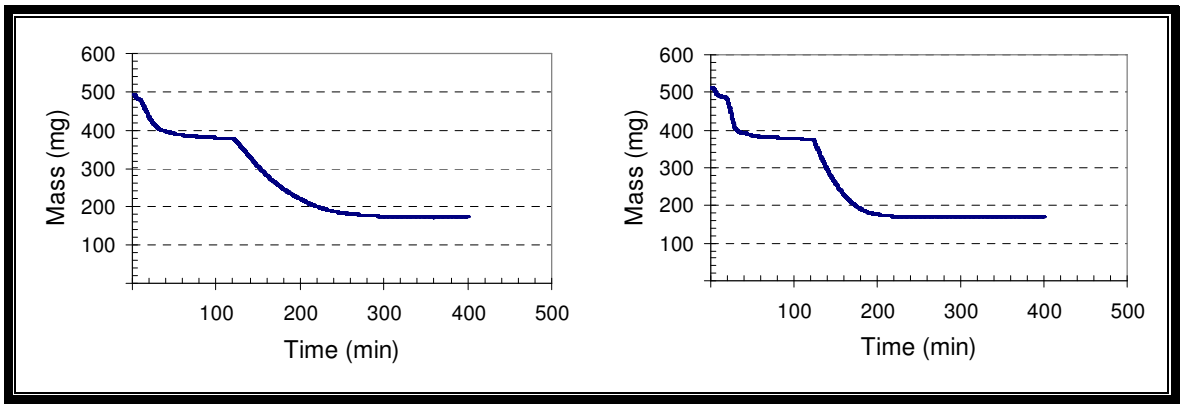


Figure C. 5: TGA curves for coal B3 at 1000ºC and 1015ºC.

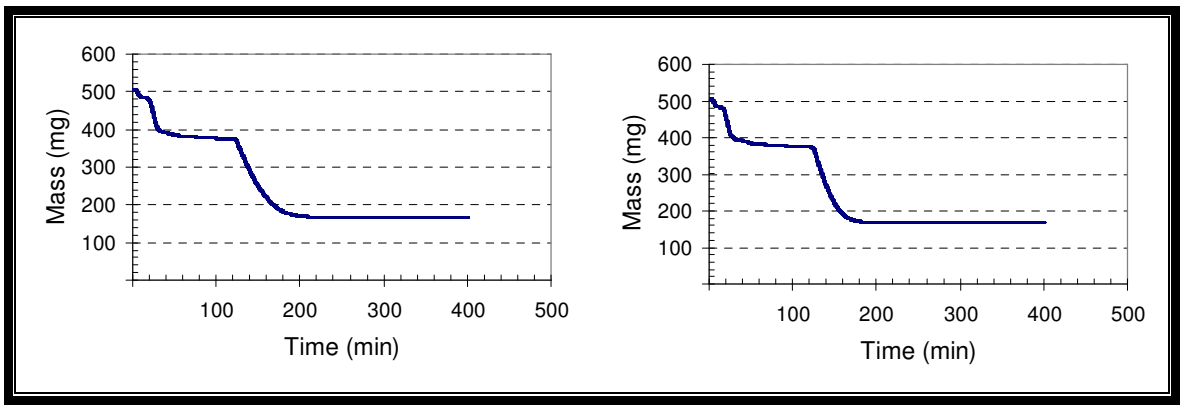


Figure C. 6: TGA curves for coal B3 at 1030ºC and 1070ºC.

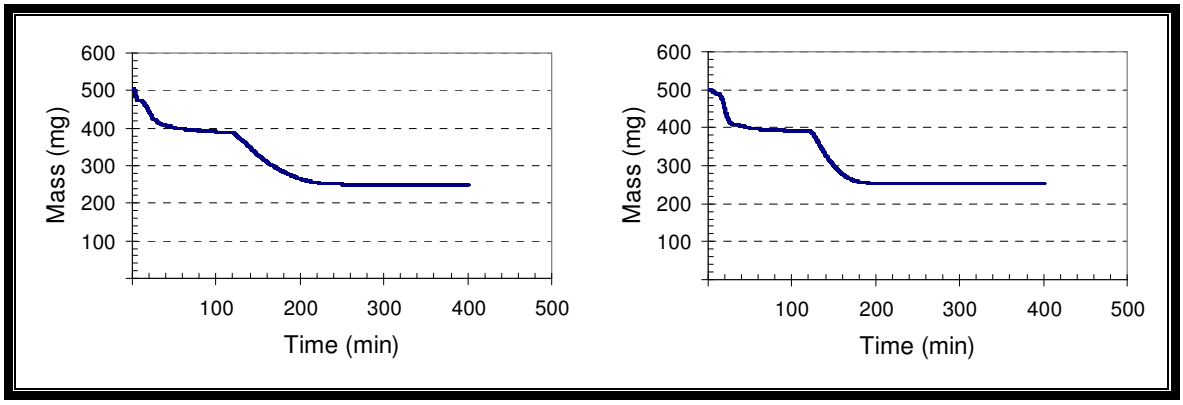


Figure C. 7: TGA curves for coal B4 at 1000ºC and 1015ºC.

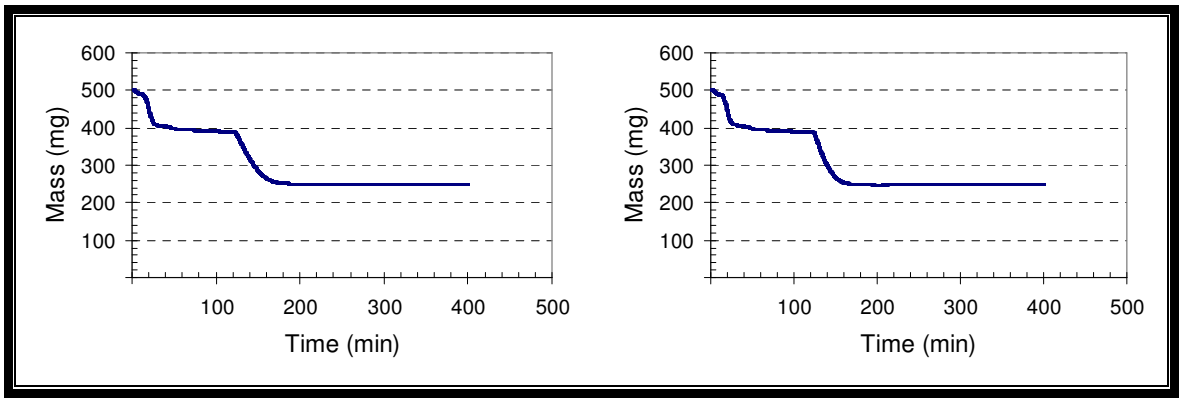


Figure C. 8: TGA curves for coal B4 at 1030ºC and 1070ºC.

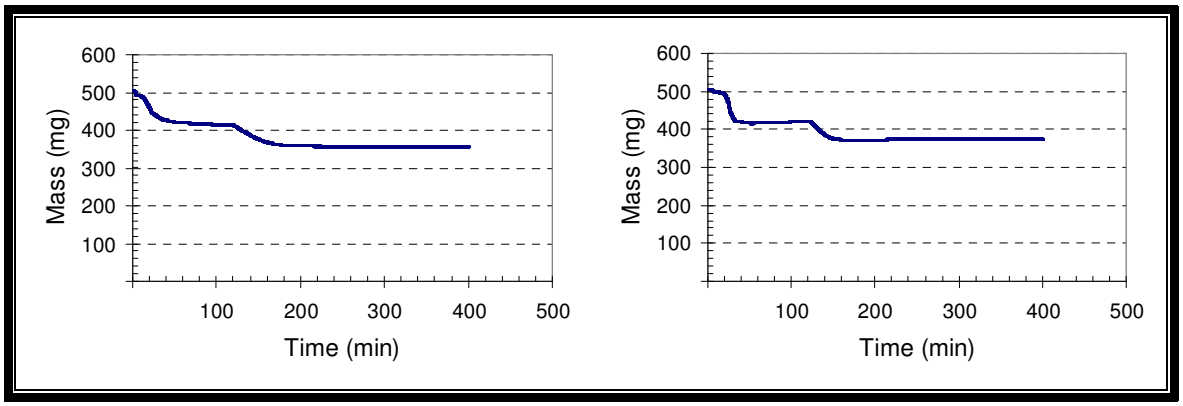


Figure C. 9: TGA curves for coal B5 at 1000ºC and 1015ºC.

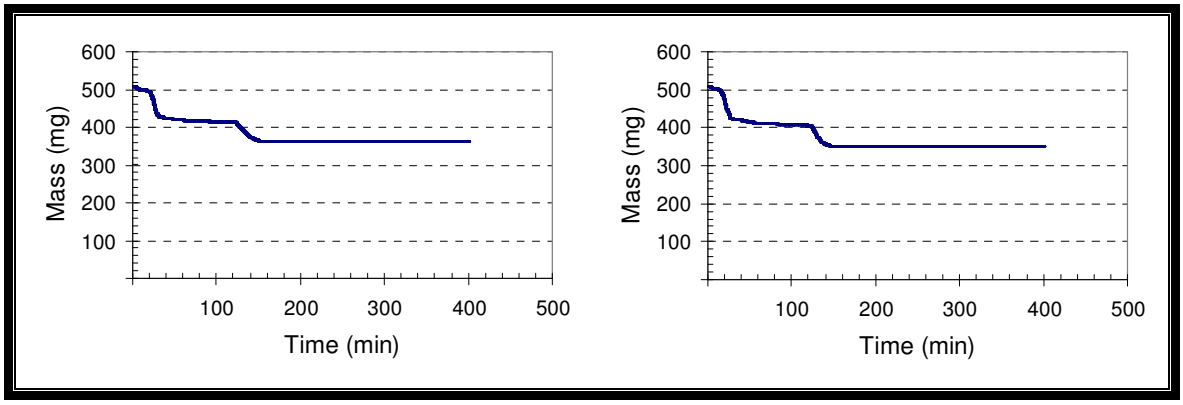


Figure C. 10: TGA curves for coal B5 at 1030ºC and 1070ºC.

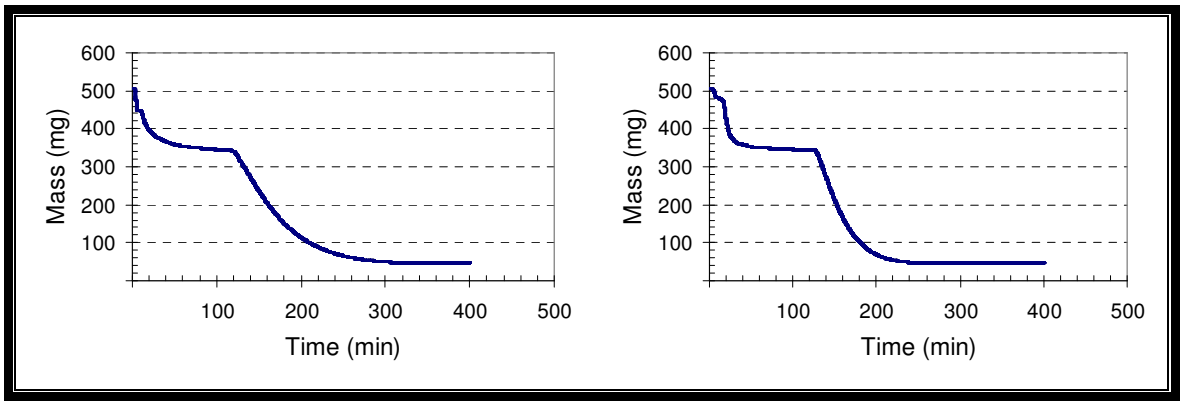


Figure C. 11: TGA curves for coal G1 at 1000ºC and 1015ºC.

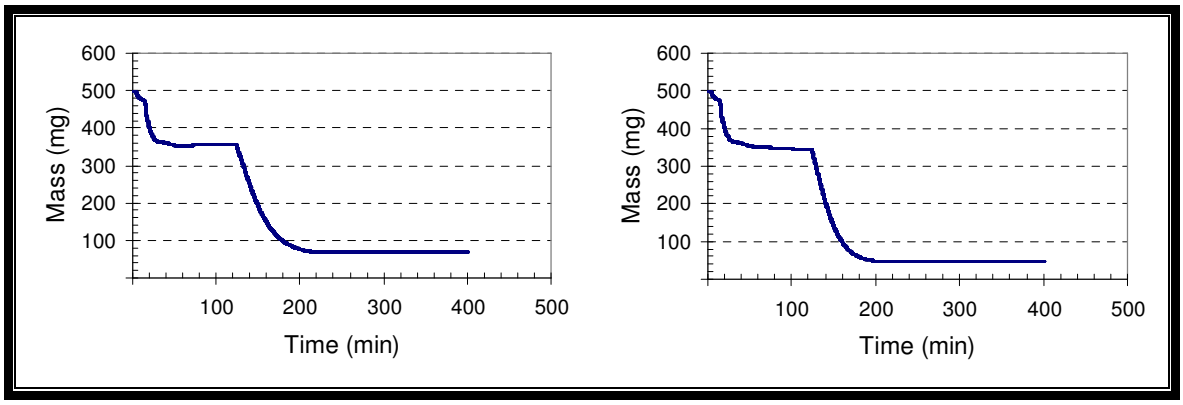


Figure C. 12: TGA curves for coal G1 at 1030ºC and 1070ºC.

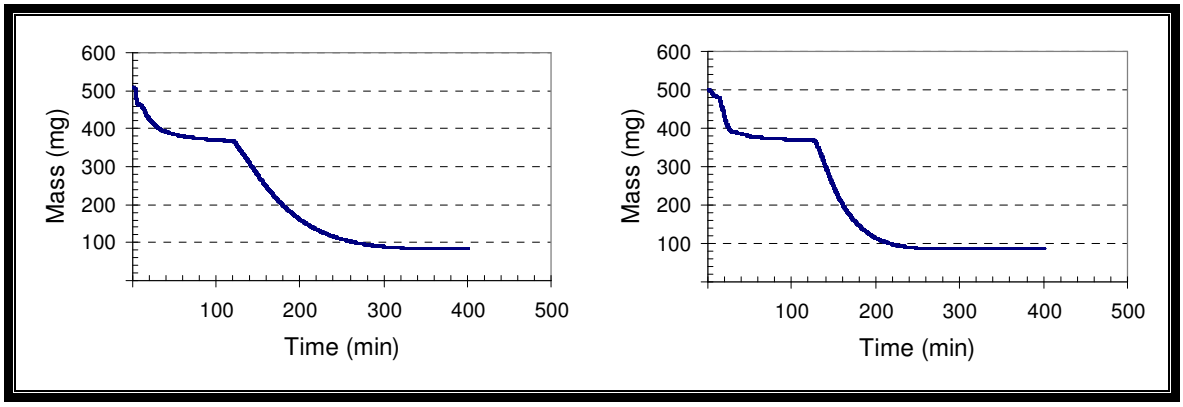


Figure C. 13: TGA curves for coal G2 at 1000ºC and 1015ºC.

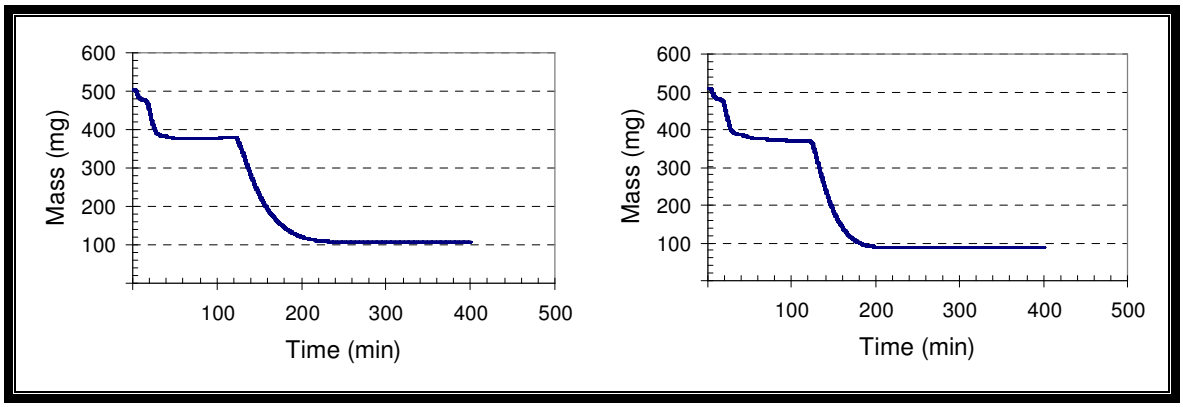


Figure C. 14: TGA curves for coal G2 at 1030ºC and 1070ºC.

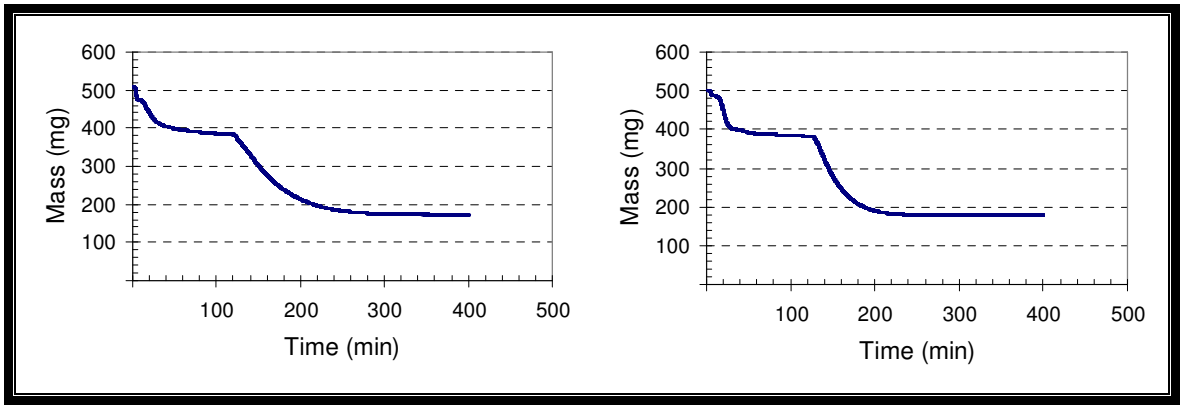


Figure C. 15: TGA curves for coal G3 at 1000ºC and 1015ºC.

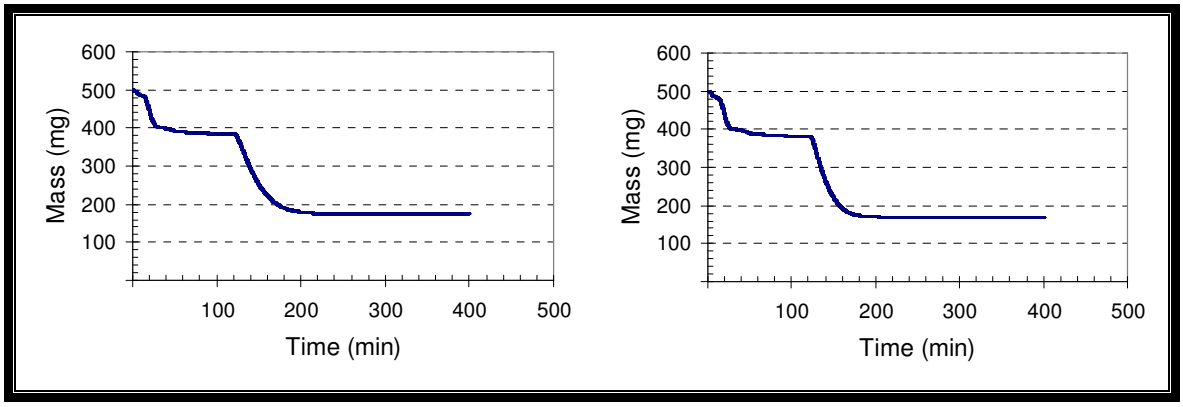


Figure C. 16: TGA curves for coal G3 at 1030ºC and 1070ºC.

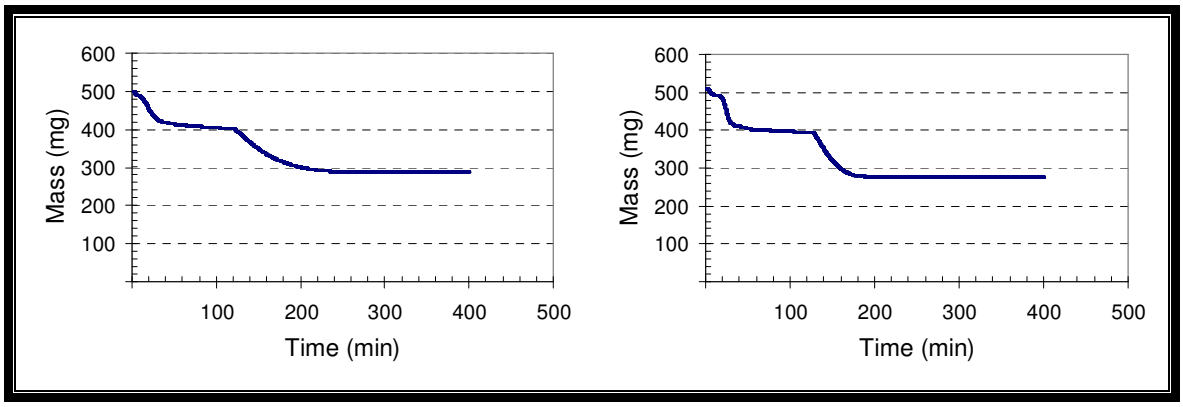


Figure C. 17: TGA curves for coal G4 at 1000ºC and 1015ºC.

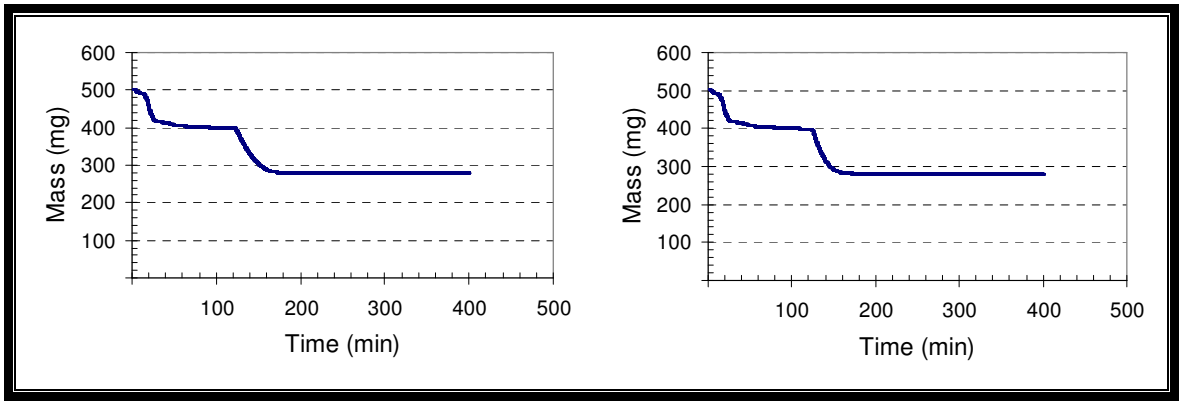


Figure C. 18: TGA curves for coal G4 at 1030ºC and 1070ºC.

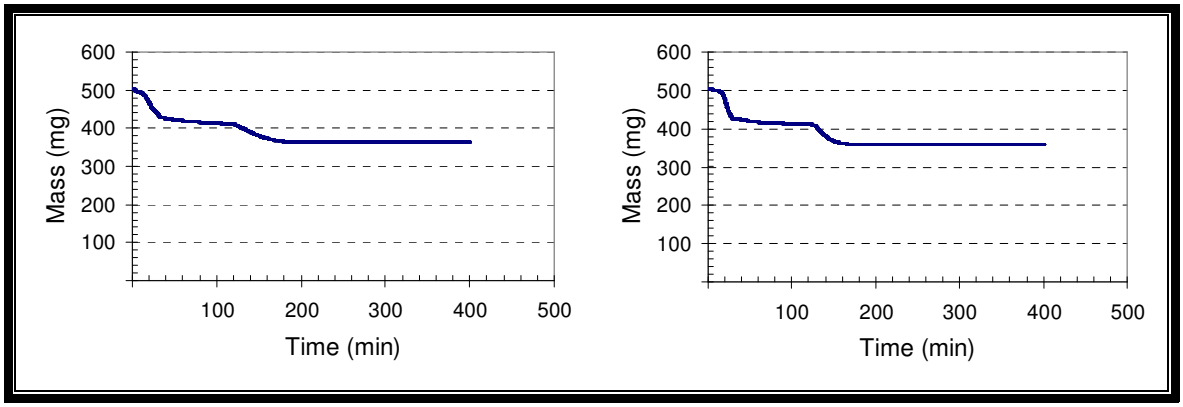


Figure C. 19: TGA curves for coal G5 at 1000ºC and 1015ºC.

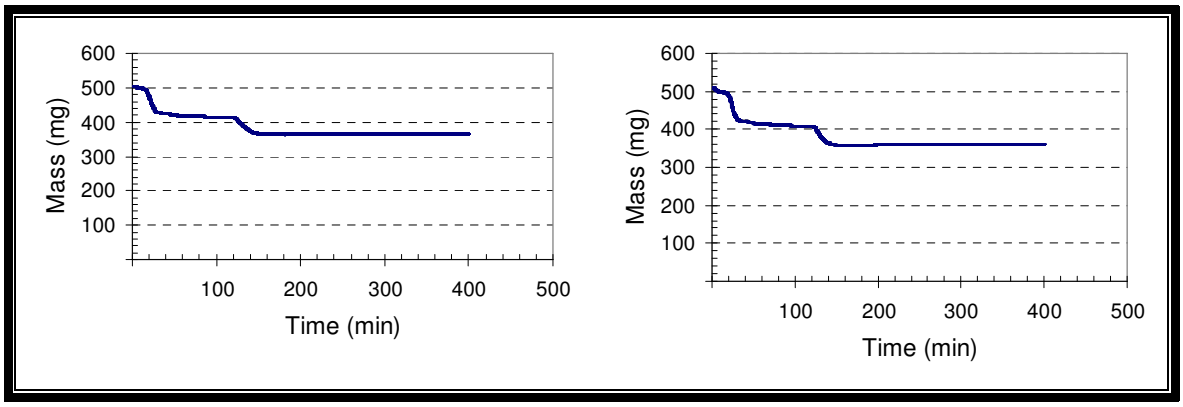


Figure C. 20: TGA curves for coal G5 at 1030ºC and 1070ºC.

# Appendix D: Conversion-time curves

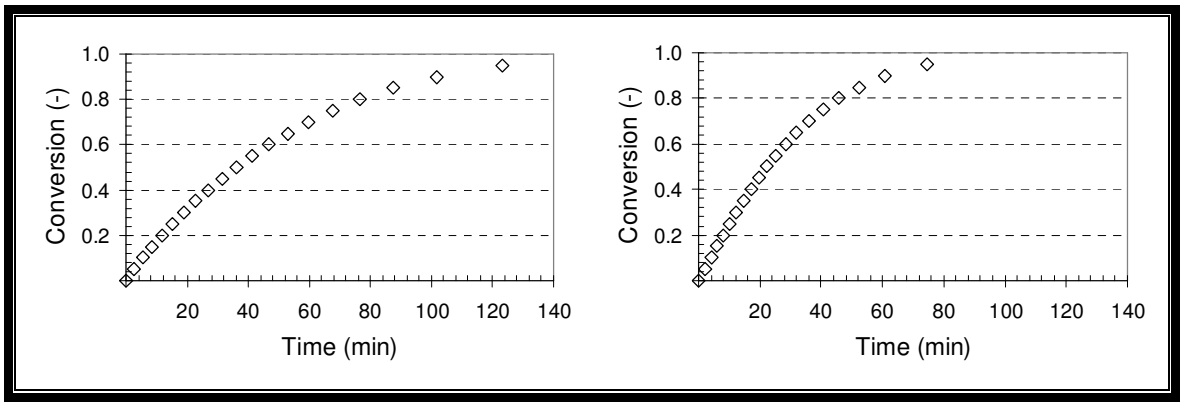


Figure D. 1: Conversion-time graphs for coal B1 at 1000ºC and 1015ºC.

Fi

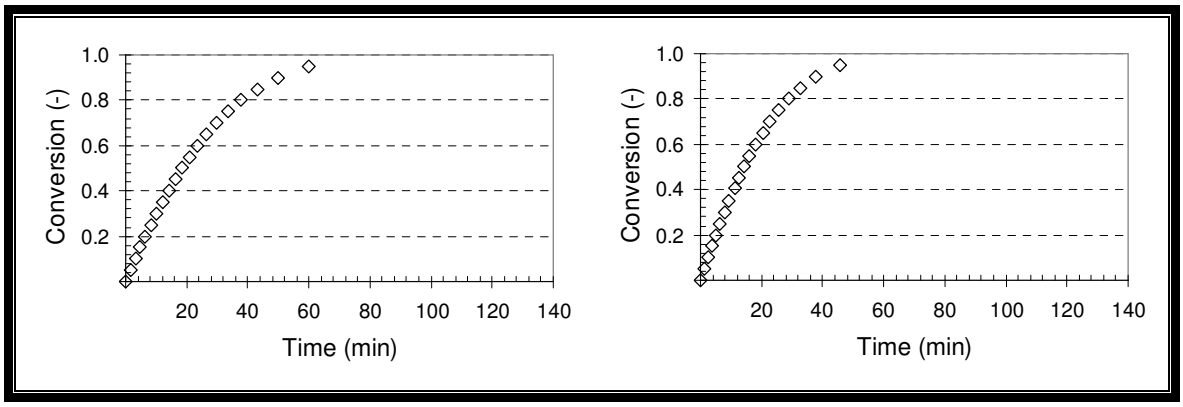


gure D. 2: Conversion-time graphs for coal B1 at 1030ºC and 1070ºC.

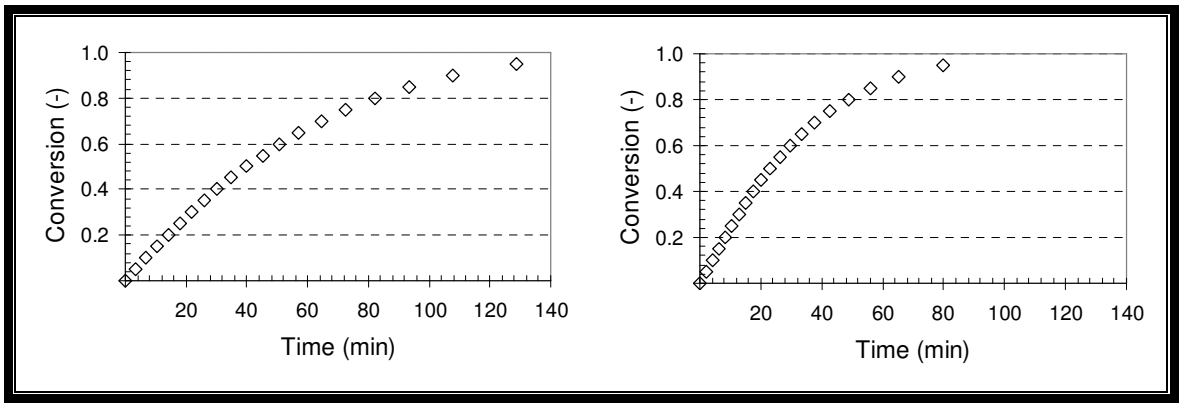


Figure D. 3: Conversion-time graphs for coal B2 at 1000ºC and 1015ºC.

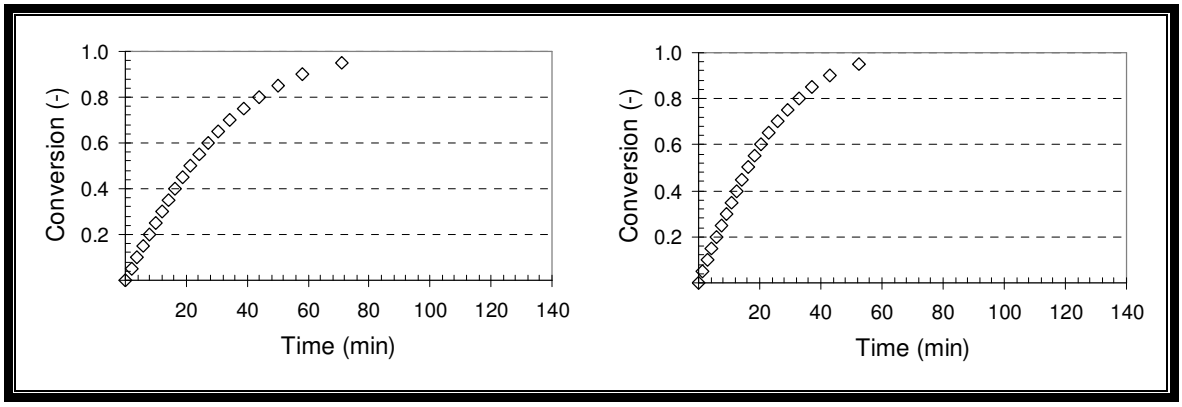


Figure D. 4: Conversion-time graphs for coal B2 at 1030ºC and 1070ºC.

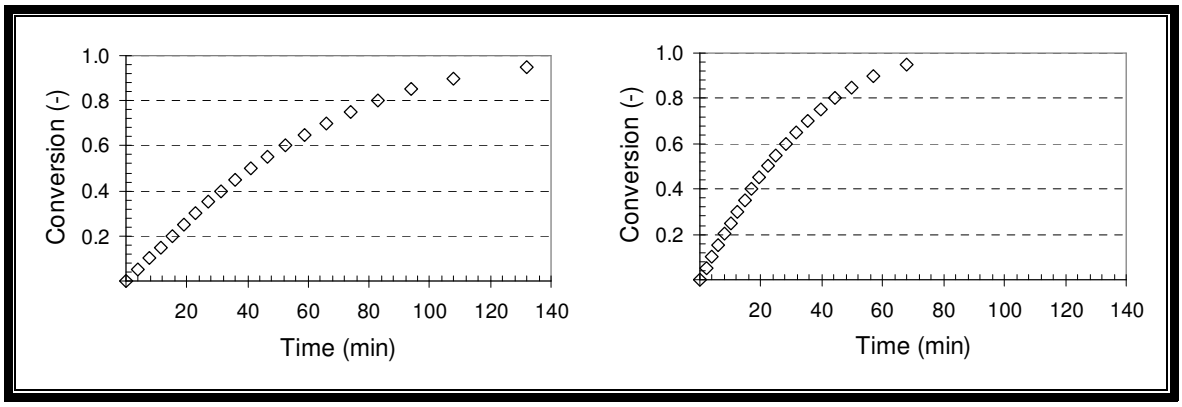


Figure D. 5: Conversion-time graphs for coal B3 at 1000ºC and 1015ºC.

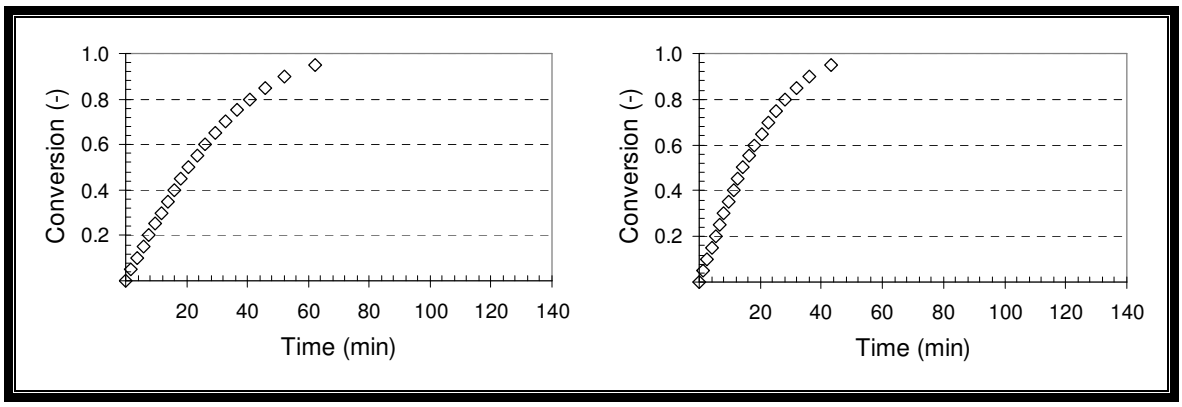


Figure D. 6: Conversion-time graphs for coal B3 at 1030ºC and 1070ºC.

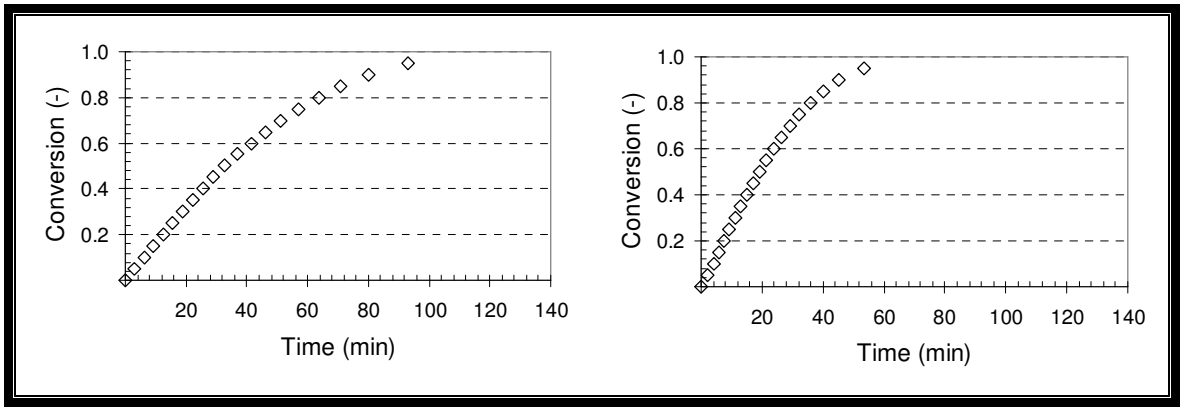


Figure D. 7: Conversion-time graphs for coal B4 at 1000ºC and 1015ºC.

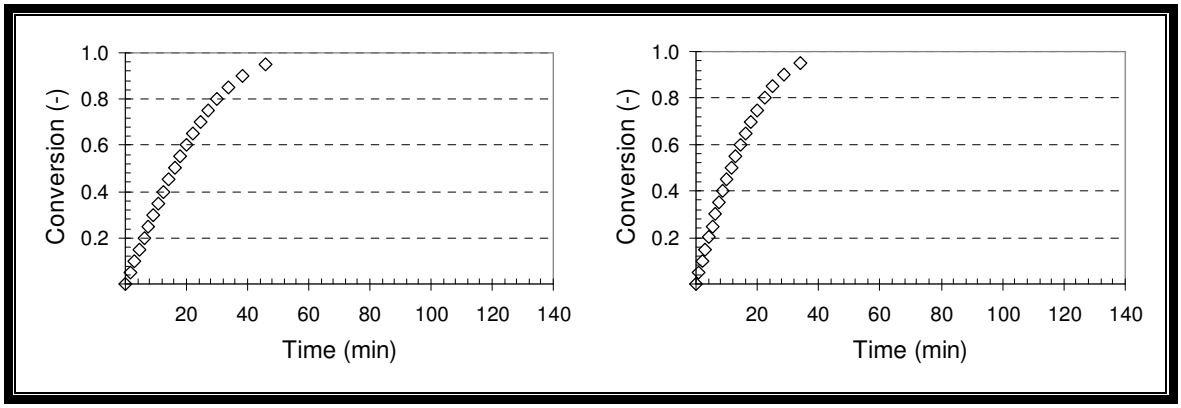


Figure D. 8: Conversion-time graphs for coal B4 at 1030ºC and 1070ºC.

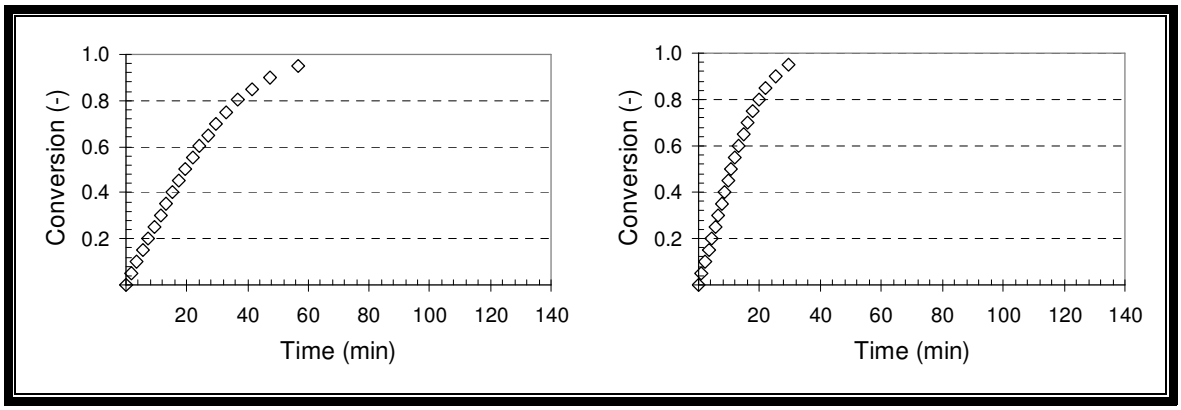


Figure D. 9: Conversion-time graphs for coal B5 at 1000ºC and 1015ºC.

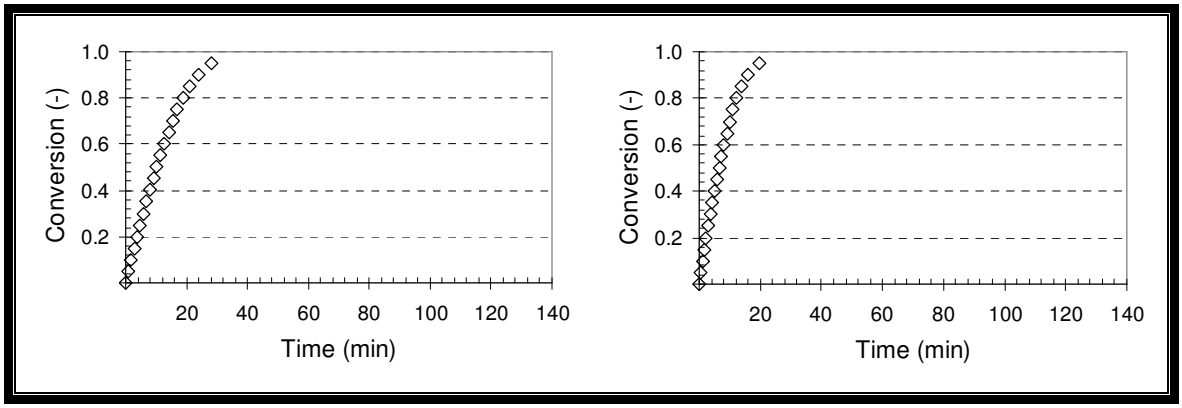


Figure D. 10: Conversion-time graphs for coal B5 at 1030ºC and 1070ºC.

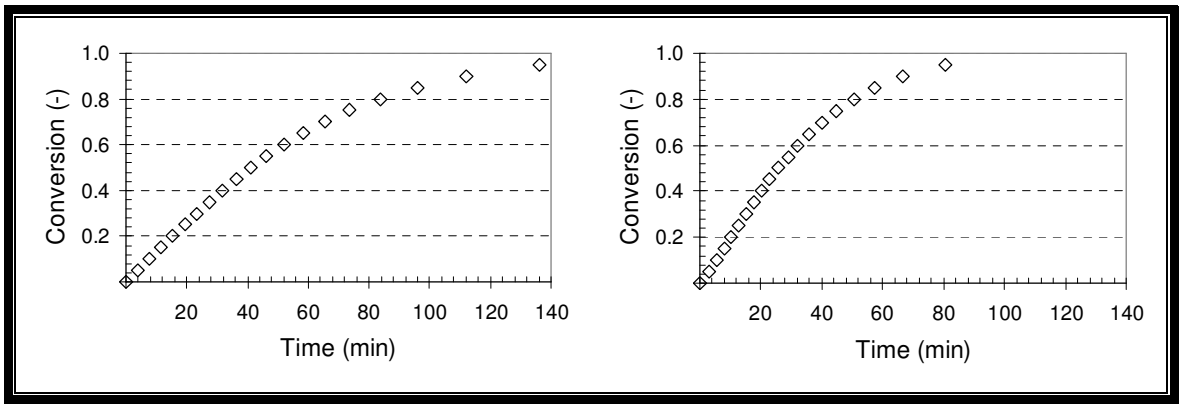


Figure D. 11: Conversion-time graphs for coal G1 at 1000ºC and 1015ºC.

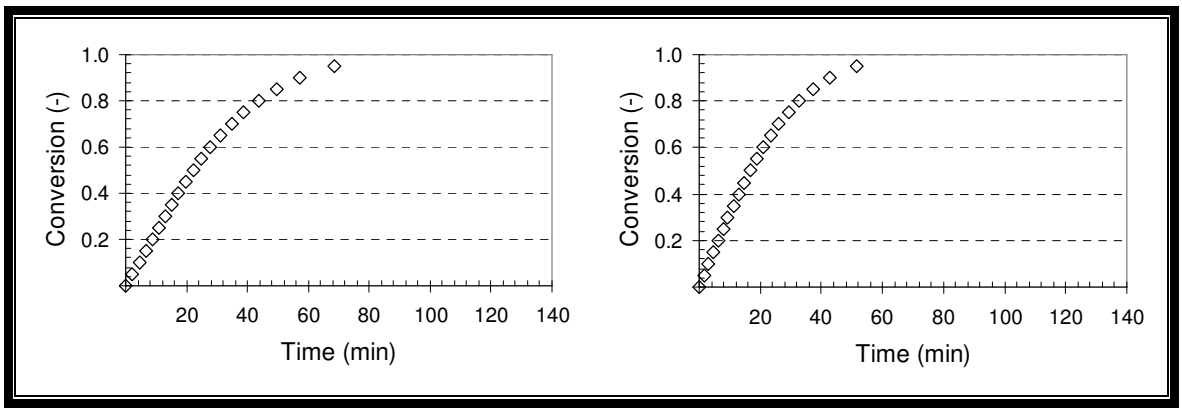


Figure D. 12: Conversion-time graphs for coal G1 at 1030ºC and 1070ºC.

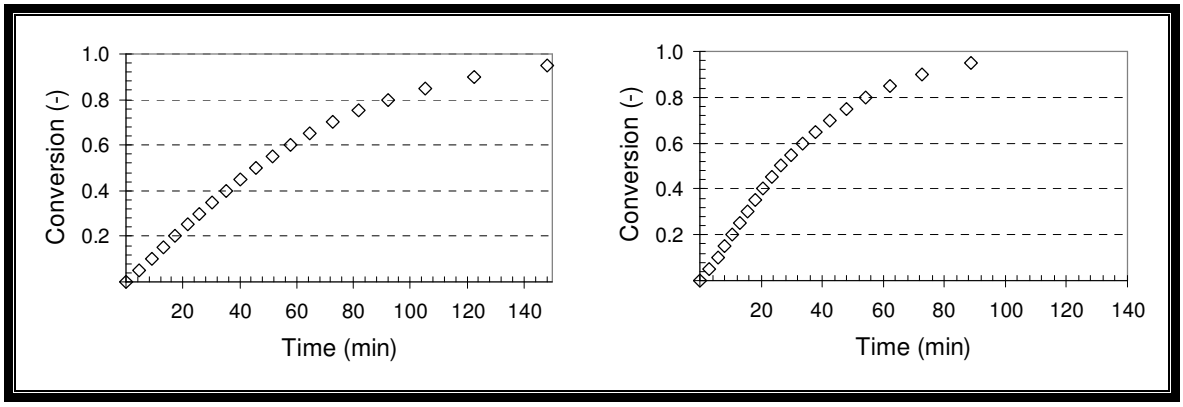


Figure D. 13: Conversion-time graphs for coal G2 at 1000ºC and 1015ºC.

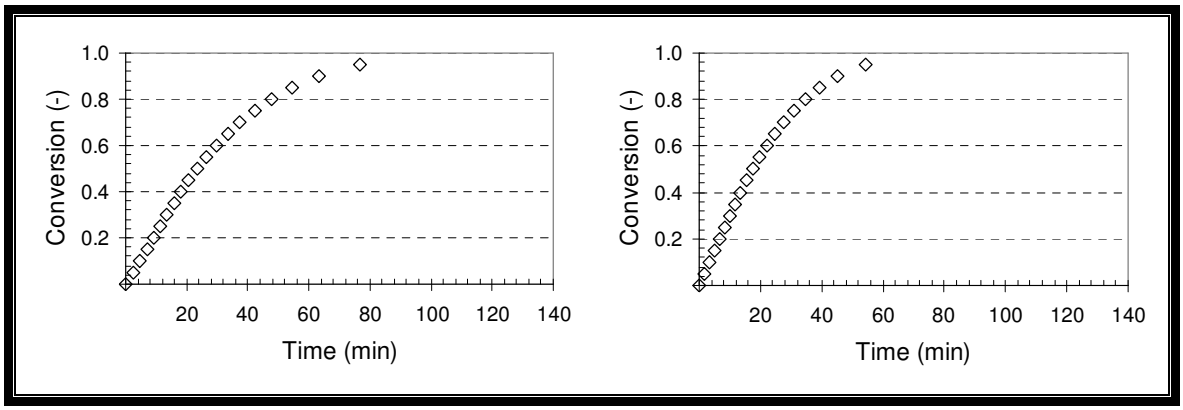


Figure D. 14: Conversion-time graphs for coal G2 at 1030ºC and 1070ºC.

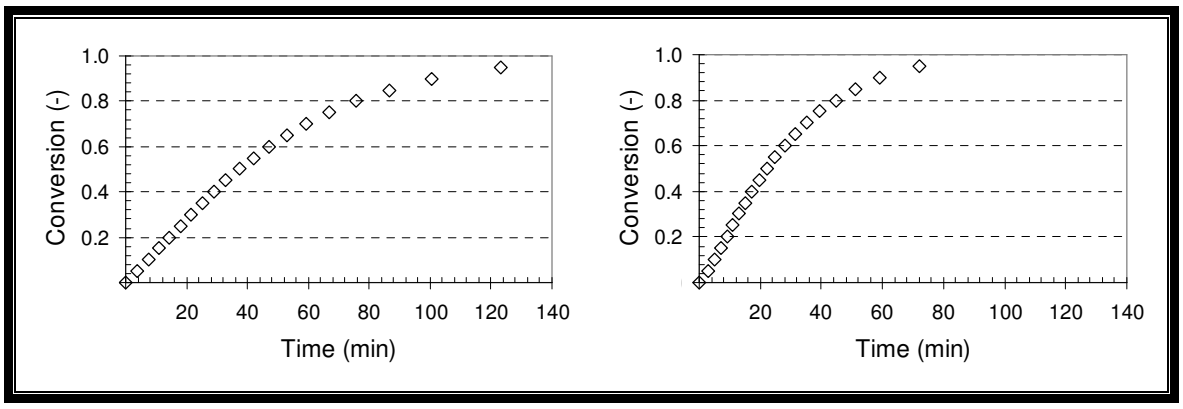


Figure D. 15: Conversion-time graphs for coal G3 at 1000ºC and 1015ºC.

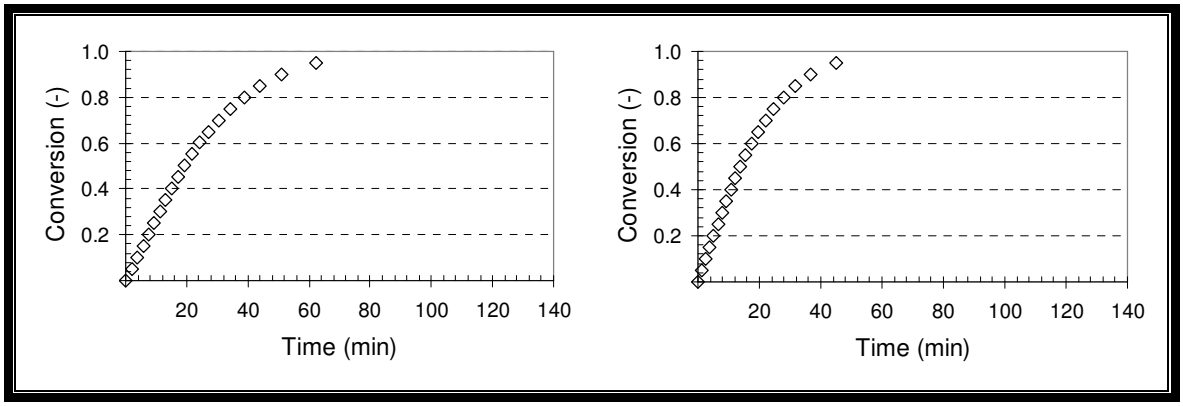


Figure D. 16: Conversion-time graphs for coal G3 at 1030ºC and 1070ºC.

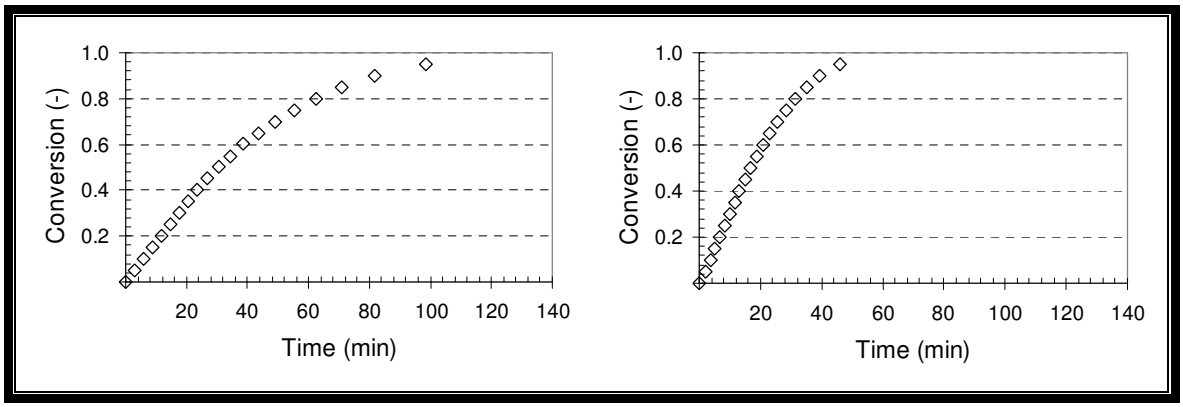


Figure D. 17: Conversion-time graphs for coal G4 at 1000ºC and 1015ºC.

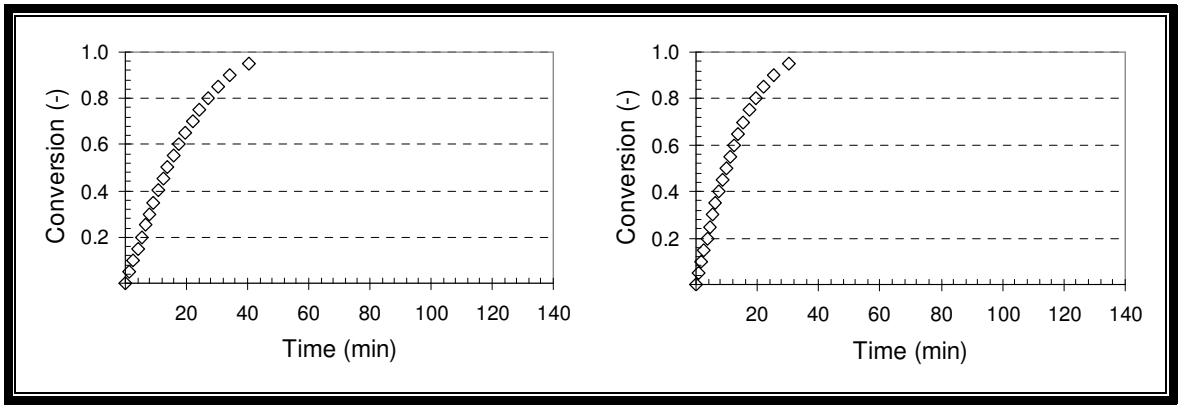


Figure D. 18: Conversion-time graphs for coal G4 at 1030ºC and 1070ºC.

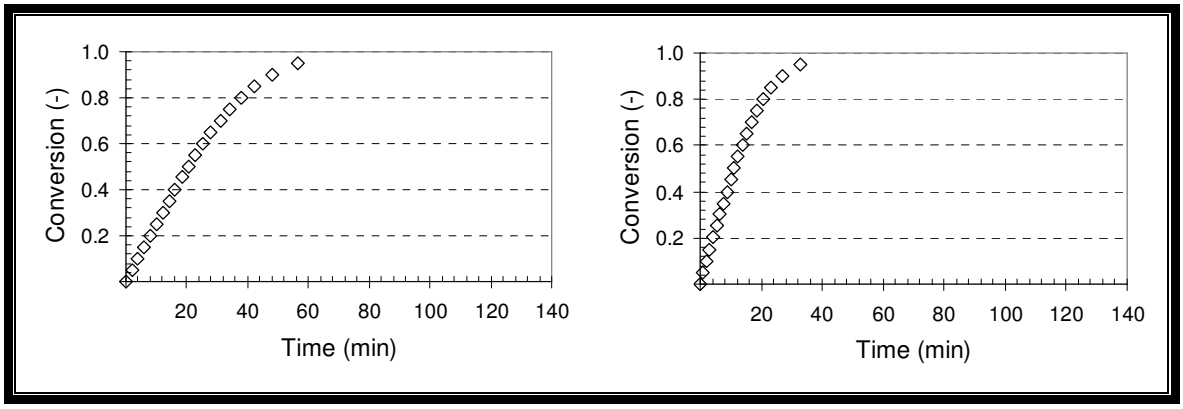


Figure D. 19: Conversion-time graphs for coal G5 at 1000ºC and 1015ºC.

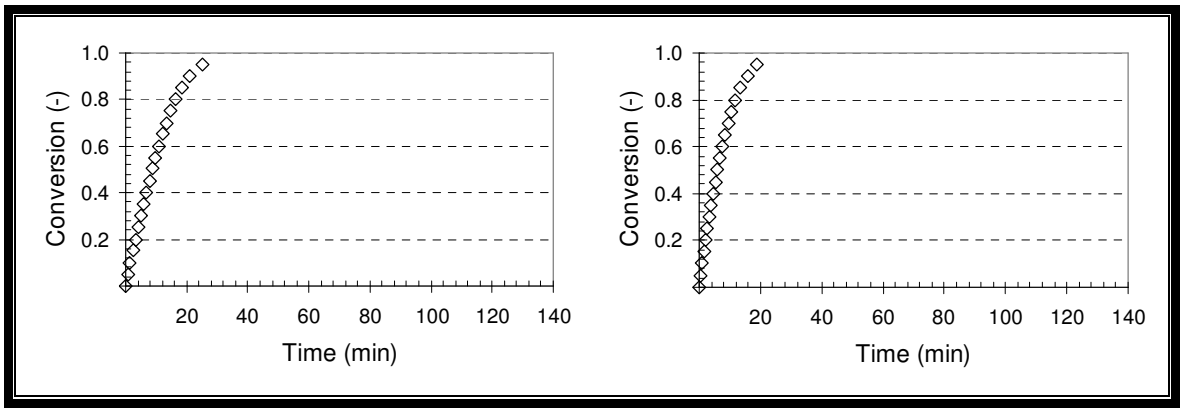


Figure D. 20: Conversion-time graphs for coal G5 at 1030ºC and 1070ºC.

# Appendix E: Influence of temperature on gasification rate

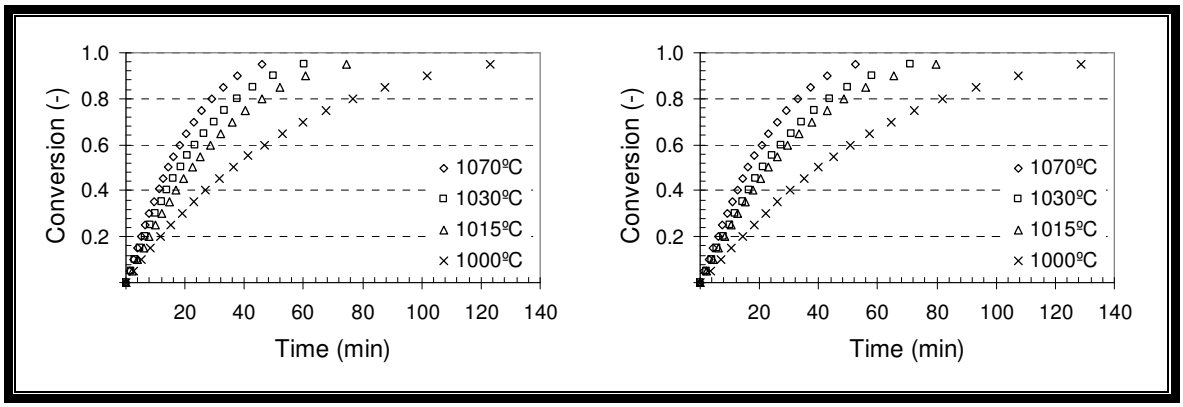


Figure E. 1: Influence of temperature on conversion rate for coal B1 and coal B2.

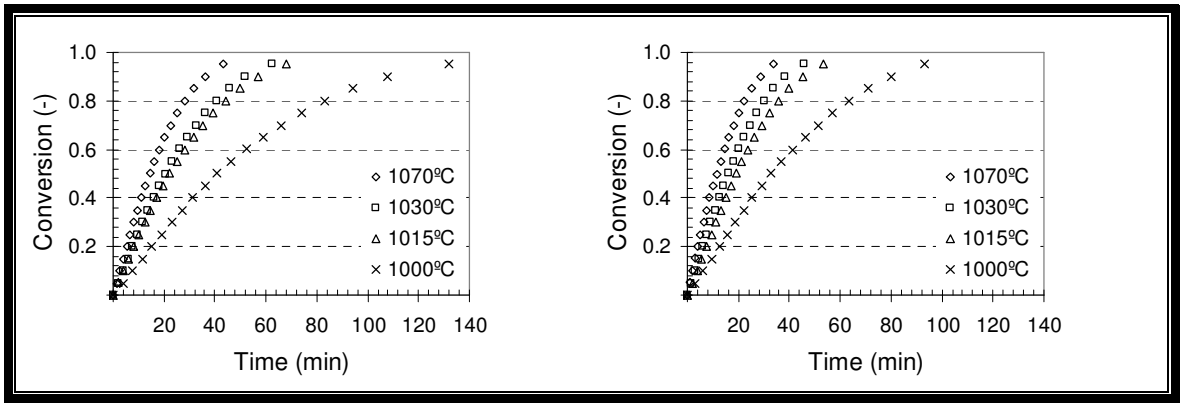


Figure E. 2: Influence of temperature on conversion rate for coal B3 and coal B4.

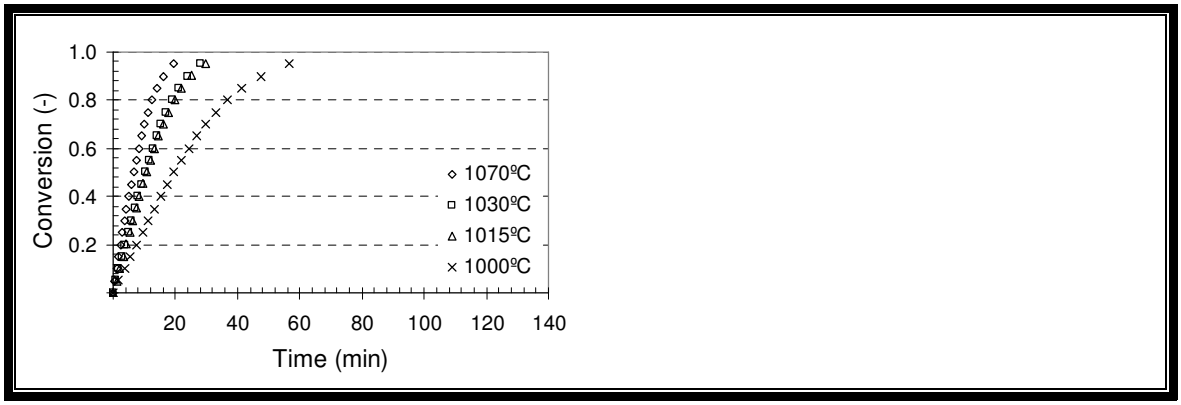


Figure E. 3: Influence of temperature on conversion rate for coal B5.

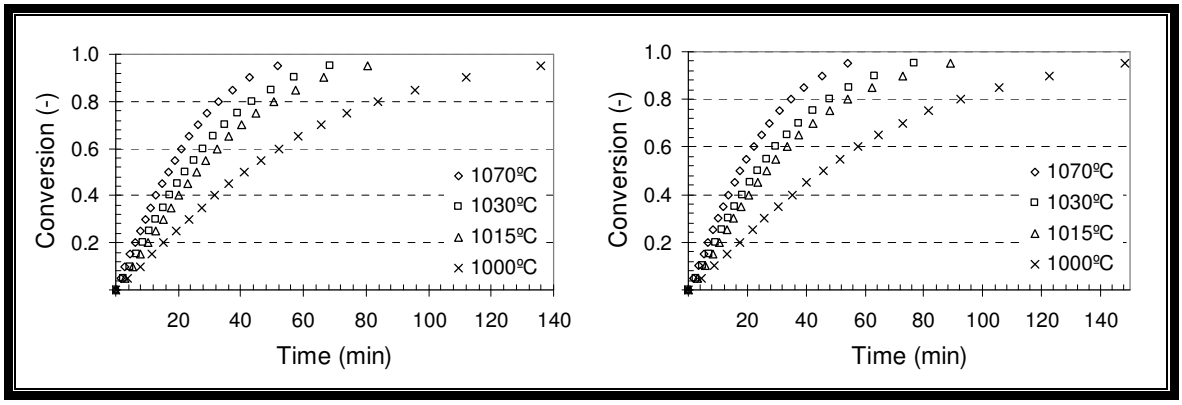


Figure E. 4: Influence of temperature on conversion rate for coal G1 and G2.

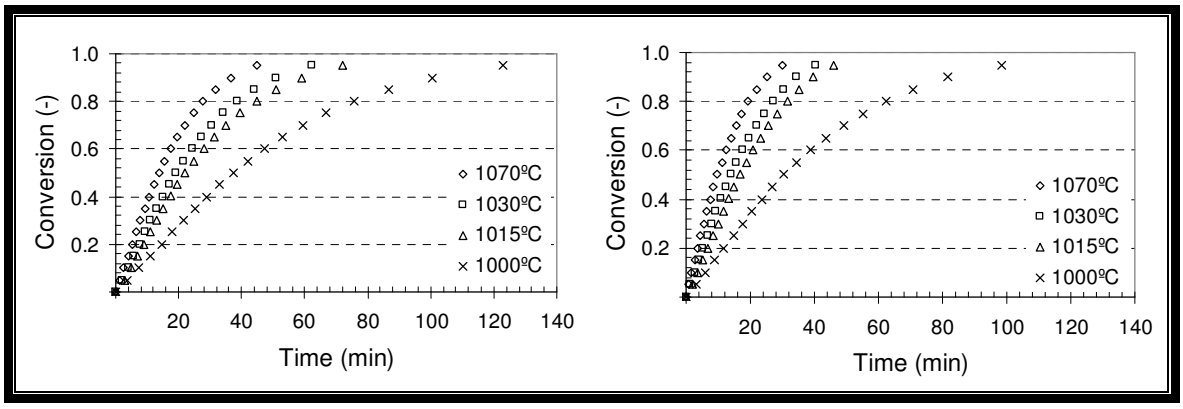


Figure E. 5: Influence of temperature on conversion rate for coal G3 and G4.

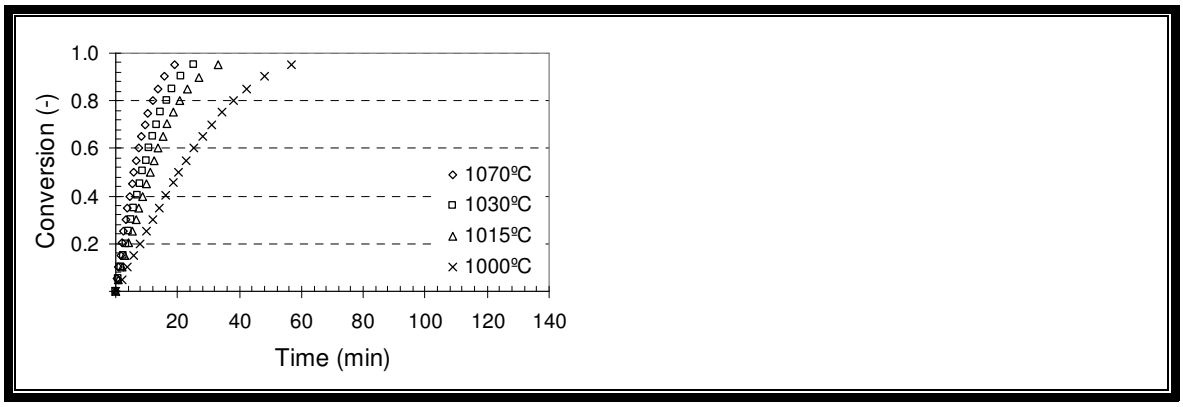


Figure E. 6: Influence of temperature on conversion rate for coal G5.

# Appendix F: Influence of density on gasification rate

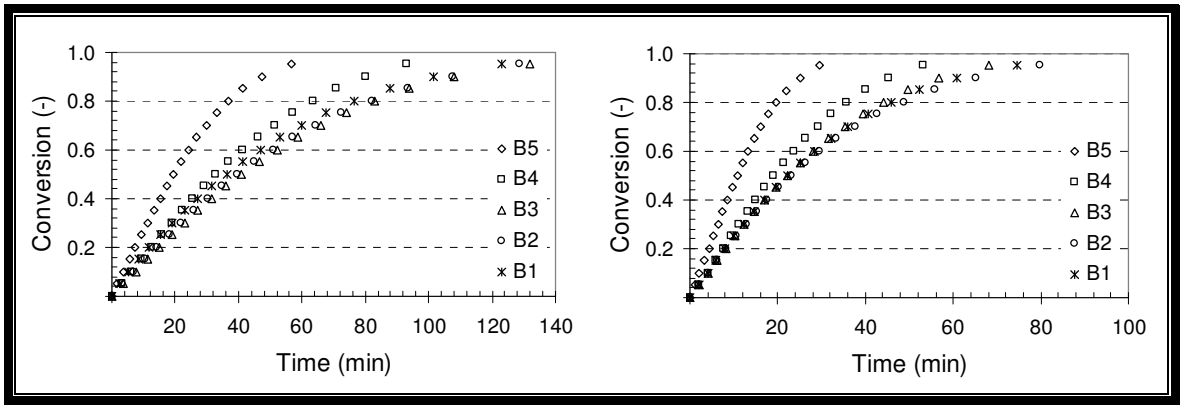


Figure F. 1: Influence of density on conversion rate for coal B at 1000ºC and 1015ºC.

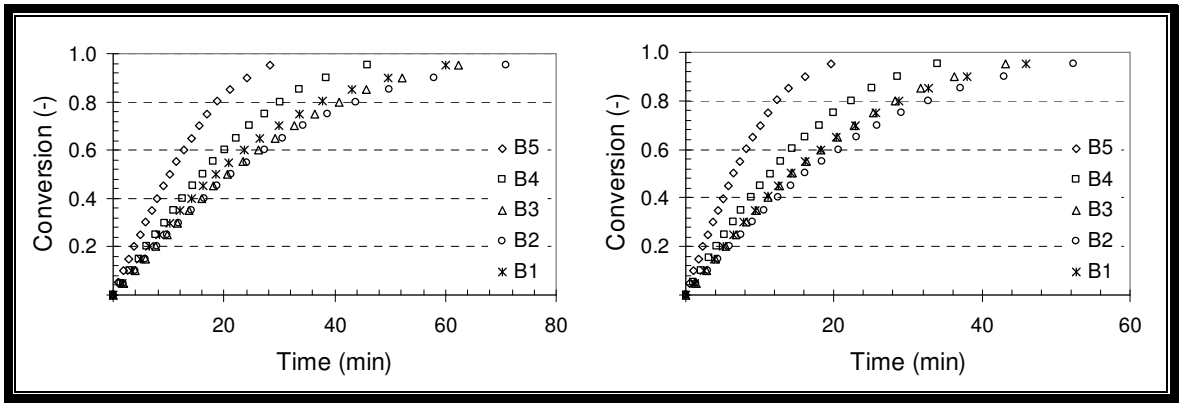


Figure F. 2: Influence of density on conversion rate for coal B at 1030ºC and 1070ºC.

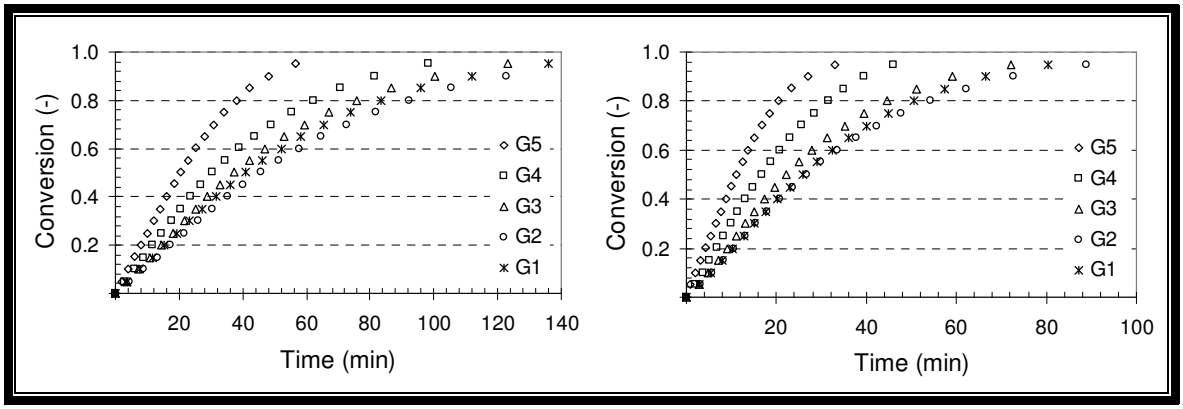


Figure F. 3: Influence of density on conversion rate for coal G at 1000ºC and 1015ºC.

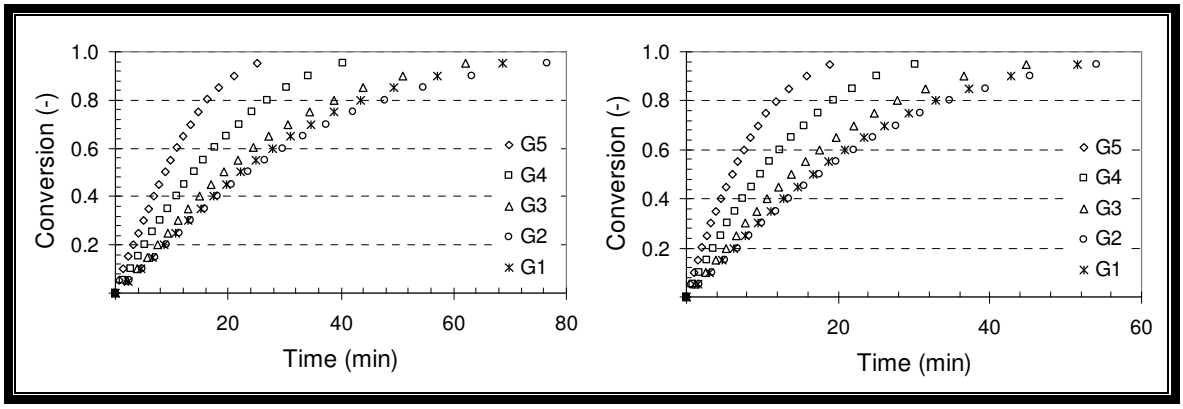


Figure F. 4: Influence of density on conversion rate for coal G at 1030ºC and 1070ºC.

# Appendix G: Determination of structural parameter

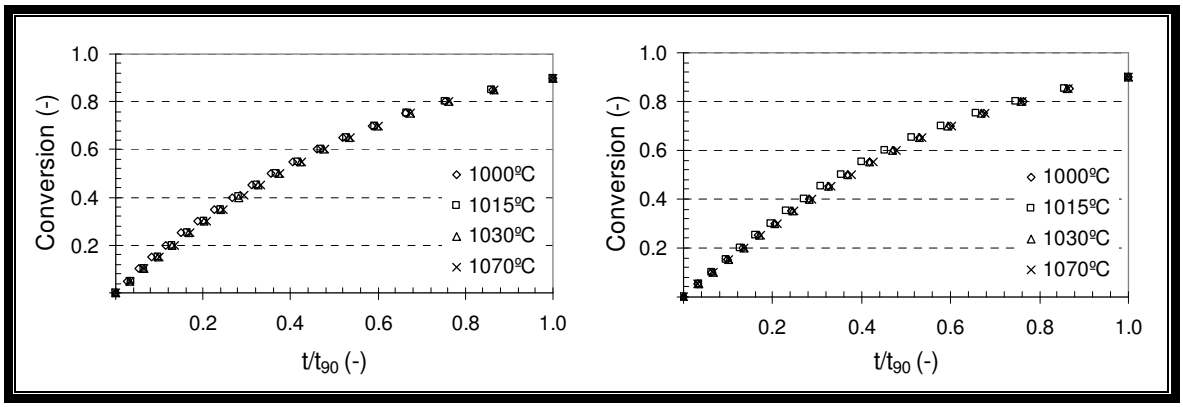


Figure G. 1: Conversion as function of reduced time for coal B1 and coal B2.

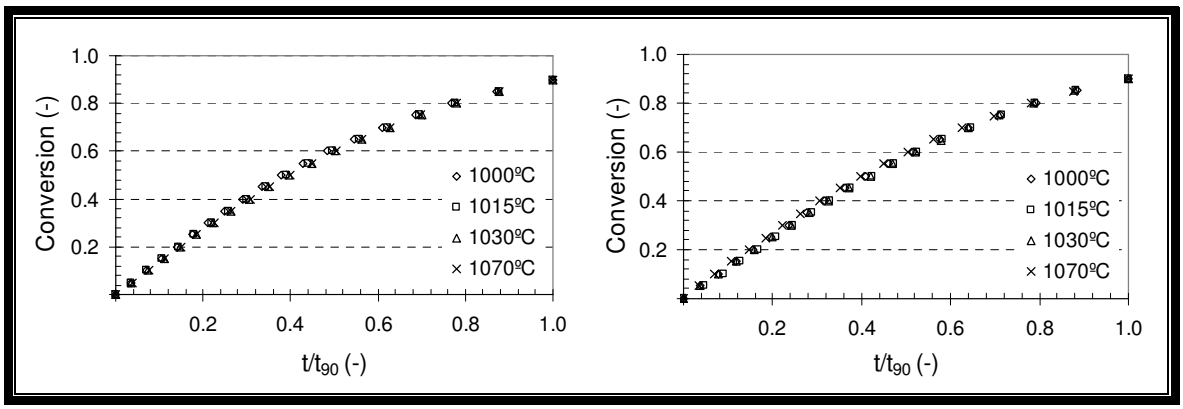


Figure G. 2: Conversion as a function of reduced time for coal B3 and coal B4.

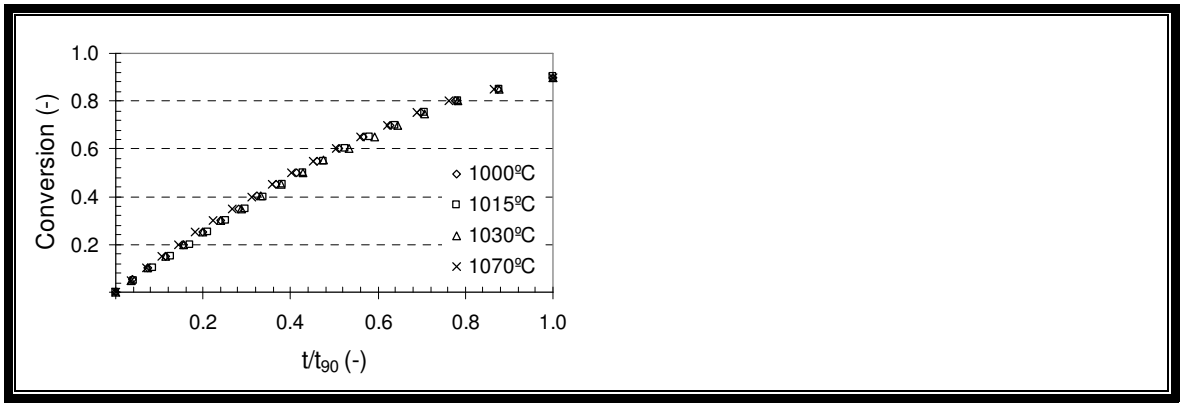


Figure G. 3: Conversion as a function of reduced time for coal B5.

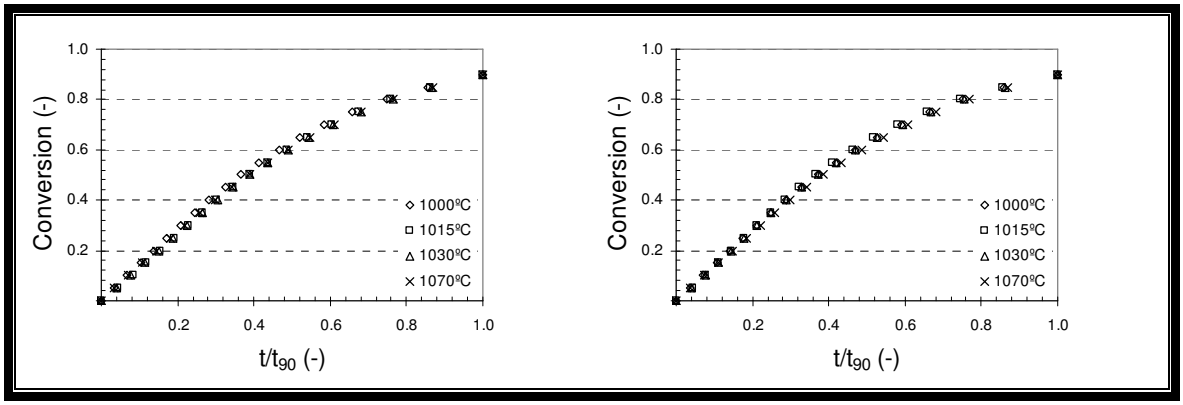


Figure G. 4: Conversion as a function of reduced time for coal G1 and coal G2.

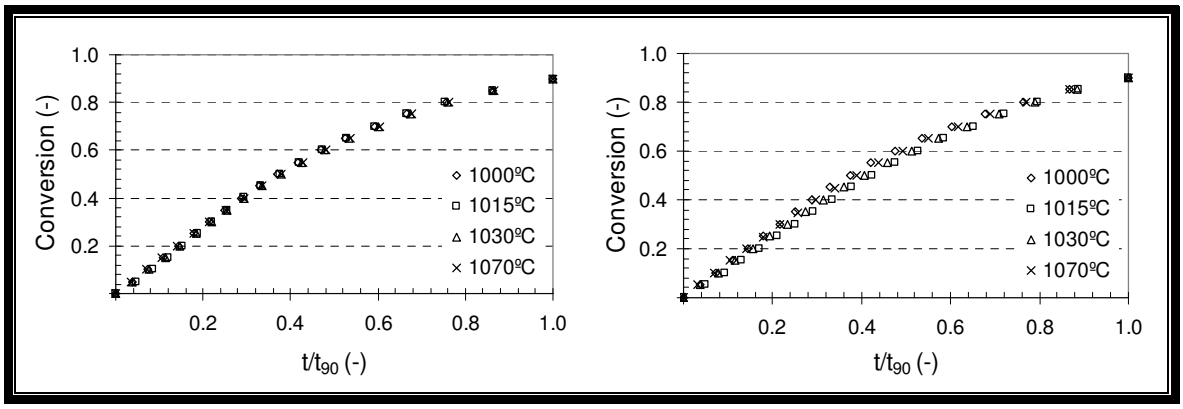


Figure G. 5: Conversion as a function of reduced time for coal G3 and coal G4.

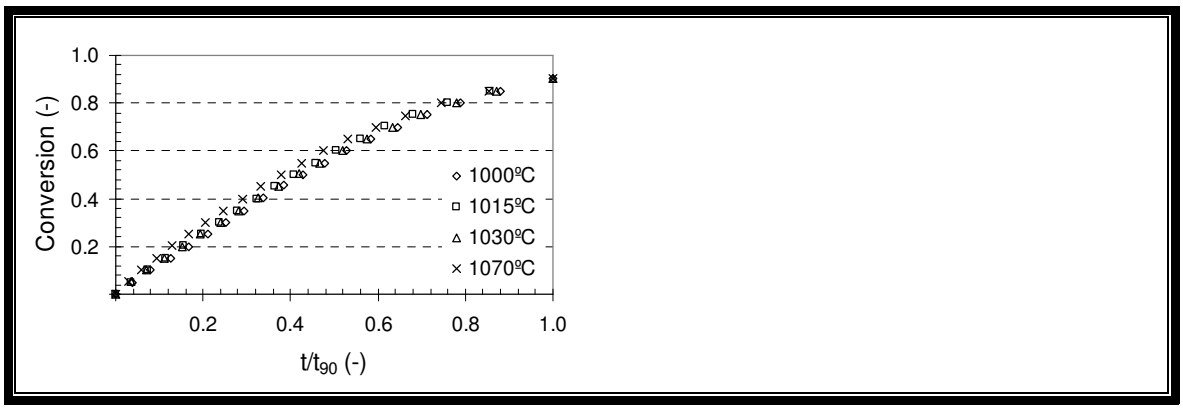


Figure G. 6: Conversion as a function of reduced time for coal G5.

# Appendix H: Fit of random pore model to experimental data

This appendix shows the fit of random pore model to the experimental data. Lines indicate modelled data.

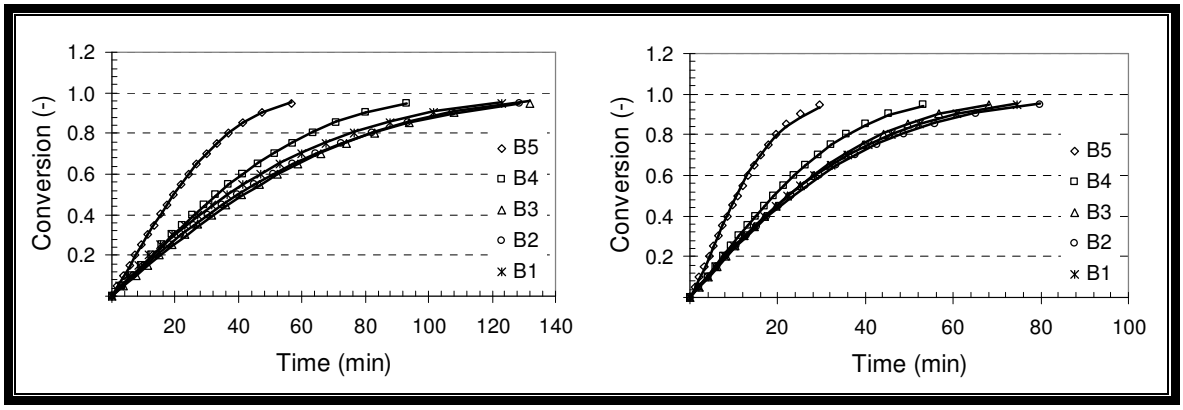


Figure H. 1: Fit of random pore model to coal B at 1000ºC and 1015ºC.

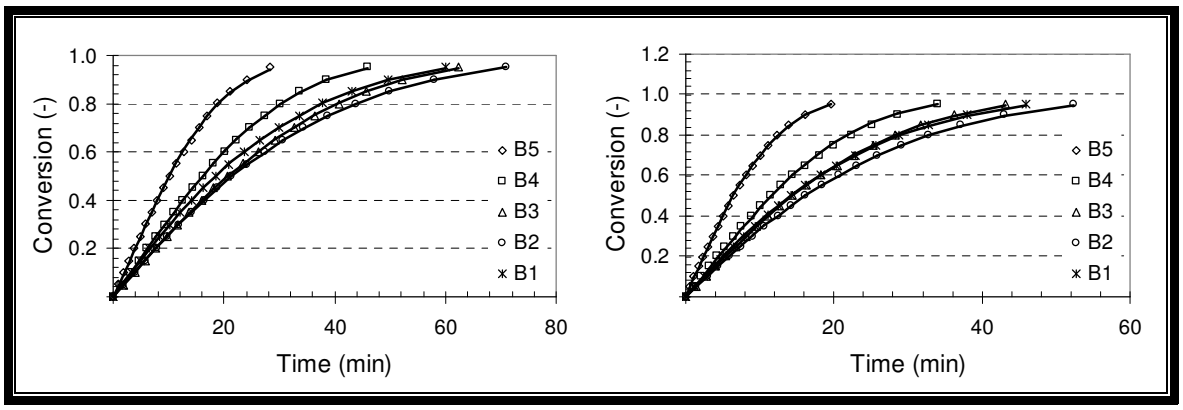


Figure H. 2: Fit of random pore model to coal B at 1030ºC and 1070ºC.

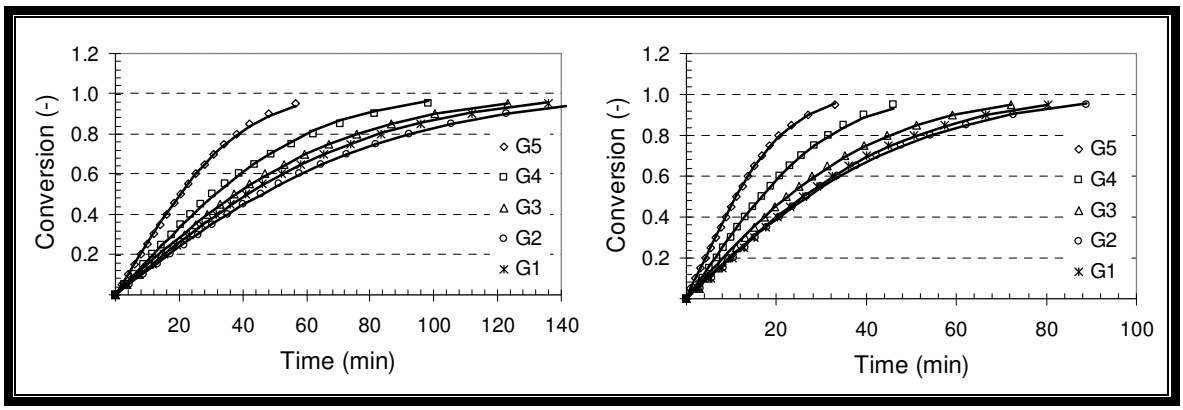


Figure H. 3: Fit of random pore model to coal G at 1000ºC and 1015ºC.

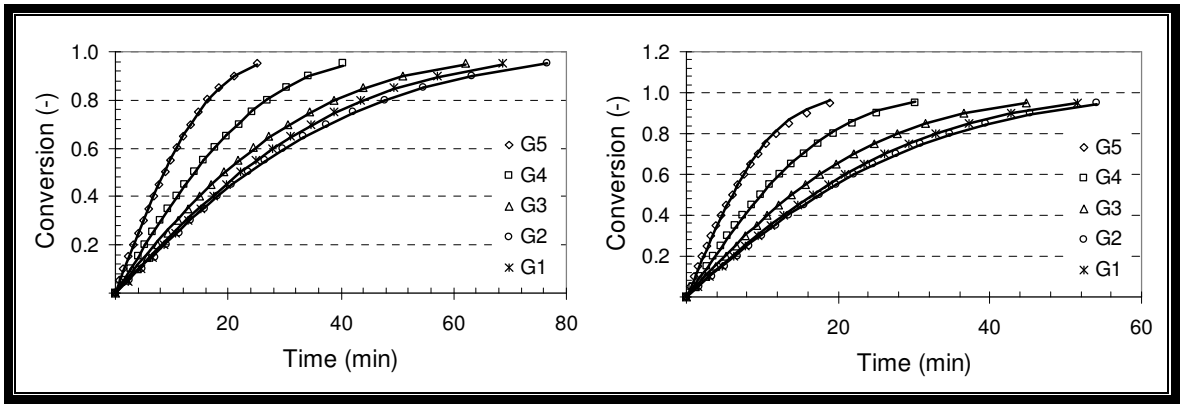


Figure H. 4: Fit of random pore model to coal G at 1030ºC and 1070ºC.

# Appendix I: Experimental error

The experimental error was calculated for gasification experiments, by comparing the time to reach 50 % conversion from 3 repeat runs done on coal fraction B5 at 1070ºC.

- Step 1: Calculate the mean of the data set. This is done by the following equation:

$$\bar{x} = \frac{1}{N}\sum_{i=1}^{N} x_i \quad \text{..... (I.1)}$$

where N is the total number of data points and $x_i$ is a individual data point.

- Step 2: Calculate the standard deviation of the data set as follows:

$$s = \sqrt{\frac{\sum_{i=1}^{N}\left(x_i - \bar{x}\right)^2}{N-1}} \quad \text{.....(I.2)}$$

- Step 3: Calculate the standard error of the mean with the following equation:

$$SE = \frac{s}{\sqrt{N}} \quad \text{.....(I.3)}$$

- Step 4: Calculate the z critical value for a 95 % confidence level, i.e. there is a 95 % probability the data points obtained from the experiments lies within the range of the calculated confidence interval. The z critical value is calculated as follows:

$$z = \frac{\bar{x} - \mu}{s/\sqrt{N}} \quad \text{.....(I.4)}$$

Where μ is the mean value for continuous variable x and N is the amount of data points.

- Step 5: Calculate the confidence interval with the following equation:

$$CI = \bar{x} \pm (SE \times z) \quad \text{.....(I.5)}$$

- Step 6: Calculate the experimental error with:

$$EE = \frac{2 \times CI}{\bar{x}} \times 100 \quad \text{.....(I.6)}$$

Table I.1 shows the calculation of an experimental error.

Table I. 1: Summary of experimental error.

| **Run number** | **$t_{50}$ (min)** |
|---|---|
| Run 1 | 129.87 |
| Run 2 | 130.95 |
| Run 3 | 130.07 |
| Average | 130.29 |
| Standard deviation | 0.58 |
| z critical value | 2.12 |
| Experimental error (%) | 1.63 |

# Appendix J: Mass transfer calculations

The Wagner-Weisz-Wheeler modulus provides an efficient theoretical estimation of how reactivity of chars is affected by internal mass transfer (Levenspiel, 1972). This parameter is defined as:

$$M_W = L^2 \frac{(-r_A''' C_A)_{Obs}}{D_{eff}} \quad \text{.....(J.1)}$$

By combining the rate of reaction, particle density and the molecular weight of carbon, Equation J.1 can be expressed as:

$$M_W = L^2 \frac{k}{D_{eff}} < 0.15 \quad \text{.....(J.2)}$$

It can therefore be assumed that when the observed Wagner-Weisz-Wheeler modulus is smaller than 0.15 that internal mass transfer does not significantly impact on the reactivity.

Several assumptions were made during the calculation of the internal pore diffusion and are stated as follows:

- Coal particles are assumed to be spheres, and therefore the characteristic length (L) can be defined as a third of the particle radius.
- Only micropores were considered in the calculation of the internal pore diffusion. The porosity and average diameter values of the micropores were obtained from $CO_2$ adsorption experiments (Table 4.27).
- The tortuosity can usually be assumed to range from 2 – 3, but is assumed as a worst-case scenario as 6.
- The apparent rate constant (k) is obtained from the initial slope of the conversion–time plot (Appendix D).
- Knudsen diffusion is assumed to be the main mechanism involved in the diffusion of gas into the micropores.

The effective diffusivity can be calculated from:

$$D_{eff} = \frac{\varepsilon_0 D_k}{\tau_t} \quad \text{(J.3)}$$

The Knudsen diffusivity can then be calculated as follows:

$$D_k = 4850 D_{AVG} \left(\frac{T}{M_{CO2}}\right)^{0.5} \quad \text{(J.4)}$$

The values of the Wagner-Weisz-Wheeler modulus were calculated for coals B1 - B5 and G1 – G5 at the highest reaction temperature used in this study, which is 1070ºC and are presented below in Table J.1.

Table J. 1: Wagner-Weisz-Wheeler modulus values for internal mass transfer.

| | **B1** | **B2** | **B3** | **B4** | **B5** | **G1** | **G2** | **G3** | **G4** | **G5** |
|---|---|---|---|---|---|---|---|---|---|---|
| **$M_W$ ($10^{-8}$)** | 4.3 | 2.8 | 3.3 | 1.8 | 4.2 | 3.4 | 3.2 | 1.9 | 2.2 | 3.4 |

It can be seen that the values of the Wagner-Weisz-Wheeler modulus are several orders of magnitude smaller than 0.15. This validates the assumption that internal mass transfer does not significantly impact on the reactivity values obtained from TGA experiments.